

SEDIMENT DIAGENESIS IN LARGE LAKES SUPERIOR AND
MALAWI, GEOCHEMICAL CYCLES AND BUDGETS AND
COMPARISONS TO MARINE SEDIMENTS

A THESIS
SUBMITTED TO THE FACULTY OF
UNIVERSITY OF MINNESOTA
BY

JYING LI

IN PARTIAL FULFILLMENT OF THE REQUIREMENTS
FOR THE DEGREE OF
DOCTOR OF PHILOSOPHY

SERGEI KATSEV

SEPTEMBER 2014

© JIYING LI 2014

ACKNOWLEDGEMENTS

This work would not have been possible without the help of many people and the great facilities provided by the Large Lakes Observatory (LLO) at the University of Minnesota Duluth (UMD). It has been great pursuing my PhD here at the LLO.

Foremost, I would like to thank my advisor Dr. Sergei Katsev, for the invaluable support throughout this endeavor. He has devoted enormous amount of time and great effort to guide me and help me improve in not only understanding the science but also in many other important skills such as scientific writing and presentations. I also appreciate the generous funding he has been providing to make my experience more productive. He has been always accessible and supportive. I enjoyed the many enlightening discussions with him, from which I've learned knowledge and skills, and also greatly inspired by his enthusiasm and curiosity for science. I am also very grateful to my coworker Sean Crowe, from whom I learned a lot of fieldwork and experimental techniques and received invaluable intellectual inputs. I also thank David Miklesh, Matthew Kistner, and Maria Dittrich, for their help with fieldwork and experiments. It has been great to work with and learn from them.

I appreciate the advice from my committee members Erik Brown, Elizabeth Minor, Josef Werne, Robert Hecky, and discussions with Tom Johnson, Robert Sterner, Jacques Finlay, and Jim Cotner. I would also like to thank Jay Austin for sharing his National Science Foundation (NSF)- funded cruised opportunities in June and October 2009. This great opportunity was very important for getting our preliminary data. Robert Sterner is also acknowledged for recovering some sediment cores for preliminary analyses. I am thankful to the captain Mike King and the crew of *R/V Blue Heron*, the captain and crew of *R/V Ndunduma*, and marine technician Jason Agnich, research associate Doug Ricketts for their help during fieldwork. They have made our work much easier. I am grateful to laboratory technician Sarah Grosshuesch who patiently helped me learn laboratory techniques and shared her expertise in instruments and experiments. I am also thankful to many other people at the LLO, Yvonne Chan, Kathy Oliver and many others, who have been always helpful and kind. I appreciate the help from Bogdana

Krivogorsky for preliminary IC data, Lauren Scott for carbon coulometry analyses, Sean Crowe (NordCEE, U of South Denmark) for methane analyses, Qiang Chen, Alfonso Mucci, and Bjorn Sundby (McGill University) for manganese and water isotope measurements, and Amy Kireta and Euan Revie (Natural Resources Research Institute, UMD) for providing some of the ^{210}Pb data. Sediment cores were split and logged at the LacCore repository, Limnological Research Center, UMN with the help of Anders Noren, Kristina Brady and others.

The work has been supported by the NSF OCE 0961720 grant, the University of Minnesota Office of International Programs (OIP) Strategic Project Grant, and the University of Minnesota Duluth start-up funds to Dr. Katsev. I am also very grateful for the support from Water Resources Science Program at UMN and the Physics Department at UMD through teaching and summer research assistantships, as well as travel funds for attending conferences.

My time in Duluth was very enjoyable in large part due to many friends and groups that became part of my life. I am grateful to all my friends, roommates, and many fellow students. I thank my friend Hongyu Li, Xiaowei Zhao, Xiuju Liu, Rozhan Zakaria and many others for their help and sharing the enjoyment. Their company means a lot to me. I am also grateful to have met Alberta Marana, Roger Mehling and their families, who not only volunteered as my English conversation teachers but also constantly helped me in many aspects of my life, helping me learn the culture, introducing fun activities, and providing advice in daily life. Being far from home these friends have made my life much easier, enjoyable and meaningful. The wonderful memories with them will be forever unforgettable.

At last I would like to thank my family, my dear parents and sister. They have been always supportive and encouraging in all my pursuits, providing unconditional love and care. With their love and support I can follow my heart and be proud of who I am.

ABSTRACT

Large freshwater lakes, despite their socioeconomic importance, are insufficiently characterized in terms of their geochemical cycling. In systems such as Lake Superior, contributions of several important processes, including those affecting biological productivity, remain poorly quantified. To understand the geochemical controls on sediment diagenesis, we investigated sediments in well-oxygenated temperate Lake Superior and tropical meromictic Lake Malawi. We characterized solid-sediment and porewater geochemistry, calculated diagenetic rates and fluxes, and investigated temporal and geographic variability for the cycles of carbon, nitrogen, phosphorus, iron, and sulfur. Revised nutrient budgets (for N and P) were constructed for both sediment and water column, suggesting a significant contribution of sediments to the geochemical cycling in both lakes. Sedimentation rate and the depth of oxygen penetration (OPD) were found to strongly affect the dynamics of carbon and nutrients. In Lake Superior, the deep (>4 cm) oxygenation of sediments in low-sedimentation areas regulates the remineralization rates of carbon and phosphorus, controls denitrification rates, and creates an unusual sulfur cycle driven by the oxidation of organic sulfur to sulfate. It also makes these deeply oxygenated sediments qualitatively distinct from sediments in nearshore high-sedimentation areas, necessitating their separate consideration in geochemical budgets. Comparisons against data from marine environments suggest that sediment processes in large lakes (both temperate and tropical) can be described by the same quantitative relationships as in marine sediments, facilitating the transfer of knowledge.

TABLE OF CONTENTS

LIST OF TABLE	vii
LIST OF FIGURES	ix
INTRODUCTION	1
Chapter 1 Carbon mineralization and oxygen dynamics in sediments in Lake Superior	7
SUMMARY	8
INTRODUCTION	9
METHODS	12
Sediment sampling and analyses	12
Oxygen fluxes and rates, carbon mineralization rates, carbon reactivity and bioturbation	16
RESULTS	21
Geographic variability in sediment properties	21
Sediment accumulation rates	23
Water column temperature and oxygen distributions	25
Oxygen penetration and uptake	28
Organic carbon content, reactivity and bioturbation rates	35
DISCUSSION	39
Spatial variability	39
Oxygen fluxes and consumption rates	40
Carbon fluxes and reactivity	42
Sediment contribution to lake-wide carbon budget	45
Controls on oxygen penetration and carbon mineralization efficiency	47
CONCLUSIONS	54
Chapter 2 Nitrogen cycling in sediments of Lake Superior and implications for marine coastal and deep ocean sediments	56
SUMMARY	57
INTRODUCTION	59
METHODS	62
Sediment sampling and analyses	62
Calculations of fluxes and rates	62
RESULTS	68
Nitrate in sediment porewaters	68
Ammonium in sediment porewaters	69
Dissolved Fe (II) in sediment porewaters	70
Nitrate and ammonium fluxes across the sediment-water interface	71
Nitrification rates	73
Nitrate reduction rates	74
N ₂ production rates	78
DISCUSSION	80

Nitrification.....	80
Nitrate reduction and N ₂ production.....	81
Nitrate reduction coupled to iron oxidation.....	83
Sediment contribution to the nitrogen budget in Lake Superior.....	83
Implications for marine sediments.....	91
CONCLUSIONS	98
Chapter 3 Phosphorus and iron cycling in Lake Superior sediments	100
SUMMARY	100
INTRODUCTION	102
METHODS	104
Sediment sampling and analyses	104
Calculations of fluxes	105
RESULTS	107
Porewater concentrations of Fe(II) and phosphorus	107
Soluble reactive phosphorus (SRP) fluxes across the sediment-water interface	109
Distributions and speciation of solid-phase iron, manganese, and phosphorus.....	111
DISCUSSION	114
Iron and manganese cycling.....	114
Interaction between the phosphorus and iron cycles	118
Controls on phosphorus fluxes across the sediment-water interface	121
Sediment contribution to the phosphorus budget of Lake Superior	124
CONCLUSIONS	127
Chapter 4 Sulfur cycling in Lake Superior sediments: controls on sulfate reduction and implications for low-carbon systems.....	129
SUMMARY	129
INTRODUCTION	131
METHODS	134
Sediment sampling and analyses	134
Calculations of fluxes and rates	134
RESULTS	137
Porewater concentrations of sulfate	137
Sulfate fluxes across the sediment-water interface.....	137
Sulfate production rates in surface sediments.....	140
Sulfate reduction rates in anoxic sediments.....	141
DISCUSSION	143
Sulfur cycling in high- vs. low-sedimentation areas.....	143
Sulfate production.....	145
Sulfate reduction	145
Lake Superior sediments as sinks for sulfur	148
CONCLUSIONS	150
Chapter 5 Sediment carbon and nutrient cycling in tropical meromictic Lake Malawi.....	152
SUMMARY	153

INTRODUCTION	154
METHODS	156
Sampling and analyses	156
Calculation of fluxes	160
RESULTS	161
Stratification and oxygen distributions	161
Sediment properties	162
Dissolved inorganic carbon in water and sediments	167
Ammonium concentrations in water and sediments	169
Nitrate concentrations in water and sediments	170
Sulfate concentrations in water column and sediments	171
Dissolved manganese, iron, and phosphorus	172
DISCUSSION	175
Geographic variability and non-steady state sedimentation	175
Carbon mineralization and preservation	176
Nitrogen cycling.....	181
Sulfur cycling.....	182
Sediment contributions to carbon and nutrient budgets in Lake Malawi	184
CONCLUSIONS	189
CONCLUSIONS	191
REFERENCES.....	195
APPENDICES	217
Appendix 1. Parameters used in calculations.	217
Appendix 2. Lake Superior sediment pH values	218
Appendix 3. Lake Superior sediment water content (WC) values.....	219
Appendix 4. Calculated porosity values for Lake Superior sediments.....	225
Appendix 5. Dissolved Fe(II) in piston and gravity cores at Sta. IR. 6, Lake Superior	231
Appendix 6. Distributions of HCl (0.5 N)- extractable iron, Lake Superior sediments	232
Appendix 7. Distributions of methane in Lake Superior sediments	233
Appendix 8. Distributions of $\delta^2\text{H}$ and $\delta^{18}\text{O}$ in piston and gravity cores at Sta. IR. 6, Lake Superior.....	234
Appendix 9. Results from sediment flow-through reactor experiments, Sta. ED, Lake Superior.....	235
Appendix 10. Distributions of $\delta^2\text{H}$ and $\delta^{18}\text{O}$ in Lake Malawi water column at Sta. CD.	238
Appendix 11. Data for other freshwater large lakes.	239

LIST OF TABLE

Table 1. 1 Sampling dates and locations in Lake Superior.....	15
Table 1. 2 Diffusive oxygen fluxes across sediment-water interface, total oxygen uptake, maximum carbon mineralization rates, organic carbon reactivity at SWI, and carbon mineralization time scale.	34
Table 2. 1 Major reactions affecting nitrogen cycling in sediments.....	64
Table 2. 2 The diffusive fluxes of nitrate ($F_{NO_3^-}$) and ammonium ($F_{NH_4^+}$) across SWI.....	72
Table 2. 3 The depth-integrated rates of nitrification ($R^*_{nitrif.}$), the fraction of the total oxygen uptake (TOU) consumed by nitrification ($R^*_{nitrif.}/TOU$), the integrated rates of nitrate consumption by denitrification and other pathways ($R^*_{NO_3^- \text{ cons.}}$), and the contribution of Fe oxidation ($R^*_{Fe^{2+}}$) to nitrate reduction.....	76
Table 2. 4 The rates of nitrogen removal to N_2 by denitrification and anammox.....	79
Table 2. 5 The nitrogen budget in Lake Superior.	86
Table 2. 6 The nitrate budget in Lake Superior.	87
Table 3. 1 Diffusive fluxes of soluble reactive phosphorus (F_{SRP}) across the SWI.	110
Table 3. 2 Depth-integrated rates of iron reduction ($R^*_{diss.Fe(II)}$, $R^*_{solid.Fe(II)}$, $R^*_{Fe \text{ total}}$), rates of phosphorus mobilization in the iron reduction zone ($R^*_{P \text{ rel. by Fe red}}$), and percentage of carbon mineralization by iron reduction ($R^*_{Fe \text{ total}} : R^*_C$).....	117
Table 3. 3 Sources and sinks of phosphorus in Lake Superior	126
Table 4. 1 The fluxes of sulfate across SWI, integrated rates of sulfate production ($R^*_{SO_4^{2-} \text{ prod.}}$), the ratio of sulfate production to carbon mineralization ($R^*_{SO_4^{2-} \text{ prod.}} : R^*_C$), integrated rates of sulfate reduction ($R^*_{SO_4^{2-} \text{ red.}}$), and percentage of carbon mineralization by sulfate reduction ($R^*_{SO_4^{2-} \text{ red.}} : R^*_C$).....	139
Table 5. 1 Sampling dates and locations in Lake Malawi	158

Table 5. 2 The infinite dilution molecular diffusion coefficients (D_i) and the tortuosity-corrected diffusion coefficients D_s	168
Table 5. 3 Fluxes of O_2 , NH_4^+ , DIC, NO_3^- , SO_4^{2-} and SRP at the sediment-water interface	168
Table 5. 4 Rates of organic carbon mineralization ($R^*_{C\ total}$), organic carbon burial ($F_{C\ burial}$), total organic carbon flux ($F_{C\ total}$), denitrification, and sulfate reduction	177
Table 5. 5 Total nitrogen budget for the Lake Malawi water column.	187
Table 5. 6 Total phosphorus budget for Lake Malawi.....	189

LIST OF FIGURES

Figure 1. 1 Sampling location in Lake Superior	14
Figure 1. 2 Optical images of Lake Superior sediment cores	22
Figure 1. 3 Unsupported ²¹⁰ Pb activity and the calculated sediment accumulation rates, apparent sediment ages, and burial velocities (vel.)	24
Figure 1. 4 Vertical temperature variations in water column of Lake Superior	26
Figure 1. 5 Vertical distributions of dissolved oxygen in water column of Lake Superior	27
Figure 1. 6 Vertical distributions of dissolved oxygen in sediments of Lake Superior....	30
Figure 1. 7 Calculated oxygen diffusive fluxes in sediments of Lake Superior	31
Figure 1. 8 Calculated oxygen consumption rates in sediments of Lake Superior.....	32
Figure 1. 9 (A) Seasonality in bottom-water oxygen concentrations determined from conductivity-temperature-depth data; (B) maximum sediment oxygen fluxes (F_{O_2}), and (C) maximum oxygen consumption rates (R_{O_2}).	33
Figure 1. 10 Organic carbon (OC) content and porosity.	36
Figure 1. 11 Organic carbon reactivity k	37
Figure 1. 12 Calculated bioturbation coefficients D_b and the burial fluxes of organic carbon that are due to bioturbation, F_b	38
Figure 1. 13 Calculated reactivity of organic carbon in Lake Superior sediments as a function of the apparent sediment age.	45
Figure 1. 14 (A) Total oxygen uptake rates and diffusive oxygen fluxes across SWI, and (B) Oxygen penetration depth (OPD) as functions of water depth.....	49
Figure 1. 15 (A) Oxygen fluxes across SWI, (B) carbon burial efficiency, (C) OPD as functions of sedimentation rate.	50
Figure 2. 1 Vertical distributions of porewater nitrate in Lake Superior sediments.	69
Figure 2.2 Vertical distributions of porewater ammonium in Lake Superior sediments..	70
Figure 2. 3 Typical profiles of dissolved Fe(II) in sediments of Lake Superior.....	71
Figure 2. 4 Calculated rates of sediment nitrification.....	75

Figure 2. 5 (A) Typical distributions of dissolved Fe^{2+} , O_2 , and NO_3^- ; (B) the corresponding nitrate fluxes, $F_{\text{NO}_3^-}$; (C) the corresponding nitrate consumption rates $R_{\text{NO}_3^-}$	78
Figure 2. 6 Nitrogen cycling in Lake Superior sediments: (A) in low-sedimentation areas with deep oxygen penetration; (B) in high-sedimentation areas with shallow oxygen penetrations.....	88
Figure 2. 7 (A, B) Fluxes of nitrate and ammonium across the SWI, (C) sediment denitrification rates, and (D) percent of deposited organic carbon mineralized by denitrification, organized by water depth.....	93
Figure 2. 8 (A) The rates of reactive nitrogen removal vs. oxygen penetration; (B) Denitrification rates vs. water depth.....	94
Figure 2. 9 Denitrification rates vs. sediment oxygen uptake.....	96
Figure 2. 10 The effect of oxygen penetration on denitrification rates.....	97
Figure 3. 1 Dissolved Fe(II) and soluble reactive phosphorus (SRP) concentrations in porewaters of Lake Superior sediments.....	108
Figure 3. 2 Scanning XRF counts for Fe, Mn, and Ti in sediments of Lake Superior..	112
Figure 3. 3 Solid phase iron and phosphorus in sediments at Sta. FWM.....	113
Figure 3. 4 Net rates of production of phosphate and dissolved Fe(II).....	119
Figure 3. 5 Depth-integrated rates of net phosphorus vs. iron remobilization in anoxic sediments.....	121
Figure 3. 6 SRP flux across the sediment-water interface as a function of total oxygen uptake.....	123
Figure 4. 1 Vertical distributions of porewater sulfate in Lake Superior sediments.....	138
Figure 4. 2 Calculated rates of sulfate production in sediments of Lake Superior.....	141
Figure 4. 3 Calculated rates of sulfate reduction in sediments of Lake Superior..	142
Figure 4. 4 (A) Typical distributions of O_2 , NO_3^- , dissolved Fe^{2+} and SO_4^{2-} ; (B) the corresponding sulfate fluxes, $F_{\text{SO}_4^{2-}}$; (C) the corresponding rates $R_{\text{SO}_4^{2-}}$	144
Figure 4. 5 Sediment sulfate reduction rates vs. sedimentation rates.....	147

Figure 4. 6 The rates of sediment sulfate reduction vs. oxygen and nitrate penetration.	148
Figure 5. 1 Sampling locations in Lake Malawi.	159
Figure 5. 2 A) Vertical distributions of temperature and dissolved oxygen in the water column of Lake Malawi. B) Deep water (> 300 m) temperature in Lake Malawi.	162
Figure 5. 3 Optical images and x-ray fluorescence scanning of total iron, manganese and titanium in Lake Malawi sediment cores.	164
Figure 5. 4 Unsupported ^{210}Pb activity, sediment accumulation rates, sediment ages, and burial velocities.	165
Figure 5. 5 Organic carbon content in Lake Malawi sediments	166
Figure 5. 6 Porosity and density (dry bulk density ($\rho_{\text{dry bulk}}$; g dry sediment per cm^3 wet sediment) or bulk density ($\rho_{\text{bulk sed.}}$; g wet sediment per cm^3 wet sediment) in Lake Malawi sediments	166
Figure 5. 7 Dissolved inorganic carbon (DIC) concentrations in water column and sediment porewaters.	167
Figure 5. 8 Ammonium concentrations in water column and sediments.	169
Figure 5. 9 Nitrate concentrations in water column and sediments.	171
Figure 5. 10 Sulfate concentrations in water column and sediments.	172
Figure 5. 11 Vertical distribution of phosphorus in the water column of Lake Malawi.	174
Figure 5. 12 Dissolved iron (II) and soluble reactive phosphorus (SRP) concentrations in sediments.	174
Figure 5. 13 Organic carbon degradation rates as a function of water depth.	178
Figure 5. 14 Organic carbon burial efficiency in Lake Malawi sediments in comparison to those in marine environments and other large lakes:	180
Figure 5. 15 Carbon export efficiency as a function of water depth.	186

INTRODUCTION

Geochemical processes in aquatic sediments are crucial for understanding the functioning of water bodies. By transforming and recycling chemical substances, including elements essential for life (carbon, nitrogen, phosphorus, sulfur, and iron), sediments regulate the ecologies of the overlying water columns. On spatial scales from local to global, sedimentary recycling or sequestration of substances affects the geochemical budgets, cycling, and nutrient availability to primary producers. Over geological time scales, sediment mineralization and burial of organic carbon determine the CO₂ and oxygen levels in the atmosphere. Understanding the geochemical controls of these processes is critical for understanding the systems' functioning as well as their responses to climate change and anthropogenic perturbations.

In contrast to marine environments, where multiple studies over the past decades have resulted in significant advances in both conceptual and quantitative understanding of sediment early diagenesis (Burdige 2007; Middelburg et al. 1996; Laursen et al. 2002; Fennel et al. 2009), sediments in large freshwater lakes are relatively understudied. Many questions remain about their rates and pathways of carbon mineralization, efficiencies of carbon preservation, and rates of nutrient transformations, removal, and recycling. Large lakes are at a particular disadvantage, as results obtained in small lakes generally cannot be transferred to these freshwater seas where sources of organic matter are predominantly autochthonous, sedimentation rates are low, and physical circulation is marine-like. As sediment processes are controlled by multiple environmental factors and mediated by resident macro- and microorganism populations that are often environment-specific, a

question arises as to how much of the information obtained in marine systems can be transferred to large freshwater lakes. Conversely, as lakes are generally more accessible than oceans, how much of the knowledge obtained in lakes can be used for extrapolating to the ocean? Direct comparison is complicated by a number of obvious differences, including in the rates of water column mixing, activities of sediment macrofauna, water chemistry (salinity, buffering capacity, and not the least the concentration of sulfate), and sediment composition. A related question concerns the applicability of results from high-sedimentation coastal marine sediments (where studies have been most plentiful) to environments such as oligotrophic Lake Superior where sediments are deeply oxygenated (Carleton et al. 1989). In the Ocean, deeply oxygenated sediments are found on the continental slope and abyssal plains and are investigated to a much lesser degree. These organic-poor sediments underlie vast areas of the Earth's ocean and account for a major fraction of global carbon and nutrient exchanges with the water column (Glud 2008). Their geochemical regimes are sensitive to the water column supplies of organic carbon and oxygen (Gobeil et al. 2001; Katsev et al. 2006). In comparison to temperate large lakes, tropical large lakes have received even less attention, despite their socioeconomic importance. Lakes such as Lake Malawi, offer a contrasting geochemical environment with a warm water column and bottom waters devoid of oxygen. Sediments are characterized by anaerobic organic carbon remineralization, similar to anoxic marine basins. No rigorous comparisons for these processes have yet been made.

Lake Superior, the world's largest lake by surface area, is poorly studied in terms of its sediment processes, with sparse geographical coverage and little information

available on the rates of critical diagenetic pathways such as denitrification, iron reduction, sulfate reduction, and phosphorus regeneration. Important elemental fluxes (e.g., of nitrate, ammonium, phosphate, and sulfate) across the sediment water interface have been only scantily quantified (Li 2011; Zigah et al. 2012; Li et al. 2013). Without this information, the geochemical budgets (e.g., of C, N, P) remain poorly constrained (Cotner et al. 2004; Sterner et al. 2007; Dolan and Chapra 2012), as are the sediment contributions to whole-lake geochemical cycling and ecosystem functioning. Lake Superior has been experiencing changes in its water column chemistry over the past several decades. Most notably, nitrate and sulfate concentrations continued to increase while the primary productivity remained low (Munawar and Munawar 1978; Sterner 2010). The primary productivity is thought to be limited primarily by the low and slightly declining concentrations of phosphorus in the water column (Sterner et al. 2004; Sterner et al. 2007). These changes have been suggested to result from changes in the internal geochemical cycling in the lake, and were tentatively linked to the dynamics of sediment processes (Finlay et al. 2007; McDonald et al. 2010; Small et al. 2013). Quantitative estimates for the essential process rates and fluxes, however, have been largely unavailable.

Lake Malawi, the ninth largest lake in the world, situated in the East African Rift system, is a hotspot of biodiversity and the site of one of the most productive fisheries in Africa that provide protein to local populations (Boostma and Hecky 2003). It is under considerable stress from both climate warming and anthropogenic changes in its watershed (Boostma and Hecky 2003; Hecky et al. 2003; Otu et al. 2011). Whereas

significant changes occurred recently in the lake's catchment (increased agriculture activity, loss of forest cover, increased nutrient loadings; Hecky et al. 2003), little information has been available for the lake-wide geochemical cycling since the mid-1990s, when Boostma and Hecky (1999) estimated the cycles of carbon and nutrients (N, P, Si). In these earlier studies, the sediment recycling of carbon and nutrients, their fluxes across the sediment-water interface and the removal processes (i.e., with the long-term burial or gas emissions) were not included, despite their potential importance.

To address these questions, this work characterizes sediment geochemistry in two very different large freshwater lakes: temperate well-mixed well-oxygenated Lake Superior and tropical meromictic anoxic Lake Malawi. Investigations based on multi-year, multi-season field surveys and subsequent laboratory and data analyses cover a large range of diagenetic regimes (well- oxygenated vs. anoxic, low vs. high sedimentation, coastal vs. pelagic). The work characterizes solid sediment and porewater compositions, quantifies the rates of individual diagenetic pathways (of carbon, nitrogen, iron, phosphorus, and sulfur) and elemental fluxes, and investigates their temporal (seasonal to decadal) dynamics and spatial heterogeneity. The geochemical budgets (of C, N, and P) are constructed or updated. Using a compilation of data from this study, as well as literature information for other freshwater lakes and marine environments, sediment diagenetic cycles are compared between freshwater large lakes and marine systems, and between temperate and tropical environments. Quantitative relationships, as well as new metrics, are established that link sediment biogeochemical rates and fluxes to environmental variables.

The obtained information should improve our understanding of the sediments' contribution to geochemical cycling in freshwater large lakes. It offers plausible explanations for the changes that occurred in the water column of Lake Superior and documents the geochemical dynamics in Lake Malawi. Established cross-system and cross-variable relationships reveal fundamental mechanisms that regulate the dynamics of sediment diagenetic processes and control geochemical fluxes. Findings presented in this thesis should allow a better understanding of the sensitivities of sediment processes to environmental variations. They also suggest implications for the diagenetic biogeochemical cycling in other systems, such as in the deep ocean, reveal several unusual and previously overlooked pathways, and may help in the interpretations of sediment records of past environmental changes.

The thesis is divided into five Chapters. Chapters 1-4 present our studies in Lake Superior, with each chapter focusing on the geochemical cycling of individual elements: Chapter 1 describes the cycling of carbon and oxygen, Chapter 2 deals with the nitrogen cycle, Chapter 3 details the interactions of iron and phosphorus, and Chapter 4 describes the sulfur cycle. Chapter 5 presents studies in Lake Malawi. Each chapter is structured independently, including the Abstract, Introduction, Methods, Results, and Discussion sections, followed by a Conclusion section that summarizes the main findings. Details of methodology are not restated in later chapters if described in previous chapters. Data compilations may include results from multiple chapters for the purpose of comparison and discussion. Additional data that are less relevant to the presented geochemical stories

are presented in the Appendix but not discussed in detail, to preserve the focus of the individual chapters on the central theme of the Thesis.

Chapter 1 Carbon mineralization and oxygen dynamics in sediments in Lake Superior

Most of the results in this Chapter have been published in Li et al. (2012): Limnology and Oceanography 57(6), 2012: 1634- 1650

Title: Carbon mineralization and oxygen dynamics in sediments with deep oxygen penetration, Lake Superior

Authors: ¹ Jiying Li, ² Sean A. Crowe, ³ David Miklesh, ^{1,3} Matthew Kistner, ² Donald E. Canfield, and ^{1,3} Sergei Katsev

¹ Large Lakes Observatory, University of Minnesota Duluth

² Nordic Center for Earth Evolution, University of Southern Denmark

³ Department of Physics, University of Minnesota Duluth

Copyright 2014 by the Association for the Sciences of Limnology and Oceanography, Inc.

In addition to the published results, this Chapter presents the data from nearshore and high-sedimentation areas that were sampled after the publication.

SUMMARY

To understand carbon and oxygen dynamics in sediments in Lake Superior, we investigated 13 locations (26-318 m depth) throughout the lake. Strong spatial variability in oxygen penetration depth (OPD) was observed (0.5 to >12 cm), corresponding to differences in sedimentation rates (0.01-0.18 g cm⁻² yr⁻¹). OPDs in offshore low sedimentation areas are deep (>3.5 cm), similar to marine sediment > 3000-m water column. Such deep penetration is explained by low sediment burial rates (0.01-0.04 cm yr⁻¹), high solubility of oxygen in cold freshwater, and a shallow (~2 cm) bioturbation zone. In response mainly to oxygen variations in the bottom waters, sediment oxygen penetration varied seasonally by as much as several cm, suggesting that temporal variability in deeply oxygenated sediments may be greater than previously acknowledged. Oxygen uptake rates (3.3- 11 mmol m⁻² d⁻¹, average 6.1 mmol m⁻² d⁻¹) and carbon mineralization efficiency (~88% of deposited carbon) were similar to those in marine hemipelagic and pelagic sediments of comparable sedimentation rates. Reactivity of organic carbon was found to decrease with age similarly to the power-law documented in marine environments. The burial flux of carbon into the deep sediment (0.73 mmol m⁻² d⁻¹) was 2.7% of the previously estimated primary production. Maximum volume-specific carbon degradation rates were 0.3 to 3.0 μmol cm⁻³ d⁻¹; bioturbation coefficient near the sediment surface was 3-8 cm² yr⁻¹. These results indicate that carbon cycling in large freshwater systems conforms to many of the same trends as in marine systems.

INTRODUCTION

Sediments of lakes and reservoirs accumulate organic carbon at a higher global annual rate than the ocean seafloor (Tranvik et al. 2009), yet their sediments remain understudied in terms of C burial, sequestration, and early diagenetic C remineralization (Cole et al. 2007; Gudasz et al. 2010). In comparison to marine environments, there is relatively little information on the rates and pathways of C degradation in lake sediments (Thomsen et al. 2004). In previous studies, carbon mineralization rates were shown to correlate with temperature (Gudasz et al. 2010) and oxygen exposure time (Sobek et al. 2009), but there have been few rigorous examinations of the relationships between C reactivity, burial efficiency, water depth, sedimentation rate, temperature, and electron acceptor availability (den Heyer and Kalff 1998; Sobek et al. 2009). Direct comparisons of freshwater environments with marine systems are complicated by a number of obvious differences in water column mixing rates and chemistry, notably the limited supply of sulfate in lakes, which through microbial sulfate reduction contributes to nearly 50% of the total carbon mineralization in marine sediments (Jørgensen 1982). Another principal difference is a lower biogeochemical reactivity of the terrigenous organic material that is brought into the lakes from the catchment and makes up a significant portion of the organic carbon pool in small and medium-size lakes (Sobek et al. 2009). The largest lakes of the world, where organic matter is predominantly autochthonous, therefore, provide the best comparisons to marine systems (Johnson et al. 1982). In this study, we investigate the carbon mineralization processes in the sediments of Lake Superior, the world's largest freshwater lake by area, where terrigenous carbon inputs to the open lake do not exceed 17% of the total carbon budget (Zigah et al. 2011).

With its great depth, cold water, and low shoreline population density, Lake Superior has the lowest primary productivity of the Laurentian Great Lakes (Munawar and Munawar 1978). Its sediments accumulate slowly ($<1 \text{ mm yr}^{-1}$) and have organic matter content below 5% (Johnson et al. 1982). The sediments are characterized by deep ($>4 \text{ cm}$) penetration of oxygen (Carlton et al. 1989), and thus oxygen is likely the dominant electron acceptor for organic carbon oxidation. Modeling studies (Katsev et al. 2006) have demonstrated that, in sediments with deep oxygen penetration, the oxygen penetration depth (OPD) may be sensitive to variations in the sedimentation flux of organic carbon and oxygen concentration in the water column. Changes in the depth of oxygen penetration indicate shifts in the mineralization pathways of organic matter and likely coincide with strong modifications of sediment composition and rates of sediment-water material exchange. Seasonal shifts in sediment OPD by several cm or more have been observed in organic-poor deep-ocean environments (Sayles 1994; Gehlen et al. 1997), and have been postulated in others, such as the deep Arctic Ocean (Gobeil et al. 2001). By sampling Lake Superior sediments at multiple locations and in multiple seasons, we aim to constrain seasonal and geographical variability in oxygen dynamics.

The budget of organic carbon in Lake Superior remains poorly constrained and the putative long-term variation in primary productivity is poorly documented (Sterner 2010). Primary production, estimated at 9.7 Tg yr^{-1} (Sterner 2010), supplies most of the organic carbon to the water column (Ostrom et al. 1998), whereas riverine and atmospheric inputs account, respectively, for $\sim 6\%$ and 9% of the total organic carbon input to the lake (Cotner et al. 2004). Losses of organic carbon are primarily through water column respiration, estimates of which ranged between 13 and 39 Tg yr^{-1} based on

measurements in offshore locations (Cotner et al. 2004), making the carbon budget appear unbalanced, as losses exceed carbon inputs (Sterner 2010). The flux of organic carbon to sediments was estimated using sediment traps at 0.83 Tg yr^{-1} (Heinen and McManus 2004). The uncertainty in these estimates with respect to the total carbon budgets of the lake is large, mostly due to a geographical sampling bias, as most measurements have been made in the western arm of the lake (McManus et al. 2003), where the primary production and terrestrial carbon inputs are thought to be higher. Data for the winter season are scant but suggest that winter production is not a negligible part of the annual carbon budget (Sterner 2010). Given the uncertainties and the inherent variability and patchiness in the water column measurements, sediment carbon degradation rates may provide a more robust estimate for the lake-average carbon sedimentation flux. Sediment studies also allow the determination of the efficiency of carbon retention in the sediment. Here, we use the sediment distributions of organic carbon and the rates of oxygen consumption to characterize the sediment carbon cycle in Lake Superior, to constrain its contributions to the lake-wide carbon budget, and to compare the characteristics of this large freshwater system to relationships established for marine sediments.

METHODS

Sediment sampling and analyses

Sediment and water column samples were taken on several cruises aboard the R/V *Blue Heron* (Table 1.1 and Fig. 1.1). Temperature and dissolved oxygen distributions in the water column were measured using a Seabird 911 plus conductivity, temperature, depth (CTD) probe with an Oxyguard flow-through oxygen sensor. The O₂ sensor was calibrated during regular probe maintenance but the calibration was not always verified prior to each cruise, hence the absolute values for oxygen in the Lake Superior water column may not be accurate for all cruises. Sediment cores of 94 mm inner diameter (i.d.) were recovered using an Ocean Instruments multi-corer. The landing sites were monitored using a Knudsen 320/R echo sounder with a 28 kHz transducer to select flat areas with laterally homogeneous sediment accumulation. The cores were subsequently stored at 4°C, which corresponds to the temperature (3 – 5°C) of Lake Superior bottom waters from May to November (*see* data below). Vertical distributions of dissolved oxygen in sediment porewaters were determined on-board in sub-sampled cores that were thermostated and allowed to equilibrate for about 40 minutes. Oxygen concentrations were measured using a Unisense (Clark-type) microelectrode (Revsbech 1989). The electrodes were calibrated at O₂ saturation in water at the in situ temperature (~4°C), and a buffered sodium ascorbate solution was used as a zero. On one cruise (October 2009), the electrodes were calibrated at 0% in water that was bubbled with nitrogen. Possible stagnation of the diffusive boundary layer during profiling is not expected to have significantly affected the oxygen gradients inside the sediment, as oxygen consumption

was slow: profile shapes changed insignificantly over several hours. Rates of total oxygen uptake were measured during the June 2009 (in cores from Sta. FWM.1, WM.1, EM.1, and Sta. 2; Table 1.1) and September 2010 (Sta. FWM.5 and Sta. IR.3) cruises in 2-4 undisturbed intact sediment cores per each sampled site. To maximize the sensitivity of the measurements, these cores were collected with only 10-15 cm of overlying water. The cores were maintained at 4°C in the dark and the overlying water was stirred at 60 revolutions per minute (rpm) using a magnetic stir bar suspended 3-4 cm above the sediment water interface. Oxygen concentrations were measured using Clark-type microelectrodes (Unisense) that were sealed into the tops of the core tubes with thick rubber stoppers. Oxygen concentrations decreased less than 10% from their in situ values and the measured decrease was linear throughout the incubation period.

Separate sediment cores were sectioned on-board under a N₂ atmosphere at vertical intervals varying from 0.5 cm at the sediment surface to 5 cm below 20 cm. The organic carbon content was determined in freeze-dried sediment samples by coulometry on a CM150 total carbon (TC), total organic carbon (TOC), total inorganic carbon (TIC) analyzer. Sediment water contents were determined by comparing the sediment sample weights before and after freeze-drying. Porosity was calculated as $\varphi = (M_w/\rho_{H_2O})/[(M_d/\rho) + (M_w/\rho_{H_2O})]$, where M_w and M_d are, respectively, the weights of interstitial water and dry sediment, ρ_{H_2O} is the density of water (1.00 g cm⁻³), and ρ is the density of dry sediment (2.65 g cm⁻³) (Johnson et al. 1982) (also *see* appendix for a list of parameters used in this Thesis). Separate intact sediment cores were split, photographed, and analyzed on a Geotek multisensor core logger at the LacCore facility of the University of Minnesota. Sediment dating using ²¹⁰Pb was performed by the Flett Research Laboratory at the

University of Manitoba on cores from Sta. EM and Sta. CM and by St. Croix laboratory of the Science Museum of Minnesota on cores from Sta. IR and Sta. FWM. The sediment age and accumulation rates ($\text{g cm}^{-2} \text{yr}^{-1}$) were determined by the analyzing laboratories using a constant rate of supply (CRS) model (Appleby and Oldfield 1978) and measured dry mass per volume of wet sediment. Burial velocities U (cm yr^{-1}) were calculated from the obtained age-vs-depth relationships as a function of depth x as

$$U = \frac{dx}{dt} \quad (1.1)$$

Whereas the CRS model likely overestimates the sedimentation rates within the bioturbation zone, in Lake Superior only the upper 2 cm of sediment are bioturbated (*see below*).

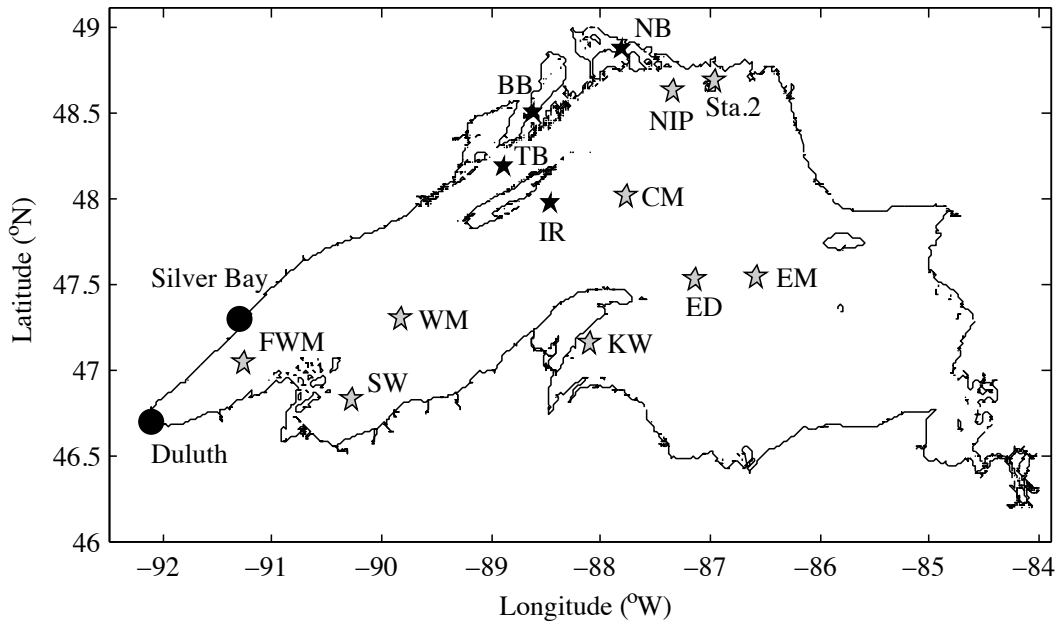


Figure 1. 1 Sampling location in Lake Superior. Distances between substations are smaller than the size of symbols (Table. 1.1). The dark symbols indicate stations with shallow oxygen penetration (termed “nearshore”; *see Results*); gray symbols indicate “offshore” stations.

Table 1. 1 Sampling dates and locations. The stations with shallow oxygen penetration (termed ‘nearshore’) are indicated by ‘†’.

Date	Station	Depth (m)	Latitude (N)	Longitude (W)
03 Jun 2009	FWM.1	170	47° 02.90′	91° 14.97′
10 Nov 2009	FWM.2	160	47° 06.26′	91° 43.19′
07 Jun 2010	FWM.3	166	47° 09.13′	91° 16.44′
20 Jul 2010	FWM.4	168	47° 02.14′	91° 16.38′
21 Sep 2010	FWM.5	166	47° 01.98′	91° 16.50′
21 Apr 2011	FWM.6	166	47° 02.15′	91° 16.31′
22 Aug 2011	FWM.7	166	47° 02.21′	91° 16.32′
05 Jun 2009	EM.1	218	47° 32.54′	86° 34.31′
06 Oct 2009	EM.2	225	47° 32.52′	86° 34.31′
10 Jun 2010	EM.3	229	47° 33.38′	86° 35.76′
22 Jul 2010	EM.4	228	47° 33.36′	86° 35.65′
22 Sep 2010	EM.5	226	47° 33.37′	86° 35.68′
26 Jul 2012	EM.6	232	47° 32.26′	86° 35.79′
04 Jun 2009	WM.1	175	47° 18.32′	89° 49.43′
04 Oct 2009	WM.2	170	47° 18.29′	89° 49.73′
11 Jun 2010	WM.3	169	47° 19.01′	89° 50.73′
22 Jul 2010	WM.4	174	47° 18.26′	89° 49.33′
25 Sep 2010	WM.5	169	47° 19.05′	89° 50.76′
23 Apr 2011	WM.6	171	47° 19.01′	89° 50.80′
08 Jun 2010	†IR.1	234	47° 58.41′	88° 28.01′
21 Jul 2010	†IR.2	237	47° 58.42′	88° 28.07′
22 Sep 2010	†IR.3	235	47° 58.41′	88° 28.08′
21 Apr 2011	†IR.4	235	47° 58.40′	88° 27.97′
25 Aug 2011	†IR.5	235	47° 58.38′	88° 28.09′
27 Jul 2012	†IR.6	235	47° 58.44′	88° 28.05′
08 Jun 2010	CM.1	252	48° 01.06′	87° 46.44′
21 Jul 2010	CM.2	236	48° 02.84′	87° 47.32′
22 Sep 2010	CM.3	235	48° 02.66′	87° 47.17′
22 Apr 2011	CM.4	239	48° 03.04′	87° 47.74′
21 Jul 2010	ED.1	316	47° 31.81′	87° 07.81′
22 Sep 2010	ED.2	318	47° 31.53′	87° 07.49′
22 Apr 2011	ED.3	312	47° 31.76′	87° 07.65′
09 Jun 2010	KW.1	84	47° 09.85′	88° 05.32′
04 Jun 2009	Sta. 2	100	48° 41.00′	86° 57.20′
22 Aug 2011	SW.1	117	46° 50.28′	90° 16.00′
24 Jul 2012	SW.2	120	46° 50.49′	90° 16.33′
25 Jul 2012	†BB.1	26	48° 30.06′	88° 36.48′
25 Jul 2012	†NB.1	29	48° 52.46′	88° 11.77′
26 Jul 2012	NIP.1	124	48° 36.62′	87° 20.52′
25 Jul 2012	†TB.1	237	48° 11.29′	88° 53.04′

Oxygen fluxes and rates, carbon mineralization rates, carbon reactivity and bioturbation

The diagenesis of solutes and solid phases can be described with a set of diagenetic equations (Berner 1980). If x is the depth below the sediment-water interface and $C_i(x,t)$ is the concentration of a chemical species i in solid phase (in mol per dry weight) or porewater (in mol per porewater volume), then for solutes (Katsev et al. 2007):

$$\frac{\partial \varphi C_i}{\partial t} = \frac{\partial}{\partial x} \left(\varphi D_i \frac{\partial C_i}{\partial x} \right) - \frac{\partial}{\partial x} (\varphi U C_i) + \varphi \alpha_{\text{irr}} (C_i^0 - C_i^{\text{burr}}) + \sum_j R_{ij} \quad (1.2)$$

and for solid phases:

$$\frac{\partial \xi C_i}{\partial t} = \frac{\partial}{\partial x} \left(\xi D_b \frac{\partial C_i}{\partial x} \right) - \frac{\partial}{\partial x} (\xi U C_i) + \sum_j R_{ij} \quad (1.3)$$

Here, D_i is the effective diffusion coefficient, U is the advection (burial) velocity, R_{ij} are the rates (mol per volume of bulk sediment) of all reactions that affect the species i , φ is the porosity, and the factor ξ is equal to $(1-\varphi)\rho$, where ρ is the density of dry sediment. The coefficient α_{irr} describes bioirrigation, which is a fauna-mediated, non-local (non-diffusive) exchange of fluids between the sediment surface (concentration C_i^0) and bioirrigated burrows (C_i^{burr}). The diffusion of solid particles is due to bioturbation (Berner 1980; Meysman et al. 2005), described by the bioturbation coefficient D_b . When temporal changes in the sediment are slow, so that the species distributions approach a dynamic equilibrium, a quasi-steady state can be described by setting the left-hand-side of these equations to zero.

For oxygen in non-permeable sediments, diffusion typically dominates over advection, so the advection term in Eq. 2 can be neglected. The bioirrigation term is an important component of oxygen fluxes in marine sediments, although in some freshwater

sediments it may be insignificant (Sweerts et al. 1991). Given the lack of data on bioirrigation in Lake Superior, the calculation of oxygen fluxes are not included, with a caveat that the actual oxygen fluxes may be higher than calculated. To estimate the maximum potential contribution from bioirrigation, the calculated diffusive oxygen fluxes are compared with the total oxygen uptakes determined in core incubations. The diffusive fluxes of oxygen, F_{O_2} ($\text{mol m}^{-2} \text{d}^{-1}$), within the sediment can be calculated using the Fick's law of diffusion:

$$F_{O_2} = -\varphi(D_s + D_{\text{enh}}) \frac{d[O_2]}{dx} \quad (1.4)$$

Here, the diffusion coefficient $D_s = D/\theta^2$ is the molecular diffusion coefficient of oxygen $D = 421 \text{ cm}^2 \text{ yr}^{-1}$ (at $T = 4^\circ\text{C}$; Boudreau 1997) corrected for sediment porosity φ using the tortuosity factor $\theta^2 = 1 - \ln(\varphi^2)$ (Boudreau 1997). The diffusion-like transport of oxygen by benthic fauna is characterized by the enhanced diffusion coefficient D_{enh} (Meile and Van Cappellen 2003). As the magnitude and depth dependence of D_{enh} are not known a priori, we adopt the same approach as for the non-local bioirrigation coefficient α_{irr} : we disregard it in the calculations but estimate its contribution later by comparing the calculated diffusive fluxes with the fluxes measured in incubations. Using Eq. 1.4, the diffusive fluxes of oxygen within the sediment were therefore calculated from high-resolution oxygen microelectrode profiles and sediment porosity (Sauter et al. 2001) as

$$F_{O_2} \approx -\varphi D_s \frac{d[O_2]}{dx} \quad (1.5)$$

To estimate the transport of particulate organic carbon by bioturbation, we use Eq. 3, building on the approach of Canfield et al. (1993) and Thomsen et al. (2004). For organic carbon, the (negative) reaction term ΣR_j represents the total rate of organic

carbon mineralization, R_C . At a quasi-steady state, the partial derivatives with respect to x in Eq. 1.3 can be replaced by ordinary derivatives. By integrating Eq. 1.3 from some depth L within the sediment to x , we obtain:

$$\xi_x D_b \left(\frac{dC}{dx} \right)_x - (\xi_x U_x C_x - \xi_L U_L C_L) - \int_L^x R_C(x') dx' = 0 \quad (1.6)$$

Here, we choose L sufficiently deep into the sediment so that $D_b(x=L)=0$. We also use the minus sign in front of the reaction term R_C to indicate explicitly that it results in consumption of organic carbon. The integral in Eq. 1.6 represents the total rate of organic carbon mineralization below the depth x . As oxygen is used to oxidize both organic carbon and products of anaerobic metabolisms (*see* below), within the oxic zone this integral can be approximated by the downward flux of oxygen at depth x . By substituting the expression for F_{O_2} from Eq. 1.5 into Eq. 1.6, we obtain the bioturbation coefficient within the oxic zone as

$$D_b = \frac{(\xi_x U_x C_x - \xi_L U_L C_L) - \varphi D_s \left(\frac{d[O_2]}{dx} \right)_x}{\xi_x \left(\frac{dC}{dx} \right)_x} \quad (1.7)$$

For the calculations in this paper, the sediment accumulation rate $\xi_L U_L$ and the organic carbon concentration C_L were evaluated at the bottom of sediment cores. The oxygen gradients were taken from the measured microprofiles, and the organic carbon concentrations and gradients were taken from the profiles determined by coulometry. As actual oxygen fluxes may be higher than molecular diffusion fluxes because of the bioirrigation and fauna-enhanced diffusion, the actual values of D_b may be correspondingly higher than calculated. Where sediment accumulation rate ($\text{g cm}^{-2} \text{ yr}^{-1}$)

can be considered approximately steady, a further simplification of Eq. 1.7 is possible, as $\xi_x U_x = \xi_L U_L$ (Meysman et al. 2005; Katsev et al. 2007).

The oxygen consumption rates per volume of sediment, R_{O_2} , were calculated assuming that the oxygen distributions were close to being in steady state, in which case oxygen consumption accounts for all changes in the vertical oxygen fluxes:

$$\frac{\partial \varphi[O_2]}{\partial t} = -\frac{\partial F_{O_2}}{\partial x} + R_{O_2} = 0 \quad (1.8)$$

Accordingly, the rates R_{O_2} ($\text{mol m}^{-3} \text{ d}^{-1}$) (per volume of bulk sediment) were calculated by taking a derivative of the oxygen flux profile (Sauter et al. 2001):

$$R_{O_2} = -\frac{\partial F_{O_2}}{\partial x} \quad (1.9)$$

These profiles were smoothed by taking sliding averages with a typical window size of 1-4 mm. Again, within the bioturbation zone, the actual oxygen consumption rates may be higher than calculated due to the benthic fauna contribution to oxygen fluxes.

Carbon degradation rates in the oxic layers can be estimated as $R_C = 6/7 R_{O_2}$ (based on the C: N ratio of 12:1 in Lake Superior sediment, and 1N: 2O₂ and 1C: 1O₂ stoichiometry of ammonium oxidation and carbon mineralization; Heinen and McManus 2004; Sterner et al. 2008), as oxygen is consumed through both aerobic respiration and oxidation of the reduced products of anaerobic metabolisms. An exception is the organic matter degraded through denitrification, as the N₂ produced is inert and not reoxidized within the sediment. Denitrification, however, is typically only a few percent of the total organic matter degradation (Canfield et al. 1993; Thomsen et al. 2004;). In Lake Superior, its contribution was previously estimated to be less than 5% (*see* Chapter 2). For carbon degradation rates limited by carbon availability (rather than by the availability

of oxidants), the mineralization rate can be written as $R_C = k\xi C$, where C is the molar concentration (mol g^{-1}) of organic carbon. The first order rate parameter k (yr^{-1}) is the effective reactivity of organic matter. As sediment organic matter consists of a large number of fractions that degrade at different rates, the effective reactivity decreases with sediment depth, as organic material ages and becomes depleted in labile fractions. Using the oxygen consumption rates, R_{O_2} (Eq. 1.9), as an approximation for the carbon degradation rates (R_C), we calculate the organic carbon reactivity (k), within the oxic zone as

$$k = \frac{R_C}{\xi C} \quad (1.10)$$

The characteristic half-life of organic C in the sediment is calculated as $\tau = \ln(2) / k$ (Table 2).

RESULTS

Geographic variability in sediment properties

Sediments in Lake Superior exhibit strong lateral variability in their visual appearance, as well as vertical positions of characteristic diagenetic layers (Fig. 1.2). The surface sediments were typically composed of dark and less compacted layers, presumably organic rich, whereas the deeper sediments contained more grey clays or light brownish layers (Fig. 1.2). Most sediment cores showed prominent Mn- and Fe-rich layers between 4 and 14 cm depth below the sediment-water interface. The layers, whose compositions were verified using scanning X-ray fluorescence (XRF) (*see* Chapter 3), were visible to the naked eye as rust-colored layers for Fe and black layers for Mn. Strikingly, some cores recovered within short distances to each other (Table 1.1) in deep Eastern (Sta. EM) and deep Western (Sta. WM) basins were markedly different in color and the number of metal-rich layers (Fig. 1.2). Variability in cores from other stations was smaller, but still significant, with the depths of metal-rich layers varying by up to several centimeters (e.g., Sta CM, and WM; Fig. 1.2).

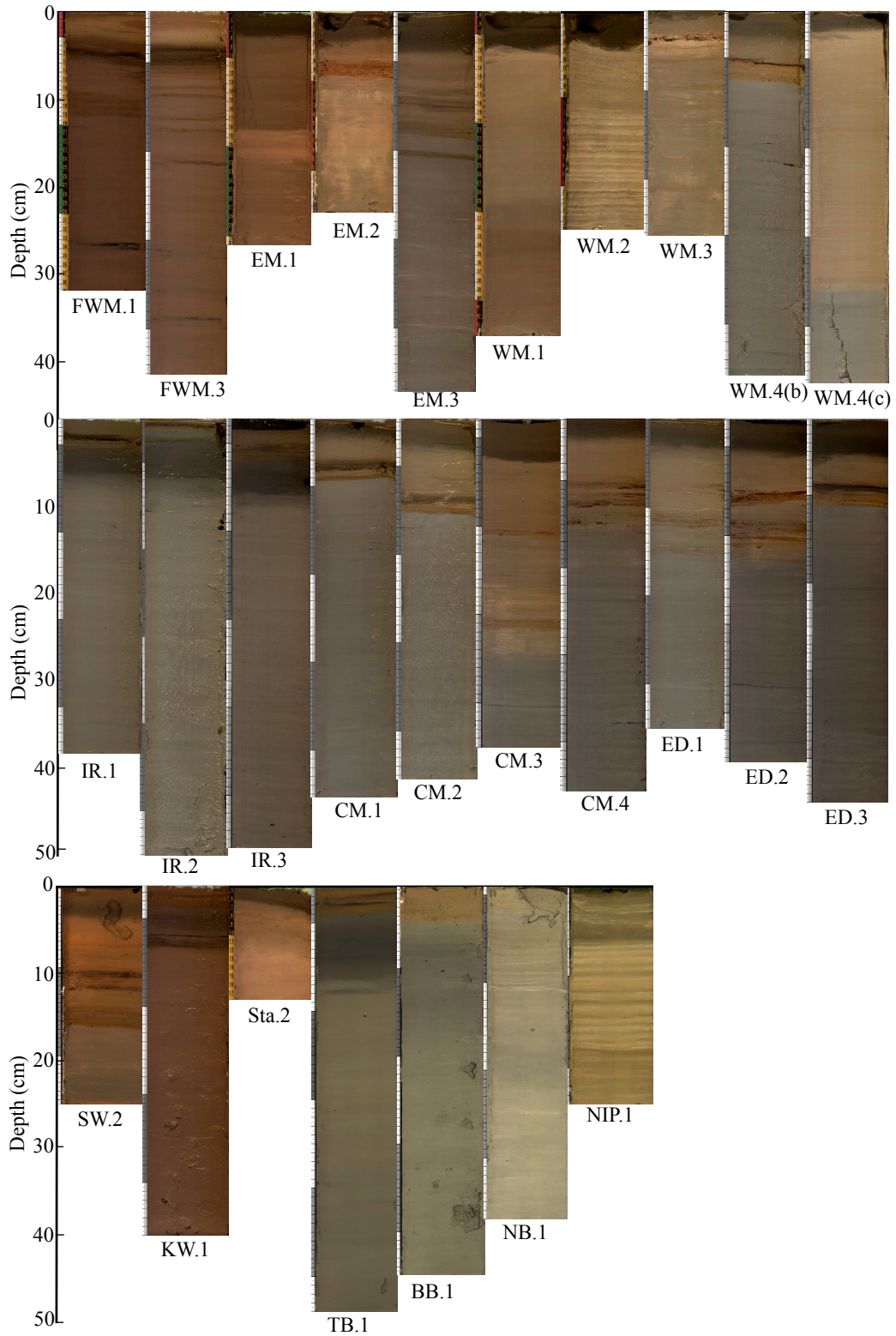


Figure 1. 2 Optical images of Lake Superior sediment cores

Sediment accumulation rates

Sediment accumulation rates ($\text{g cm}^{-2} \text{ yr}^{-1}$) determined from ^{210}Pb analyses are shown in Fig. 1.3. At Sta. FWM, the data show a temporary increase in sedimentation by more than a factor of 2 in the mid-20th century. This is likely associated with the discharge of taconite tailings (depleted iron ore) into the lake by the Silver Bay Mining Company (Fig. 1.1). The discharges continued from 1950s to 1980s and led to a markedly increased sedimentation in parts of the Western Arm of Lake Superior (Li 2011). Another contributing factor may be the variations in the amount of coarse grained sediment carried into the lake by the St. Louis River, at the westernmost end of the lake. At other stations, sediment accumulation varied throughout the 20th century to a much smaller degree. Among these stations, Sta. IR has the highest sediment accumulation rate, around $0.02 \text{ g cm}^{-2} \text{ yr}^{-1}$. The sites Sta. CM and Sta. EM, located, respectively, in the central and eastern-central parts of the lake, have significantly lower sedimentation rates, around $0.01 \text{ g cm}^{-2} \text{ yr}^{-1}$. The burial velocities (cm yr^{-1}), which are the solid particle velocities relative to the sediment-water interface, decrease downcore due to sediment compaction, from $\sim 0.1 \text{ cm yr}^{-1}$ near the sediment-water interface to $0.02\text{-}0.03 \text{ cm yr}^{-1}$ below 10 cm depth.

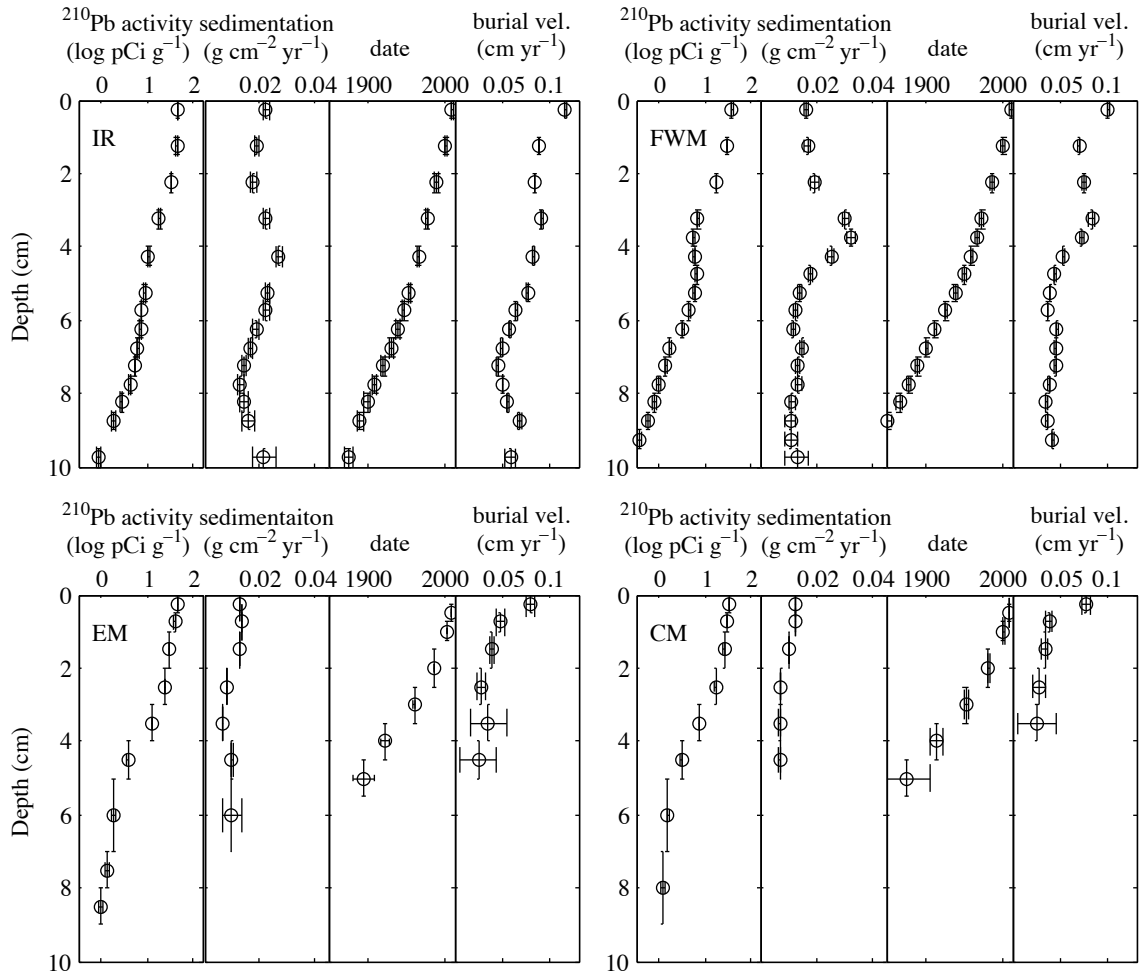


Figure 1. 3 Unsupported ^{210}Pb activity and the calculated sediment accumulation rates, apparent sediment ages, and burial velocities (vel.) at Sta. IR, FWM, EM, and CM. Horizontal error bars reflect the propagated uncertainties in the ^{210}Pb activity. Vertical error bars indicate the depth intervals of analyzed samples.

Water column temperature and oxygen distributions

Temperature profiles in the water column (Fig. 1.4) at all stations indicated typical dimictic stratification, with spring overturn in early June and winter overturn known to occur in December. Temperatures in the bottom waters remained near the maximum-density temperature (4°C) year round, with surface temperatures varying between 0°C in winter and 17°C in summer. Oxygen concentrations in the bottom waters were typically high after the overturn in June and remained high over the summer but declined in fall as stratification develops (Fig. 1.5). The oxygen dynamics during winter months are poorly known. Depth variation in oxygen within the epilimnion typically mirrored the temperature profiles, suggesting their control by oxygen solubility: lower concentrations were found in warmer surface waters during summer stratification.

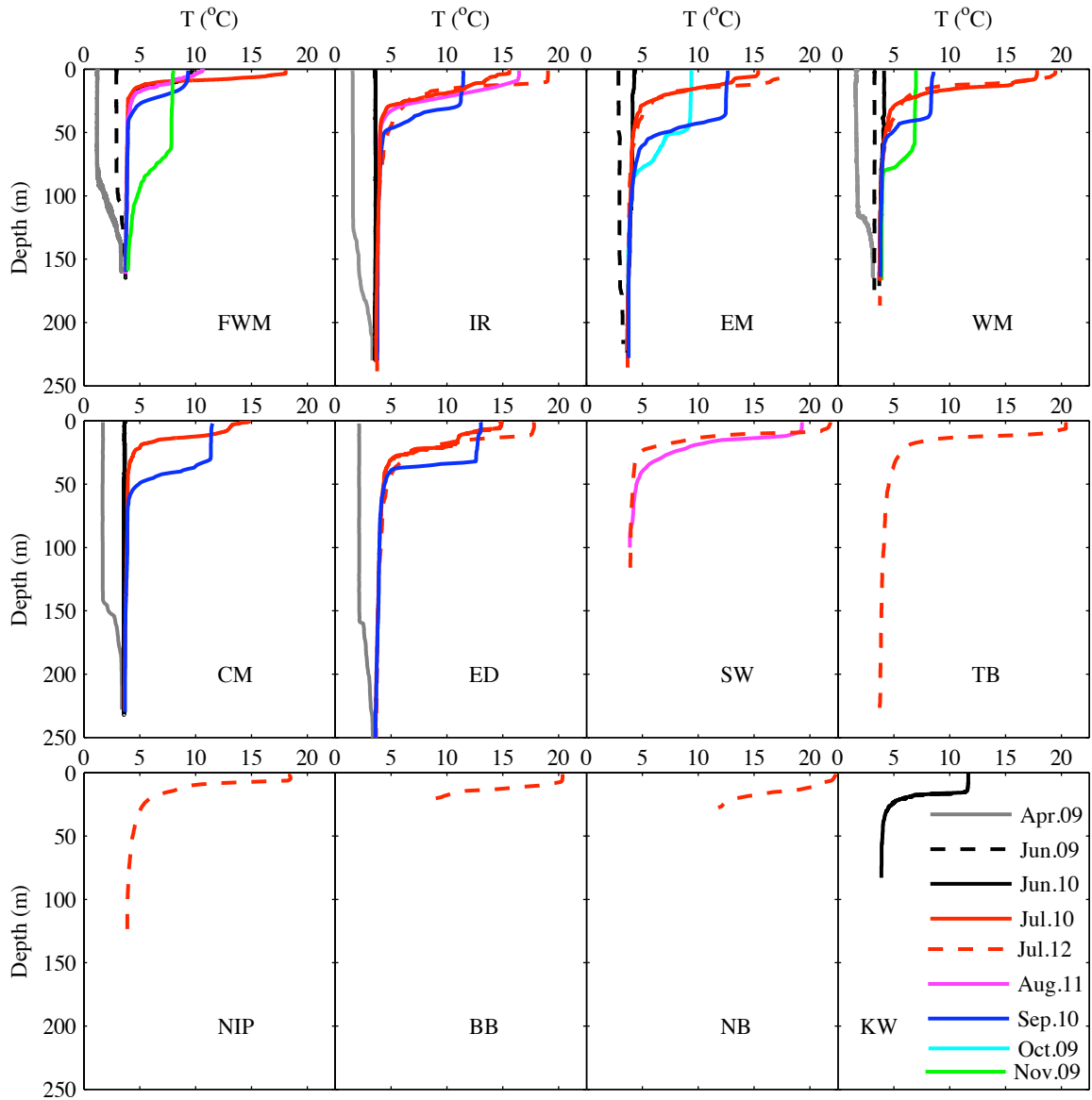


Figure 1. 4 Vertical temperature variations in water column of Lake Superior

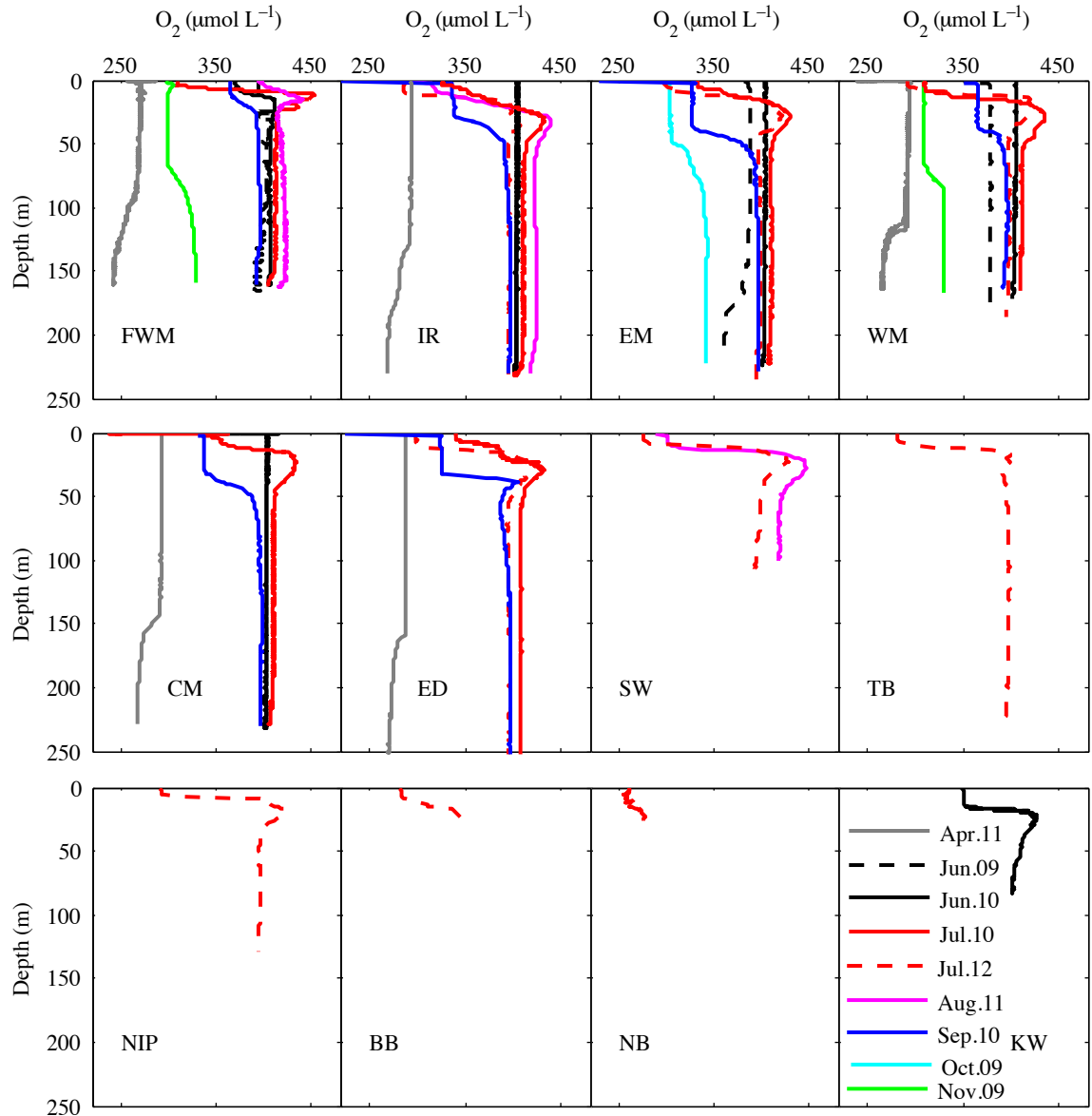


Figure 1. 5 Vertical distributions of dissolved oxygen in water column of Lake Superior. (Note: CTD oxygen sensor, although calibrated during routine probe maintenance, was not calibrated prior to each cruise, thus absolute concentration values should be treated with caution.)

Oxygen penetration and uptake

At the locations where sedimentation rates are low (typically offshore), oxygen penetrated deeply into the sediments (Fig. 1.6): the oxygen penetration depth (OPD), defined at the detection limit of the microelectrode ($0.5 \mu\text{mol L}^{-1}$), was between 4 and 11 cm in cores from Sta. FWM, WM, CM, ED, and KW and several cores from Sta. WM, SW, and EM. In several other cores from the Sta. WM and Sta. EM (EM.1, EM.2, WM.1, WM.2, WM.3, WM.4c), oxygen concentrations remained high ($>80 \mu\text{mol L}^{-1}$) to depths greater than 12 cm, the maximum depth that could be reached with our microelectrode. At Sta. NIP, the depth of oxygen penetration was 42 cm, as verified by profiling from the bottom of the core. At some stations where sediment cores from different samplings were similar in appearance (e.g., Sta. IR, ED, selected cores from Sta. EM), the depth of oxygen penetration varied between samplings throughout the summer of 2010 by several mm. Oxygen penetration typically deepened from June and July to September, especially at the sites with deep OPDs (Sta. EM and CM; Fig. 1.6). With the exception of Sta. CM, the oxygen penetration in April of 2011 was significantly shallower (by ~ 2 cm) at all sampled locations (Fig. 1.6). In contrast to the offshore low sedimentation sites, OPD in the enclosed bays and other locations with high sedimentation (e.g., Sta. TB, BB, NB, IR) were shallower, from 0.5 cm to 3 cm (Fig. 1.6).

Sediment oxygen uptake fluxes measured in core incubations varied between $4.4 \text{ mmol m}^{-2} \text{ d}^{-1}$ at Sta. WM to $7.7 \text{ mmol m}^{-2} \text{ d}^{-1}$ at St. 2, with an average of $6.1 \text{ mmol m}^{-2} \text{ d}^{-1}$ (Table 1.2). Figure 1.7 presents the diffusive oxygen fluxes, which were calculated from representative microelectrode oxygen profiles (Fig. 1.6). The calculated diffusive fluxes were consistently below the fluxes in incubations (Table 1.2), with the average diffusive

flux being approximately half the average flux in incubations. For example, at Sta. IR, where sediment composition appeared to be most consistent between samplings, the diffusive flux ($3.29 \text{ mmol m}^{-2} \text{ d}^{-1}$) in September of 2010 was 67% of the total uptake flux ($4.9 \pm 0.8 \text{ mmol m}^{-2} \text{ d}^{-1}$) measured on the same cruise.

The calculated rates of oxygen consumption (Fig. 1.8) are highest within the top 1 cm of the sediment, with typical maximum values between 0.4 and $3.0 \mu\text{mol cm}^{-3} \text{ d}^{-1}$ (Fig. 1.8; Table 1.2). The rates monotonically decrease downcore, with the exception of some nearshore stations (e.g., Sta. IR and TB) where the depth of oxygen penetration was shallow and oxygen consumption had an apparent peak at around the OPD (e.g., in Sta. IR.1 core, oxygen consumption increased from $0.03 \mu\text{mol cm}^{-3} \text{ d}^{-1}$ at 3.4 cm to $0.14 \mu\text{mol cm}^{-3} \text{ d}^{-1}$ at 3.5 cm. Fig. 1.8). Figure 1.9 plots the calculated uptake fluxes, maximum volume-specific oxygen consumption rates, and oxygen concentrations in the bottom waters (Fig. 1.5) as a function of time of the year.

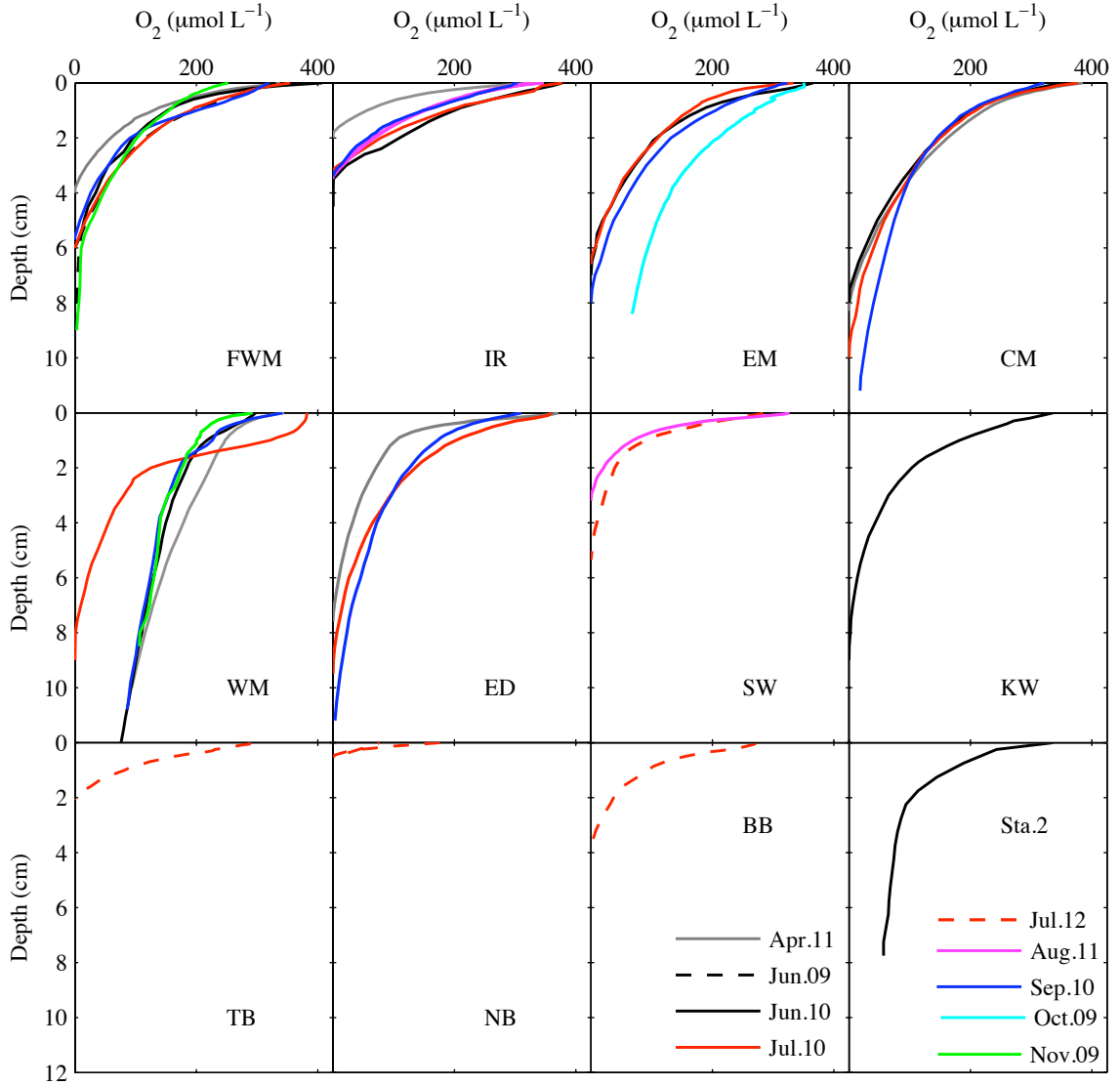


Figure 1. 6 Vertical distributions of dissolved oxygen in sediments of Lake Superior. Replicate profiles taken in different cores of similar visual appearance from the same station during the same cruise differed in their OPDs by < 2 mm.

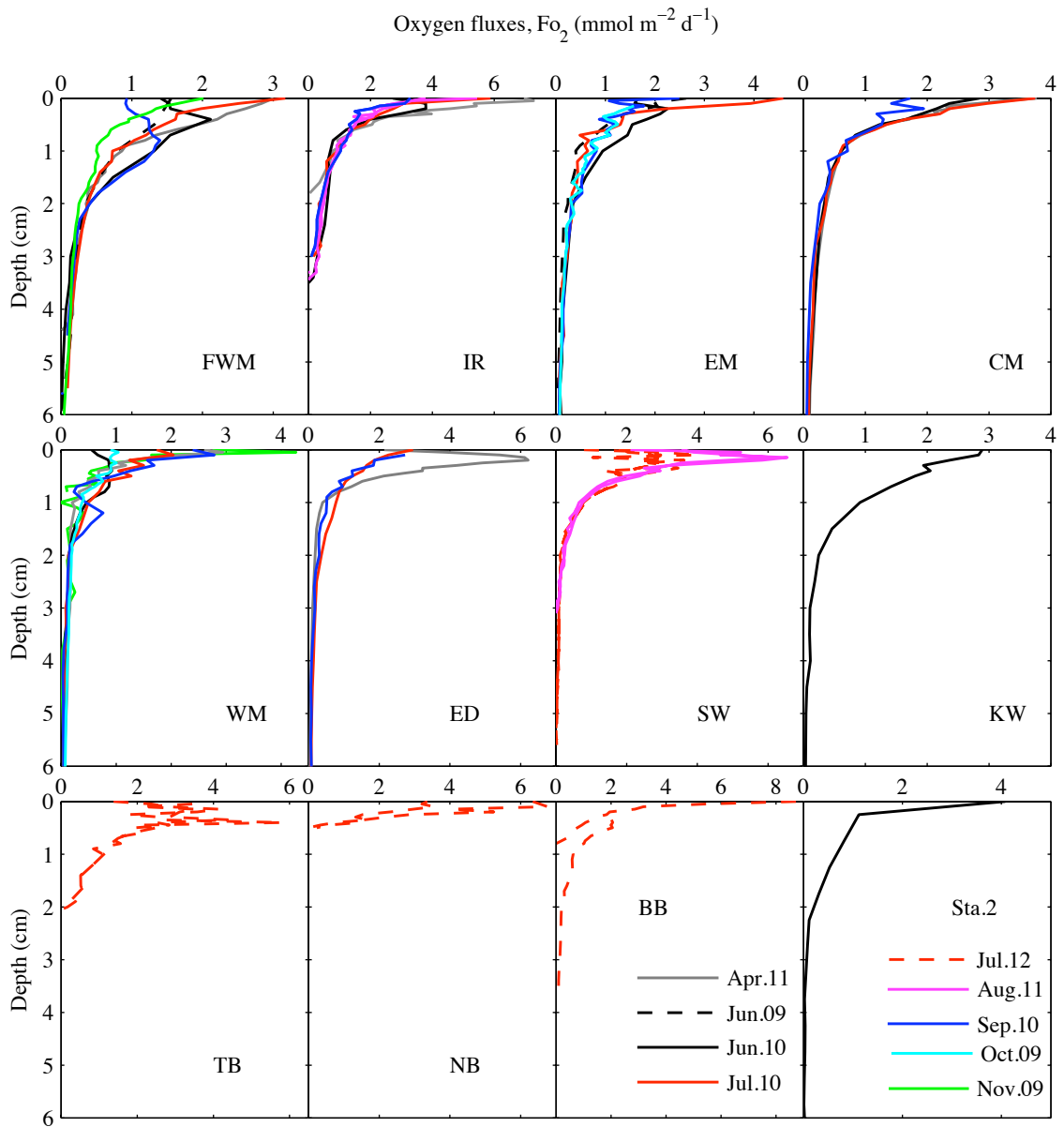


Figure 1. 7 Calculated oxygen diffusive fluxes in sediments of Lake Superior

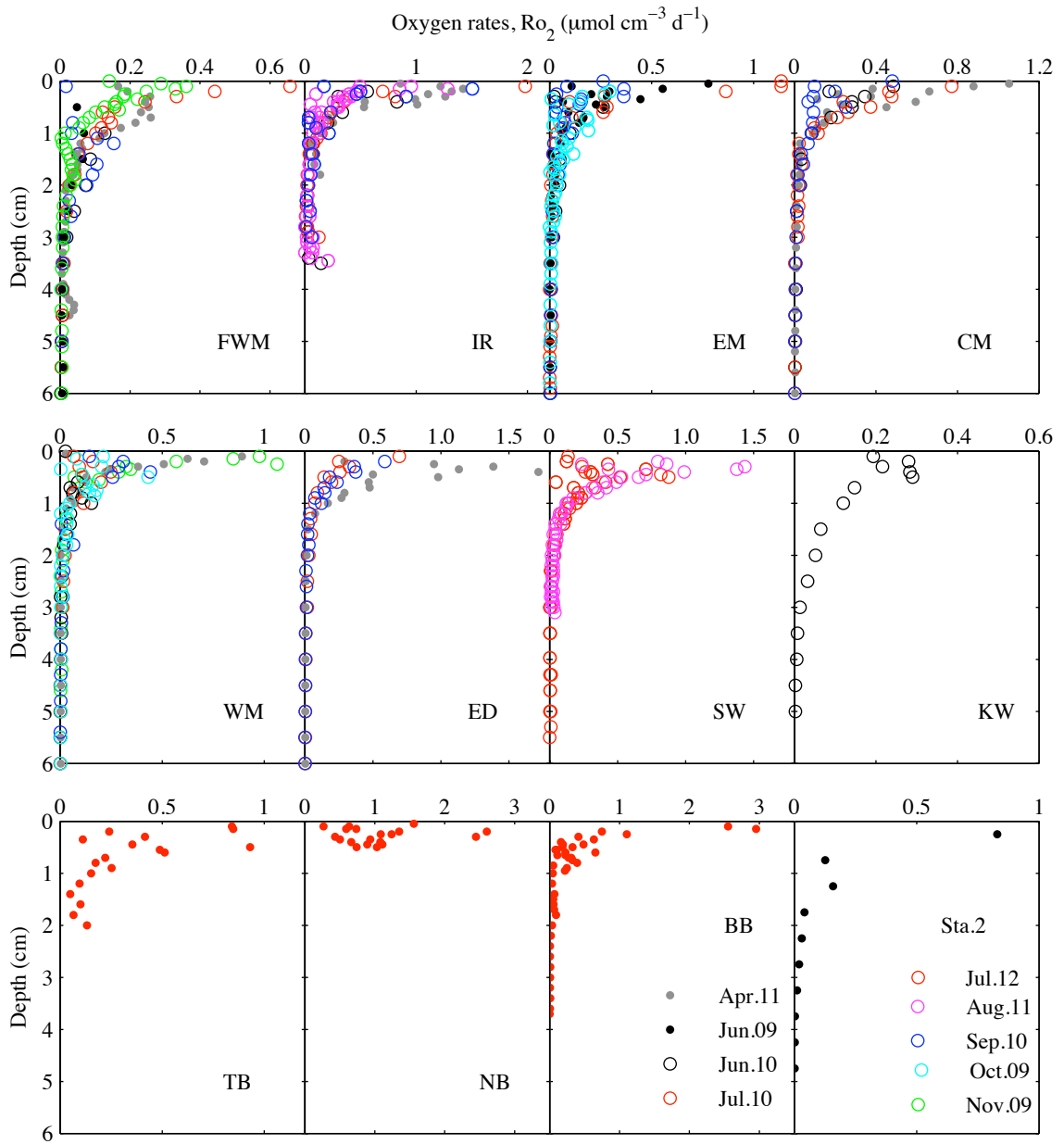


Figure 1. 8 Calculated oxygen consumption rates in sediments of Lake Superior

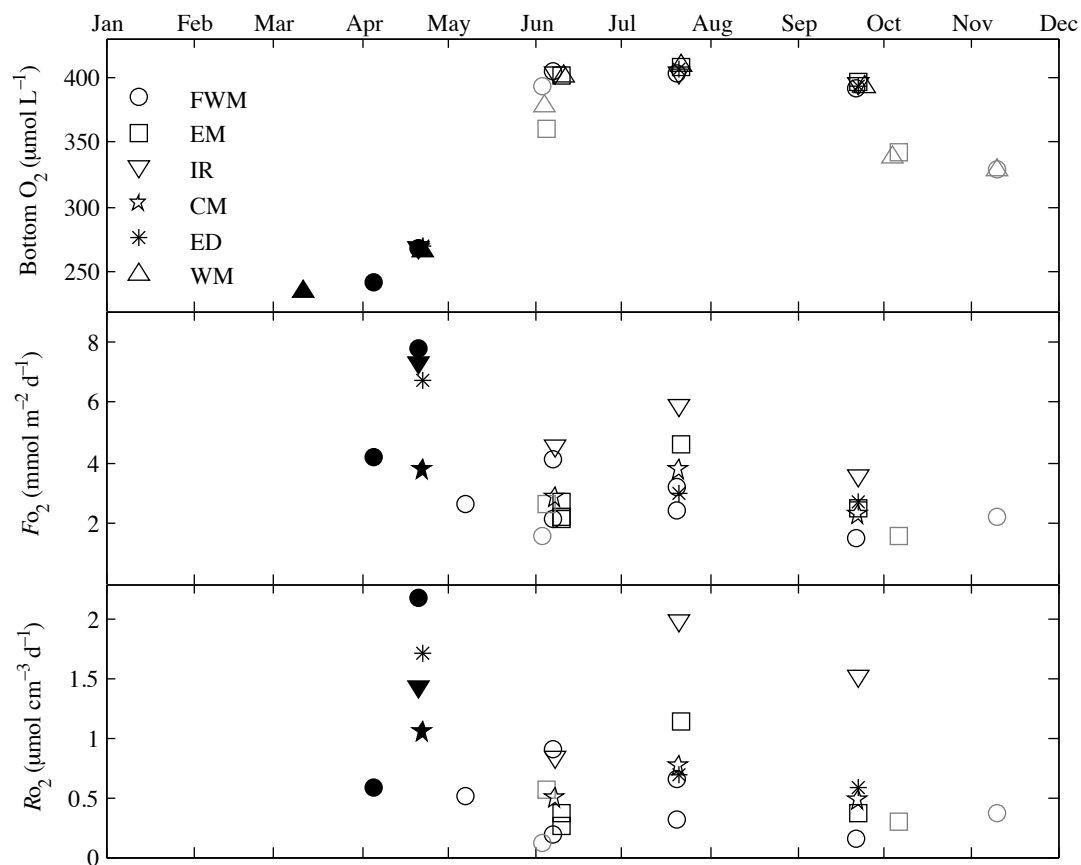


Figure 1. 9 (A) Seasonality in bottom-water oxygen concentrations determined from conductivity-temperature-depth data (see note on O₂ sensor calibration above); (B) maximum sediment oxygen fluxes (F_{O_2}), and (C) maximum oxygen consumption rates (R_{O_2}). Black open symbols are the results from 2010; gray open symbols are from 2009; black solid symbols are the results from 2011; gray solid symbols are from 2012.

Table 1. 2 Diffusive oxygen fluxes across sediment-water interface, total oxygen uptake, maximum carbon mineralization rates, organic carbon reactivity at SWI, and carbon mineralization time scale. Numbers given are averages over all available measurements with minimum and maximum values given in brackets. The total oxygen uptake values are from whole-core incubations. Integrated carbon degradation rate (C degradation flux) and maximum carbon degradation rates are calculated from oxygen flux and consumption rates (Fig. 1.7 and 1.8; $F_C = 6/7 F_{O_2}$; $R_C = 6/7 R_{O_2}$), averaged over all available profiles.

	O ₂ diffusive flux (mmol m ⁻² d ⁻¹)	Total O ₂ uptake (mmol m ⁻² d ⁻¹)	Integrated C degradation rate (mmol m ⁻² d ⁻¹)	Maximum C degradation rate, R _C (μmol cm ⁻³ d ⁻¹)	Organic carbon reactivity at SWI, k (yr ⁻¹)	Mineralization time scale, τ (yr)
FWM	3.0 (1.1– 7.8)	6.4 ¹ ; 7.1± 1.1 ² ; 4.5 [*]	5.5 ¹ ; 6.1 ² ; 3.9 [*]	0.47 (0.094 -0.77)	1.3	0.52
†IR	5.0 (2.7- 7.3)	4.9± 0.8 ² ; 7.5 [*]	4.2 ² ; 6.4 [*]	1.1 (0.71- 1.3)	2.6	0.26
EM	2.9 (1.3- 4.6)	4.4 [*]	3.8 [*]	0.50 (0.27- 0.94)	1.3	0.52
WM	2.2 (1.1- 3.2)	4.4 ¹ ; 3.3 [*]	3.8 ¹ ; 2.8 [*]	0.47 (0.13- 0.94)		
CM	3.2 (2.3- 3.8)	4.8 [*]	4.1 [*]	0.61 (0.41- 0.94)	0.78	0.89
ED	4.2 (2.7- 6.8)	6.3 [*]	5.4 [*]	0.76 (0.51- 1.2)	0.74	0.94
SW	4.9 (3.9- 6.5)	7.4 [*]	6.4 [*]	0.94 (0.75- 1.2)		
KW	2.9	4.4; 4.4 [*]	3.8 ¹ ; 3.8 [*]	0.25		
Sta.2	4.1	7.7 ¹ ; 6.2 [*]	6.6 ¹ ; 5.3 [*]	0.71		
†TB	5.1 (4.4- 5.8)	7.7 [*]	6.6 [*]	0.80		
†BB	7.1 (8.7- 5.4)	11 [*]	9.4 [*]	2.6		
†NB	6.4 (5.9- 6.8)	9.8 [*]	8.4 [*]	2.2		
Average	4.3 ± 1.5	6.1± 1.4 ^{1,2} ; 6.4 [*]	5.7± 1.8		1.4± 0.8	0.63

Note: ¹ measured in June 2010; ² measured in September 2010; ^{*} Total oxygen uptake calculated from diffusive oxygen fluxes accounting for bioirrigation ($R_{O_2 \text{ total}} = 1.5 R_{O_2 \text{ diff}}$); † indicates stations termed in the text as ‘nearshore’.

Organic carbon content, reactivity and bioturbation rates

The organic carbon content of the sediments decreases downcore from 3.5-5.0 weight percent (wt %) at the sediment surface to about 2 wt % in the deeper sediment (Fig. 1.10). The concentration of organic carbon remains relatively constant below 10-15 cm depth compared to the decrease trend in the surface. At Sta. FWM, both the organic carbon concentration and water content varied non-monotonously (Fig. 1.10). The dip in the Sta. FWM profile at 4 cm depth indicates the presence of dense organic-poor particles, which matches the period of increased sedimentation (Fig. 1.3) and the time period during which taconite tailings were being discharged from Silver Bay (Li 2011). The depth variation in the effective reactivity of organic carbon calculated from Eq. 1.10 is illustrated in Fig. 1.11. The reactivity of organic carbon decreases drastically within the upper 1 cm of the sediment. At the sediment-water interface the reactivity k is around 1 yr^{-1} , whereas in the depth interval 1-2 cm it falls to approximately 0.05 yr^{-1} .

Figure 10 shows the values of the bioturbation coefficient calculated from Eq. 1.7, as a function of depth within the sediment. Bioturbation is limited to the upper 2 cm of sediment, and most intense at the sediment surface, where the bioturbation coefficient reaches values of $3\text{-}4 \text{ cm}^2 \text{ yr}^{-1}$.

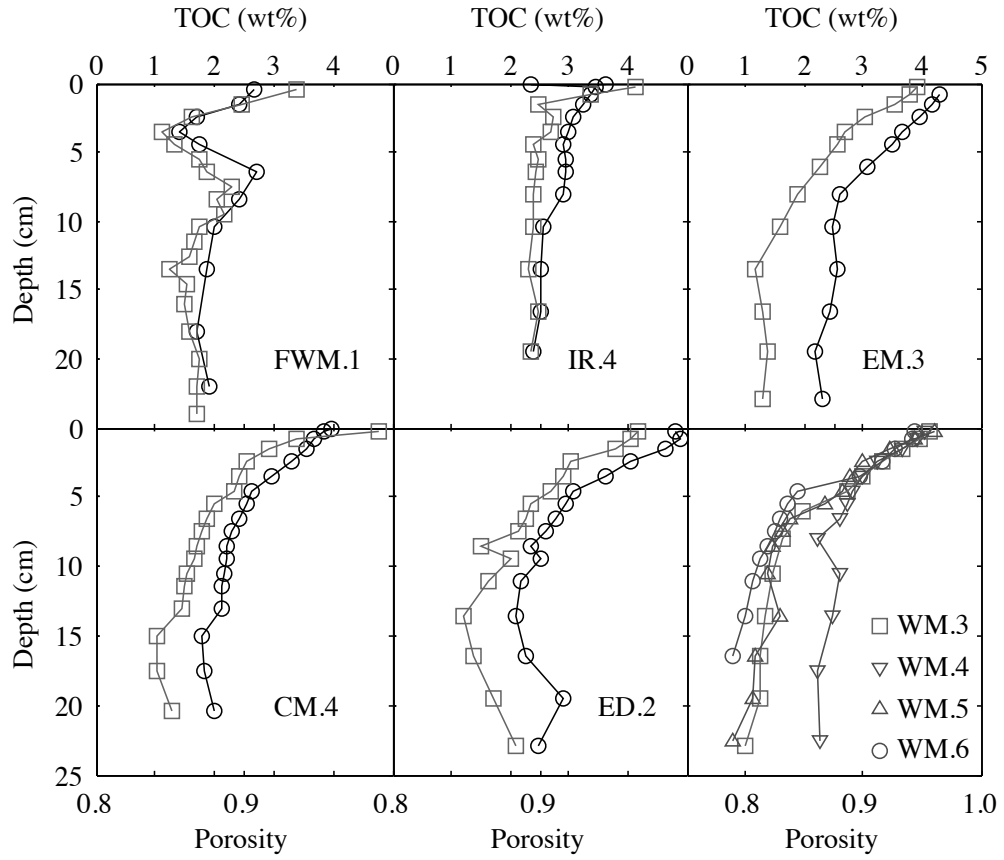


Figure 1. 10 Organic carbon (OC) content (black) and porosity (gray). The total inorganic carbon content (TIC) was negligible in all coulometric measurements.

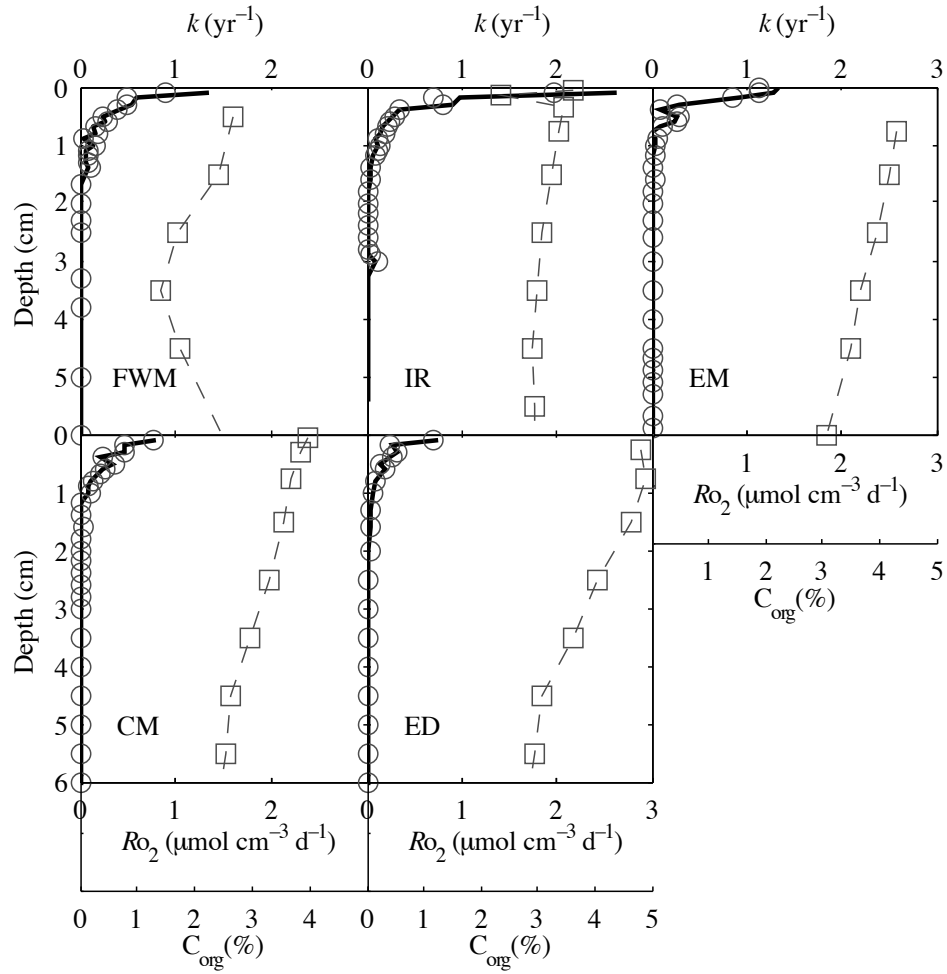


Figure 1.11 Organic carbon reactivity k (black line). Data is calculated from O_2 consumption rate (gray circles) and the total organic carbon content (gray squares, interpolated between measurements as shown by the dashed line).

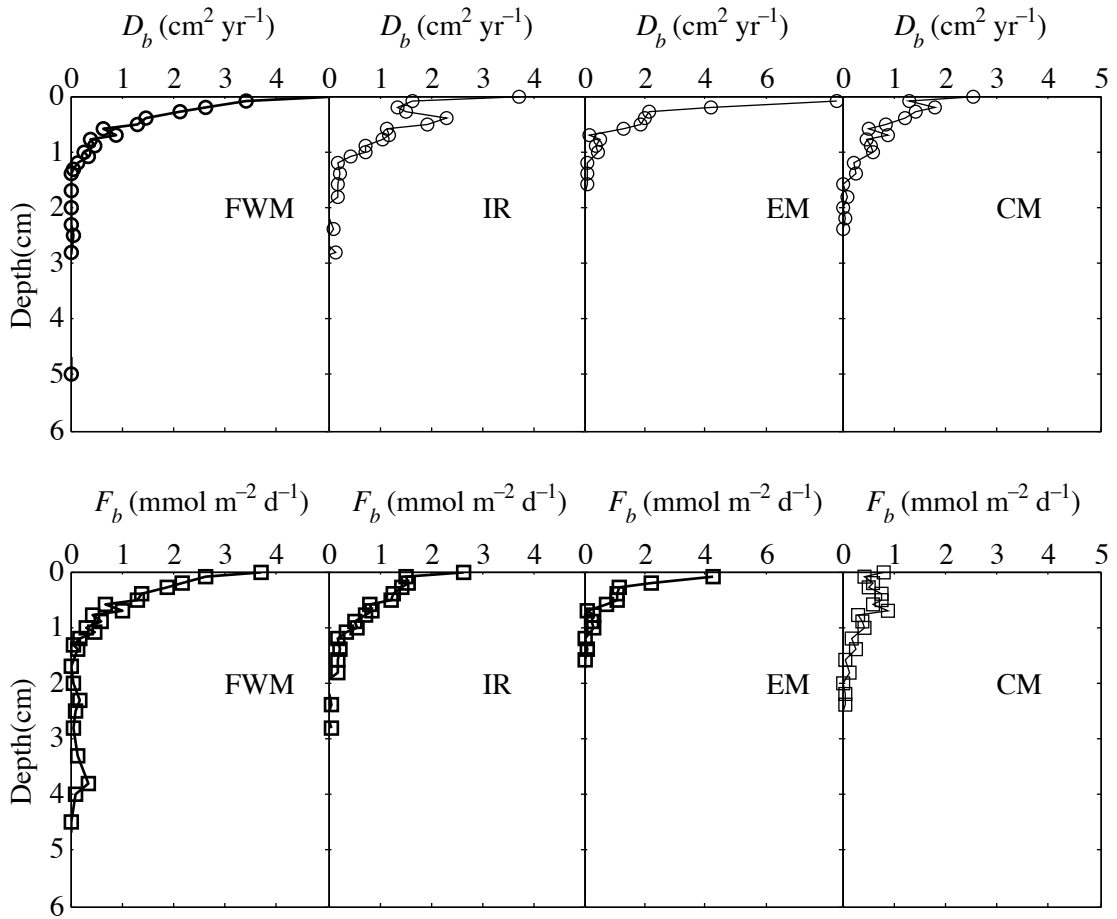


Figure 1. 12 Calculated bioturbation coefficients D_b and the burial fluxes of organic carbon that are due to bioturbation, F_b

DISCUSSION

Spatial variability

Our results reveal strong lateral variability in Lake Superior sediment properties, not only between sampling stations located hundreds of kilometers apart, but also over hundreds of meters. On large geographical scales, variability can be expected due to differences in sediment provenance, organic matter fluxes, and bottom current velocities. The higher phytoplankton abundance (Munawar and Munawar 1978) and sedimentation rates (Fig. 1.3; Kistner 2013; Kemp et al. 1978; Evans et al. 1981) in the bays and some productive regions result in shallower oxygen penetration (e.g. Sta. IR, SW, TB, NB, BB; Fig. 1.6) and relatively higher fluxes of oxygen across the sediment-water interface (Table 1.2), while in the open-water, low-productive basins oxygen penetration were deeper (e.g., Sta. 2, EM, CM, WM, ED, NIP; Fig. 1.6) with lower oxygen fluxes across the SWI (Table. 1.2). In analogy to marine systems, where coastal sediments typically have higher sedimentation rates, shallower OPD and greater oxygen uptakes than do pelagic sediments, in the later discussion (and the later chapters) we will refer to such sediments as “nearshore”, for convenience, in contrast to the “offshore” sites with deep OPDs.

On a much smaller scale, however, sediments at several sites also exhibited strong variability. For example, our Sta. EM.1 core had no visible Fe-rich layer (Fig. 1.2) and an OPD >12 cm (Fig. 1.6), whereas our Sta. EM.2 core had a prominent Fe layer at 6 cm depth (Fig. 1.2) yet an OPD >8 cm (Fig. 1.6). Another core from the same site, Sta. EM.3, had a Fe-rich layer at ~8.5 cm and an OPD of 6.5 cm (Figs. 1.2, 1.6). These cores were recovered within several hundred meters of each other. Such small-scale variability

was strongest at the Sta. WM and Sta. EM stations, in the middle of the Western and Eastern deep basins, respectively. The strong variability in sediment properties in our cores may be linked to the spatial heterogeneity of the Lake Superior floor that was reported in recent seismic surveys (van Alstine, 2006). The surveys, which focused on areas close to our Sta. WM, revealed that the lake floor contains multiple pockmarks, as well as linear and ring-shaped depressions that were ~2 m deep and spanned hundreds of meters. Sediment core analyses suggested that the depressions expose the hard-packed post-glacial sediments that may contain little recently deposited material (van Alstine 2006). The origin of these features is unclear, they have been hypothesized to be expressions of glacial ice scouring and dewatering of post-glacial sediments (T. Johnson and N. Wattrus pers. comm.). Our observations with a shipboard echosounder indicate that these features are ubiquitous in both the Eastern and Western basins of the lake.

Oxygen fluxes and consumption rates

The total oxygen uptake rates (Table 1.2) measured in our incubations were greater than oxygen fluxes driven by molecular diffusion, suggesting a non-negligible contribution from processes such as fauna-enhanced diffusion, non-local bioirrigation, or hydrodynamic flow (Lorke et al. 2003; Glud 2008). The observed differences suggest that these processes may account for 30-50% of the total oxygen flux. This is at the low end of the range for the contribution of biologically enhanced fluxes in marine sediments with similar total oxygen uptakes (Meile and Van Cappellen 2003). For non-local bioirrigation, using the typical rates ($\alpha_{\text{irr}}C_0 = 10\text{-}20 \text{ mmol L}^{-1} \text{ yr}^{-1}$) in marine sediments (Meile and Van Cappellen 2003), and integrating the bioirrigation rate over 2 cm (the

depth interval affected by benthic fauna in Lake Superior, Fig. 1.12), we calculate that the non-local bioirrigation flux of oxygen in Lake Superior is about $0.3 \text{ mmol m}^{-2} \text{ d}^{-1}$. This is less than 10% of the total uptake flux. A similarly small figure is obtained when the bioirrigation rates are calculated using the bioirrigation coefficients that were measured in microcosm experiments in Lake Erie sediments ($\alpha_{\text{irr}}=10^{-6} \text{ s}^{-1}$; Matisoff and Wang 1998). This suggests that in Lake Superior the benthic fauna contributes to the solute transport primarily through enhanced diffusion, rather than non-local fluid exchange. Given the magnitude of this contribution (30-50% of the total uptake flux), the calculated rates of oxygen consumption (Fig. 1.8) and values of bioturbation coefficient (Fig. 1.12) likely underestimate the rates and coefficients by 30-50%.

Whereas the rates of oxygen consumption (R_{O_2}) in Fig. 1.8 were calculated (Eq. 1.9) with the assumption of a steady state, the data in Fig. 1.9 allow us to quantify the contribution of the time-explicit term in Eq. 1.8. The fastest change in the bottom water oxygen concentrations seems to have occurred in April-May. Based on the CTD measurements, concentrations increased from 8 mg L^{-1} ($250 \mu\text{mol L}^{-1}$) to 13 mg L^{-1} ($400 \mu\text{mol L}^{-1}$) over a period of approximately 60 days. This translates into the rate of change at the sediment-water interface of $\frac{\partial [O_2]}{\partial t} = 0.0025 \mu\text{mol cm}^{-3} \text{ d}^{-1}$, which is two orders of magnitude lower than the typical rate of oxygen consumption (Fig. 1.8). As temporal variations below the sediment surface are expected to be even lower, the steady state approximation given by Eq. 1.9 should be sufficiently precise. As R_{O_2} approximately corresponds to the rate of organic carbon degradation (R_C), Fig. 1.8 illustrates that the rates of organic carbon degradation in Lake Superior are highest near the sediment-water interface and decrease substantially within the upper 1-2 cm of sediment. A significant

fraction of organic carbon is thus mineralized in the upper sediment layer, where oxygen, which penetrates well below the bioturbation zone, is present at high concentrations. Only profiles from some nearshore stations (e.g., Sta. IR, TB) indicate a substantial consumption of oxygen by the products of anaerobic metabolisms, as reflected by a local maximum in oxygen consumption at the oxic-anoxic boundary, which corresponds with the accumulation of Mn and Fe (oxyhydr)oxides (*see* later Chapters) and likely develops due to the oxidation of upward diffusing reduced chemical constituents by O₂ (Canfield et al. 1993; also *see* later Chapters).

Carbon fluxes and reactivity

The rate of carbon burial into the deep sediment, $F_{C_{bur}}$, can be estimated from the sediment accumulation rate, $U\xi$, and the total organic carbon concentration (C), at a depth L where the concentration of organic carbon no longer varies appreciably with depth: $F_{C_{bur}}=C_L U_L \xi_L$. The sediments below 15 cm depth contain about 1-2% TOC (0.9-1.7 mmol C g⁻¹; Fig. 1.10; Kistner 2013) and the typical sediment accumulation rates at our stations are 0.015 g cm⁻² yr⁻¹ offshore (Fig. 1.3) and 0.06 – 0.18 g cm⁻² yr⁻¹ nearshore (Kemp et al. 1978; Evans et al. 1981; Li 2011). Accordingly, organic carbon is being buried into the deep sediments at a rate of ~0.7 mmol C m⁻² d⁻¹ (~3 g C m⁻² yr⁻¹) in the offshore basins of Lake Superior and ~ 1.0 mmol m⁻² d⁻¹ nearshore.

The downward flux of carbon at the sediment-water interface (SWI) is due to both sediment accumulation and bioturbation:

$$F_{C_{SWI}} = -\xi D_b \left(\frac{dC}{dx} \right)_0 + \xi_0 U_0 C_0 \quad (1.11)$$

For the bioturbation coefficient of $3 \text{ cm}^2 \text{ yr}^{-1}$, the TOC concentration at the sediment surface of 4 wt%, and the organic carbon and porosity gradients shown in Fig. 1.10, these fluxes are on the order of $6 \text{ mmol m}^{-2} \text{ d}^{-1}$ for offshore sediments (average of Sta. FWM, CM, and EM) and $\sim 10 \text{ mmol m}^{-2} \text{ d}^{-1}$ nearshore (calculated from data at Sta. IR). This necessarily matches the sum of integrated carbon degradation rates (Table 1.2) and the carbon burial fluxes calculated above.

The reactivity of organic matter in the surface sediment is high, with a characteristic time scale of degradation on the order of 1 year (Table 1.2; Fig. 1.11), suggesting that the most labile organic fractions may decompose over a seasonal time scale. The reactivity decreases sharply within the top 2 cm, which is reflected in a much stronger decrease in the oxygen consumption rates (R_{O_2}), than in the organic carbon concentration (Fig. 1.10). The most reactive organic fractions are thus mineralized within the bioturbation zone and well above the depth of oxygen penetration. Below the bioturbation zone, the reactivity of organic carbon can be estimated by calculating the rate of organic carbon mineralization from the profile of TOC. At a steady state, by setting the left-hand-side of Eq. 3 to zero and using $U\xi=\text{constant}$, one obtains

$$R_C = -\xi U \frac{dC}{dx} \quad (1.12)$$

The reactivity k then can be calculated similarly to Eq. 1.10 as:

$$k = \frac{R_C}{\xi C} = -\frac{U}{C} \frac{dC}{dx} \quad (1.13)$$

For example, using the burial velocities, U , from Fig. 1.3 and the TOC concentrations, C , from Fig. 1.10 we obtain that the reactivity k below the depth of oxygen penetration at Sta. IR (4 cm) is on the order of 0.001 yr^{-1} .

Figure 1.13 illustrates the decrease in the reactivity of sediment organic matter, k , with age. In constructing this figure, the results for the reactivity calculated as a function of depth within the sediment (Fig. 1.11, Eqs. 1.10, 1.13) were combined with the relationship between the sediment depth and age shown in Fig. 1.3. In marine systems, the aging of organic material is often described by the Middelburg power law (Middelburg 1989; Middelburg et al. 1993), which holds over six orders of magnitude. Figure 1.13 shows that the reactivity of organic matter in the sediments of Lake Superior decreases with time after sediment deposition according to a similar power law. The reactivities calculated here for Lake Superior fall within the typical range of values observed in marine systems (Fig. 1.13). Given the low fraction (<17%) of terrestrial organic material in these sediments (Zigah et al. 2011), this suggests that the relationships established for the decomposition of organic matter in marine environments may be transferable to the organic material produced in large freshwater lakes. The slope of the power-law line in Lake Superior, however, is steeper than the slope of the Middelburg line. The difference is statistically significant (at the two sigma confidence level), suggesting that the degradation of organic material in Lake Superior occurs faster than in typical marine systems.

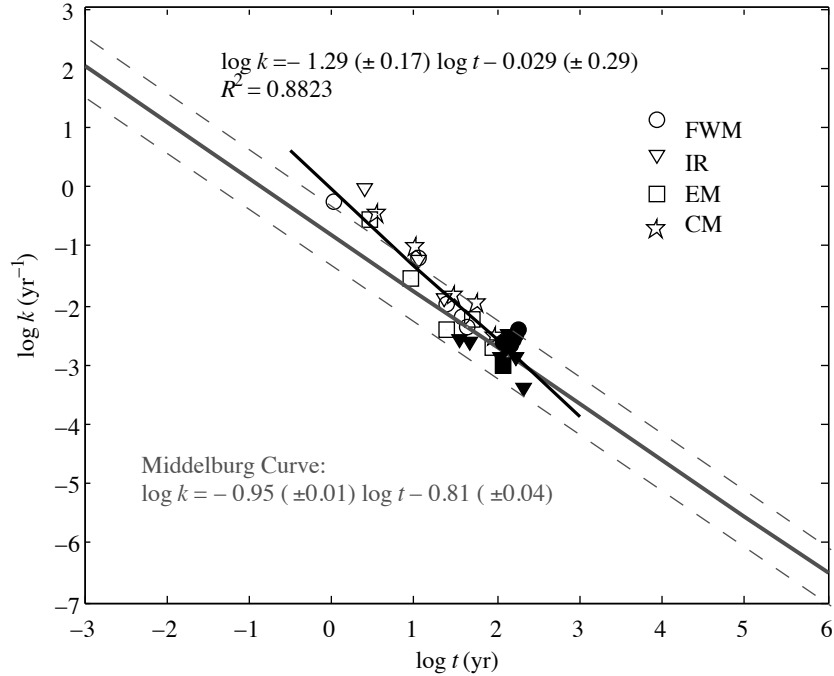


Figure 1. 13 Calculated reactivity of organic carbon in Lake Superior sediments as a function of the apparent sediment age. The gray line is Middelburg’s model (Middelburg 1989) for the reactivity of organic matter in marine sediment. Open symbols correspond to the values of k calculated within the oxic zone using Eq. 1.10; filled symbols correspond to the values calculated in the sediment below oxygen penetration using Eq. 1.13. Dotted gray lines outline the typical range of values in marine sediments (Burdige 2007).

Sediment contribution to lake-wide carbon budget

The total oxygen uptake by Lake Superior sediments (Table 1.2) suggests a carbon degradation rate of $4.8 \pm 1.0 \text{ mmol m}^{-2} \text{ d}^{-1}$ in the offshore sediments and $7.7 \pm 1.4 \text{ mmol m}^{-2} \text{ d}^{-1}$ in the nearshore sediments. Combined with the permanent burial fluxes ($0.7 \text{ mmol C m}^{-2} \text{ d}^{-1}$ offshore and $1.0 \text{ mmol C m}^{-2} \text{ d}^{-1}$ nearshore) this indicates that the total flux of organic carbon to the lake floor is $\sim 5.5 \text{ mmol m}^{-2} \text{ d}^{-1}$ offshore and $8.7 \text{ mmol m}^{-2} \text{ d}^{-1}$

¹ nearshore. This is slightly higher but broadly consistent with previous estimates. The organic sedimentation flux was previously estimated in sediment traps in the Western arm of the lake at $2.3 \text{ mmol m}^{-2} \text{ d}^{-1}$ (Heinen and McManus 2004), in the central lake at $5\text{-}7.5 \text{ mmol m}^{-2} \text{ d}^{-1}$ (Baker et al. 1991; perhaps with a contribution from resuspended sediment), and in the Eastern basin at $2.5\text{-}3.5 \text{ mmol m}^{-2} \text{ d}^{-1}$ (Klump et al. 1989). Given the high reactivity of organic carbon (Table 1.2), the settling organic material may undergo substantial degradation while in sediment traps, and even poisoned traps are known to underestimate carbon amounts (Gardner 2000). Our estimates based on the total oxygen uptake therefore offer a complementary estimate.

The efficiency of sediment carbon mineralization is $\sim 88\%$ ($4.8/5.5 = 87\%$ offshore and $7.7/8.7 = 89\%$ nearshore), i.e., only $\sim 11\%$ of the deposited organic carbon becomes buried into the deep sediments (below 15 cm depth). Such high efficiency is not unusual in aquatic sediments, but in marine environments it is more typical of hemipelagic and pelagic oceanic sediments (Reimers and Seuss 1983) rather than sediments in ~ 200 m water depth. Assuming the offshore-type sediments (low sedimentation rate, deep OPD, low carbon mineralization rate) underlie $\sim 90\%$ of the lake (as an estimate, actual number unknown) and the rest $\sim 10\%$ of the lake floor is covered by nearshore-type sediments (high sedimentation rate, shallow OPD, low carbon mineralization rate), organic carbon mineralization in the sediments of Lake Superior can be estimated at $1.5 \times 10^{11} \text{ mol C yr}^{-1}$ (or 1.8 Tg yr^{-1} ; $4.8 \times 90\% + 7.7 \times 10\% = 5.1 \text{ mmol m}^{-2} \text{ d}^{-1}$ and a total area of 82100 km^2). This is $\sim 20\%$ of the carbon being produced by gross primary production, which was recently estimated based on measurements at selected locations at 9.7 Tg yr^{-1} (Sterner et al 2010). Given that large areas (up to as much as two

thirds) of the lake floor may be non-depositional (do not retain fine-grained sediments; Kemp et al. 1978), and the primary productivity may have been underestimated as measurements were conducted in offshore areas where primary production is lower than in nearshore regions (Munawar and Munawar 1978), the actual contribution of sediments to carbon mineralization is probably somewhat lower. The 20% number is close to values observed in similar water depths in marine environments (Suess 1980), but higher than a previous estimate for Lake Superior. The fraction of primary-produced organic carbon that reaches the sediments was previously estimated at 5%, based on the amount of carbon collected in open-water sediment traps (Baker et.al. 1991). The burial flux into the deep sediments (0.26 Tg yr^{-1} ; $0.7 \times 90\% + 1.0 \times 10\% = 0.71 \text{ mmol m}^{-2} \text{ d}^{-1}$ and a total area of 82100 km^2 ; projected from our measurements for the entire lake) represents 2.7% of the estimated gross primary production, which agrees well with the typical range for deep temperate lakes (Alin and Johnson 2007).

Controls on oxygen penetration and carbon mineralization efficiency

The oxygen fluxes, $2\text{-}7 \text{ mmol m}^{-2} \text{ d}^{-1}$ for diffusive fluxes and $3\text{-}11$ for total fluxes, and the rates of carbon mineralization, $\sim 1 \mu\text{mol cm}^{-3} \text{ d}^{-1}$ (Fig. 1.8) in the upper sediment layer are similar to those found in marine sediments in similar water depths, $\sim 200 \text{ m}$ (Fig. 1.14 A; Sauter et al. 2001; Glud 2008). However, in coastal marine sediments, oxygen penetration rarely exceeds a few mm (Glud 2008; Mouret et al. 2010; Fig. 12), whereas in the low sedimentation basins (offshore-type) of Lake Superior it is routinely below 3 cm (Figs. 1.5, 1.14 B), which is similar to those of marine sediments under $\sim 3000 \text{ m}$ depth (Fig. 1.14 B). When plotted against the sedimentation rate (~ 0.015

$\text{g cm}^{-2} \text{ yr}^{-1}$; $\sim 0.03 \text{ cm yr}^{-1}$), both oxygen uptake and carbon burial efficiency (1-88%=12%) match well the corresponding values in marine sediments, whereas the oxygen penetration depth is at the upper limit of the corresponding marine range (Fig. 1.15). As most carbon mineralization in Lake Superior occurs in the upper few cm of sediment (Fig. 1.8), the low sedimentation rate translates to slow burial of organic material, allowing sufficient time for mineralization and a low oxygen demand in the deep sediment. In addition, several other factors, absent in marine sediments, contribute to the deep oxygen penetration in Lake Superior. The solubility of oxygen in freshwater is about 30% higher than in saltwater of the same temperature. The cold (3-5°C year round) bottom waters of Lake Superior, renewed regularly by overturns, thus routinely carry more oxygen than oceanic bottom waters. In addition, compared to marine sediments where bioturbation extends to 10 cm depth or deeper (Boudreau 1998), the shallow bioturbation zone ($\sim 2 \text{ cm}$; Fig. 1.12) in Lake Superior and the typically lower number of burrowing organisms in freshwater than marine sediments (Solan and Herringshaw 2008) lead to a less efficient transport of reactive organic material into the deep sediment, lowering the oxygen demand there.

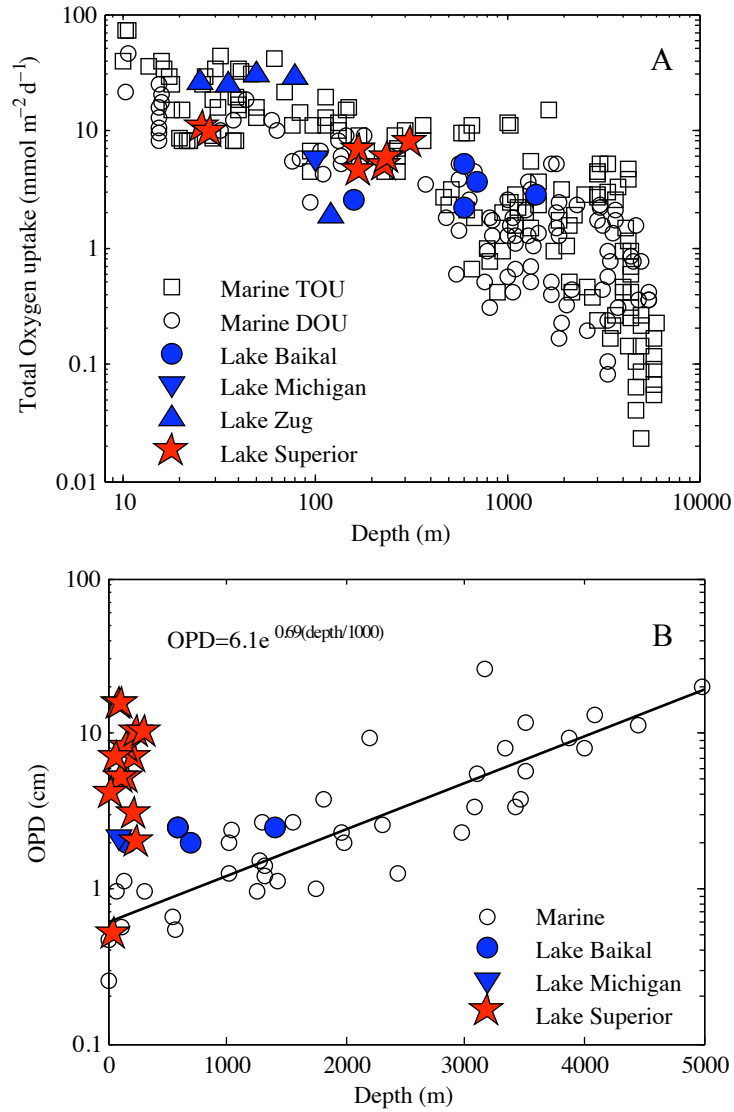


Figure 1. 14 (A) Total oxygen uptake rates across SWI, and (B) Oxygen penetration depth (OPD) in freshwater large lakes as functions of water depth, compared to marine environments. The data are from Lake Superior (this study), Lake Baikal (Maerki et al. 2006), Lake Michigan (Thomsen et al. 2004), Lake Zug (Maerki et al. 2009) and marine sediments (den Heyer and Kalff 1998; Glud 2008).

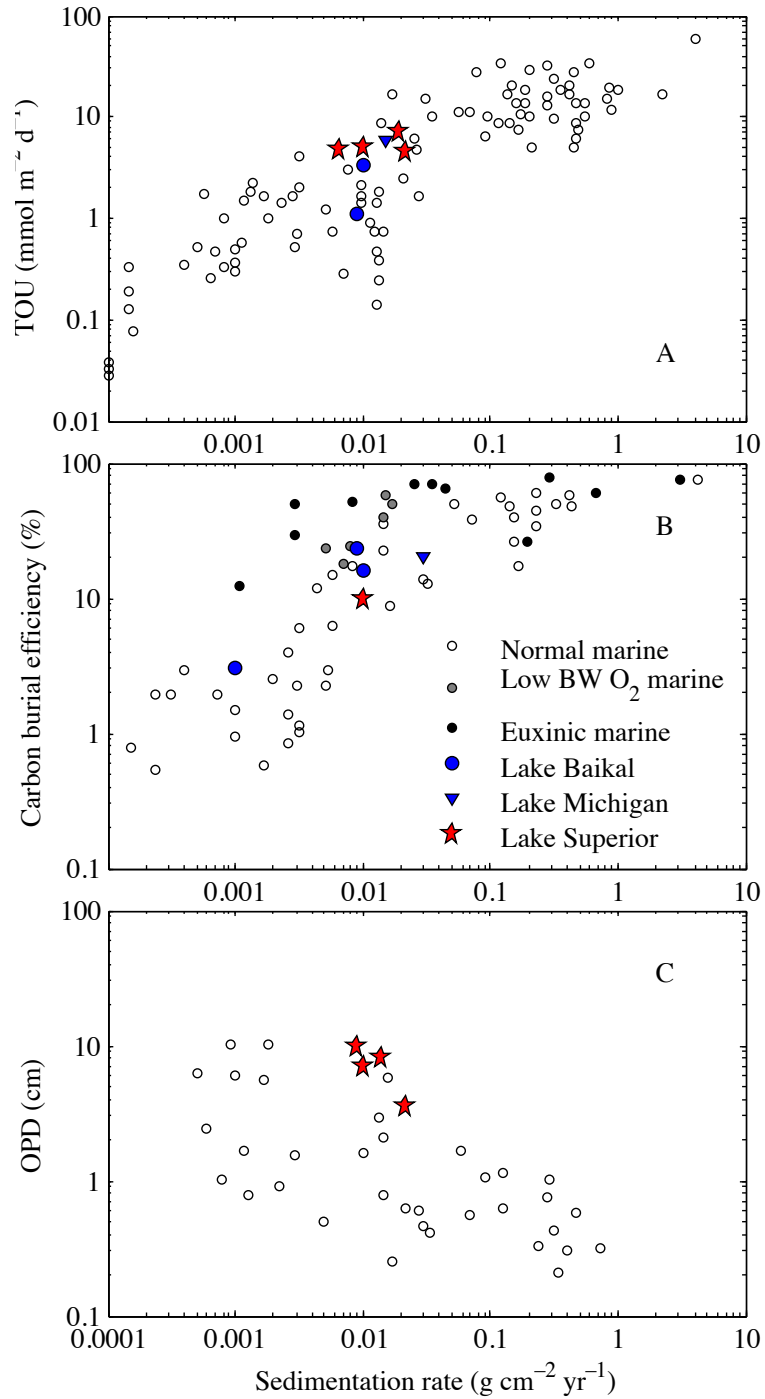


Figure 1. 15 (A) Oxygen fluxes across SWI, (B) carbon burial efficiency, (C) OPD as functions of sedimentation rate. Lake Superior data are from this study; Marine data are replotted from Canfield (1989, 1994) and Burdige (2009).

Non-steady state diagenesis

Despite the spatial heterogeneity of Lake Superior sediments (Figs. 1.2, 1.8), our dataset allows inferences about the temporal variability. Our results suggest that in Lake Superior the sediment depth of oxygen penetration experiences significant (by up to 2 cm) seasonal variations (Fig. 1.5). The OPD reflects the balance between the availability of oxygen from the bottom waters and the rate of oxygen consumption in the sediment. Numerical simulations of Katsev et al. (2006) demonstrated that the OPD is especially sensitive to this balance in deeply oxygenated sediments. The simulations also showed that in such sediments variations in bottom water oxygen levels modify the OPD more strongly, and on shorter time scales, than changes in the amount of settling organic matter. The reason is that, to affect the OPD, the reactive organic material needs to be transported into the deep sediment by burial or bioturbation. Our observations in Lake Superior support these predictions. Although the deposited organic matter is sufficiently reactive for some of its fractions to decompose on a seasonal time scale (Table 1.2) and carbon decomposition rates near the sediment surface appear to vary seasonally (Figs. 1.7, 1.8, 1.9), the burial rates are slow (Fig. 1.3) and the bioturbation is shallow (Fig. 1.12). Accordingly, no significant correlation can be found between the fluxes of oxygen (Fig. 1.7) and the OPD. In contrast, that the shallowest oxygen penetration was observed at the end of winter stratification, when the oxygen levels in the bottom waters were at their lowest (~67% saturation at atmospheric pressure) (Figs. 1.5, 1.9), suggests that the seasonal variations in OPD are regulated by the oxygenation of the water column (Fig. 1.5). Changes in the bottom water oxygen levels displace the OPD on the time scale of

diffusion, $\tau = x^2/(2D_s)$; for example, diffusion to $x=8$ cm takes ~ 2 months (for $D=421$ $\text{cm}^2 \text{yr}^{-1}$ used above). In Lake Superior, therefore the OPD should respond with time lags ranging from several weeks (for shallower OPDs, e.g., Sta. IR) to several months (for deeper OPDs, e.g., Sta. CM and ED). At stations with deep OPDs, the oxygenation of the water column in June (Fig. 1.5, 1.9) therefore would result in a deepening OPD in mid-to-late summer, consistent with our observations (Fig. 1.6).

Organic C sedimentation may modify the OPD on decadal and longer time scales. These may be long enough for the positions of the redox boundary to become marked by the accumulation of Fe and Mn (Katsev et al. 2006), such as in Fig. 1.2. The trends in organic sedimentation in Lake Superior are unclear, as the historical data on primary productivity are scarce. If we assume that the organic sedimentation in Lake Superior followed the availability of phosphorus, the limiting nutrient (Nalewajko et al. 1981), then the sedimentation flux of organic carbon probably doubled between the beginning of the 20th century and the mid-1970s and then declined in the 1990s (Lesht et al. 1991). This would result in a temporary shallowing of the redox boundary and the accumulation of Fe and Mn at shallower depths. These layers could now be located within the presently oxic sediment, in violation of the steady state redox sequence. Given the strong lateral heterogeneity of the sediments (Fig. 1.2), however, this hypothesis is difficult to test. It is possible that local redox changes over a variety of time scales could be caused by physical disturbances. For instance, bottom currents (Bennington et al. 2010) may episodically remove (or deposit) the organic-rich upper sediment layer, thereby exposing (or covering) the underlying organic-poor sediment.

The observed cm-scale migrations in oxygen penetration depth suggest that temporal redox variability in deeply oxygenated sediments may be greater than previously acknowledged. These changes may lead, in particular, to the variability in the transformations of other redox-sensitive elements, such as nitrogen, iron (and iron bound phosphorus), which are of particular interest in nutrient cycling in Lake Superior and will be discussed in later Chapters. That sediment OPD responds to the oxygen supply from the bottom waters also suggests that sediment redox chemistry may be affected by the physical stratification of the water column, which is now being affected by climate warming (Austin and Colman 2008). Given the similarity to marine hemipelagic sediments (Fig. 1.14, 1.15), analogous processes could be expected in oceanic sediments in response to changing ocean ventilation, such as during oceanic anoxia events.

CONCLUSIONS

- Sediments in Lake Superior exhibit strong spatial heterogeneity. Striking differences were observed in oxygen penetration depths (OPD) and locations of metal-rich layers within the sediment column on spatial scales as small as hundreds of meters.
- Strong spatial variability in oxygen penetration, oxygen fluxes and consumption rates parallel the spatial heterogeneity in sedimentation. Sediments in the low sedimentation areas (typically offshore) are characterized by deep OPDs (4 to > 12 cm), low oxygen fluxes ($5.8 \pm 1.2 \text{ mmol m}^{-2} \text{ d}^{-1}$) and low carbon degradation rates ($0.59 \pm 0.21 \mu\text{mol cm}^{-3} \text{ d}^{-1}$), whereas sediments in the high sedimentation nearshore areas are typically characterized by shallow OPDs (< 4 cm), high oxygen fluxes ($8.7 \pm 2.1 \text{ mmol m}^{-2} \text{ d}^{-1}$) and high carbon degradation rates ($1.7 \pm 0.9 \mu\text{mol cm}^{-3} \text{ d}^{-1}$).
- The depth of oxygen penetration varies on seasonal as well as decadal scales. OPD in the deeply oxygenated sediment is sensitive (varied by as much as several cm) to seasonal oxygen variations in bottom waters. Long-term changes in organic carbon fluxes may also have contributed to large excursions in oxygen penetration (evidenced by multiple metal-rich layers, some of which are present in the currently oxidized sediment zone). Thus, temporal variability in deeply oxygenated sediments may be greater than previously acknowledged. Similarly large excursions may be expected in marine systems that can be considered analogous in terms of the sediment redox dynamics, such as in the deep Arctic ocean sediments in response to the seasonality in carbon sedimentation or long term increases in productivity brought about by climate change.

- Oxygen uptake rates (average $6.1 \text{ mmol m}^{-2} \text{ d}^{-1}$) and organic carbon mineralization efficiency (88%) in the sediments Lake Superior are similar to those in marine sediments with comparable sedimentation rates and similar water depths. The reactivity of organic carbon was found to decrease with age similarly to the power-law documented in marine environments. The burial flux of carbon into the deep sediment (average $0.73 \text{ mmol m}^{-2} \text{ d}^{-1}$) was 2.7% of the primary productivity, similar to marine environments with similar water depth. These results indicate that carbon cycling in large freshwater systems conforms to many of the same trends as in marine systems.
- The exceptional deep OPD ($>3.5 \text{ cm}$) in the offshore low sedimentation areas are similar to marine sediment in 3000 m water depth, despite the average depth of Lake Superior of ~ 200 meters. Such deep penetration is explained by low sedimentation rates ($0.01\text{-}0.04 \text{ cm yr}^{-1}$), high solubility of oxygen in freshwater, and a shallow ($\sim 2 \text{ cm}$) bioturbation zone.

Chapter 2 Nitrogen cycling in sediments of Lake Superior and implications for marine coastal and deep ocean sediments

Most of the results in this Chapter were published in Li and Katsev (2014), Limnology and Oceanography 59(2), 2014: 465- 481

Title: Nitrogen cycling in deeply oxygenated sediments: Results in Lake Superior and implications for marine sediments

Authors: ¹Jiying Li and ^{1,2}Sergei Katsev

¹ Large Lakes Observatory, University of Minnesota Duluth

² Department of Physics, University of Minnesota Duluth

Copyright 2014 by the Association for the Sciences of Limnology and Oceanography, Inc.

SUMMARY

To understand the nitrogen (N) cycle in sediments with shallow versus deep oxygen penetration, the work measured porewater profiles of N species and calculated diagenetic N fluxes and rates at 13 locations in Lake Superior, in 26 to 318 m water depth. The results reveal that sediments with high oxygen demand, such as in nearshore or high-sedimentation areas, contribute disproportionately to benthic nitrogen removal, despite covering only a small portion of the lake floor. These sediments are nitrate sinks (average $0.16 \text{ mmol m}^{-2} \text{ d}^{-1}$) and have denitrification rates (average $0.76 \text{ mmol m}^{-2} \text{ d}^{-1}$) that are comparable to those in coastal marine sediments. The deeply oxygenated (4 to >12 cm) offshore sediments are nitrate sources (average efflux $0.26 \text{ mmol m}^{-2} \text{ d}^{-1}$) and generate N_2 at lower rates (average $0.10 \text{ mmol m}^{-2} \text{ d}^{-1}$). Ammonium is nitrified with high efficiency (90%), and nitrification supports >50% of denitrification nearshore and ~100% offshore. About 2% of nitrate reduction is coupled to the oxidation of iron, a rarely detected pathway. Our revision of the Lake Superior N budget indicates significant contributions from sediment-water exchanges and N_2 production, and the updated budget is closer to balance than previous ones. Sediment nitrification is a major source of nitrate to the system (contributing 84% of nitrate inputs), suggesting that changes in sediment processes are the most likely cause of the increased nitrate concentrations in Lake Superior. Our results reveal that sediment nitrogen cycling in large freshwater lakes is similar to that in marine systems. They further suggest that denitrification rates in slowly accumulating well-oxygenated sediments cannot be described by the same relationship

with total oxygen uptake as in high-sedimentation areas, hence global models should treat the abyssal ocean sediments differently than coastal and shelf sediments.

INTRODUCTION

Transformations of nitrogen in aquatic sediments are an important part of the global nitrogen cycle. Sediments actively exchange the reactive nitrogen— nitrate and ammonium – with the water column and contribute to its recycling and removal, accounting for 50-70% of the denitrification in the global ocean (Codispoti et al. 2001). Denitrification (reductive conversion of nitrate to dinitrogen) and nitrification (oxidation of ammonium to nitrate) are the most commonly considered reactions in the sediment nitrogen cycle, though anammox (anaerobic oxidation of ammonium to N_2 with NO_2^- as the electron acceptor) is increasingly recognized as a significant pathway of nitrogen removal in marine sediments (Dalsgaard et al. 2005). As the reaction rates (Laursen and Seitzinger 2002) and sediment-water exchange fluxes of nitrogen in marine sediments are highly variable (Devol and Christensen 1993), for the purposes of the phenomenological descriptions and global N-cycle modeling sediments are often categorized based on water depth and environment: estuaries, bays, shelf and coastal oceans, deeper continental margins, and deep oceans (Middelburg et al. 1996; Fennel et al. 2009; Glud et al. 2009). To link the N transformation rates to commonly measured quantities, the rates of nitrification and denitrification have been correlated to sediment oxygen consumption, sedimentation rates, and water depth (Middelburg et al. 1996; Seitzinger et al. 2006). Whereas in marine environments such relationships have been described relatively well, nitrogen cycling in large freshwater lakes has received less attention.

Lake Superior, the world's largest lake by surface area, provides an opportunity to investigate the nitrogen cycle in a freshwater endmember system that in many respects is

similar to marine systems. Characterized by relatively low organic carbon content (3-5 wt%) and slow accumulation rates (*see* Chapter 2 and Kistner 2013), the offshore sediments of Lake Superior exhibit an exceptionally deep penetration of oxygen (3 to >16 cm in water depths between 120-300 m; *see* Chapter 2), typical of oceanic hemipelagic sediments in > 3000 m water depth (Glud 2008). The organic carbon mineralization rates and carbon burial efficiencies in these sediments are similar to those in the deep Ocean. The nitrogen dynamics in Lake Superior have been enigmatic (Sternner et al. 2007). Over the last century the lake experienced an unusual increase in water column nitrate concentrations, leading to an extreme N:P ratio of 10,000 (Guildford and Hecky 2000). The nitrate accumulation has been suggested to result at least partly from the ammonium oxidation in the lake (Finlay et al. 2007), and tentative links to sediment N cycling have been suggested (Finlay et al. 2013; Small et al. 2013). The sediments' role in the nitrogen cycling in Lake Superior is poorly quantified (Sternner et al. 2007; Li 2011; Small et al. 2013), with scarce geographical coverage and little information available on the rates of critical geochemical pathways, such as nitrification and denitrification. The sediments in Lake Superior exhibit strong temporal and spatial variability, with oxygen penetration varying seasonally by as much as 2 cm (*see* Chapter 1), especially at locations with deep oxygen penetration, and lateral heterogeneity on scales from tens to hundreds of meters (*see* Chapter 1). This variability complicates comparisons among different sediment cores and necessitates a large number of samplings to obtain representative averages, on the other hand also provide great opportunity for investigation of nitrogen cycling dynamics/variability and their controls.

This chapter reports the results from the multi-year multi-season investigation of the sediment nitrogen cycle in Lake Superior. We estimate the nitrate and ammonium fluxes across the sediment-water interface, calculate the rates of sediment nitrification and denitrification, and discuss the controls on the sedimentary nitrogen cycling in areas of both high and low sedimentation, nearshore and offshore. The sediment contributions to the reactive N recycling in Lake Superior are quantified and an updated geochemical budget for the lake is presented. Results are analyzed further to infer the trends in nitrogen cycling across sediments with different sedimentation rates and redox conditions, and compared to the phenomenological relationships suggested previously for the marine environments.

METHODS

Sediment sampling and analyses

Sediments and overlying waters were sampled across Lake Superior on multiple cruises aboard the R/V *Blue Heron* in 2009-2012 (Fig. 1.1; Table 1.1), and processed using the procedures described in Chapter 1. Pore waters were immediately extracted from the sediment sections in the N₂-filled glove bag using Rhizon porous polymer micro samplers (0.1 μm membrane pore size) (Dickens et al. 2007). The porewater samples for nitrate and ammonium analyses were frozen at -18°C until they were measured, and samples for the dissolved Fe(II) analyses were acidified with hydrochloric acid (1% of 6 mol L⁻¹ HCl) immediately after collection and stored at 4°C. Dissolved nitrate concentrations were measured in porewater and bottom water samples using colorimetric method (Grasshoff et al. 1999) on a Lachat Quickchem 8000 flow injection auto-analyzer. Ammonium concentrations were determined by Orthophthaldialdehyde (OPA) fluorometry (Holmes et al. 1999). Dissolved Fe(II) concentrations were determined spectrophotometrically with Ferrozine (Viollier et al. 2000).

Calculations of fluxes and rates

In addition to the diffusive and total oxygen fluxes described in Chapter 1, the molecular diffusion fluxes (F_i) of nitrate, ammonium and dissolved Fe²⁺ were also calculated using Fick's law of diffusion similar to Eq. 1.5

$$F_i = -\varphi D_s \frac{dC_i}{dx} \quad (2.1)$$

where x is depth below sediment-water interface, C_i is solute concentration (mol per porewater volume), φ is porosity, and $D_s = D/(1-\varphi^2)$, is the appropriate molecular diffusion coefficient corrected for sediment tortuosity (Boudreau 1997). At 4°C, the bulk molecular diffusion coefficients D_i are $D_{\text{NO}_3^-} = 349 \text{ cm}^2 \text{ yr}^{-1}$, $D_{\text{NH}_4^+} = 352 \text{ cm}^2 \text{ yr}^{-1}$, and $D_{\text{Fe}^{2+}} = 123 \text{ cm}^2 \text{ yr}^{-1}$ (Boudreau 1997). Porosity was determined as a function of depth within the sediment as shown in Chapter 1. Where concentration gradients near the sediment-water interface were poorly resolved, the diffusive fluxes across the interface were calculated using the measured porewater concentrations below the interface, the measured bulk bottom water concentrations and a boundary layer thickness of 1 cm (based on the 0.05 cm resolution oxygen profiles; *see* Chapter 1). For oxygen fluxes, the contributions from processes other than molecular diffusion, such as bioirrigation (Meile et al. 2005; Glud 2008), were estimated in Chapter 1 at 30-50% of the total sediment oxygen uptake. Assuming, for lack of information, a similar effect on the fluxes of other solutes, the total effluxes of NO_3^- and NH_4^+ may be up to 50% higher than the calculated diffusive fluxes. Bioturbation in Lake Superior is limited to the upper 2 cm of sediment (*see* Chapter 1), thus no contributions from benthic fauna are expected below this depth.

The geochemical reaction rates of solutes within the sediment were estimated from the measured vertical concentration profiles using the diagenetic reaction-diffusion equation (*see* Chapter 1, Eq 1.2; Boudreau 1997). At steady state (and neglecting solute advection and bioirrigation), the reaction rates are related to the diffusive transport as:

$$0 = \frac{d}{dx}(\varphi D_s \frac{dC_i}{dx}) + \sum_j R_{ij} \quad (2.2)$$

where R_j are the rates of individual reactions that affect the concentration of solute C_i (Table 2.1). Using the reaction stoichiometries in Table 2, the rate equations for porewater nitrate and ammonium, NO_3^- and NH_4^+ , can be written as:

$$\frac{d}{dx}(\varphi D_{s-\text{NO}_3} \frac{dC_{\text{NO}_3^-}}{dx}) + R_{\text{nitrif.}}(x) - R_{\text{ammonif.}}(x) - R_{\text{denitrif.}}(x) - R_{\text{anammox}}(x) = 0 \quad (2.3)$$

$$\frac{d}{dx}(\varphi D_{s-\text{NH}_4^+} \frac{dC_{\text{NH}_4^+}}{dx}) - R_{\text{nitrif.}}(x) + R_{\text{ammonif.}}(x) - R_{\text{anammox}}(x) + R_{\text{NH}_4^+ \text{ prod.}}(x) = 0 \quad (2.4)$$

Here $R_{\text{nitrif.}}$, $R_{\text{ammonif.}}$, $R_{\text{denitrif.}}$, and R_{anammox} are the rates of nitrification, nitrate ammonification (dissimilatory nitrate reduction to ammonium), denitrification, and anammox, as defined in Table 2.1 $R_{\text{NH}_4^+ \text{ prod.}}$ is the rate of ammonium production from organic nitrogen during the organic matter mineralization (Table 2.1).

Table 2. 1 Major reactions affecting nitrogen cycling in sediments

Processes		Rate
Aerobic respiration	$(\text{CH}_2\text{O})_x(\text{NH}_3)_y + x \text{O}_2 \rightarrow x \text{CO}_2 + y \text{NH}_3 + x \text{H}_2\text{O}$	$R_C = -x/y R_{\text{NH}_4^+ \text{ prod.}}$
Denitrification	$(\text{CH}_2\text{O})_x(\text{NH}_3)_y + 4x/5 \text{NO}_3^- \rightarrow x/5 \text{CO}_2 + 4x/5 \text{HCO}_3^- + 2x/5 \text{N}_2 + y \text{NH}_3 + x \text{H}_2\text{O}$	$R_C = 5/4 R_{\text{denitrif.}}$
Nitrification	$\text{NH}_4^+ + 2 \text{O}_2 + 2 \text{HCO}_3^- \rightarrow \text{NO}_3^- + 2 \text{CO}_2 + 3 \text{H}_2\text{O}$	$R_{\text{nitrif.}}$
¹ Nitrate ammonification	$\text{NO}_3^- + 8 e^- + 7 \text{H}_2\text{O} \rightarrow \text{NH}_4^+ + 10 \text{OH}^-$	$R_{\text{ammonif.}}$
Anammox	$\text{NH}_4^+ + \text{NO}_3^- \rightarrow \text{N}_2 + 2 \text{H}_2\text{O}$	R_{anammox}
Anaerobic Fe oxidation	$\text{Fe}^{2+} + \frac{1}{8} \text{NO}_3^- + \frac{7}{8} \text{H}_2\text{O} + \frac{7}{4} \text{OH}^- \rightarrow \frac{1}{8} \text{NH}_4^+ + \text{Fe}(\text{OH})_3$	$R_{\text{Fe}^{2+} \text{ oxidation}}$

Notes: ¹The listed half-reaction may be coupled with the oxidation of organic C, reduced Fe, or S (Hulth et al. 2005).

The rates of nitrification (Table 2.1) can be obtained in the oxic sediment zone from Eq. 2.3 by considering that the rates of ammonification, denitrification, and anammox ($R_{\text{ammonif.}}$, $R_{\text{denitrif.}}$, and R_{anammox}) are negligible at high O_2 concentrations ($> 6 \mu\text{mol L}^{-1}$; Seitzinger 1988; Dalsgaard et al. 2005):

$$R_{\text{nitrif.}}(x) = -\frac{d}{dx}(\varphi D_{\text{s-NO}_3} \frac{dC_{\text{NO}_3}}{dx}) \quad (2.5)$$

The exceptionally deep oxygenation of sediments in Lake Superior (Chapter 1, Fig. 1.6) thus allows the calculation of nitrification rates ($R_{\text{nitrif.}}$) from nitrate concentration profiles (Eq. 2.5). In surface sediment where bioirrigation may be important, Eq. 2.5 should be properly written as:

$$R_{\text{nitrif.}}(x) = -\frac{d}{dx}(\varphi D_{\text{s-NO}_3} \frac{dC_{\text{NO}_3}}{dx}) - \varphi \alpha_{\text{irr}} (C_{\text{NO}_3}^0 - C_{\text{NO}_3}^{\text{burr}}) \quad (2.6)$$

where C^0 and C^{burr} are the concentrations of nitrate, respectively, above the sediment surface and within the bioirrigated burrows, and α_{irr} is the bioirrigation coefficient (Katsev et al. 2007). For a typically concentration gradient for nitrate in Lake Superior ($C^0 - C^{\text{burr}} < 0$, see below), Eq. 2.5 yields the minimum nitrification rates and the actual rates could be higher. The area-specific (integrated over the sediment depth) nitrification rates ($\text{mmol m}^{-2} \text{d}^{-1}$) can be calculated by integrating Eq. 5 from the sediment-water interface (SWI; $x=0$) to the bottom of the nitrification zone L :

$$\begin{aligned} R_{\text{nitrif.}}^* &= \int_0^L R_{\text{nitrif.}}(x) dx = -\int_0^L \frac{d}{dx}(\varphi D_{\text{s-NO}_3} \frac{dC_{\text{NO}_3}}{dx}) dx \\ &= \left(\varphi D_{\text{s-NO}_3} \frac{dC_{\text{NO}_3}}{dx} \right)_{x=0} - \left(\varphi D_{\text{s-NO}_3} \frac{dC_{\text{NO}_3}}{dx} \right)_{x=L} = F_{\text{NO}_3(x=L)} - F_{\text{NO}_3(x=0)} \end{aligned} \quad (2.7)$$

Here $R_{\text{nitrif.}}^*$ is the depth-integrated nitrification rate, and $F_{\text{NO}_3^-}(x=0)$ and $F_{\text{NO}_3^-}(x=L)$ are the diffusive fluxes at the SWI and $x=L$, respectively. The depth L can be chosen at the depth within the oxygenated zone where $F_{\text{NO}_3^-}$ reaches a maximum (*see* Results for details).

The porewater nitrate can be removed through denitrification, anammox, or the dissimilatory nitrate reduction (DNR) to ammonium (ammonification) (Table 2.1; Hulth et al. 2005). The net rate of nitrate consumption, $-\Sigma R_{\text{NO}_3^-}$, by all three of these pathways can be described at steady state and neglecting bioirrigation (Eq. 2.2) as:

$$\Sigma R_{\text{NO}_3^-}(x) = -\frac{dF_{\text{NO}_3^-}}{dx} = \frac{d}{dx}(\varphi D_{s-\text{NO}_3^-} \frac{dC_{\text{NO}_3^-}}{dx}) \quad (2.8)$$

where $F_{\text{NO}_3^-}$ is the vertical flux of nitrate. By integrating Eq. 2.8 from L , the upper boundary of the zone of net nitrate reduction, to L^∞ , the depth where the nitrate gradients vanish, the depth-integrated rates of net nitrate consumption ($R_{\text{NO}_3^- \text{ cons.}}^*$) can be expressed as:

$$R_{\text{NO}_3^- \text{ cons.}}^* = -\int_L^{L^\infty} R_{\text{NO}_3^-}(x)dx = \left(\varphi D_{s-\text{NO}_3^-} \frac{dC_{\text{NO}_3^-}}{dx} \right) \Bigg|_{x=L}^{x=L^\infty} = F_{\text{NO}_3^-}(x=L) \quad (2.9)$$

where $F_{\text{NO}_3^-}(x=L)$ is the diffusive flux at L (i.e., the maximum downward flux; *see* below for details).

The rates of reactive nitrogen removal to N_2 by denitrification and anammox (Table 2.1) can be calculated by neglecting nitrification in anoxic sediment. Denitrification is typically the dominant pathway of nitrogen removal in freshwater (Hulth et al. 2005) but anammox was recently also found to be significant (Schubert et al.

2006; Zhu et al. 2013), including in Lake Superior (S. A. Crowe unpubl.), so anammox cannot be a priori neglected. By rearranging Eqs. 2.3 and 2.4, we obtain

$$\begin{aligned}
 R_{\text{N removal}} &= R_{\text{denitrif.}}(x) + 2R_{\text{anammox}}(x) \\
 &= \frac{d}{dx}(\varphi D_{\text{s-NH}_4^+} \frac{dC_{\text{NH}_4^+}}{dx}) + \frac{d}{dx}(\varphi D_{\text{s-NO}_3^-} \frac{dC_{\text{NO}_3^-}}{dx}) - R_{\text{NH}_4^+ \text{ prod.}}(x)
 \end{aligned} \tag{2.10}$$

Here, $R_{\text{NH}_4^+ \text{ prod.}}$ is the rate of ammonium production from organic nitrogen during organic matter mineralization. To calculate the area-specific rates of nitrogen removal, Eq. 2.8 can be integrated from SWI ($x=0$) to some maximum depth L^∞ where the concentrations of NO_3^- and NH_4^+ no longer vary with depth and their diffusive fluxes are negligible. The total nitrogen removal rate (Eq. 2.11) then can be calculated as a difference between the total ammonium production within the sediment and the NO_3^- and NH_4^+ fluxes out (negative) of the sediment:

$$\begin{aligned}
 R_{\text{N removal}}^* &= -\int_0^{L^\infty} R_{\text{denitrif.}}(x) dx + 2\int_0^{L^\infty} R_{\text{anammox}}(x) dx \\
 &= \left(\varphi D_{\text{s-NH}_4^+} \frac{dC_{\text{NH}_4^+}}{dx} \right) \Big|_{x=0}^{x=L^\infty} + \left(\varphi D_{\text{s-NO}_3^-} \frac{dC_{\text{NO}_3^-}}{dx} \right) \Big|_{x=0}^{x=L^\infty} + \int_0^{L^\infty} R_{\text{NH}_4^+ \text{ prod.}}(x) dx \\
 &= F_{\text{NO}_3^-(x=0)} + F_{\text{NH}_4^+(x=0)} + 1/12R_C^*
 \end{aligned} \tag{2.11}$$

The last term in Eq. 2.11 describes the production of ammonium from organic N, based on the C mineralization rate, R_C^* (Chapter 1, Table 1.2) and the C: N ratio of 12:1 in Lake Superior (Heinen and McManus 2004; Sterner 2008). In N-rich Lake Superior, the variation in the C:N ratio with depth in the sediment does not exhibit a clear pattern (Ostrom et al. 1998).

RESULTS

Nitrate in sediment porewaters

The porewater nitrate distributions (Fig. 2.1) at sites with deep OPDs exhibit peaks several mm below the sediment-water interface, a common feature in carbon-poor sediments (Coloway and Bender 1982; Burdige 2006) resulting from aerobic oxidation of ammonium (Middelburg 1996). The resultant increased concentrations in the surface sediments than the overlying waters indicate the diffusive fluxes of nitrate from sediments into the water column (Eq. 2.1). The nitrate concentrations below the peaks decrease into the anoxic sediment, indicating nitrate reduction (Table 2.1). Nitrate is typically exhausted within several cm of the OPD (Chapter 1, Fig. 1.6). In sediments with deep oxygen penetrations (e.g., >10 cm at Sta. EM and WM), the nitrate penetrations are also deep; in sediments with shallow OPDs (e.g., Sta. IR, NB, BB, and TB), the nitrate penetrations are shallow, typically less than 4 cm (Fig. 2.1). The nitrate concentrations at Sta. TB were negligible below the SWI (not shown), despite the $28.7 \mu\text{mol L}^{-1}$ concentration in the overlying water column.

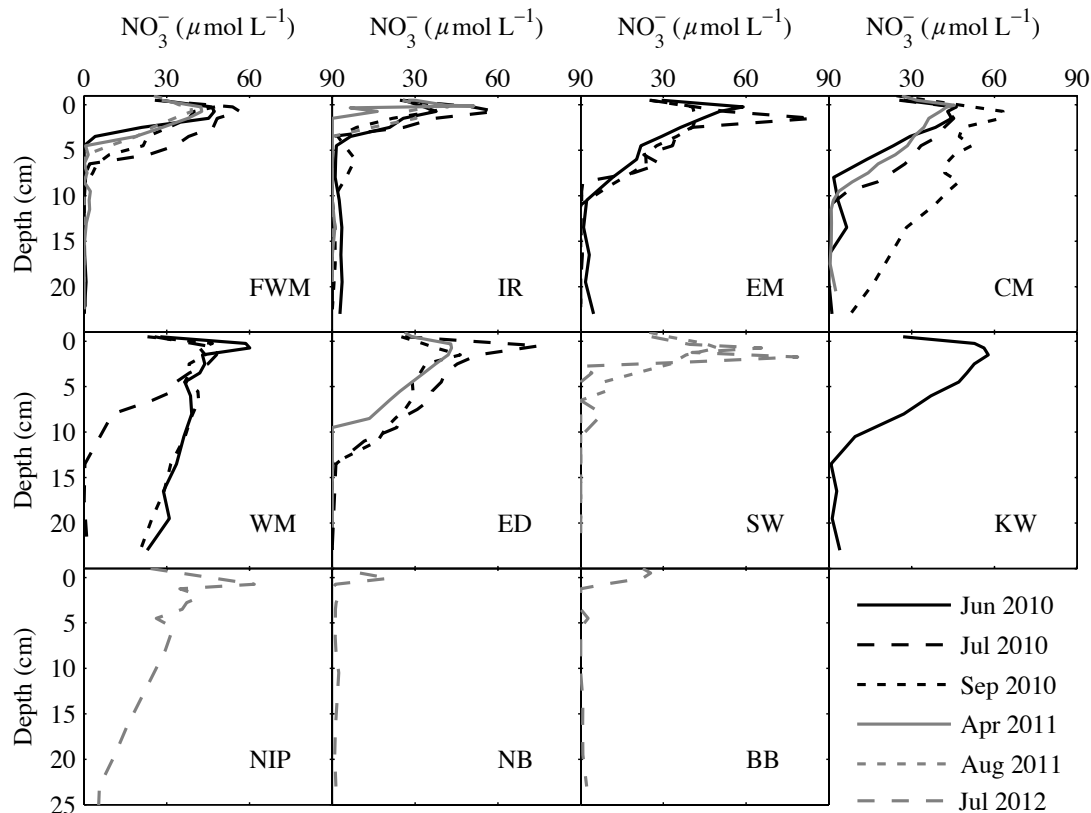


Figure 2. 1 Vertical distributions of porewater nitrate in Lake Superior sediments.

Ammonium in sediment porewaters

The concentrations of ammonium, which is produced during organic matter mineralization, increase with depth within the sediment at all stations (Fig. 2.2). The ammonium concentration gradients at the SWI indicate effluxes into the water column. The nitrate and ammonium profiles (Figs. 2.1, 2.2) exhibit high variability among samplings, consistent with the heterogeneity of the sediments (*see* Chapter 1). Though this variability precluded the detection of seasonal trends, the large number of profiles allowed the calculation of the average fluxes and rates (Table 2.2, 2.3 and 2.4).

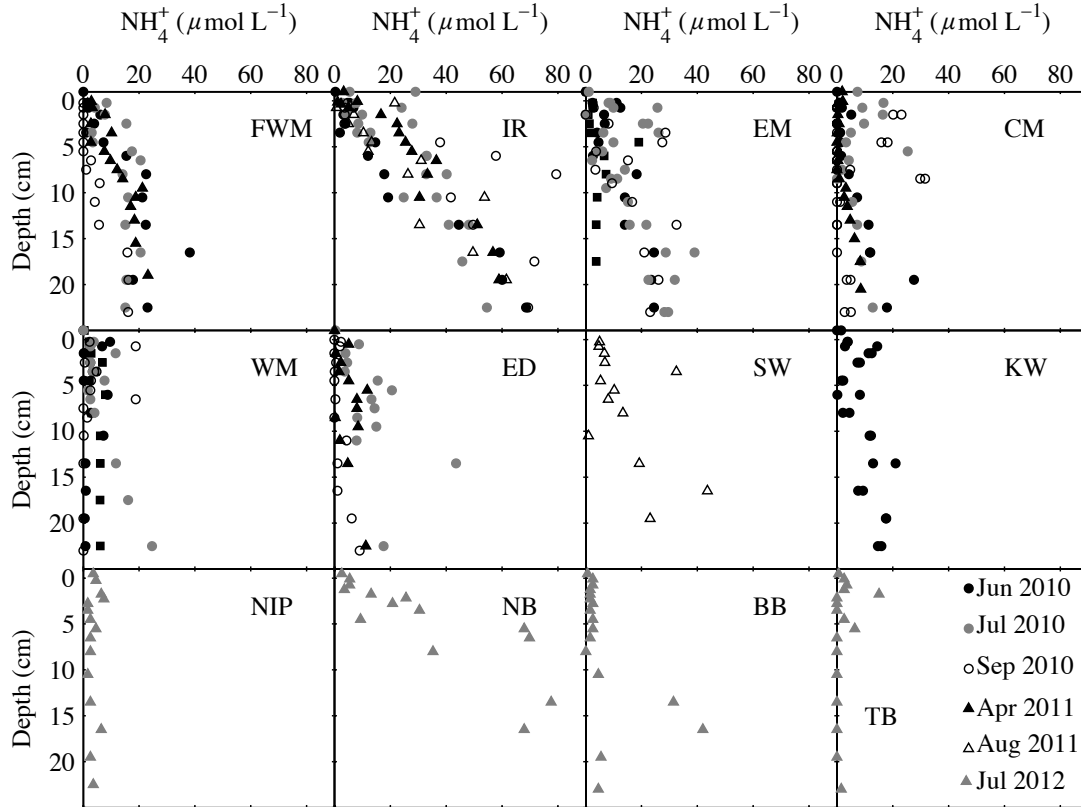


Figure 2.2 Vertical distributions of porewater ammonium in Lake Superior sediments

Dissolved Fe (II) in sediment porewaters

The concentrations of dissolved Fe^{2+} (Fig. 2.3) increase with depth below the OPD, suggesting iron reduction in the anoxic sediment and Fe^{2+} oxidation near the depth of oxygen penetration. In Lake Superior, prominent Fe- and Mn-rich sediment layers that result from metal oxidation are often visible to the naked eye (*see* optical images in Chapter 1 (Fig. 1.2) and scanning x-ray fluorescence profiles in later Chapter 3 (Fig. 3.2)). In cores where nitrate penetrated significantly below the OPD, Fe^{2+} appears in porewaters below the depth of nitrate penetration.

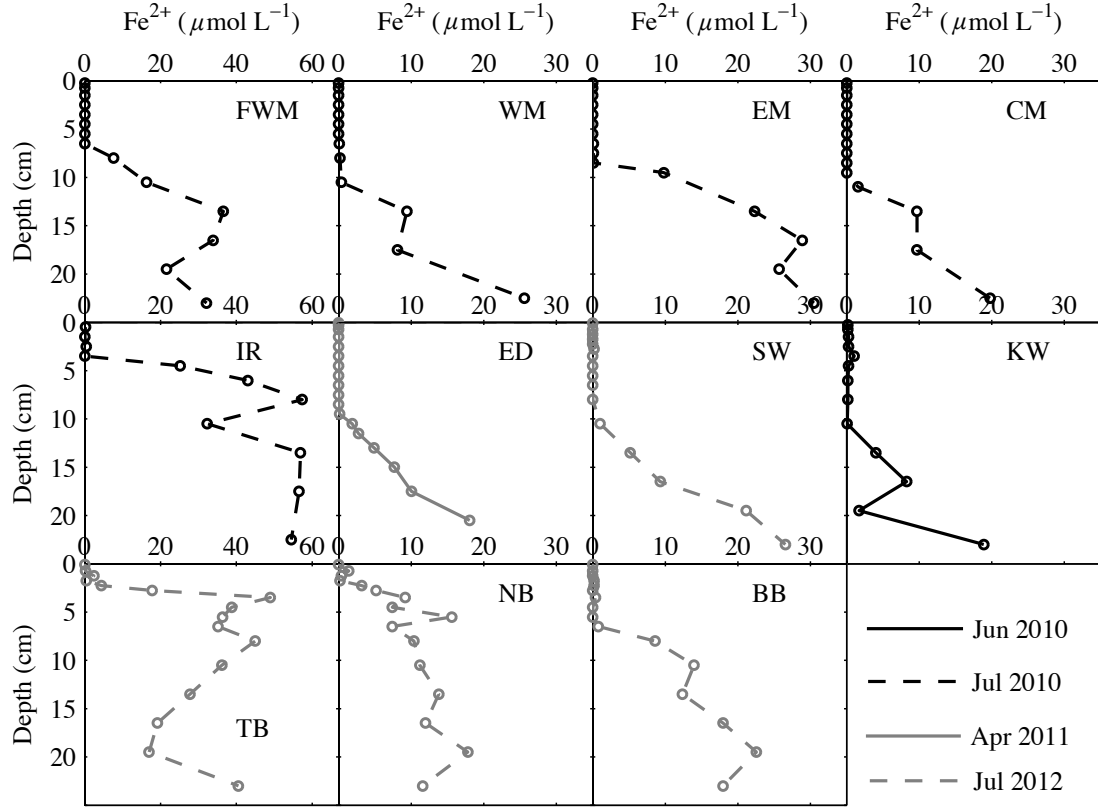


Figure 2. 3 Typical profiles of dissolved Fe(II) in sediments of Lake Superior. Scales are different amount stations.

Nitrate and ammonium fluxes across the sediment-water interface

Sediments with deep penetration of nitrate (> 3 cm; Fig. 2.1; Sta. FWM, EM, WM, CM, ED, SW, KW and NIP) were sources of nitrate to the overlying waters, with diffusive effluxes of 0.19 - 0.33 $\text{mmol m}^{-2} \text{d}^{-1}$ (Table 2.2). At Sta. NB where nitrate was depleted < 1 cm, the efflux was significantly lower, 0.076 $\text{mmol m}^{-2} \text{d}^{-1}$. At the enclosed-bay sites Sta. TB and BB, the diffusive fluxes were into the sediment, at 0.52 and 0.047 $\text{mmol m}^{-2} \text{d}^{-1}$, respectively. The effluxes of ammonium were small at all stations (0.0087 - 0.081 $\text{mmol m}^{-2} \text{d}^{-1}$; Table 2.2). Bioirrigation is expected to affect the nitrate and ammonium fluxes to a lesser degree than oxygen fluxes (30-50%; Chapter 1), as the

bioirrigation coefficients for nitrate and ammonium are lower (Meile et al. 2005) and the respective concentration gradients are weaker.

Table 2. 2 The diffusive fluxes of nitrate ($F_{NO_3^-}$) and ammonium ($F_{NH_4^+}$) across SWI (positive into the sediment)

Station	$F_{NO_3^-}$ (mmol m⁻² d⁻¹)	$F_{NH_4^+}$ (mmol m⁻² d⁻¹)
FWM.1	-0.11	-0.0091
FWM.3	-0.23	-0.017
FWM.4	-0.34	
FWM.5	-0.17; -0.29	0
FWM.6	-0.13; -0.10	
FWM.7	-0.10; -0.23	
Average	-0.19 ± 0.09	-0.0087 ± 0.0085
EM.1	-0.15	-0.024
EM.2	-0.27	
EM.3	-0.36	-0.13
EM.4	-0.20	-0.091
EM.5	-0.12; -0.16	-0.0087; -0.018
EM.6	-0.13	-0.029
Average	-0.20 ± 0.09	-0.050 ± 0.049
WM.1	-0.19	-0.020
WM.2	-0.28	
WM.3	-0.37	-0.11
WM.4	-0.17	-0.045; -0.022
WM.5	-0.17; -0.20	
Average	-0.23 ± 0.08	-0.049 ± 0.04
CM.1	-0.23	-0.019
CM.2	-0.24	-0.11
CM.3	-0.20	
CM.4	-0.22	
Average	-0.22 ± 0.02	-0.065 ± 0.06
†IR.1	-0.09	-0.034
†IR.2	-0.32	
†IR.3	-0.13; -0.15	0
†IR.4	-0.92; -0.54	
†IR.5	-0.07	
†IR.6	-0.91; -0.31	
Average	-0.38 ± 0.29	-0.017
ED.1	-0.44	-0.10; -0.061
ED.2	-0.11	

ED.3	-0.17; -0.44	
Average	-0.29 ± 0.17	-0.081 ± 0.027
SW.1	-0.15	
SW.2	-0.15; -0.58	-0.025
Average	-0.29 ± 0.15	-0.025
KW.1	-0.33	-0.030
Sta.2	-0.31	-0.036
†TB.1	0.52	-0.029
NIP.1	-0.27	-0.015
†NB.1	-0.076	-0.044
†BB.1	0.047	-0.029

Note: The stations with shallow oxygen penetration (termed ‘nearshore’) are indicated by ‘†’. All fluxes and integrated rates are in $\text{mmol m}^{-2} \text{d}^{-1}$.

Nitrification rates

The calculated nitrification rates (Fig. 2.4) indicated active nitrification in the upper 4 cm of sediment. The rates peaked 0.5-1.5 cm below the sediment-water interface, independently of the oxygen penetration depth. The maximum rates varied between 0.02 and $0.15 \mu\text{mol cm}^{-3} \text{d}^{-1}$ (Fig. 2.4). The nitrification rates decreased below 2 cm and became negligible below 4 cm at all locations. The depth-integrated nitrification rates (Table 2.3) ranged between 0.21 and $0.74 \text{mmol m}^{-2} \text{d}^{-1}$ (average $0.35 \text{mmol m}^{-2} \text{d}^{-1}$). The effect of bioirrigation on these integrated rates can be estimated by integrating the bioirrigation term in Eq. 6 over the bioturbated upper 2 cm of sediment. For a typical bioirrigation coefficient of $\alpha_{\text{irr}} < 10^{-6} \text{s}^{-1}$ (Matisoff and Wang 1998) and the nitrate concentration gradient of $C^0 - C^{\text{bur}} < 30 \mu\text{mol L}^{-1}$ (Fig. 2.1), bioirrigation should increase the nitrification rate by less than $0.05 \text{mmol m}^{-2} \text{d}^{-1}$, which is within the uncertainty (Table. 2.3).

Nitrate reduction rates

Nitrate reduction (by denitrification, anammox, and dissimilatory nitrate reduction to ammonium; Fig. 2.5) typically occurred 2-5 cm below the sediment surface in the high-sedimentation regions and below 3-7 cm in the low-sedimentation regions, within several centimeters of the OPD. Figure 2.5 shows the calculated vertical fluxes of nitrate, $F_{NO_3^-}$, and the net nitrate consumption rates $-\Sigma R_{NO_3^-}$ (Eq. 2.8) in two typical sediments. As the upper boundary of the nitrate reduction zone (L in Eq. 2.9) is below the bioturbation zone (Fig. 2.5), the calculated nitrate reduction rates are essentially unaffected by bioturbation and bioirrigation. The depth-integrated rates of nitrate consumption (Eq. 2.9) range between 0.032 and 0.24 $\text{mmol m}^{-2} \text{d}^{-1}$ (Table 2.3). They are lower in sediments with deep oxygen penetrations (0.032-0.12 $\text{mmol m}^{-2} \text{d}^{-1}$ at Sta. FWM, EM, WM, CM, KW, ED, average 0.080 $\text{mmol m}^{-2} \text{d}^{-1}$) and higher in sediments with shallower OPDs (0.18-0.24 $\text{mmol m}^{-2} \text{d}^{-1}$ at Sta. IR, NB, and BB, average 0.20 $\text{mmol m}^{-2} \text{d}^{-1}$).

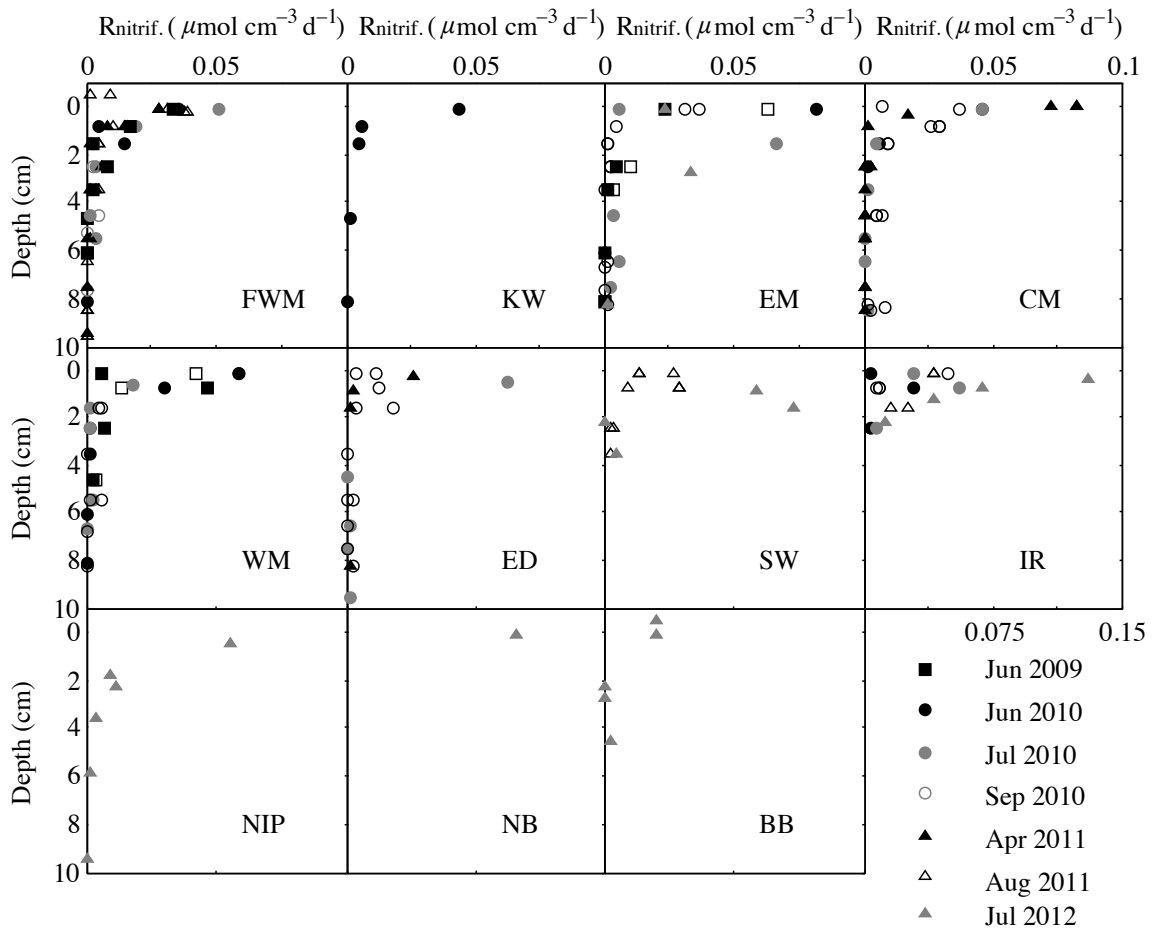


Figure 2. 4 Calculated rates of sediment nitrification

Table 2. 3 The depth-integrated rates of nitrification ($R^*_{\text{nitrif.}}$), the fraction of the total oxygen uptake (TOU; *see* Chapter 1 Table 1.2) consumed by nitrification ($R^*_{\text{nitrif.}}:\text{TOU}$), the integrated rates of nitrate consumption by denitrification and other pathways ($R^*_{\text{NO}_3^- \text{ cons.}}$), and the contribution of Fe oxidation ($R^*_{\text{Fe}^{2+}}$) to nitrate reduction. All fluxes and integrated rates are in $\text{mmol m}^{-2} \text{d}^{-1}$.

Station	$R^*_{\text{nitrif.}}$	$R^*_{\text{nitrif.}}:\text{TOU}$	$R^*_{\text{NO}_3^- \text{ cons.}}$	$R^*_{\text{NO}_3^- \text{ cons.}}:R^*_{\text{nitrif.}}$	$R^*_{\text{Fe}^{2+}}$	$R^*_{\text{Fe}^{2+}}:R^*_{\text{NO}_3^- \text{ cons.}}$
FWM.1	0.21		0.085			
FWM.3	0.39		0.15			
FWM.4	0.44		0.084			
FWM.6	0.27		0.088; 0.086			
FWM.7	0.21; 0.29; 0.27		0.092; 0.074; 0.061			
Average	0.28± 0.09	8.4%	0.090± 0.03	32%		
EM.2	0.39; 0.37		0.11; 0.091			
EM.3	0.51		0.14		0.0009	0.8%
EM.4	0.48		0.28			
EM.5	0.23; 0.31		0.034; 0.040		0.0022	5.5%
EM.6	0.29		0.15			
Average	0.37± 0.10	8.9%	0.12± 0.08	32%		
WM.1	0.33					
WM.2	0.35					
WM.3	0.56					
WM.4	0.21		0.036		0.0007	1.9%
WM.5	0.33					
Average	0.36± 0.08	16%	0.036± 0.015	10%		
CM.1	0.29		0.049			
CM.2	0.29		0.036			
CM.3	0.39; 0.26; 0.39		0.046; 0.087			
CM.4	0.33; 0.35		0.096; 0.060		0.0012	1.5%
Average	0.32± 0.05		0.066± 0.024	21%		

Table 2.3 Continued

Station	R* _{nitrif.}	R* _{nitrif.} :TOU	R* _{NO₃ cons.}	R* _{NO₃⁻ cons.:} R* _{nitrif.}	R* _{Fe²⁺}	R* _{Fe²⁺ cons.:} R* _{NO₃⁻ cons.}
†IR.1	0.21		0.11			
†IR.2	0.53		0.21			
†IR.3	0.36; 0.34; 0.36		0.14; 0.12; 0.14			
†IR.5	0.25		0.13			
†IR.6	0.74		0.42			
Average	0.40 ± 0.18	16%	0.18 ± 0.11	45%		
ED.1	0.63		0.17			
ED.2	0.18; 0.22		0.079; 0.061			
ED.3	0.21		0.045		0.0005	1.1%
Average	0.37 ± 0.20	9.6%	0.087 ± 0.055	28%		
SW.1	0.23; 0.27		0.066; 0.11		0.0004	0.9%
SW.2	0.61				0.0032	3.7%
Average	0.37 ± 0.16		0.088	24%		
KW.1	0.36		0.032	8.8%	0.0006	1.9%
NIP.1	0.62					
†NB.1	0.32		0.24	76%		
†BB.1	0.13		0.17	131%		

Note: The stations with shallow oxygen penetration (termed ‘nearshore’) are indicated by ‘†’. All fluxes and integrated rates are in mmol m⁻² d⁻¹.

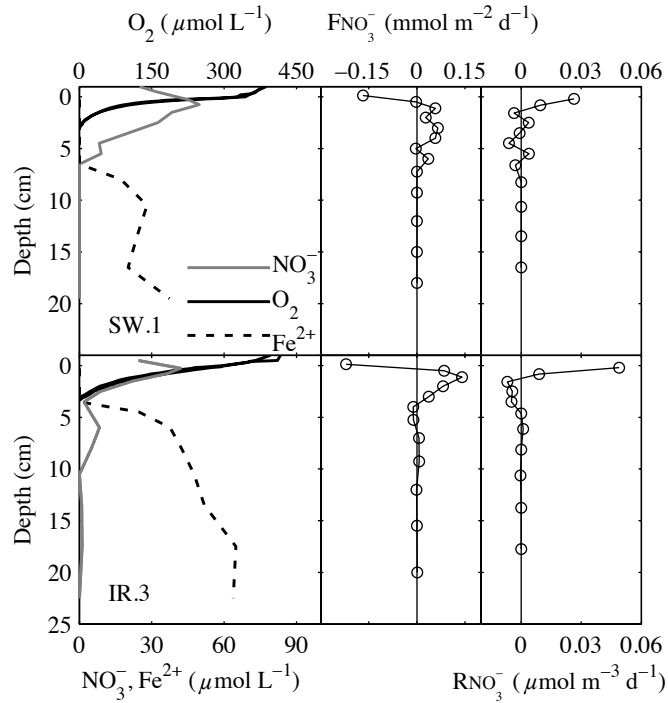


Figure 2. 5 (A) Typical distributions of dissolved Fe^{2+} , O_2 , and NO_3^- ; (B) the corresponding nitrate fluxes, $F_{NO_3^-}$ (negative if into the water column; Table 3); (C) the corresponding nitrate consumption rates $R_{NO_3^-}$ (positive for nitrate production). The depth L where $R_{NO_3^-}$ falls to zero and $F_{NO_3^-}$ reaches maximum separates the zones of net nitrate production (above) and consumption (below).

N_2 production rates

The calculated rates of N_2 production by denitrification and anammox (Table 2.1; Eq. 2.11) are presented in Table 2.4. At deeply oxygenated sites (Sta. EM, WM, CM, ED), the rates are small ($<0.05 \text{ mmol m}^{-2} \text{ d}^{-1}$). For example, at these rates, denitrification would account for less than 5% of the total organic carbon mineralization. In contrast, at the high-sedimentation sites with shallower OPDs (Sta. TB, BB, NB), the rates of the reactive nitrogen removal to N_2 (Eq. 2.11) are an order of magnitude higher ($>0.5 \text{ mmol}$

$\text{m}^{-2} \text{d}^{-1}$; Table 2.4). Denitrification at these rates would account for 12-31% of the total carbon mineralization. The calculated rates of N_2 production in Table 2.4 are only weakly sensitive to bioirrigation: based on Eq. 2.11, a conservatively estimated 100% uncertainty in the total fluxes of NO_3^- , NH_4^+ , and O_2 translates into a 30% uncertainty in the depth-integrated rates.

Table 2. 4 The rates of nitrogen removal to N_2 by denitrification and anammox ($R_{\text{N removal}}^*$; Eq. 2.11). The stations with shallow oxygen penetration (termed ‘nearshore’) are indicated by ‘†’. See Chapter 1 for the measured total oxygen uptakes (TOU); for locations (indicated by ‘*’), to account for bioirrigation, the total fluxes of NO_3^- , NH_4^+ , and O_2 were increased by 50% compared to diffusive fluxes.

Stations	Oxygen diffusive fluxes ($\text{mmol m}^{-2} \text{d}^{-1}$)	Total oxygen uptake, TOU ($\text{mmol m}^{-2} \text{d}^{-1}$)	Nitrogen removal to N_2 ($\text{mmol m}^{-2} \text{d}^{-1}$)	Organic C mineralized by denitrification
FWM	3.0 (1.1 -7.8)	6.7	0.19 ± 0.01	<4%
EM	2.9 (1.3 – 4.6)	4.4*	0.031 ± 0.06	<2%
WM	2.2 (1.1 – 3.2)	4.4	0.029 ± 0.024	<2%
CM	3.2 (2.3 – 3.8)	4.8*	<0.035	<1%
†IR	5.0 (2.7 – 7.3)	4.9	0.26 ± 0.05	<8%
ED	4.2 (2.7 – 6.8)	6.3*	<0.049	<1%
SW	4.9 (3.9-6.5)	7.4*	0.25 ± 0.03	<5%
†TB	5.1 (4.4, 5.8)	7.7*	1.4 ± 0.1	<31%
†BB	7.1 (8.7, 5.4)	11*	0.84 ± 0.06	<16%
†NB	6.4 (6.8, 5.9)	10*	0.54 ± 0.04	<12%

DISCUSSION

The reactions in the sediment nitrogen cycle are tightly coupled (Table 2.1). Organic matter mineralization mobilizes organic N as ammonium, which subsequently can be oxidized to either nitrate (nitrification) or N₂ (anammox). The produced nitrate is used in denitrification to oxidize organic carbon and is reduced in the process to N₂ (Hulth et al. 2005). The porewater nitrate and ammonium may be exchanged with the water column, thus recycling the reactive nitrogen into the ecosystem, whereas the unmineralized fraction of organic nitrogen may be buried into the deep sediment. Below these processes are analyzed in more detail, identify the trends in their rates, and used them to compile geochemical budgets.

Nitrification

Nitrification is a major biogeochemical pathway that transforms ammonium to nitrate. Besides the calculation method based on Eq. 2.7, the gross rate of ammonium production can be estimated from the total sediment oxygen uptake ($\sim 6.1 \text{ mmol m}^{-2} \text{ d}^{-1}$ offshore; *see* Chapter 1). As 1 mol of O₂ is needed to oxidize 1 mol of organic carbon and 2 mols of O₂ are needed to oxidize 1 mol of NH₄⁺ (Table 2), the 12C:1N:14O₂ stoichiometry of the organic matter oxidation leads to a gross ammonium production rate of approximately $6.1/14 = 0.44 \text{ mmol m}^{-2} \text{ d}^{-1}$. Subtracting the previously calculated average efflux of ammonium ($0.045 \text{ mmol m}^{-2} \text{ d}^{-1}$; Table 3) yields an ammonium oxidation rate that closely matches the nitrification rates calculated from Eq. 5 ($0.28\text{-}0.40 \text{ mmol m}^{-2} \text{ d}^{-1}$; Table 2.3). These in situ rates are about an order of magnitude lower than the potential rates (Small et al. 2013) determined in sediment slurries amended with

ammonium ($1.5\text{--}6.5\text{ mmol m}^{-2}\text{ d}^{-1}$ nearshore and $38\text{ mmol m}^{-2}\text{ d}^{-1}$ offshore; Stark 2009). The mismatch suggests that in the well-oxygenated sediments of Lake Superior nitrification is limited by the availability of ammonium (Rysgaard et al. 1994), thus the potential rates may strongly exceed the in situ rates.

The efficiency of ammonium oxidation is high: a ratio of the ammonium efflux ($0.045\text{ mmol m}^{-2}\text{ d}^{-1}$) to ammonium production ($0.44\text{ mmol m}^{-2}\text{ d}^{-1}$) yields $1 - (0.045/0.44) = 90\%$. Despite this, in Lake Superior, nitrification accounts for only 9-16% (average 12%) of the total sediment oxygen uptake (Table 2.3), which is a noticeably smaller fraction than in marine sediments: 35% in the coastal regions (Seitzinger et al. 1984), 21% on the continental shelf (Laursen and Seitzinger 2002), and 21-45% on the continental slope and abyssal plains (Christensen and Rowe 1984). The reason seems to be the higher C:N ratio in the organic material in Lake Superior (11 to 13; Heinen and McManus 2004; Sterner et al. 2008). For the organic matter oxidation stoichiometry above, a complete oxidation of the produced ammonium should consume $2 \times 1 / (12 + 2) = 14\%$ of the total O_2 flux (which matches our result), as opposed to 23% for the Redfield ratio of 6.6.

Nitrate reduction and N_2 production

Sediment nitrate can be removed through denitrification, anammox, or dissimilatory nitrate reduction (DNR) to ammonium (ammonification) (Table 2.1; Hulth et al. 2005). Ammonification recycles nitrate to ammonium whereas denitrification and anammox remove the reactive nitrogen from the system by converting it to N_2 . The

calculated nitrate reduction rates (Table 2.3) indicate that in Lake Superior these processes remove between 9% and 100% of the nitrate produced by nitrification. The rest escapes the sediment in the form of nitrate effluxes, which are significantly higher in the deeply oxygenated offshore sediments (Table 2.2) where they remove between 44% and 91% of the produced nitrate. Accordingly, the efficiency of nitrate removal is lower at the sites with deep OPDs (e.g., 8.8% at Sta. KW and 32% at Sta. FWM and EM) and higher at sites with shallower OPDs (45% at Sta. IR, 76% at Sta. NB, and 100% at Sta. BB). Similarly, the overall rates of N_2 production by denitrification and anammox are higher in sediments characterized by high sedimentation and shallow oxygen penetrations, such as the nearshore sites Sta. BB, NB, TB, and IR (0.26-1.4, average 0.76 $\text{mmol m}^{-2} \text{d}^{-1}$; Table 2.4), than in sediments at the low-sedimentation offshore sites (0.029-0.25, average 0.10 $\text{mmol m}^{-2} \text{d}^{-1}$). These calculated rates of N_2 production are similar to the ones reported in Lake Superior by Small et al. (2013). At high-sedimentation sites, the nitrate for denitrification (and anammox) is supplied by both nitrification (average about 50%; Table 2.3, Table 2.4) and nitrate fluxes (50%) from the water column (average 0.16 $\text{mmol m}^{-2} \text{d}^{-1}$; Table 2.2). At the low-sedimentation offshore sites, nitrification in the oxic sediment layer is the only source of nitrate for the deeper anoxic sediment and thus an important control on the rates of reactive nitrogen removal. This parallels the situation in marine sediments (Seitzinger 1988) where nitrification supports between 60 and 100% of the total denitrification in the continental shelf sediments (Devol et al. 1997; Laursen and Seitzinger, 2002).

Nitrate reduction coupled to iron oxidation

Studies have suggested that nitrate reduction may be coupled to the oxidation of reduced Fe (Straub et al. 1996; Benz et al. 1998): in pelagic marine sediments, ferrous iron (Fe^{2+}) often appears in porewater only below the depth of nitrate penetration (Burdige 1993). At several of our sites, the depth of iron oxidation coincided with the penetration depth of nitrate (NPD) rather than oxygen. For example, at Sta. EM, CM and SW, nitrate penetrated 3 cm deeper than oxygen, and Fe^{2+} appeared only below the depth of nitrate penetration (Figs. 2.1, 2.3, 2.5, and Fig 1.6 in Chapter 1). This suggests that in Lake Superior nitrate reduction is at least partially coupled to Fe^{2+} oxidation. The depth-integrated iron oxidation rates can be estimated from the Fe^{2+} fluxes immediately below the oxidation depth (L'):

$$R_{\text{Fe}^{2+} \text{ oxidation}}^* = - \left(\varphi D_{\text{s-Fe}^{2+}} \frac{dC_{\text{Fe}^{2+}}}{dx} \right)_{x=L'} \quad (2.12)$$

At sites where the OPD and NPD are clearly separated (Sta. EM, CM, SW), the calculated rates and the reaction stoichiometry $1/8R_{\text{Fe}^{2+} \text{ oxidation}} = R_{\text{NO}_3^-}$ (Table 2.1) suggest that the DNR coupled to iron oxidation accounts for <2.2% of the total nitrate consumption (Table 2.3). At the locations where the OPD, NPD, and the depth of iron oxidation overlap (Fig. 2.5), the reduced iron is likely oxidized predominantly by O_2 , as oxygen is a more favorable electron acceptor.

Sediment contribution to the nitrogen budget in Lake Superior

The nitrogen budget in Lake Superior has recently attracted attention (Finlay et al. 2007; Sterner et al. 2007; Small et al. 2013), as it appeared imbalanced (Sterner et al.

2007; Li 2011), with inputs of nitrogen exceeding outputs. Previous studies quantified the total nitrogen inputs into the lake with the direct precipitation, tributary inflows, and outflows (Sterner et al. 2007), but sediment contributions remained unclear (Li 2011). Some of the sediment fluxes were quantified in the coastal regions of the lake and denitrification rates were estimated (at 0 -0.04 mmol m⁻² d⁻¹) near the Keweenaw Peninsula (Carlton et al. 1989), but few measurements existed for the offshore regions (Heinen and McManus 2004; Stark 2009). Although recent efforts (Small et al. 2013) provided more information, the contributions to the lake-wide nitrogen budget from processes such as sediment denitrification and anammox, permanent burial of organic nitrogen, and nitrogen exchanges in the potential hotspots of denitrification, such as enclosed bays, remain insufficiently quantified.

Tables 2.5 and 2.6 show the updated Lake Superior total nitrogen and nitrate budgets, respectively, which include our results for the sediment-water exchanges, sedimentary removal of reactive nitrogen to N₂, and burial of organic nitrogen. The results reveal that, similarly to the situation in the global ocean where coastal sediments contribute disproportionately to N cycling and removal (Dalsgaard et al. 2005), the N cycle in Lake Superior needs to be considered separately for the areas of high and low sedimentation. Figure 2.6 compares the deeply oxygenated sediments in low-sedimentation regions, typically offshore, to the typical sediments with shallow OPDs. The disparity in the N₂ production rates indicates that the offshore-type sediments, while covering most of the lake floor (90% as an estimate, actual numbers are unknown; *see* sensitivity analyses below (Tables 2.5 and 2.6)), may account for a disproportionately

small fraction (46%) of the total benthic nitrogen removal to N_2 . In contrast, the nearshore-type sediments, while representing 10% of the lake floor area, may account for 54% of the nitrogen removal. For comparison, in the Global Ocean the continental margin sediments in <150 m water depth, while accounting for less than 20% of the ocean floor area, contribute 50% to the benthic N_2 production (Dalsgaard et al. 2005).

Table 2. 5 The nitrogen budget in Lake Superior. Contributions from this work are in italics; all others are from Sterner et al. 2007. All fluxes and rates are area-specific ($\mu\text{mol m}^{-2} \text{d}^{-1}$); the surface area of Lake Superior is 82,100 km^2 . Positive fluxes are into the reservoir of interests, e.g., sediment or water column.

Sources or sink	Contribution to N budget		
	Water Column	Sediment	Entire Lake
Atmospheric deposition (NO_3^- and NH_4^+)	82		82
Watershed input (NO_3^- , NH_4^+ and organic N)	90		90
N fixation	Unknown		
Outflow (NO_3^- , NH_4^+ and organic N)	-78		-78
	Offshore (90% area)	Nearshore (10% area)	Weighted average
Organic N sedimentation	470	650	-490
Organic N burial	54	78	-56
NO_3^- flux at SWI	-270	160	227
NH_4^+ flux at SWI	-45	-27	43
DON flux at SWI		Unknown	Unknown
Removal to N_2 by denitrification/anammox	100	760	-170
Total input			442
Total output			-568
Imbalance			-172 ~ -187

Note on Sensitivity Analysis: The range of imbalance represents the variation by varying the extent of the nearshore areas, from 10% to 20% of lake floor area as nearshore vs. 90% to 80% area as offshore. The imbalance for N budget for both the water column and entire lake is lower, accounting for non-depositional areas in the lake (Kemp et al. 1978): assuming 10% of the nearshore lake floor and 30% of the offshore lake floor are non-depositional, the imbalance of total nitrogen for the water column decrease to $-74 \mu\text{mol m}^{-2} \text{d}^{-1}$ and the imbalance for entire lake decreases to $-78 \mu\text{mol m}^{-2} \text{d}^{-1}$.

Table 2. 6 The nitrate budget in Lake Superior. Contributions from this work are in italic; all others are from Sterner et al. 2007. All fluxes and rates are area-specific ($\mu\text{mol m}^{-2} \text{d}^{-1}$); the surface area of Lake Superior is 82,100 km^2 ; Positive fluxes are into the reservoir of interests, e.g., sediment or water column.

Sources or sink	Contribution to N budget		
	Water Column	Sediment	Entire Lake
Atmospheric deposition	47		47
Watershed input (runoff and groundwater)	19		19
Nitrification	Unknown		
Biological uptake	Unknown		
Outflow	-61		-61
	Offshore (90% area)	Nearshore (10% area)	Weighted average
Nitrification	<i>350</i>	<i>370</i>	<i>350</i>
NO_3^- flux at SWI	-270	160	227
Removal to N_2 or NH_4^+	74	200	-87
Total input			293
Total output			-61
Imbalance			232

Note on Sensitivity Analysis: increasing the nearshore areas by 100% (20% area nearshore vs. 80% area offshore) does not affect the nitrate budget balance for the entire lake significantly ($< 3\%$; new imbalance 256 $\mu\text{mol m}^{-2} \text{d}^{-1}$). This decreases the nitrate input into the water column from sediments and increases the nitrate output for the sediments, leading to less imbalance in the water column nitrate budget (new imbalance 189 $\mu\text{mol m}^{-2} \text{d}^{-1}$). The imbalance for both the water column and entire lake is lower when accounting for the non-depositional areas in the lake (Kemp et al. 1978): assuming 10% of the nearshore lake floor and 30% of the offshore lake floor are non-depositional, the imbalance of nitrate for the water column decrease to 161 $\mu\text{mol m}^{-2} \text{d}^{-1}$ and imbalance of nitrate for the entire lake decreases to 194 $\mu\text{mol m}^{-2} \text{d}^{-1}$.

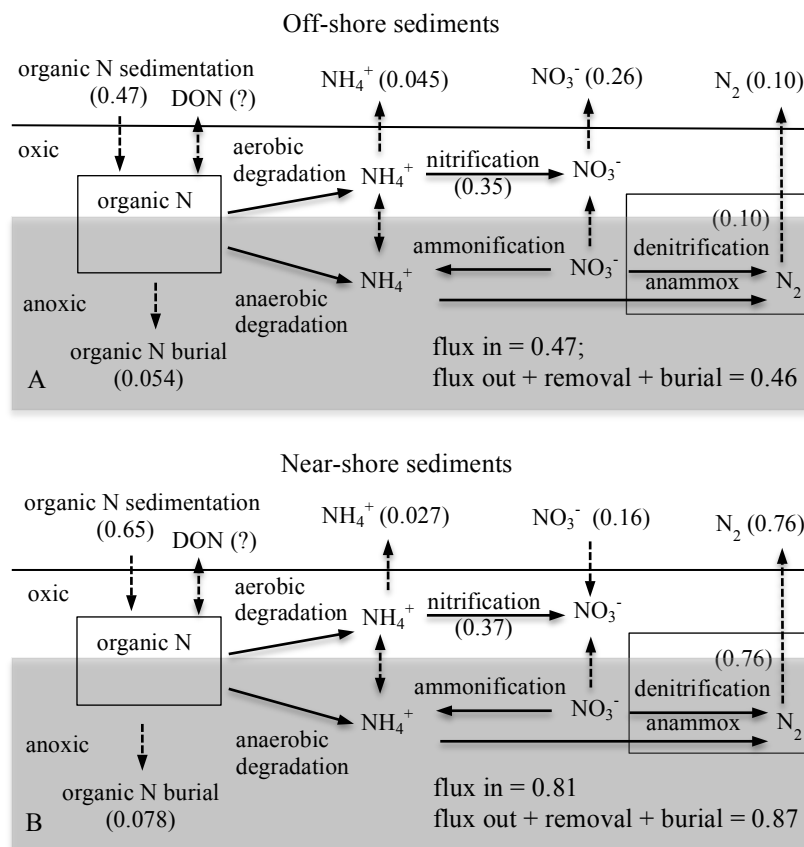


Figure 2. 6 Nitrogen cycling in Lake Superior sediments: (A) in low-sedimentation areas with deep oxygen penetration (Sta. FWM, EM, WM, CM, SW, ED, NIP); (B) in high-sedimentation areas with shallow oxygen penetrations (Sta. IR, TB, BB, NB). All fluxes and integrated rates are in $\text{mmol N m}^{-2} \text{d}^{-1}$. Horizontal solid lines indicate the SWI; solid arrows indicate diagenetic reactions; dashed arrows indicate sedimentation and diffusion fluxes. The values are averages from Tables 2.2, 2.3 and 2.4. The organic nitrogen fluxes are discussed in the text.

Our calculated effluxes of nitrate for the offshore stations (0.19-0.33, average 0.27 mmol m⁻² d⁻¹) are higher than the previous estimates in Lake Superior (0.15 mmol m⁻² d⁻¹; Heinen and McManus, 2004) and significantly higher than the recent estimate of 0.031 mmol m⁻² d⁻¹ by Small et al. (2013) who worked closer to shore. For the average nearshore flux of nitrate into the sediments of 0.16 mmol m⁻² d⁻¹ (Fig. 2.6), the lake-average nitrate efflux is into the water column at 0.23 mmol m⁻² d⁻¹. The effluxes of ammonium are small at all locations (average 0.042 mmol m⁻² d⁻¹). The dissolved organic nitrogen (DON) fluxes are poorly constrained (0.34± 0.31 mmol m⁻² d⁻¹ by Stark (2009) and 0.059± 0.173 mmol m⁻² d⁻¹ by Small et al. (2013)). In marine sediments, DON fluxes are typically small, less than 5% of the fluxes of inorganic nitrogen (NO₃⁻ and NH₄⁺) (Devol and Christensen, 1993; Burdige and Zheng, 1998). Based on the DON flux estimates in Lake Superior (Stark 2009; Small et al. 2013), the fluxes of inorganic nitrogen (nitrate and ammonium) from the sediments account for 24 to 61% of the total nitrogen inputs into the water column of Lake Superior (Table 2.5).

The burial of organic nitrogen into the deep offshore sediments is estimated at 0.054 mmol N m⁻² d⁻¹, based on the organic carbon burial rate of 0.7 mmol m⁻² d⁻¹ (*see* Chapter 1) and a 12 C:1N stoichiometry (Stark 2009). The burial rate in the nearshore sediments is only slightly higher: 0.078 mmol N m⁻² d⁻¹. (This estimate is based on the organic carbon burial rate of 0.51 -1.52 mmol m⁻² d⁻¹ (average 1.07 mmol m⁻² d⁻¹) in the nearshore-type sediments (*see* Chapter 1). This yields the average lake-wide burial of nitrogen of ~0.056 mmol N m⁻² d⁻¹. This is comparable to the loss of nitrogen from the lake with the outflow (0.078 mmol m⁻² d⁻¹) and corresponds to 33% of the estimated combined inputs of total nitrogen from the atmosphere and watershed (the nitrogen

fixation rate is not known; Sterner et al. 2007). The sediment contributions to the total nitrogen budget in Lake Superior are thus significant and need to be considered.

For the water column of the lake, the total nitrogen losses ($0.57 \text{ mmol m}^{-2} \text{ d}^{-1}$) exceed the total nitrogen inputs ($0.44 \text{ mmol m}^{-2} \text{ d}^{-1}$; Table 2.5). The difference of $0.13 \text{ mmol m}^{-2} \text{ d}^{-1}$ may be attributable to the uncertainties in the budget numbers, unquantified contributions, such as from nitrogen fixation and DON fluxes, and the existence of non-depositional areas (Kemp et al. 1978). The total nitrogen budget for the sediment column appears to be nearly balanced (Fig. 2.6; Table 2.5): the present-day net flux of N across the SWI matches the long-term burial flux. The sediments of Lake Superior, being sources of inorganic nitrogen to the water column, are therefore sinks for total nitrogen: they remove nitrogen as N_2 and bury the non-reactive organic N. These two nitrogen sinks account for 73% of the total nitrogen removal in the lake. The total nitrogen losses ($0.31 \text{ mmol m}^{-2} \text{ d}^{-1}$) for the entire lake (Table 2.5) exceed the total nitrogen inputs ($0.17 \text{ mmol m}^{-2} \text{ d}^{-1}$). This budget is closer to balance than the previous one (Sterner et al. 2007) where inputs outweighed losses even without the contribution from nitrogen fixation.

The increase in nitrate concentrations in the lake can likely be attributed to the sediment processes. For the nitrate budget of the entire lake (both water column and sediments), the nitrate inputs ($0.42 \text{ mmol m}^{-2} \text{ d}^{-1}$) exceed the total nitrate output ($0.15 \text{ mmol m}^{-2} \text{ d}^{-1}$; Table 2.6), with sediment nitrification contributing 84% of all nitrate inputs. For the water column budget, the nitrate inputs ($0.29 \text{ mmol m}^{-2} \text{ d}^{-1}$) still exceed the total nitrate outputs ($0.061 \text{ mmol m}^{-2} \text{ d}^{-1}$; Table 2.6), with the sediment nitrate effluxes contributing 77% of the inputs. The imbalance of $0.23 \text{ mmol m}^{-2} \text{ d}^{-1}$ (Inputs - outputs) could lead to a nitrate increase of $\sim 30 \mu\text{mol L}^{-1}$ over 60 years (measured ~ 20

$\mu\text{mol L}^{-1}$). This suggests that changes in the nitrification-driven nitrate effluxes from sediments are the most likely factor that could cause increases in the nitrate levels in Lake Superior.

Implications for marine sediments

In marine environments, the sediment nitrogen cycle is often discussed based on water depth, with coastal and abyssal sediments as endmembers (Middelburg 1996). In water depths similar to those in Lake Superior (0-200 m), marine sediments are typically nitrate sinks where nitrate moves from the water column into the sediment (Fig. 2.7A). In Lake Superior this is the case only for the locations with relatively high sedimentation rates, typically near shore. The rates of nitrogen removal in these sediments are comparable to those in coastal marine environments (Fig. 2.7C), with denitrification accounting for 10-20% of the organic carbon mineralization (Fig. 9D; Table 2.4). The offshore sediments in Lake Superior, however, are more analogous to the oceanic hemipelagic and pelagic sediments than to coastal sediments. Where oxygen penetrates deeply (3 to > 15 cm) and sedimentation rates are low ($\sim 0.01 \text{ g cm}^{-2} \text{ yr}^{-1}$; *see* Chapter 1), the nitrate effluxes and removal rates (Tables 2.2, 2.3 and 2.4) are similar to those in the marine sediments in ~ 3000 m of water. Denitrification accounts for only <5 % of the organic carbon mineralization (Fig. 2.7C). The effluxes of ammonium in Lake Superior are lower than in marine sediments in similar water depths (Fig. 2.7B) but comparable to those in the deeply oxygenated carbon-poor sediments of the deep ocean (>3000 m). This suggests that the categorization of sediments based on oxygen penetration (or sedimentation rate, which is a correlated quantity; *see* Chapter 1), is more appropriate

than the one based on water depth. The importance of oxygen penetration can be seen in other lakes as well: for example, the well-oxygenated sediments in Lake Michigan (OPD > 2 cm; Thomsen et al. 2004) are nitrate sources to the water column and have lower denitrification rates than the shallowly oxygenated sediments in Lake Zug (OPD < 0.2 cm; Maerki et al. 2009) that are nitrate sinks (Fig. 2.7A). Figure 2.8 A shows the negative correlation between the OPD and the rates of nitrogen removal for the sediments of lakes Superior, Michigan, and Baikal, and in the deep continental margins (~ 1500 m). The rates of nitrogen removal decrease with oxygen penetration, as longer oxygen exposure times leave less reactive carbon for denitrification. Extrapolate this relationship (Fig. 2.8A) to the deep Ocean sediments using their OPDs (Glud 2008) allows estimating the rates of denitrification (Fig. 2.8B) there. The calculated denitrification rates in the deep ocean sediments are consistent with those estimated in previous studies (Middelburg et al. 1996).

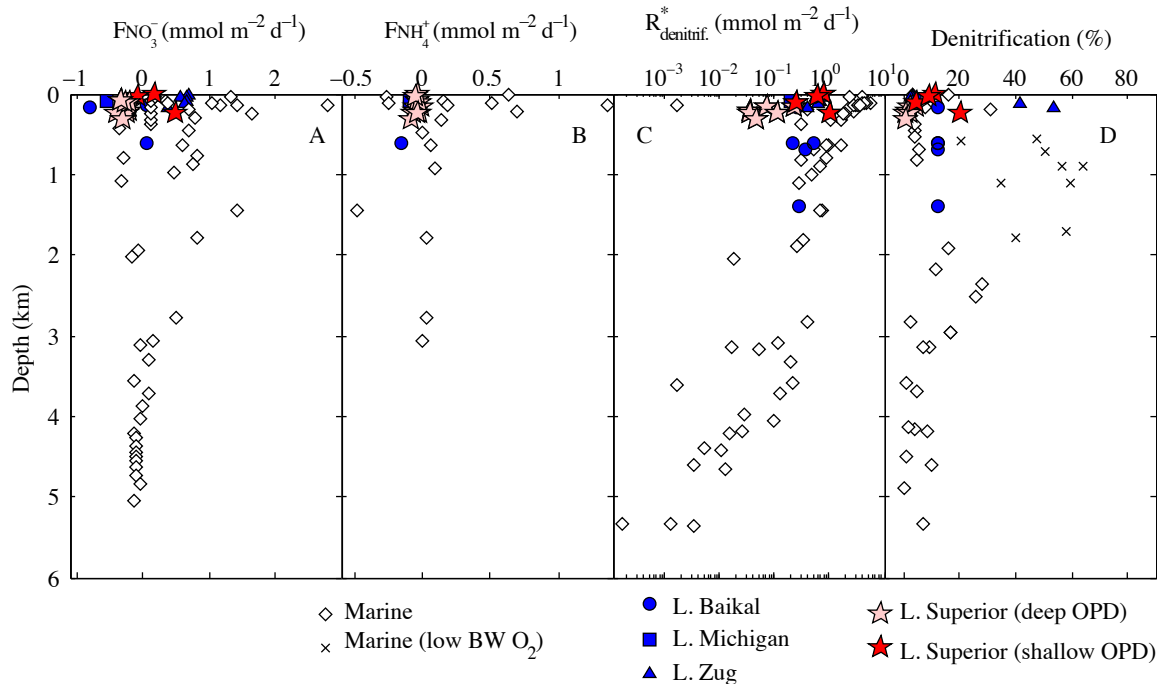


Figure 2. 7 (A, B) Fluxes of nitrate and ammonium across the SWI, (C) sediment denitrification rates, and (D) percent of deposited organic carbon mineralized by denitrification, organized by water depth. The data are from Lake Superior (this study), Lake Baikal (Maerki et al. 2006), Lake Michigan (Thomsen et al. 2004), Lake Zug (Maerki et al. 2009), and marine sediments (Devol and Christensen 1993; Middelburg et al. 1996; Burdige 2006; Glud et al. 2009). BW O_2 – bottom water O_2 .

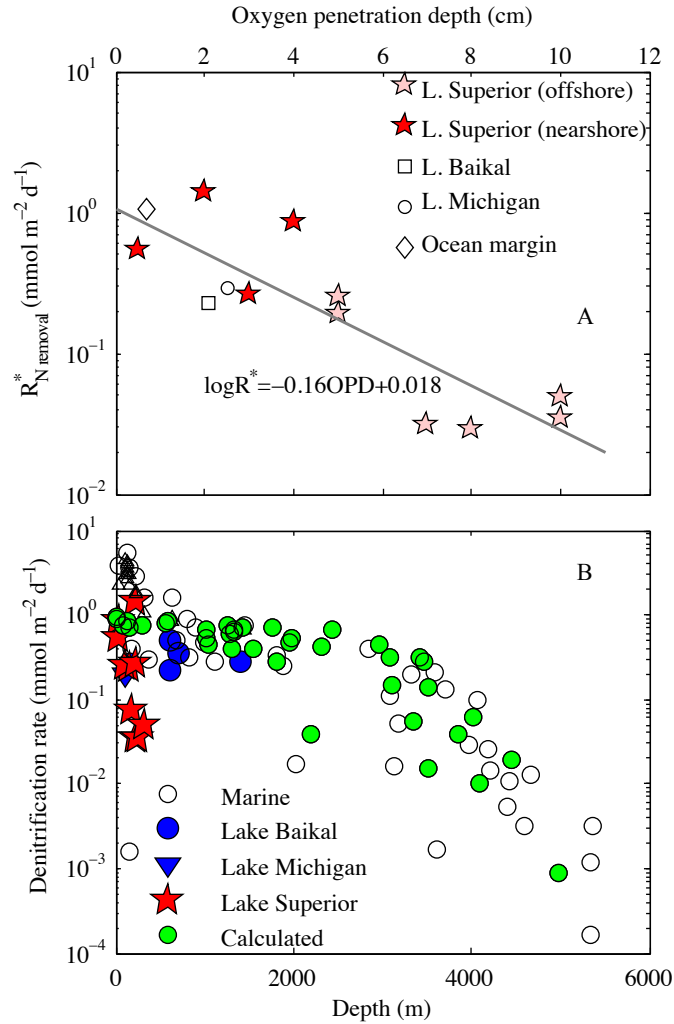


Figure 2. 8 (A) The rates of reactive nitrogen removal vs. oxygen penetration; (B) Denitrification rates vs. water depth. The data are from Lake Superior (this study), Lake Baikal (Maerki et al. 2006), Lake Michigan (Thomsen et al. 2004), and ocean margin sediments (Middelburg et al. 1996; Glud 2008; Glud et al. 2009).

The total oxygen uptake (TOU), a common measure of organic carbon sedimentation (Glud 2008), was previously found to correlate linearly with the denitrification rates in the continental slope and shelf sediments (Fig. 2.9): $R_{\text{denitrif.}}^* = 0.116 \times \text{TOU}$ ($r = 0.80$; Seitzinger and Giblin, 1996) and $R_{\text{denitrif.}}^* = 0.105 \times \text{TOU}$ ($r = 0.76$; Laursen and Seitzinger, 2002). The linear relationship is reasonable when denitrification is limited by the supply of nitrate, as nitrification both consumes oxygen and supplies nitrate for denitrification (Laursen and Seitzinger, 2002). However, in carbon-poor sediments, our results suggest that the relationship may be stronger than linear (Fig. 2.9). Besides being dependent on the supply of nitrate, the denitrification rate is regulated by the amount and reactivity of organic carbon that reaches the denitrification zone. Whereas the carbon amount is reflected in the TOU, the depth of the denitrification zone is linked to the depth of oxygen penetration (Fig. 2.10), which in deeply oxygenated sediments depends on the rate of carbon sedimentation nonlinearly (Katsev et al. 2006). The combined effect of these factors results in a stronger-than-linear relationship between the TOU and the denitrification rates (Fig. 2.9). Whereas the nearshore sediments in Lake Superior conform to the same relationship as marine coastal sediments (Fig. 2.9), the deeply oxygenated sediments are characterized by significantly lower denitrification rates (Fig. 2.9). Our results (Figs. 2.9 and 2.10) indicate that the total oxygen uptake cannot be uniquely correlated to the rates of sediment denitrification. Sediments characterized by the same oxygen uptake (i.e., receiving effectively the same sedimentation flux of organic carbon) may exhibit radically different denitrification rates, depending on the depth of oxygen penetration, which is deeper in slowly accumulating sediments (Fig. 2.10). This suggests that the deeply oxygenated abyssal sediments in the

Ocean may not conform to the same relationships as coastal and continental shelf sediments, and need to be treated differently in geochemical models that address the global nitrogen cycle. For the freshwater nitrogen cycle, our results suggest that large oligotrophic lakes generally conform to the trends observed in marine systems, so models from marine environments may be transferable to lakes.

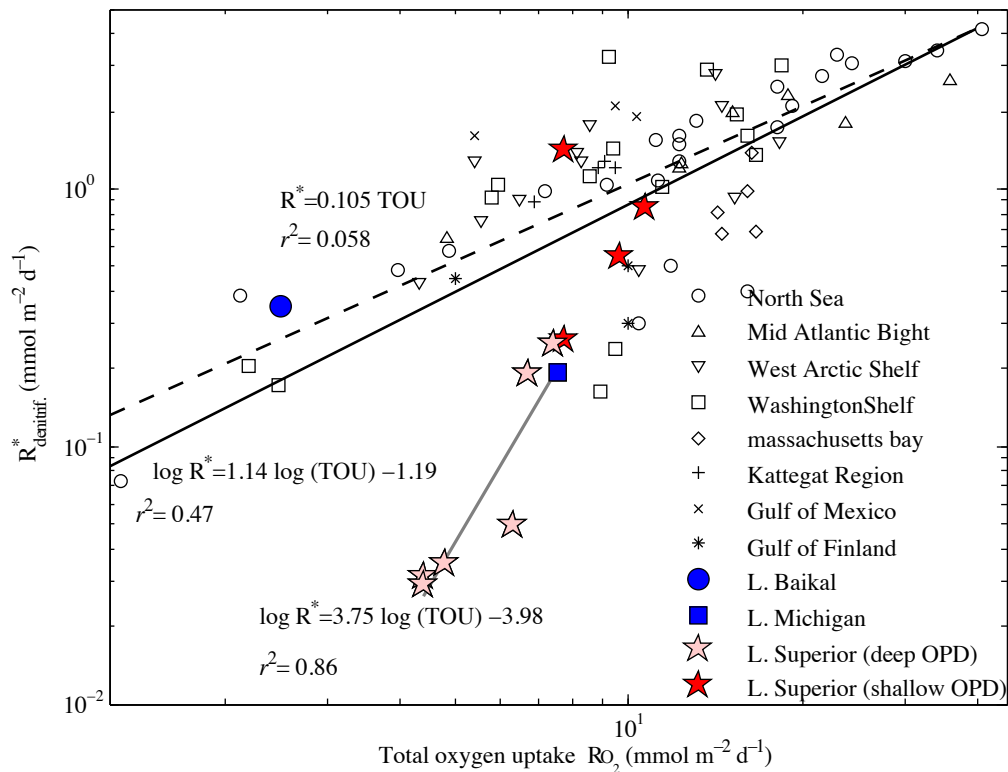


Figure 2. 9 Denitrification rates vs. sediment oxygen uptake. The data are from lakes Superior (this study), Baikal (Maerki et al. 2006), Michigan (Thomsen et al. 2004), and marine sediments (Canfield et al. 1993; Laursen and Seitzinger 2002; Hietanen and Kuparinen 2008; Glud et al. 2009). The lines are the linear model of Laursen and Seitzinger (2002) (dashed), the fit to the data from coastal and shelf marine sediments, other large lakes and Lake Superior in this study.

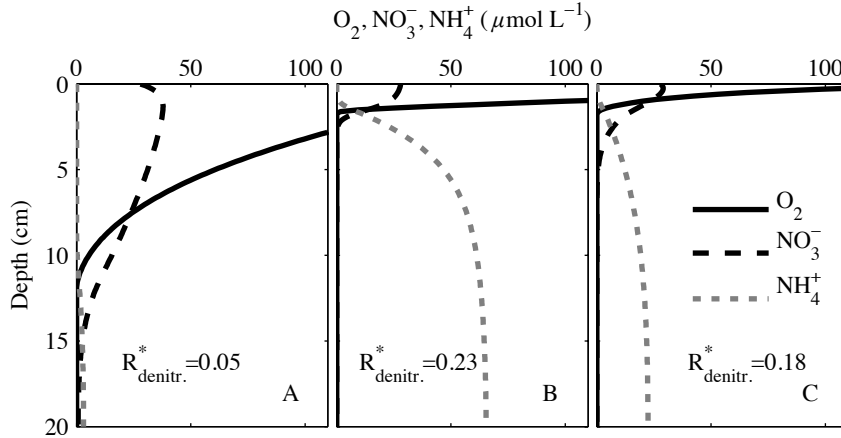


Figure 2. 10 The effect of oxygen penetration on denitrification rates. The rates and vertical concentration profiles of oxygen, nitrate, and ammonium were generated, for illustration purposes, using the diagenetic model LSSE-Mega (Katsev et al. 2007). (A) Conditions typical for the Lake Superior offshore sediments: burial velocity of 0.2 mm y^{-1} (at 20 cm depth, after compaction); oxygen and nitrate concentrations at the SWI of 350 and $28 \mu\text{mol L}^{-1}$, respectively. (B) Same, but the burial velocity is 2 mm y^{-1} . (C) Same as (A), but oxygen concentration at the SWI is $175 \mu\text{mol L}^{-1}$. The depth-integrated denitrification rates, $R^*_{\text{denitrif.}}$, are in $\text{mmol m}^{-2} \text{ d}^{-1}$ (compare to Fig. 11). The total sediment oxygen uptake (TOU) is the same in all cases, about $4 \text{ mmol m}^{-2} \text{ d}^{-1}$.

CONCLUSIONS

- The nitrogen cycling in sediments of Lake Superior exhibits strong spatial heterogeneity and needs to be considered separately for the areas of high and low sedimentation. The low-sedimentation offshore sediments (OPD > 4 cm) are characterized by lower denitrification rates ($0.10 \text{ mmol m}^{-2} \text{ d}^{-1}$), whereas the sediments in high sedimentation areas (OPD < 4 cm) exhibit high denitrification rates ($0.76 \text{ mmol m}^{-2} \text{ d}^{-1}$) and contribute disproportionately to benthic nitrogen removal (54% of N_2 removal despite covering only ~ 10% of the lake floor). The deeply oxygenated offshore sediments are nitrate sources to the water column (efflux $0.26 \text{ mmol m}^{-2} \text{ d}^{-1}$), whereas the shallow oxygenated nearshore sediments serve as nitrate sinks (nitrate flux in at $0.16 \text{ mmol m}^{-2} \text{ d}^{-1}$).
- Sediments in Lake Superior contribute significantly to the N budgets of both the water column and the entire lake. The lake-average nitrate and ammonium efflux into the water column ($0.27 \text{ mmol m}^{-2} \text{ d}^{-1}$) accounts for 24 – 61% of the total nitrogen inputs into the water column. The sediments serve as sinks of nitrogen for the entire lake via nitrogen removal to N_2 and long-term burial of the non-reactive nitrogen, which together account for 73% of the total nitrogen removal in the lake. The updated nitrogen budget is closer to balance than the previous one, with total nitrogen losses exceeding the total nitrogen input and an unknown contribution from nitrogen fixation. Sediment nitrification in Lake Superior, which leads to the flux out of nitrate into the water column, is a major source of nitrate to the system (contributing 84% of nitrate inputs), which suggests that changes in sediment denitrification are the most likely cause of the increased nitrate concentrations in Lake Superior.

- In Lake Superior sediments nitrification is limited by the availability of ammonium. Ammonium oxidation efficiency is high (90%), despite the fact that nitrification only accounts for ~ 12% of the total sediment oxygen uptake, which is a result of higher C: N ratio (12C: N), compared to > 20% in marine sediments (6.6C: 1N).
- The nitrate and dissolved iron profiles suggest that ~2% of nitrate reduction is coupled to the oxidation of iron, a rarely detected pathway.
- Sediment nitrogen cycling in large freshwater lakes is found to be similar to the N cycling in marine systems. Sedimentation rate and oxygen penetration depth are more appropriate than water depth as parameters for the categorization of sediments and parameterization of the nitrogen fluxes and rates.
- In contrast to coastal marine sediments, in deeply oxygenated sediments the relationship between sediment denitrification and total oxygen uptake (C sedimentation) is stronger than linear. This is because denitrification rates are regulated by several factors associated with organic carbon sedimentation: the organic matter deposition supplies both the organic C substrate for denitrification and the nitrate (via ammonium oxidation within the sediment). In addition, the amount and reactivity of organic carbon affect the depth of oxygen penetration nonlinearly in deeply oxygenated sediments, which may introduce nonlinearity in the dependence of the denitrification rates on C supply. Thus, denitrification rates in slowly accumulating well-oxygenated sediments cannot be described by the same relationship with total oxygen uptake as in high-sedimentation areas.

Chapter 3 Phosphorus and iron cycling in Lake Superior sediments

SUMMARY

To understand the phosphorus cycling in the sediments of Lake Superior and its contribution to the lake-wide phosphorus budget, we investigated 13 locations (26-318 m depth) throughout the lake. Porewater and solid-phase profiles of iron and phosphorus were measured, and their transformation rates and vertical fluxes were calculated. Results suggest that the cycles of carbon, phosphorus and iron in the sediments of Lake Superior are tightly linked. Iron reduction ($0.047 \text{ mmol m}^{-2} \text{ d}^{-1}$) mobilizes dissolved phosphorus in deep sediment, whereas re-oxidation of dissolved iron at the redox boundary immobilizes it. The efflux of dissolved phosphorus (2.5 to $7.0 \mu\text{mol m}^{-2} \text{ d}^{-1}$) from sediment into the water column is controlled by the balance between the organic phosphorus release from organic matter and its adsorption near the sediment surface. In these deeply oxygenated sediments, the P efflux is only weakly affected by the rates of iron reduction. The P recycling efficiency is low ($\sim 12\%$), primarily due to the high iron sedimentation, high Fe:P ratio (~ 40 - 80) in the surface sediments, and deep oxygen penetration. The updated Lake Superior phosphorus budget suggests that sediments contribute significantly to the lake-wide P cycling, primarily by acting as a sink. The sediment efflux of dissolved reactive P contributes $>13\%$ of the total P inputs into the water column, whereas burial of P into the deep sediments serves as the main sink for total phosphorus in the lake. The new P budget appears imbalanced (outputs exceed inputs), with the imbalance

significantly exceeding the historical decline in TP in the water column, suggesting that sources of P may have been underestimated.

INTRODUCTION

Phosphorus (P) is an essential nutrient for primary productivity in aquatic systems. In freshwater lakes it is most frequently the limiting nutrient that determines their trophic state (Hecky and Kilham 1988). Sediments, being long-term net sinks of P, play an important role in the lakes' P cycle, and sediment P retention capacity is the major factor that regulates the concentrations of reactive phosphorus in the water column (Katsev et al. 2006; Hupfer and Lewandowski 2008). The classical model of "oxygen-controlled P mobilization" describes the coupling between the iron (Fe) and P cycles and links P releases to the sediment redox conditions (Mortimer 1942): under oxic conditions the high sorption capacity of sedimentary iron oxyhydroxides (FeOOH) with respect to P prevents P release into the overlying waters, whereas under anoxic conditions the adsorbed P is released upon the reduction of oxidized iron phases. Whereas this model was supported by studies of many freshwater and marine systems (Hupfer and Lewandowski 2008 and reference therein), other alternative mechanisms have been suggested for controlling phosphorus retention capacity of sediments. The long term phosphorus recycling efficiency and fluxes across the SWI are affected by multiple factors, such as the sedimentation flux of iron oxyhydroxides, the extent of sulfate reduction that causes precipitation of iron sulfides, which have lower P sorption capability, and regeneration of P during organic matter mineralization (Katsev et al. 2006). Studies have suggested that P recycling efficiencies in freshwater sediments are generally low compared to marine systems (Caraco et al. 1990). To understand the benthic P cycling in Lake Superior, this chapter investigates the interactions of the phosphorus and iron diagenetic cycles, the balance between processes that regulate the

fluxes of dissolved phosphorus across the sediment-water interface, and their spatial and temporal variability.

Lake Superior is a carbon-poor, oligotrophic system that has low concentrations of phosphorus. In contrast to the increasing nitrate concentrations in the lake's water column, historical data have shown a constant or small declining trend in TP concentrations (TP decreased from ~ 0.19 to $0.10 \mu\text{mol L}^{-1}$ since the mid-1960s; Sterner et al. 2007), following the regulation of phosphorus loadings by the International Joint Commission (IJC) in the 1970s (Chapra and Dolan 2012). The present water column total phosphorus (TP) levels are $< 2 \mu\text{g L}^{-1}$ (Chapra and Dolan 2012), and soluble reactive phosphorus (SRP) is low ($\sim 10 \text{ nmol L}^{-1}$; Baehr and McManus 2003). Primary production in Lake Superior is limited by the availability of reactive phosphorus (Sterner et al. 2004), and the internal sources and the recycling of phosphorus within the lake are considered important in supporting the primary productivity (Heinen and McManus 2004). The phosphorus losses via riverine outflow are small ($\sim 10\%$ of allochthonous inputs; Heinen and McManus 2004), suggesting that sediments are important phosphorus sinks. Their contributions, however, have not been well constrained. The P settling rates and benthic recycling efficiency have been previously estimated only in the Western Arm of Lake Superior (Heinen and McManus 2004). As our results in the preceding Chapters suggest a strong spatial (as well as temporal) variability in sediment properties in Lake Superior, a lake-wide investigation of the sediment phosphorus cycling is essential for constraining its geochemical budgets. This Chapter estimates the sediments contributions to the lake-wide phosphorus cycling, and presents an updated phosphorus budget for the lake.

METHODS

Sediment sampling and analyses

Sediments and overlying waters were sampled across Lake Superior on multiple cruises aboard the R/V *Blue Heron* in 2009-2012 (Fig. 1.1; Table 1.1), and processed using the procedures described in Chapter 1 and 2. The splited sediment were scanned for major elements at 200 μm spatial resolution using an ITRAX X-ray fluorescence (XRF) scanning sediment analyzer at the Large Lakes Observatory, University of Minnesota Duluth. The porewater samples for the dissolved Fe(II) and soluble reactive phosphorus (SRP) analyses were acidified with hydrochloric acid (1% of 6 mol L⁻¹ HCl) immediately after collection and stored at 4°C. Dissolved Fe(II) concentrations were determined spectrophotometrically with Ferrozine (Viollier et al. 2000). Frozen wet sediment samples (in 15 mL Falcon tubes) were thawed and analyzed for an operationally defined biologically available iron fraction (amorphous Fe(III) oxides and solid-phase Fe(II) compounds) by a 0.5 N HCl extraction (Roden et. al. 2002). Separate frozen sediment samples were freeze-dried, ground, and homogenized, and the distribution of iron phases in them was determined using the sequential extraction procedure of Poulton and Canfield (2005): extractions by magnesium chloride, sodium acetate, and sodium dithionite were used, respectively, to extract exchangeable iron, carbonate iron (siderite and ankerite), and reducible iron oxides (ferrihydrite, lepidicrocite, goethite, hematite and akaganeite). Solid sediments were also analyzed for phosphorus fractions, following the SEDEX sequential extraction procedure of Ruttenberg (1992), which separates the sediment phosphorus into five pools: exchangeable P, ferric Fe-bound P, authigenic carbonate fluorapatite + carbonate fluorapatite + biogenic apatite + calcium carbonate

associated P, detrital apatite P of igneous or metamorphic origin, and organic P. Dissolved Fe concentrations in both the extracts and filtered porewater samples were determined by Ferrozine colorimetric method (Viollier et al. 2000) using a Thermo Spectronic GENESYS™ 6 Spectrophotometer. SRP concentrations in porewaters, bottom water samples, and sediment extracts were measured using the molybdenum blue method (Grasshoff et al. 1999) on a Lachat Quickchem 8000 flow injection auto-analyzer.

Calculations of fluxes

The molecular diffusive fluxes (F_i) of dissolved Fe^{2+} and SRP were calculated using the Fick's law of diffusion (Eq.1.5 and Eq.2.1). The bulk molecular diffusion coefficients D_s at the in-situ temperature 4°C, with correction for sediment tortuosity, are $D_{\text{Fe}^{2+}} = 123 \text{ cm}^2 \text{ yr}^{-1}$, $D_{\text{H}_2\text{PO}_4^-} = 155 \text{ cm}^2 \text{ yr}^{-1}$, and $D_{\text{HPO}_4^{2-}} = 125 \text{ cm}^2 \text{ yr}^{-1}$ (see Chapter 1 and 2 for details). In determining the fluxes of SRP (mostly HPO_4^{2-} and H_2PO_4^- at the in situ pH), the diffusion coefficients for the two ionic species were averaged, and the calculated fluxes are presented here with uncertainties that account for the possible variations in the composition ratios. Where concentration gradients near the sediment-water interface were poorly resolved, the diffusive fluxes across the interface were calculated from the gradients calculated from the measured porewater concentrations below the interface, the measured bulk bottom water concentrations, and the assumed thickness of boundary layer of 1 cm (based on the 0.05 cm resolution oxygen profiles; see Chapter 1). With contributions from processes other than molecular diffusion, such as bioirrigation (Meile et al. 2005; Glud 2008), the total fluxes of P may be higher than molecular diffusion

fluxes (e.g., for oxygen Li et al. (2012) estimated the difference at 30- 50%). Bioturbation in Lake Superior is limited to the upper 2 cm of sediment (Li et al. 2012), thus no contributions from benthic fauna are expected below this depth.

RESULTS

Porewater concentrations of Fe(II) and phosphorus

In sediments where oxygen and nitrate concentrations in the sediments (> 20 cm) remained high, the sediments contained no detectable dissolved Fe(II) (< 1 $\mu\text{mol L}^{-1}$), indicating the absence of active iron reduction at these depths (e.g. in the entire core of EM.1, WM. 1, 2, 4, Sta.2, NIP, and the oxic layers of others; Fig. 3.1). In the deep sediments where oxygen and/or nitrate were depleted completely, dissolved Fe (II) concentrations increased below the depths of oxygen and/or nitrate penetrations, suggesting active iron reduction. Porewater SRP concentrations were close to zero (below the detection limit of 0.5 $\mu\text{mol L}^{-1}$) at the SWI, increased to low but detectable concentrations (0-5 $\mu\text{mol L}^{-1}$) within the surface oxic sediments where dissolved Fe(II) was not detectable (e.g., *see* profiles for WM that are scaled in Figure 3.1 to smaller concentrations, for better visibility), and increased significantly into the deep anoxic sediments (typically reaching 40 – 90 $\mu\text{mol L}^{-1}$), paralleling the increases in dissolved Fe(II).

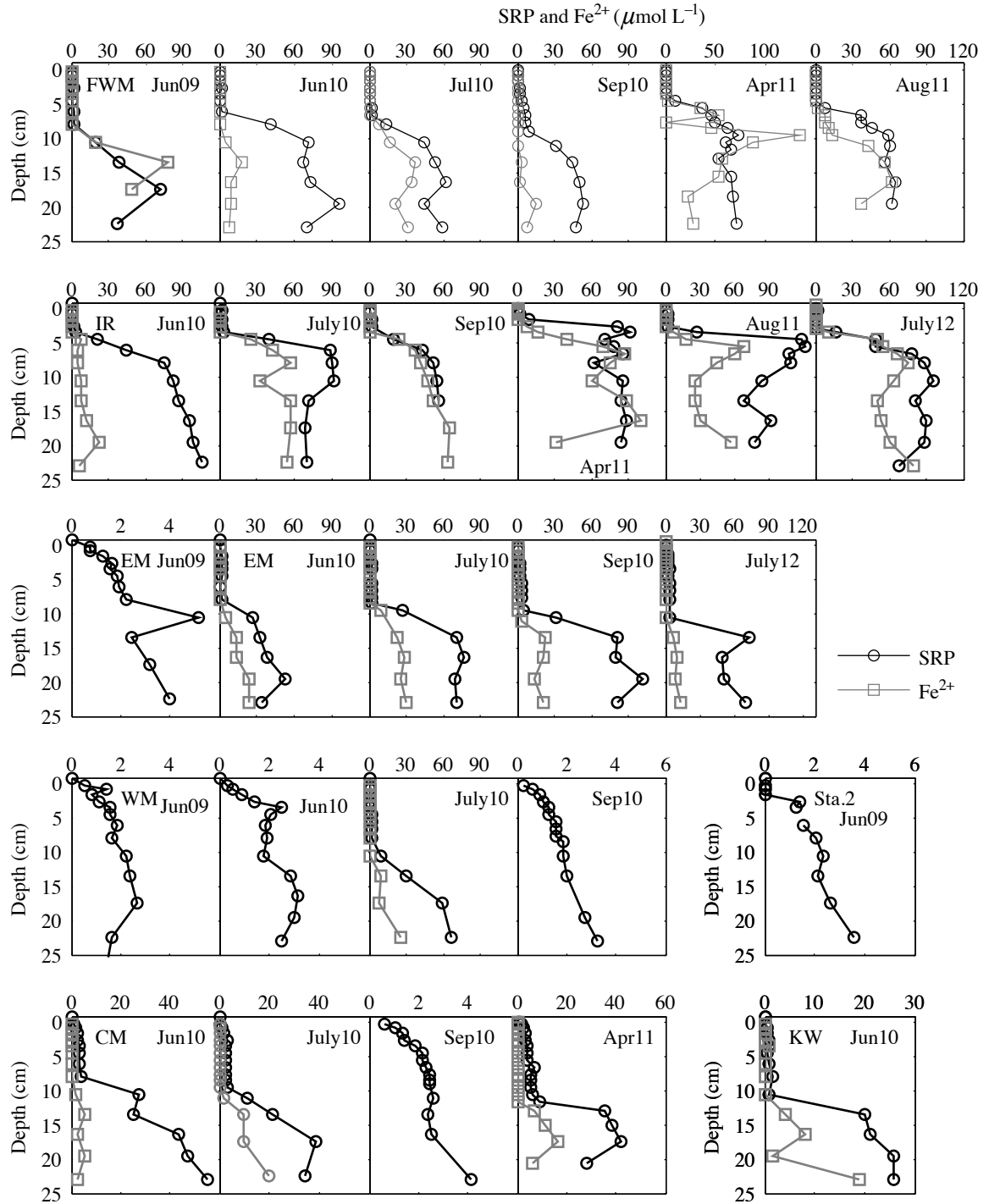


Figure 3. 1 Dissolved Fe(II) and soluble reactive phosphorus (SRP) concentrations in porewaters of Lake Superior sediments (continued on next page).

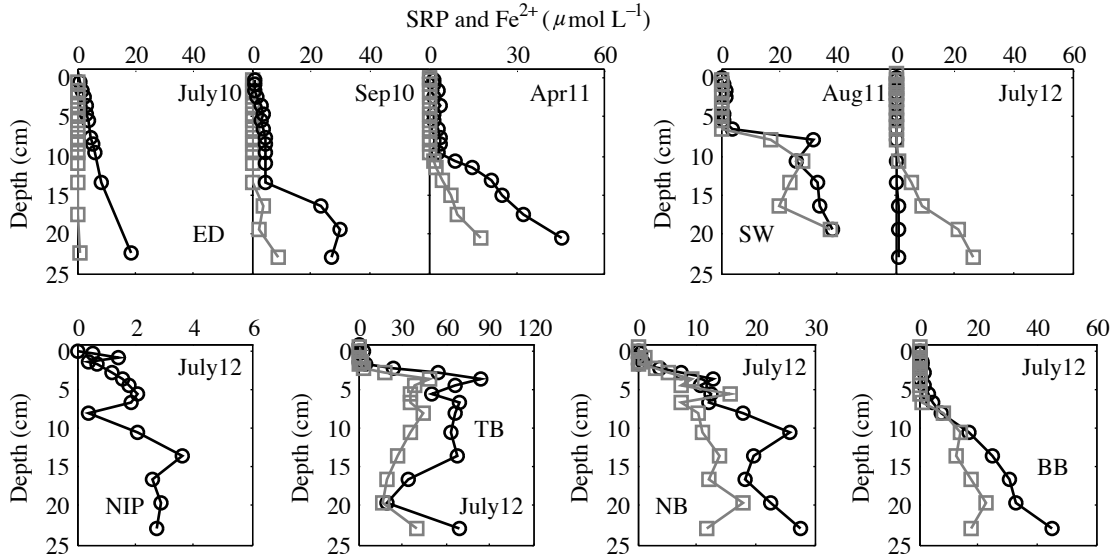


Figure 3.1 Dissolved Fe(II) and soluble reactive phosphorus (SRP) concentrations in porewaters of Lake Superior sediments (continued from previous page).

Soluble reactive phosphorus (SRP) fluxes across the sediment-water interface

The elevated concentrations of SRP in sediment porewaters relative to the bottom water levels indicate effluxes of dissolved phosphorus from sediments into the water column at all sites. The diffusive effluxes calculated from the measured SRP gradients ranged from 2.5 to 7.0 $\mu\text{mol m}^{-2} \text{d}^{-1}$ (Table. 3.1).

Table 3. 1 Diffusive fluxes of soluble reactive phosphorus (F_{SRP}) across the SWI. Fluxes are positive into the sediments (see Chapter 1 for the diffusive oxygen fluxes (F_{O_2}) and the measured and calculated (indicated by *) total oxygen uptakes (TOU). P recycling efficiency is defined as the ratio of phosphorus effluxes to the total sedimentation flux of organic phosphorus.

Station	F_{O_2} (mmol m ⁻² d ⁻¹)	TOU (mmol m ⁻² d ⁻¹)	F_{SRP} (μmol m ⁻² d ⁻¹)	P Recycled E
FWM.1	1.6	6.4	-2.9 ± 0.3	
FWM.3	4.1; 2.1		-3.0 ± 0.3	
FWM.4	3.2; 2.5		-2.1 ± 0.2	
FWM.5	1.5	7.1	-1.6 ± 0.2	
FWM.6	3.3; 3.1; 4.2; 7.8		-3.1 ± 0.3; -5.9 ± 0.7	
Average	3.3	6.8	-2.8 ± 0.7	11%
EM.1	2.6		-3.4 ± 0.4	
EM.3	3.1; 2.3		-2.5 ± 0.3	
EM.4	4.6		-5.3 ± 0.5	
EM.5	2.5		-2.3 ± 0.2	
EM.6	2.1; 2.7		-4.9 ± 0.5	
Average	2.9	4.4*	-3.7 ± 0.5	16%
WM.1	3.4	4.4	-3.7 ± 0.2	
WM.3	1.2		-1.6 ± 0.2	
WM.4	2.2; 2.1		-2.2 ± 0.2	
WM.5	2.8		-2.6 ± 0.3	
Average	2.3	4.4	-2.5 ± 0.3	14%
IR.1	4.5		-3.9 ± 0.4	
IR.2	5.9		-5.4 ± 0.3	
IR.3	3.6	4.9 ± 0.8	-5.0 ± 0.6	
IR.4	5.7; 7.3		-11 ± 1; -6.0 ± 0.7	
IR.5	3.8		-4.3 ± 0.5; -3.6 ± 0.4	
Average	5.1	7.7*	-5.4 ± 1.0	13%
CM.1	2.8		-4.9 ± 0.5	
CM.2	3.7		-3.3 ± 0.2	
CM.3	1.9		-3.3 ± 0.4	
CM.4	3.8		-11 ± 1.0	
Average	3.2	4.8*	-5.6 ± 3.0	21%
ED.1	3.0		-2.5 ± 0.3	
ED.2	2.7		-2.7 ± 0.3	
ED.3	6.8		-11 ± 1	
Average	4.2	6.3*	-5.4 ± 2	16%
SW.1	6.5		-3.7 ± 0.4	
SW.2	4.0; 3.9		-4.3 ± 0.5	
Average	4.9	7.4*	-4.0 ± 0.5	10%
KW.1	2.9	4.4*	-2.1 ± 0.2	9%
NIP.1			-6.6 ± 0.7; -1.6 ± 0.2	
NB.1	6.8; 6.1	9.7*	-6.5 ± 0.7	12%

BB.1	8.7; 5.4	11 [*]	-4.0 ± 0.3	7%
TB.1	4.4; 5.8	7.7 [*]	-7.0 ± 0.7	17%

Distributions and speciation of solid-phase iron, manganese, and phosphorus

Scanning XRF profiles of total iron and manganese reveals multiple Fe- and Mn-rich layers (Fig. 3.2; also visible to a naked eye, *see* Fig. 1.2 in Chapter 1). Figure 3.3 shows the typical distributions of solid phase iron and phosphorus fractions obtained in sequential extractions (more profiles are given in the Appendix). The iron-rich layers are dominated by the 0.5-HCl extractable or dithionite-extractable iron fractions, which correspond to the operationally defined reactive (reduceable) iron. These enrichments in reactive solid phase Fe match the enrichments in iron-bound phosphorus (Fig 3.3C). The Fe (III) : Fe-bound P ratio in the surface sediments is high (~ 40 - 80), decreases slightly with depth within the oxic layer, and strongly decreases below the depth of iron and phosphorus enrichments (Fig. 3.3D).

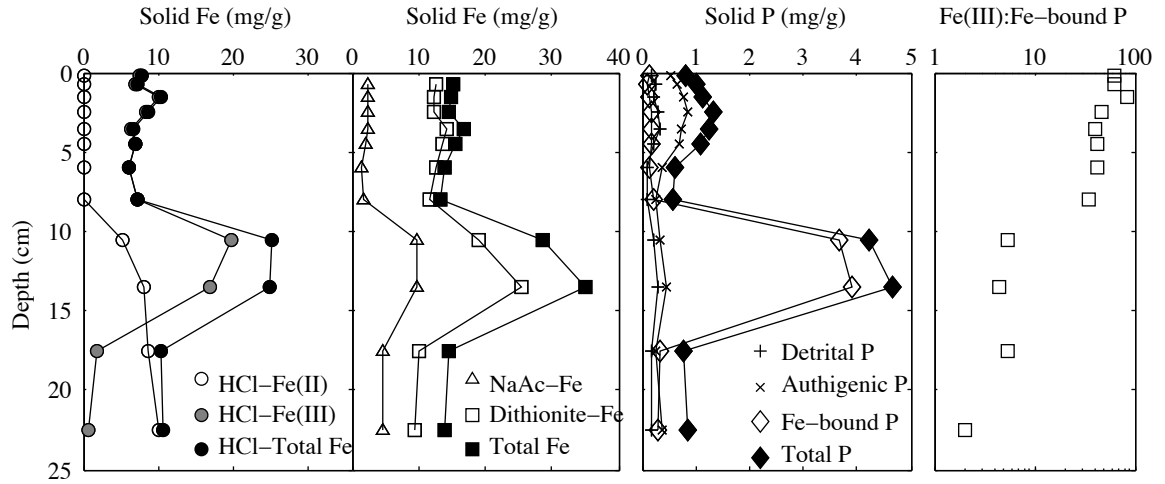


Figure 3. 3 Solid phase iron and phosphorus in sediments at Sta. FWM. The Fe(III): Fe-bound P ratio is a molar ratio, calculated from the 0.5 N HCl extractable Fe(III) and extractable Fe-bound P contents.

DISCUSSION

Iron and manganese cycling

The presence of broad and/or multiple metal-rich layers in Lake Superior sediments (Fig 3.2) is consistent with the ease of temporal excursions in the sediment redox boundary described in Chapter 1. Comparison of the XRF iron and manganese profiles with the distributions of Ti, which is an element typically associated with the detrital sediment components, suggests that these Fe- and Mn-rich layers are diagenetic in origin (Fig 3.2). This is further supported by the distributions of dissolved iron (Fig 3.1) and solid phase iron speciations (Fig 3.3A, B): Increases in dissolved Fe^{2+} and solid-phase Fe(II) below the OPD indicate iron reduction, whereas enrichments in solid-phase Fe(III) are indicative of the oxidation of the upward-diffusing Fe^{2+} at the depth where it meets oxygen (or an alternative electron acceptor such as nitrate or Mn oxides). Manganese layers located immediately above the uppermost iron layers are consistent with the typical diagenetic redox sequence: manganese oxides are more thermodynamically favorable as electrode accepters for organic carbon degradation than iron oxides, thus they are reduced (and re-precipitated) above the zone of iron reduction. The positions of the metal layers relative to the present-day OPD provide further insights into the redox boundary excursions. Taking the Sta. FWM core for example, millimeter-wide Mn and Fe-rich layers are found within the oxic sediment layer, ~ 4 cm above the measured OPD. Below the depth of oxygen penetration, there are several more iron-rich layers (Fig. 3.2; *see* Fig. 1.6 in Chapter 1 for oxygen profiles). This violation of the traditional redox sequence suggests that the OPD had been shallower in the past but deepened to its present location. The sediment redox chemistry at the Sta. FWM is

complicated by the deposition of taconite (depleted iron ore) tailings after 1950s, which increased the oxygen demand and shifted the OPD upward, leading to the precipitation of Mn and Fe at the new redox boundary. Upon the cessation of taconite discharges after 1980 and the oxidation of the deposited taconite particles, the redox boundary migrated downward to its present location (*see* more details and evidence in Li 2011).

The rates of iron reduction can be estimated from the concentration profiles of the produced dissolved Fe^{2+} and solid-phase Fe(II) using the diagenetic equations described in Chapter 1 (Eqs. 1.2 and 1.3). Briefly, under nearly steady state conditions and, the diagenesis of iron can be described below the bioturbation zone (<2 cm; *see* Chapter 1) as

$$0 = \frac{d}{dx} \left(\varphi D_{\text{diss.Fe(II)}} \frac{dC_{\text{diss.Fe(II)}}}{dx} \right) + R_{\text{diss.Fe(II)}} \quad (3.1)$$

$$0 = \frac{d}{dx} \left(\xi U C_{\text{solid.Fe(II)}} \right) + R_{\text{solid.Fe(II)}} \quad (3.2)$$

Here $D_{\text{diss.Fe(II)}}$ is the diffusive coefficient for dissolved Fe(II), $C_{\text{diss.Fe(II)}}$ and $C_{\text{solid.Fe(II)}}$ are the concentrations of dissolved Fe(II) and solid-phase Fe(II), respectively, and $R_{\text{diss.Fe(II)}}$ and $R_{\text{solid.Fe(II)}}$ are the iron reduction rates that affect the dissolved and solid-phase concentrations of Fe(II); x is the sediment depth; U is the burial velocity and ξ is equal to $(1-\varphi)\rho$. By integrating equations (3.1-3.2) from the upper boundary of iron reduction ($x=L$) to the deep sediment where both the dissolved and solid-phase Fe(II) concentrations no longer change with depth ($x=\infty$), the depth-integrated rates (in $\text{mmol m}^{-2} \text{d}^{-1}$) can be written as:

$$R_{diss.Fe(II)}^* = \varphi D_{diss.Fe(II)} \frac{dC_{diss.Fe(II)}}{dx} \Big|_{x=L}^{x=\infty} = -\varphi D_{diss.Fe(II)} \frac{dC_{diss.Fe(II)}}{dx} \Big|_{x=L} = F_{diss.Fe(II), x=L} \quad (3.3)$$

$$R_{solid.Fe(II)}^* = \xi UC_{solid.Fe(II)} \Big|_{x=L}^{x=\infty} = \xi UC_{solid.Fe(II), x=\infty} - \xi UC_{solid.Fe(II), x=L} \quad (3.4)$$

The total net rate of iron reduction can be estimated as $R_{Fe}^* = R_{diss.Fe(II)}^* + R_{solid.Fe(II)}^*$. This iron reduction rate calculated from eqs. (3.3-3.4) is $R_{Fe}^* = 0.047 \text{ mmol m}^{-2} \text{ d}^{-1}$ (Table 3.2). At this rate, iron reduction accounts for < 0.2% of total carbon mineralization ($5.7 \text{ mmol m}^{-2} \text{ d}^{-1}$; see Chapter 1).

Table 3. 2 Depth-integrated rates of iron reduction ($R_{\text{diss.Fe(II)}}^*$, $R_{\text{solid.Fe(II)}}^*$, $R_{\text{Fe total}}^*$), rates of phosphorus mobilization in the iron reduction zone ($R_{\text{P rel. by Fe red}}^*$; Eq.3.5), and percentage of carbon mineralization by iron reduction ($R_{\text{Fe total}}^* : R_{\text{C}}^*$). All rates are in $\text{mmol m}^{-2} \text{d}^{-1}$.

Station	$R_{\text{diss.Fe(II)}}^*$	$R_{\text{solid.Fe(II)}}^*$	$R_{\text{Fe total}}^*$	$R_{\text{P rel. by Fe red}}^*$	R_{C}^*	$R_{\text{Fe total}}^* : R_{\text{C}}^*$
FWM.1	0.022			0.0095		
FWM.3	0.0047	0.0031		0.032		
FWM.4	0.0077			0.017		
FWM.5	0.0011			0.015		
FWM.6	0.051			0.051		
FWM.7	0.023			0.024		
Average	0.018		0.049	0.025	5.2	0.1%
IR.1	0.015	0.0031		0.034		
IR.2	0.044			0.073		
IR.3	0.043			0.028		
IR.4	0.046			0.18		
IR.5	0.080			0.18		
IR.6	0.068			0.063		
Average	0.045		0.076	0.010	5.3	0.2%
EM.3	0.0033	0.001		0.014		
EM.4	0.012			0.035		
EM.5	0.0090			0.037		
EM.6	0.0027			0.030		
Average	0.0067		0.017	0.029	3.8	0.1%
WM.4	0.0034			0.009	3.3	
CM.1	0.0014			0.013		
CM.2	0.0037			0.0072		
CM.4	0.0049			0.022		
Average	0.0033			0.014	4.1	
ED.2	0.0013			0.0077		
ED.3	0.0020			0.0083		
Average	0.0017			0.0080	5.4	
KW.1	0.0015			0.0083	3.8	
SW.1	0.016			0.029		
SW.2	0.0041			0.017		
Average	0.0099			0.023	6.4	
NB	0.0092			0.016	8.4	
TB	0.079			0.14	6.6	
BB	0.007			0.0055	9.4	
AVERAGE	0.018		0.047	0.034	5.7	1%

Interaction between the phosphorus and iron cycles

The porewater phosphorus concentrations and the SRP fluxes across the sediment-water interface are determined by the balance between the P mobilization rates and its adsorption in the surface sediment. The two major sources of phosphate to the porewaters are regeneration of organic phosphorus and release of phosphate from Fe-oxides during iron reduction. The immobilization of phosphate in sediments happens mostly through its adsorption to the Fe-oxide mineral surfaces and co-precipitation with Fe during iron reoxidation (Carignan and Flett 1981; Roden and Edmonds 1997) or formation of reduced iron phosphates such as vivianite. The strong interaction of phosphate with iron oxides is evident in Lake Superior sediments by the dominance of the iron bound solid phosphorus pool at the depth of the diagenetic iron peak (Fig. 3.3). This is consistent with the increase in SRP concentrations into the anoxic sediments where iron reduction releases the previously bound phosphorus. The relatively smaller increase in porewater SRP levels in the near-surface oxic sediments most likely results from the regeneration of phosphorus from organic matter there. The effect is muted by the phosphate adsorption to oxidized sediment solids, most notably iron oxides and oxyhydroxides. The net rate of phosphorus production (release) and consumption (adsorption), as well as the rates of dissolved Fe(II) production can be estimated (below bioturbation zone) as

$$R_i = -\frac{d}{dx} \left(\varphi D_i \frac{dC_i}{dx} \right) \quad (3.5)$$

where R_i is the net rate of phosphate or dissolved Fe(II) production (positive for production), D_i is the diffusion coefficient of phosphate/Fe²⁺, and C_i is the concentration of phosphate (SRP) or dissolved Fe(II). As shown in Figure 3.4, phosphate production in the anoxic sediment is associated with the release of dissolved Fe(II), whereas

immediately above the iron reduction zone oxidation of Fe(II) coincides with the consumption of phosphorus, matching the peak in the iron-bound phosphorus. The net phosphate production rates in the surface oxic sediments are small compared to the respective rates in the anoxic deep sediments (in the zone of iron reduction), despite the availability of fresh organic matter near the sediment-water interface. This must reflect the high adsorption capacity of the oxidized surface sediments with respect to phosphate relative to the anoxic deep sediments.

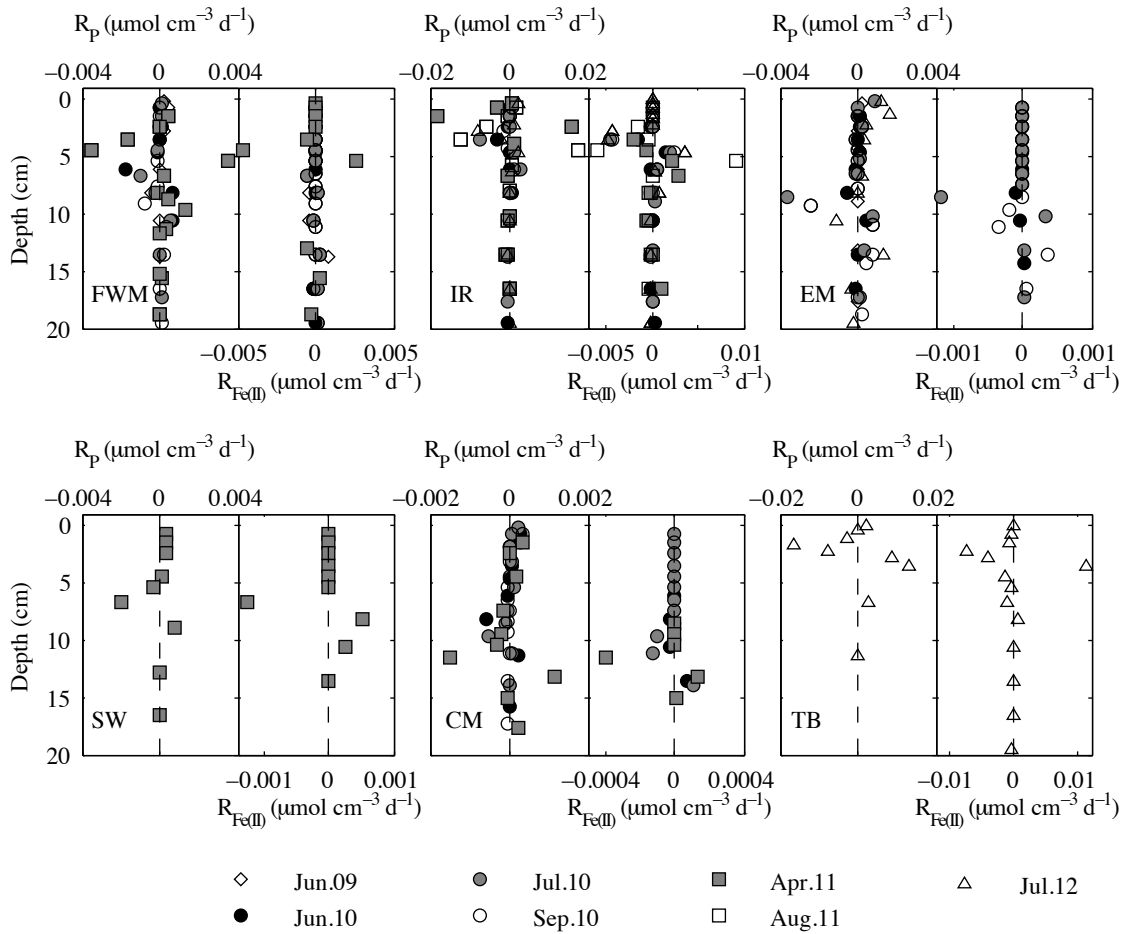


Figure 3. 4 Net rates of production of phosphate and dissolved Fe(II).

The depth-integrated rate of P mobilization in the anoxic sediment can be estimated from fluxes of SRP at the upper boundary of the iron reduction zone (Table 3.2), similarly to the calculation for the integrated iron reduction rates above. A comparison of the depth-integrated production rates for dissolved Fe(II) ($R_{\text{Fe(II)}}^*$) and phosphate (R_{SRP}^*) suggest a phosphorus-to-iron remobilization ratio of ~ 1.8 (Fig. 3.5). This is strikingly different from the 0.2–0.5 P:Fe ratio (2-6 Fe:P ratio) in the solid phase (Fig 3.3D): significantly more P is released relative to Fe than becomes buried into the iron reduction zone as iron-bound P. A typical Fe:P ratio at which the surfaces of iron oxyhydroxides become saturated with phosphate is 7 to 15 (Caraco et al. 1993; Jensen et al. 1992; Roden and Edmonds 1997). This ratio (or P:Fe ratio of 0.07-0.10) is reached at the bottom of the Fe-rich layer (Fig. 3.3D). The higher P:Fe ratio for the mobilization of dissolved constituents into the porewater is likely because a large proportion of reduced Fe is immobilized as solid Fe(II) phases (Fig 3.3A) (presumably, as Fe sulfides), which do not strongly adsorb phosphate. Additionally, phosphate is also released from organic matter, which continues to be mineralized below the zone of Fe reduction. In contrast, the surface sediments are characterized by large Fe(III):P ratios (40-80), indicating that these sediments are not saturated with phosphate and can strongly bind phosphate that is regenerated during organic matter decomposition.

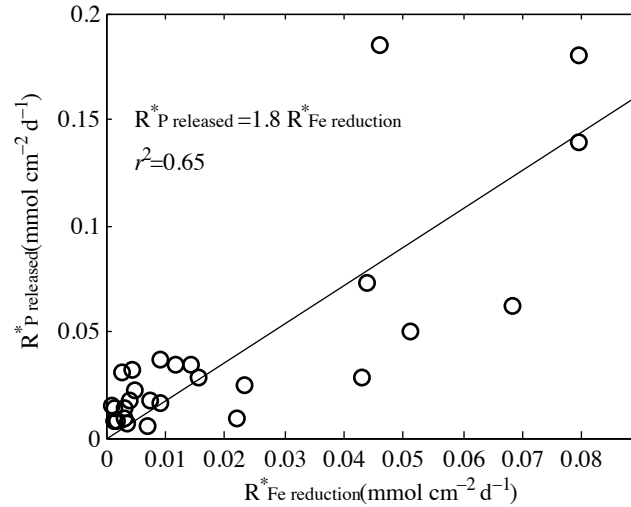


Figure 3. 5 Depth-integrated rates of net phosphorus vs. iron remobilization in anoxic sediments.

Controls on phosphorus fluxes across the sediment-water interface

The deep oxygen penetration, the correspondingly deep zone of iron reduction, and the strong P-absorption capacity of surface sediments in Lake Superior suggest that the sediment-water exchanges of phosphorus can be only weakly affected by iron reduction. This is in contrast to many shallower and more productive lakes where seasonal variations in the sediment redox regime cause the reduction of iron and, in fact, regulate the delivery of sediment P into the water column (i.e. the ‘classical model’ of Einsele-Mortimer; Mortimer 1942). In Lake Superior, the flux of phosphate across the SWI is largely controlled by the balance between the organic phosphorus regeneration and phosphate adsorption by iron oxides in the surface (oxic) sediment. As far enough from the saturation the adsorption can be a linear function of porewater P, the effluxes of SRP across the SWI likely behave as a nearly a linear function of organic carbon loading: a nearly fixed fraction of the phosphorus deposited to the sediment surface with organic matter is released back into the water column as SRP. Comparing the net rates of

phosphate production and carbon mineralization in the surface sediment allows estimating the efficiency of P recycling: taking Sta. FWM as an example, the P release rate of $< 0.001 \mu\text{mol cm}^{-3} \text{ d}^{-1}$ accounts for only $\sim 13\%$ of the phosphate that is expected to be released based on the estimated $0.8 \text{ C } \mu\text{mol cm}^{-3} \text{ d}^{-1}$ rate of carbon degradation (calculated from 1P:106 C stoichiometry (Heinen and McManus 2004); *see* Chapter 1 for carbon degradation rates). The remaining 87% of phosphate must be immobilized in the sediment. Comparing the SRP fluxes across the SWI to the oxygen uptake rates shows a SRP:O₂ flux ratio of 0.001:1.1, suggesting a similar P recycling efficiency of $\sim 12\%$ (given the 1P:106O₂ stoichiometry; Fig. 3.6). This P regeneration efficiency in Lake Superior sediments is consistent with the typical P recycling efficiency 5-20% in other freshwater lakes (Caraco et al. 1990), although higher values are found in anoxic or more productive and seasonally anoxic lakes (e.g., Moor et al. 1998; and results from Lake Malawi in Chapter 5) Marine sediments with similar rates of carbon mineralization typically have higher P regeneration efficiencies ($> 50\%$; Sundby et al. 1992; Caraco et al. 1990; McManus et al. 1997). There, the C_{ox}: P regeneration ratios are generally consistent with those expected from the decomposition of Redfield organic matter.

The capacity of surface sediments for immobilizing P released from organic matter is likely determined by the availability of oxidized iron. It was commonly believed that high P recycling efficiency resulted from the high rates of sulfate reduction in the sediments, which decrease the abundance of iron oxides and decrease P absorption (Caraco et al. 1990; Caraco et al. 1993; Capone and Kiene 1988). However, in the deep ocean sediment ($\sim 3000 \text{ m}$) where the zone of sulfate reduction is deep (deep OPD, similar to Lake Superior) and P fluxes at the SWI are mostly controlled by the organic

mineralization in the surface sediment, P regeneration efficiency is also high, consistent with the Redfield decomposition of organic matter. This suggests that the composition of surface sediments (i.e., the deposited material) may be important for controlling the P regeneration near the sediment surface (Hupfer and Lewandowski 2008). The acetate- and dithionite-extractable iron (carbonate iron and reducible iron oxides) are the major components that absorb phosphorus (Ruttenberg 1992; Fig. 3.3). In Lake Superior they account for 1.5–3.5% of the solid sediment weight. In marine sediments, in contrast, dithionite extractable iron typically accounts for only 0.2 ~ 1.5% (Canfield 1989). In addition, the high P retention in Lake Superior relative to marine sediments may result from the deep oxygen penetration (see Chapter 1 for OPD comparison to marine sediments), as OPD determines the thickness of the surface sediment layer that contains iron oxides.

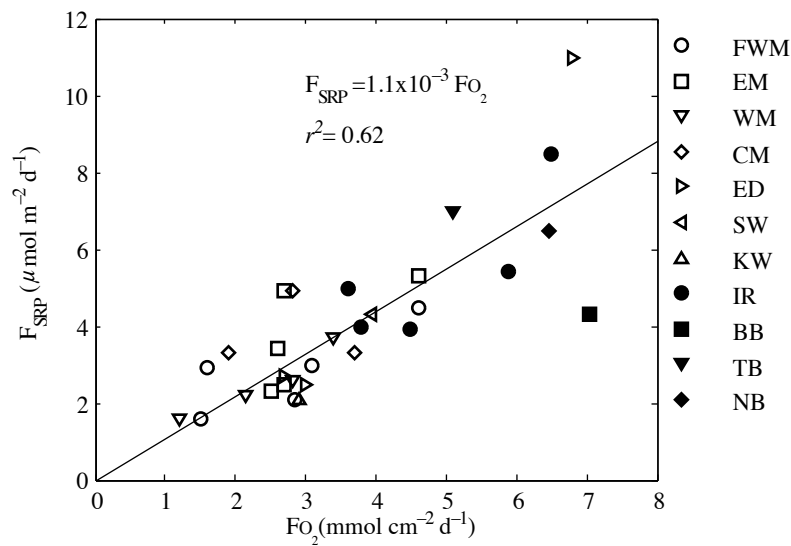


Figure 3. 6 SRP flux across the sediment-water interface as a function of total oxygen uptake.

Sediment contribution to the phosphorus budget of Lake Superior

An updated phosphorus budget in Lake Superior is presented in Table 3.3, with contributions from sediments that were not well constrained previously. Heinen and McManus (2004) calculated a lake-wide phosphorus budget based on sedimentation flux measurements from sediment traps in the Western Arm. However the sediment traps may have underestimated the P sedimentation flux, as organic material may undergo substantial degradation while in traps (*see* discussion in Chapter 1 comparing C flux measured in traps and organic carbon degradation rates measured in cores). In Table 3.3 the lake-wide P budget is updated, and also the most recent P input data (atmospheric deposition, watershed loading, point-source pollution, etc.), which were not available previously (Dolan and Chapra 2012). The organic P sedimentation of $-49 \text{ mmol m}^{-2} \text{ d}^{-1}$, appears to be a major sink of P for the Lake Superior water column. Our calculated diffusive effluxes of phosphorus from sediments ($2.5 - 7.0 \text{ } \mu\text{mol m}^{-2} \text{ d}^{-1}$; average $4.4 \text{ } \mu\text{mol m}^{-2} \text{ d}^{-1}$) are broadly consistent with the fluxes that were previously estimated in sediment core incubations in the Western Arm of the lake ($5 \pm 6 \text{ } \mu\text{mol m}^{-2} \text{ d}^{-1}$; Heinen and McManus, 2004). The total P flux across the sediment-water interface may be 30-50% larger than the diffusive flux due to processes such as bioirrigation (*see* Chapter 1 for discussion). Using the estimated P recycling efficiency (12-13%), this flux can be estimated at $\sim 7.3 \text{ } \mu\text{mol m}^{-2} \text{ d}^{-1}$. This would account for $\sim 50\%$ of the total P input into the water column, indicating a significant contribution from sediments to supplying the reactive P that supports primary production.

A large percentage of the deposited phosphorus (87%) is buried in the sediments (burial flux $43 \text{ } \mu\text{mol m}^{-2} \text{ d}^{-1}$; as detrital or non-reactive organic P). Assuming steady state,

this burial flux appears to be a major long-term sink of phosphorus in Lake Superior (Table 3.3). The burial flux of P (e.g., at FWM) can also be estimated from the solid-phase phosphorus concentration (C_L ; Fig. 3.3) and the known burial velocity (U_L) and porosity (φ_L) in the deep sediment (*see* Chapter 1) as $F_{\text{burr.}} = C_L U_L (1 - \varphi_L) \rho$, with the estimated value of $\sim 25 \mu\text{mol m}^{-2} \text{d}^{-1}$. This value is smaller but the same order of magnitude as the estimate above ($43 \mu\text{mol m}^{-2} \text{d}^{-1}$) that was based on organic P sedimentation and the P recycling efficiency. The difference may be attributable to the underestimation of total P in the deep sediments, as not all P phases were extracted (only detrital, authigenic and Fe-bound P were characterized).

The current P budget for the entire lake appears imbalanced, with P sinks significantly exceeding sources (Table 3.3). We hypothesize that phosphorus inputs from shoreline erosion were probably underestimated in previous studies, as data were largely unavailable (Chapra and Sonzogni 1979). Nevertheless, assuming the lake to be nearly in steady state with respect to the annually-averaged P cycling (P inputs equal outputs) as the TP concentrations leveled off since the 1990s (Sterner et al. 2007), the flux of dissolved phosphorus across the interface would still account for $> 13\%$ of the total P input into the water column, and sediment burial is a major sink of P for the entire lake (Table 3.3). These significant contributions from sediments suggest that the sediment cycling of P needs to be taken into account when modeling the P cycle in Lake Superior and assessing the P controls in the Lake (Chapra and Dolan 2012). The $-34 \mu\text{mol m}^{-2} \text{d}^{-1}$ imbalance in P fluxes would correspond to a $3 \mu\text{mol L}^{-1}$ decrease in the water column TP levels (calculated using surface area of 82100 km^2 and volume of 11920 km^3) over 40 years (the time period since regulations of P loading took effect in the 1970s; Lesht et al

1991). Historical data for the water column TP concentrations in the Laurentian Great Lakes suggested a decline in TP in lakes Michigan, Huron, and Erie, but showed much smaller decreases in Lake Superior (less than $0.1 \mu\text{mol L}^{-1}$ over the past 40 years). This further supports our hypothesis that some source of P to Lake Superior may have been underestimated.

Table 3. 3 Sources and sinks of phosphorus in Lake Superior ($\mu\text{mol m}^{-2} \text{d}^{-1}$). Organic P sedimentation flux is calculated from the organic carbon settling rate of $5.8 \text{ mmol m}^{-2} \text{d}^{-1}$, with a 106C:1P stoichiometry (Heinen and McManus 2004), assuming 10% of the lake floor is non-depositional (actual number not known; Kemp et al. 1978). The flux of P across the SWI is estimated using the organic P sedimentation and P recycling efficiency of 12%; numbers in *italics* are contributions from this study.

Sources or sink	Contribution to P budget		
	Water Column	Sediment	Entire Lake
Atmospheric deposition	0.87 ¹		0.87
Watershed input (tributary)	2.3 ¹		2.3
Point source (municipal and industrial)	0.29 ¹		0.29
Shoreline erosion	4.1 ²		4.1
Outflow	-0.43 ³		-0.43
Organic P sedimentation	<i>-49</i>	<i>49</i>	
Organic P burial		<i>-43</i>	<i>-43</i>
P flux at SWI	<i>5.9</i>	<i>-5.9</i>	
Total input	<i>15</i>	<i>49</i>	<i>7.6</i>
Total output	<i>-49</i>	<i>-49</i>	<i>-43</i>
Imbalance	<i>-34</i>	<i>0</i>	<i>-34</i>

Reference: ¹Dolan and Chapra 2012; ²Chapra and Sonzogni 1979; ³Weiler 1978. The imbalance for both the water column and entire lake is lower when accounting for the non-depositional areas in the lake (Kemp et al. 1978): assuming 30% of lake floor are non-depositional, the imbalance of phosphorus for the water column decrease to $-22 \mu\text{mol m}^{-2} \text{d}^{-1}$ and imbalance for the entire lake decreases to $-23 \mu\text{mol m}^{-2} \text{d}^{-1}$.

CONCLUSIONS

- In Lake Superior sediments, active iron reduction ($0.047 \text{ mmol m}^{-2} \text{ d}^{-1}$) occurs below the penetration depth of oxygen or nitrate, accounting for $< 0.2\%$ of carbon degradation. Dissolved ferrous iron that is produced by iron reduction in the anoxic sediments is re-oxidized at the redox boundaries leading to enrichments in solid phase iron. The presence of multiple metal layers in the sediments of Lake Superior is consistent with redox boundary excursions described in previous Chapters.
- Phosphorus cycling is strongly associated with the cycling of iron. Iron reduction in the anoxic sediment and its re-oxidation at the redox boundary strongly affect the mobilization of phosphorus in the deep sediments. Dissolved phosphorus in the oxic surface sediments comes mostly from regenerated organic phosphorus.
- The sediments in Lake Superior are significant sources of dissolved phosphorus to the water column (effluxes of 2.5 to $7.0 \mu\text{mol m}^{-2} \text{ d}^{-1}$). These fluxes are controlled by the balance between organic phosphorus regeneration and phosphate adsorption in the surface sediments, and only weakly affected by the iron reduction in deeper sediment. The sediment P recycling efficiency is low (12-13%), especially compared to marine sediments with similar oxygen uptake rates ($>50\%$), indicating a strong P retention capacity of Lake Superior sediments. It results from high iron sedimentation in Lake Superior, high Fe:P ratio (>50) in surface sediments, and deep oxygen penetration.
- The updated phosphorus budget for Lake Superior shows non-negligible contributions from sediments. Sediment burial is the major sink of phosphorus (-

43 $\mu\text{mol m}^{-2} \text{d}^{-1}$), whereas the flux of dissolved phosphorus across the SWI accounts for > 13% of the total P inputs into the water column. The updated P budget appears imbalanced, with outputs exceeds inputs. The imbalance ($-40 \mu\text{mol m}^{-2} \text{d}^{-1}$) is greater than what can be accounted for by the documented historical decline in the total phosphorus levels in the Lake Superior water column, suggesting that some significant sources of P, such as phosphorus inputs from shoreline erosion, may have been underestimated.

Chapter 4 Sulfur cycling in Lake Superior sediments: controls on sulfate reduction and implications for low-carbon systems

SUMMARY

To understand the sediment sulfur cycle in Lake Superior, porewater profiles of sulfate were measured and diagenetic fluxes and reaction rates were measured at 13 locations in Lake Superior, in 26 to 318 m water depth. The results reveal that sediment sulfur cycling in Lake Superior differs markedly between the areas of high vs. low sedimentation. Sulfate reduction rates are lower (average $0.012 \text{ mmol m}^{-2} \text{ d}^{-1}$) in the offshore low-sedimentation areas. There, in a striking contrast to the conventional paradigm of diagenetic sulfur cycling, sulfate is supplied to the sediment porewaters through the regeneration of organic sulfur. It is this production of sulfate within the oxidized sediment layer that supports deeper sediment sulfate reduction, while excess sulfate is released into the water column (average efflux $0.020 \text{ mmol m}^{-2} \text{ d}^{-1}$). In contrast, in high-sedimentation nearshore sediments, sulfate reduction rates are higher (average $0.085 \text{ mmol m}^{-2} \text{ d}^{-1}$), and sulfate is drawn from the water column (flux $0.063 \text{ mmol m}^{-2} \text{ d}^{-1}$). Sulfate reduction in Lake Superior sediments accounts for 0.3-3% of organic carbon mineralization. The importance of organic sulfur regeneration as a source of sulfate (supplying >50% of sulfate) suggests that the organic matter supply in this oligotrophic low-sulfate ($\sim 40 \text{ }\mu\text{M}$) system is a major control on sediment sulfate reduction. Our analyses suggest that sedimentary sulfate reduction in low-carbon systems is better correlated to the sedimentation rate and the depth of oxygen and nitrate penetration than

to sulfate concentrations in the overlying waters. This implies that relationships that link the accumulation of sulfide phases (such as pyrite preserved in sedimentary records) and their associated isotopic signatures to the historical sulfate levels may be different in oligotrophic systems than in carbon-rich systems, with possible implications for the modern deep ocean and the low-productivity low-sulfate ancient Oceans.

INTRODUCTION

Sulfur cycling in freshwater sediments has received less attention than in marine systems, as sulfate concentrations are typically low ($0.01\text{-}0.5\text{ mmol L}^{-1}$) compared to those in marine waters (28 mmol L^{-1}). The importance of sulfur cycle in freshwater sediments, however, cannot be neglected as its spatial and temporal dynamics strongly interact with cycles of other elements such as iron and phosphorus (Roden and Edmonds 1997; Caraco et al. 1998; Katsev et al. 2006). The reduction of sulfate in sediments, a process that occurs when organic carbon input is in excess of the availability of more favorable electron acceptors (oxygen, nitrate, and manganese and iron oxides), typically creates an important sink for sulfur in freshwater systems. The reduced sulfide (H_2S) can react with iron to form the diagenetically immobile iron sulfide minerals (e.g., the operationally defined acid-volatile sulfide (AVS, FeS) and eventually pyrite (FeS_2); Morse et al. 1987) or with organic carbon to form organic C-bonded S compounds (Rudd et al. 1986). These phases can then be buried and preserved in the sediment record. It has been suggested that the sediment sulfur storage can be used as a record for past changes in the water-column sulfate concentrations, e.g. for tracking the history of sulfur pollution (Nriagu 1984; Glavin et al. 1990). This relies on a hypothesis that sulfate reduction and sulfur burial are controlled by the sulfate levels in the overlying waters, an idea that is supported by strong correlations between the sediment sulfur content and water column sulfate levels (Gorham et al. 1974; Nriagu 1984). Generalizing these correlations, however, could be problematic if, in addition to sulfate availability, sediment sulfur reduction is also controlled by other factors, such as organic carbon supply or redox conditions. Moreover, the sulfate for sulfate reduction may come from multiple sources

such as reoxidation of sulfides and hydrolysis of sulfate-esters during organic matter mineralization (Holmer and Storkholm 2001; King and Klug 1982). Understanding the sources of sulfate is also crucial for interpreting the relationships between the sulfur isotope signatures in the preserved sedimentary sulfides and water-column sulfate levels. Such relationships have been used, for example, for inferring the sulfate concentrations in the ancient Oceans (Habicht et al. 2002), based on the isotopic fractionations ($\Delta^{34}\text{S}$ sulfate-sulfide) during sulfate reduction. Additional sulfate sources may complicate such interpretations, as different fractionations may be imparted on the source sulfate (Canfield 2001).

In Lake Superior, the sulfate concentrations are low ($\sim 40 \mu\text{mol L}^{-1}$) compared to marine waters, while the sediment carbon and nitrogen cycles are similar to those in the marine environments (*see* previous Chapters). The sediment sulfur cycle has not been characterized, with some work in the 1980s suggesting insignificant contributions of sulfate reduction to sediment carbon mineralization, based on model estimates from one location in the lake (Carton et al. 1989). Similarly to the increasing trend in nitrate concentrations in the water column (Chapter 2), sulfate concentrations have also increased over the past decades, though to a lesser degree (increase by $\sim 15 \mu\text{mol L}^{-1}$ since the 1960s). This increase has been attributed to an increase in fossil-fuel usage (Chapra et al. 2012). The potential effects of these trends on the sediment sulfur cycle and sediment-water feedbacks are not known. This chapter characterizes the sediment sulfur cycle in Lake Superior and discusses the controls on sediment sulfate reduction and sediment sulfur storage in the lake. The sensitivity of the sediment sulfur cycle to water column sulfate concentrations in low-carbon systems is analyzed to discuss the implications of

these results for using sediment S accumulation as a paleolimnological tracer for sulfate inputs in freshwater lakes, as well as complications for interpreting sediment sulfur records in analogous marine environments, such as the oligotrophic deep oceans or the low-sulfate ancient oceans.

METHODS

Sediment sampling and analyses

Sediments and overlying waters were sampled across Lake Superior on multiple cruises aboard the R/V *Blue Heron* in 2009-2012 (Fig. 1.1; Table 1.1), and processed using the procedures described in Chapter 1 and 2. The porewater samples for sulfate analyses were frozen at -18°C until measurements. Sulfate concentrations were measured by ion chromatography (DIONEX ICS 1100).

Calculations of fluxes and rates

The molecular diffusive fluxes (F_i) of sulfate were calculated using Fick's law of diffusion described in previous Chapters (Eq. 1.5 and Eq. 2.1), using the bulk molecular diffusion coefficient $D_{\text{SO}_4^{2-}} = 183 \text{ cm}^2 \text{ y}^{-1}$ at the in-situ temperature of 4°C with correction for sediment tortuosity (*see* Chapters 1 and 2 for details):

The rates of sulfate production (release and oxidation of sulfide) and consumption (reduction) can be estimated from the measured vertical concentration profiles of sulfate using the diagenetic diffusion-reaction equation described in previous Chapters (*see* Chapter 1, Eq 1.2, Chapter 2, Eq 2.2). Under steady-state conditions, the rate equations for porewater sulfate can be written as

$$\frac{d}{dx} \left(\varphi D_{\text{s-SO}_4^{2-}} \frac{dC_{\text{SO}_4^{2-}}}{dx} \right) + R_{\text{SO}_4^{2-} \text{ prod.}}(x) - R_{\text{SO}_4^{2-} \text{ red.}}(x) + \varphi \alpha_{\text{irr}} \left(C_{\text{SO}_4^{2-}}^0 - C_{\text{SO}_4^{2-}}^{\text{burr}} \right) = 0 \quad (4.1)$$

Here $R_{\text{SO}_4^{2-} \text{ prod.}}$ and $R_{\text{SO}_4^{2-} \text{ red.}}$ are the rates of sulfate production and sulfate consumption (reduction); C^0 and C^{burr} are the concentrations of sulfate, respectively, above the sediment surface and within the bioirrigated burrows, and α_{irr} is the bioirrigation

coefficient (Katsev et al. 2007). In the oxic sediment zone (*see* Chapter 1 for oxygen profiles) where sulfate reduction is negligible (sulfate reduction occurs only below the depth of oxygen penetration; Burdige 2006), the rate of sulfate production can be obtained as

$$R_{\text{SO}_4^{2-} \text{ prod.}}(x) = -\frac{d}{dx} \left(\varphi D_{\text{s-SO}_4^{2-}} \frac{dC_{\text{SO}_4^{2-}}}{dx} \right) - \varphi \alpha_{\text{irr}} \left(C_{\text{SO}_4^{2-}}^0 - C_{\text{SO}_4^{2-}}^{\text{burr}} \right) \quad (4.2)$$

The exceptionally deep oxygenation of sediments in Lake Superior (Chapter 1, Fig. 1.6) thus allows the calculation of sulfate production rates ($R_{\text{SO}_4^{2-} \text{ prod.}}$) in the surface sediments. By neglecting bioirrigation, Eq. 4.2 can be written as

$$R_{\text{SO}_4^{2-} \text{ prod.}}(x) = -\frac{d}{dx} \left(\varphi D_{\text{s-SO}_4^{2-}} \frac{dC_{\text{SO}_4^{2-}}}{dx} \right) \quad (4.3)$$

For a typical concentration gradient for sulfate in Lake Superior ($C^0 - C^{\text{burr}} < 0$, *see* results below), Eq. 4.3 yields the minimum sulfate production rates and the actual rates in the surface sediments could be higher (Eq. 4.2). In deeper sediment (> 2 cm), bioirrigation is negligible (*see* results in Chapter 1). The area-specific (integrated over sediment depth) net sulfate production rates ($\text{mmol m}^{-2} \text{d}^{-1}$) in oxic surface sediments can be calculated by integrating Eq. 4.3 from the sediment-water interface (SWI; $x=0$) to the upper boundary of sulfate reduction L (using a similar method as described in Chapter 2, Eq. 2.7; also see Results and Discussion for more details on choosing L and uncertainties estimation):

$$\begin{aligned} R_{\text{SO}_4^{2-} \text{ prod.}}^*(x) &= \int_0^L R_{\text{SO}_4^{2-} \text{ prod.}}(x) dx = -\int_0^L \frac{d}{dx} \left(\varphi D_{\text{s-SO}_4^{2-}} \frac{dC_{\text{SO}_4^{2-}}}{dx} \right) dx \\ &= \left(\varphi D_{\text{s-SO}_4^{2-}} \frac{dC_{\text{SO}_4^{2-}}}{dx} \right)_{x=0} - \left(\varphi D_{\text{s-SO}_4^{2-}} \frac{dC_{\text{SO}_4^{2-}}}{dx} \right)_{x=L} = F_{\text{SO}_4^{2-}(x=L)} - F_{\text{SO}_4^{2-}(x=0)} \end{aligned} \quad (4.4)$$

Here $R_{\text{SO}_4^{2-} \text{ prod.}}^*$ is the depth-integrated sulfate production rate, and $F_{\text{SO}_4^{2-}(x=0)}$ and $F_{\text{SO}_4^{2-}(x=L)}$ are the diffusive fluxes at the SWI and $x=L$, respectively. L can be chosen at the depth where $F_{\text{SO}_4^{2-}}$ reaches a maximum (this depth typically coincides with the depth of oxygen and/or nitrate penetration; see also Chapter 2, Eq. 2.7 and Discussion in this Chapter for more details).

The net rates of sulfate reduction in the deep sediments can be estimated, assuming that sulfide reoxidation in the anoxic sediment and sulfate production from organic sulfur in the reactive carbon-depleted deep sediment are negligible, as:

$$R_{\text{SO}_4^{2-} \text{ red.}}(x) = \frac{d}{dx} \left(\varphi D_{\text{s-SO}_4^{2-}} \frac{dC_{\text{SO}_4^{2-}}}{dx} \right) \quad (4.5)$$

The area-specific rates of sulfate reduction ($R_{\text{SO}_4^{2-} \text{ red.}}^*$; $\text{mmol m}^{-2} \text{d}^{-1}$) can be estimated by integrating Eq. 4.5 from the upper boundary of sulfate reduction (L in Eq. 4.4) to L^∞ , the depth where the sulfate gradients vanish:

$$R_{\text{SO}_4^{2-} \text{ red.}}^*(x) = \int_L^\infty \frac{d}{dx} \left(\varphi D_{\text{s-SO}_4^{2-}} \frac{dC_{\text{SO}_4^{2-}}}{dx} \right) dx = \left(\varphi D_{\text{s-SO}_4^{2-}} \frac{dC_{\text{SO}_4^{2-}}}{dx} \right) \Bigg|_{x=L}^{x=\infty} = F_{\text{SO}_4^{2-}(x=L)} \quad (4.6)$$

where $F_{\text{NO}_3^-(x=L)}$ is the diffusive flux at L (see Results for details).

RESULTS

Porewater concentrations of sulfate

In a striking departure from the conventional diagenetic profiles of sulfate where sulfate concentrations decrease monotonically downward from the sediment-water interface, typical porewater sulfate distributions (Fig. 4.1) in Lake Superior sediments exhibit peaks at or several mm below the interface. The exceptions are Sta. NB and several cores at Sta. IR where sulfate concentrations were higher in the overlying waters than in the sediments (Fig. 4.1). The sulfate concentrations below the peaks typically decrease into the anoxic sediments, with the exception of Sta. NIP where sulfate concentrations continue to increase with depth. At stations where oxygen and nitrate penetrations are relatively shallow (*see* O₂ and NO₃⁻ profiles in Chapters 1 and 2), sulfate is exhausted in the sediment below the depth of nitrate penetration (e.g., Sta. IR, NB, TB, BB, and several cores at Sta. FWM, EM, ED, and SW). In sediments with deep oxygen and nitrate penetrations, the sulfate penetrations are also deep (e.g., Sta. WM, CM, and several cores at Sta. FWM, ED, SW).

Sulfate fluxes across the sediment-water interface

The higher sulfate concentrations in surface sediments than in overlying waters (Fig. 4.1) suggest that at most locations the sediments are sources of sulfate to the water column (effluxes range from 0.007 mmol m⁻² d⁻¹ at Sta. EM to 0.047 mmol m⁻² d⁻¹ at Sta. TB; Table 4.1). At some nearshore high-sedimentation sites (e.g., Sta. NB and several cores at Sta. IR), however, sulfate influxes from the water column to the sediments (flux

in $0.026 \text{ mmol m}^{-2} \text{ d}^{-1}$ at Sta. IR and $0.010 \text{ mmol m}^{-2} \text{ d}^{-1}$ at Sta. NB; Table 4.1). Bioirrigation is expected to affect the sulfate fluxes to a much lesser degree than oxygen fluxes (30-50%; Chapter 1), as the bioirrigation coefficients for sulfate are lower ($D_{\text{bio-SO}_4^{2-}}$ is $\sim 20\%$ of $D_{\text{bio-O}_2}$; Meile et al. 2005).

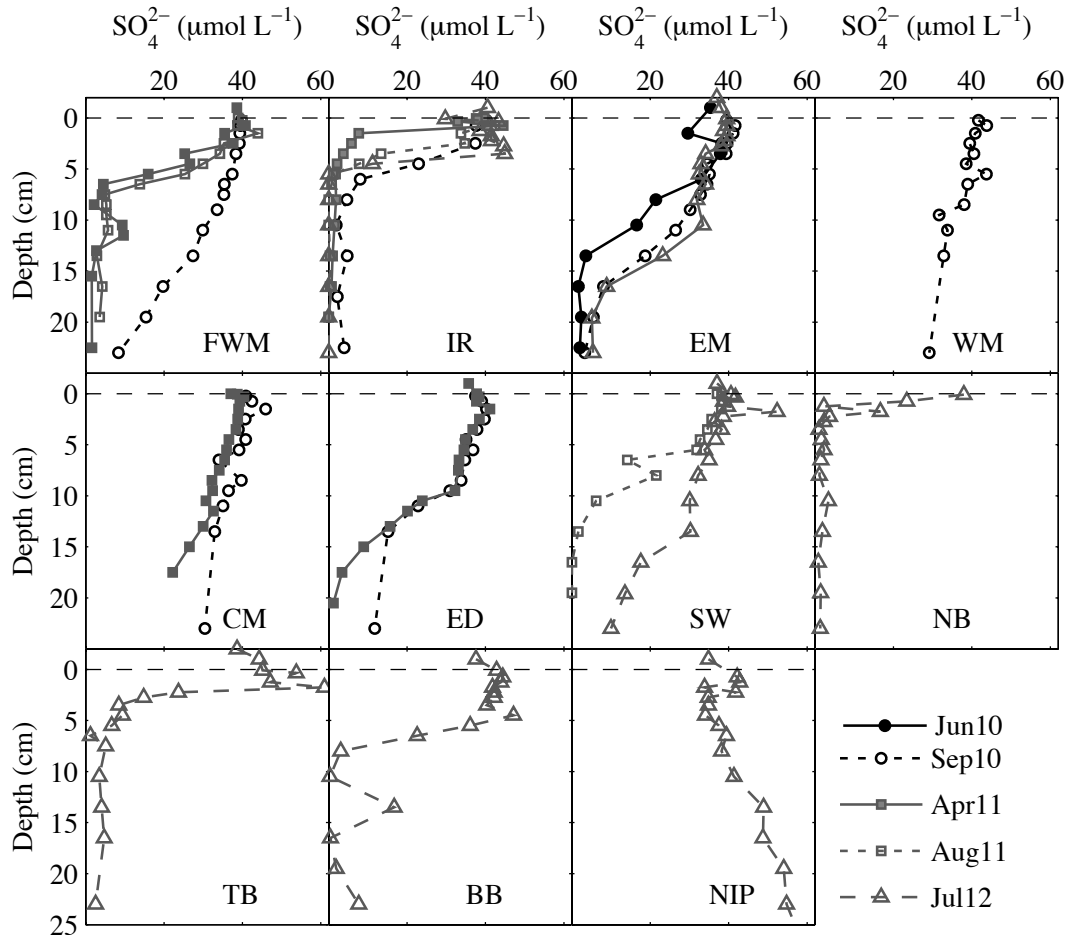


Figure 4. 1 Vertical distributions of porewater sulfate in Lake Superior sediments.

Table 4. 1 The fluxes of sulfate across SWI (positive indicate flux into the sediment), integrated rates of sulfate production ($R^*_{\text{SO}_4^{2-} \text{ prod.}}$), the ratio of sulfate production to carbon mineralization ($R^*_{\text{SO}_4^{2-} \text{ prod.}} : R^*_C$), integrated rates of sulfate reduction ($R^*_{\text{SO}_4^{2-} \text{ red.}}$), and percentage of carbon mineralization by sulfate reduction ($R^*_{\text{SO}_4^{2-} \text{ red.}} : R^*_C$). All rates are in $\text{mmol m}^{-2} \text{ d}^{-1}$.

Station	TOU	$F_{\text{SO}_4^{2-}}$	$R^*_{\text{SO}_4^{2-} \text{ prod.}}$	$R^*_{\text{SO}_4^{2-} \text{ prod.}} : R^*_C$	$R^*_{\text{SO}_4^{2-} \text{ red.}}$	$R^*_{\text{SO}_4^{2-} \text{ red.}} : R^*_{\text{SO}_4^{2-} \text{ prod.}}$	$R^*_{\text{SO}_4^{2-} \text{ red.}} : R^*_C$
FWM.6	6.4	-0.0075	0.032		0.025		
FWM.7	5.2	-0.019	0.044		0.025; 0.018		
Average	5.8	-0.013	0.038	0.008	0.023	60±18%	0.9%
IR.3	5.4	0.0053	0.018; 0.023		0.023		
IR.4	10.3	0.052	0.060		0.11		
IR.5	6.9	0.035; 0.013	0.050		0.063		
IR.6			0.099		0.087		
Average	7.5	0.026	0.050	0.008	0.071	127±40%	2.2%
EM.3	3.7	-0.0049	0.013		0.0076		
EM.5	3.7		0.025		0.0055		
EM.6	3.6	-0.0091	0.017		0.0076		
Average	3.7	-0.007	0.018	0.006	0.0069	42±18%	0.4%
ED.2	4.1	-0.014	0.023		0.0095		
ED.3	9.6	-0.012	0.027; 0.018		0.015; 0.0065		
Average	6.9	-0.013	0.023	0.004	0.010	45±4%	0.3%
CM.3	2.9	-0.013	>0.013				
CM.4	5.7		0.04				
Average	4.3		0.027	0.007			
SW.1	9.3	-0.021	0.036		0.011		
SW.2	5.9	-0.019	0.026		0.0067		
Average	7.6	-0.020	0.031	0.002	0.009	56%	0.3%
†NB.1	10	0.10	0.060	0.007	0.16	217%	3%
†TB.1	7.7	-0.047	0.13;	0.02	0.083	77%	2.5%
†BB.1	13	-0.028	0.057;	0.005	0.029;	51%	0.6%

Sulfate production rates in surface sediments

The higher concentrations of sulfate in surface sediments than in the overlying waters at most locations indicate production of sulfate within the sediment (Fig. 4.1). The calculated rates of sulfate production (Fig. 4.2) indicate that it occurs in the upper 10 cm of sediment, above the depth of oxygen and nitrate penetrations. The rates are highest near the sediment surface (maximum rates $\sim 0.005\text{-}0.04 \mu\text{mol cm}^{-3} \text{ d}^{-1}$), decrease with depth, and become negligible below 10 cm. As discussed above, these are minimum rates, as bioirrigation in the surface sediment was neglected (Eq. 4.2). For a typical bioirrigation coefficient of $\alpha_{\text{irr}} < 10^{-6} \text{ s}^{-1}$ (Matisoff and Wang 1998) and the sulfate concentration difference $C^0 - C^{\text{burr}}$ (between and overlying water and the bioirrigated burrows) of $< 5 \mu\text{mol L}^{-1}$, the approximate increase in sulfate production due to bioirrigation would be less than $0.0003 \mu\text{mol cm}^{-3} \text{ d}^{-1}$, which is $< 10\%$ of the maximum sulfate production rates in the surface sediment. The rates below the bioturbation zone (2 cm) should not be affected. The depth-integrated sulfate production rates (Table 4.1) range between 0.018 and $0.13 \text{ mmol m}^{-2} \text{ d}^{-1}$ (average $0.049 \text{ mmol m}^{-2} \text{ d}^{-1}$). The effects of bioirrigation on these rates can be estimated by integrating the bioirrigation term in Eq. 4.2 over the upper 2 cm of sediments, using parameters described above. This yields an increase in sulfate production of $< 0.003 \text{ mmol m}^{-2} \text{ d}^{-1}$, which is also $< 10\%$ of the calculated rates.

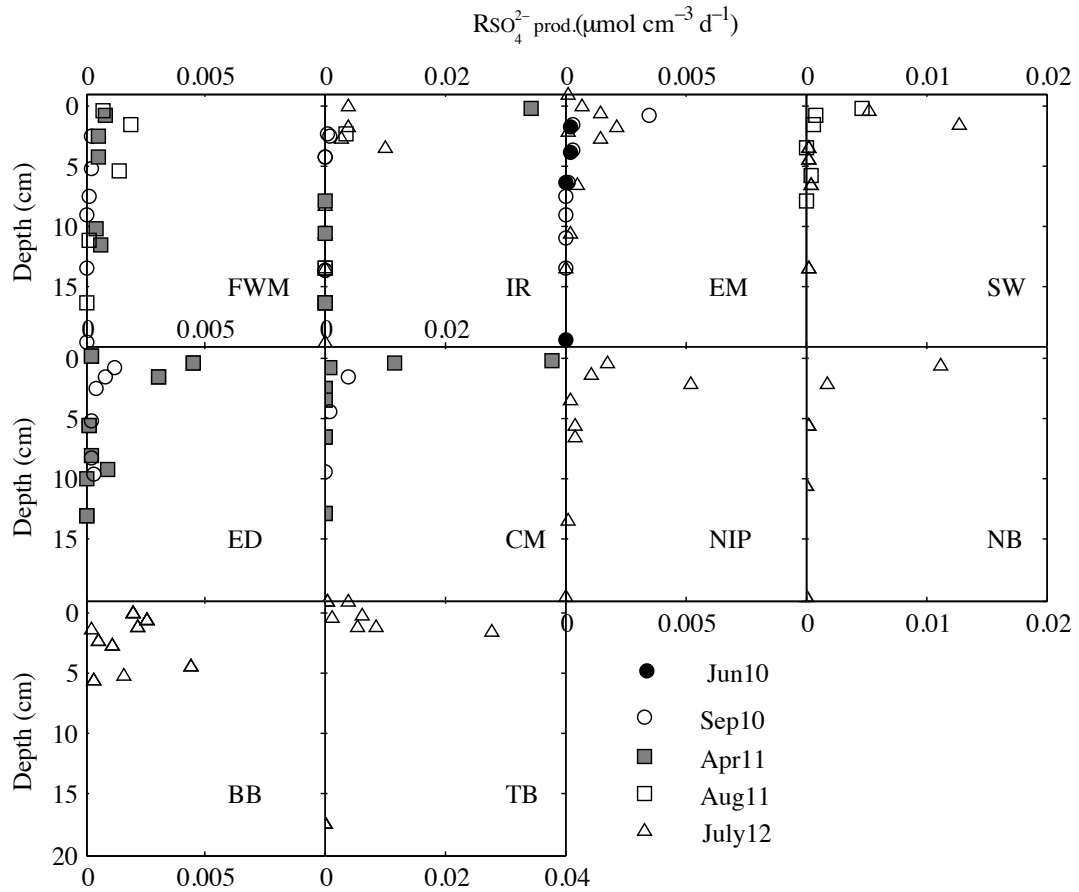


Figure 4. 2 Calculated rates of sulfate production in sediments of Lake Superior

Sulfate reduction rates in anoxic sediments

The decrease in sulfate concentrations into the deep anoxic sediments suggests active sulfate reduction (which must be coupled to carbon mineralization and/or oxidation of methane) at all stations except Sta. NIP (Fig. 4.1). Sulfate reduction typically occurs below the depth of nitrate penetration (NPD); the rates peak within several mm of the NPD and decrease into the deeper sediment (Fig. 4.3). As the upper boundaries of sulfate reduction (L in Eq. 4.6) are below the bioturbation zone, the calculated sulfate

reduction rates should be unaffected by bioturbation and bioirrigation. The depth-integrated rates of sulfate reduction (Eq. 4.6) range from 0.007 mmol m⁻² d⁻¹ (at Sta. EM) to 0.13 mmol m⁻² d⁻¹ (at Sta. NB).

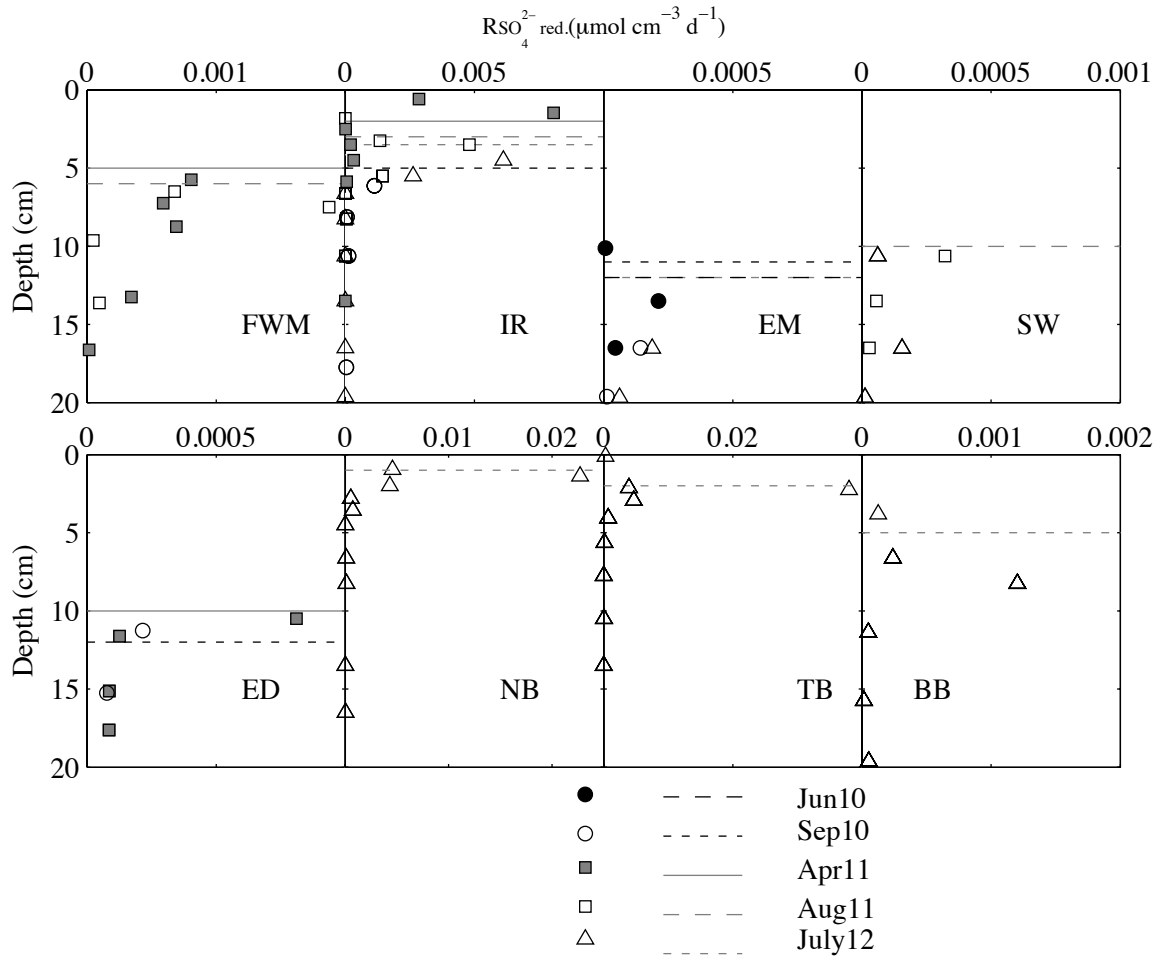


Figure 4. 3 Calculated rates of sulfate reduction in sediments of Lake Superior. The corresponding (seasonally varying) depths of oxygen and nitrate penetration that affect the vertical extent of the sulfate reduction zones are described in Chapters 1 and 2.

DISCUSSION

Sulfur cycling in high- vs. low-sedimentation areas

The sulfur cycle in the sediments of Lake Superior exhibits strong spatial heterogeneity, similarly to the cycles of carbon and nitrogen (*see* Chapters 1 and 2). Figure 4.4 compares the calculated vertical sulfate fluxes ($F_{\text{SO}_4^{2-}}$) and net sulfate production/consumption rates ($R_{\text{SO}_4^{2-}}$) in two typical sediments in Lake Superior. In both sediments sulfate is produced in the surface oxic sediments, supporting sulfate reduction in the deeper anoxic sediment (Fig. 4.4 C). In sediment from an ‘offshore’ low-sedimentation area where oxygen and nitrate penetrations are deep (e.g. Sta. FWM in Fig. 4.4 A), sulfate reduction is supported by the sulfate produced in the surface sediment, and excess sulfate exits the sediments into the water column. The average sulfate effluxes ($0.020 \text{ mmol m}^{-2} \text{ d}^{-1}$) in these sediments account for 43% of the net sulfate production ($0.046 \text{ mmol m}^{-2} \text{ d}^{-1}$), while the remaining 57% is reduced in the sediment (average sulfate reduction rate $0.027 \text{ mmol m}^{-2} \text{ d}^{-1}$; Table 4.1). In ‘nearshore’ high sedimentation areas where oxygen and nitrate penetrations are shallow (e.g., Sta. IR; Fig. 4.4), sulfate reduction rates are higher (average $0.12 \text{ mmol m}^{-2} \text{ d}^{-1}$), exceeding the rates of sulfate production ($0.06 \text{ mmol m}^{-2} \text{ d}^{-1}$). There, the sulfate produced in the surface sediment supports ~50% of sulfate reduction, while the remaining 50% is supplied by sulfate fluxes from the water column ($0.063 \text{ mmol m}^{-2} \text{ d}^{-1}$). In the discussion below we analyze these processes and their controls in more detail.

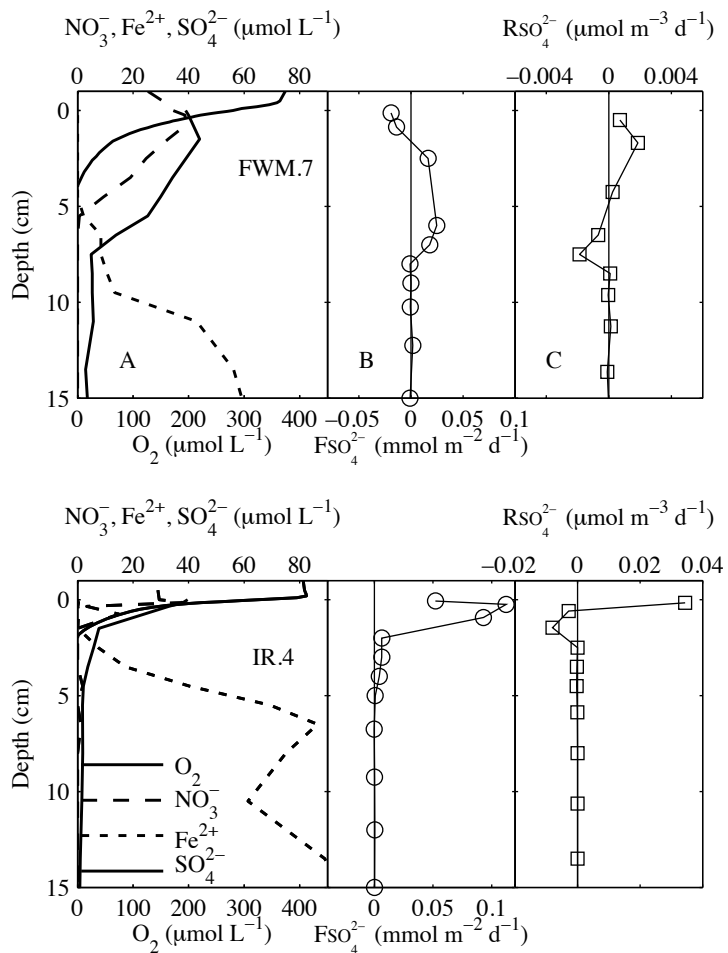


Figure 4.4 (A) Typical distributions of O_2 , NO_3^- , dissolved Fe^{2+} and SO_4^{2-} ; (B) the corresponding sulfate fluxes, $F_{\text{SO}_4^{2-}}$ (negative into the water column); (C) the corresponding rates $R_{\text{SO}_4^{2-}}$ (positive for sulfate production and negative for sulfate reduction). The depth L where $R_{\text{SO}_4^{2-}}$ falls to zero and $F_{\text{SO}_4^{2-}}$ reaches maximum separates the zones of net sulfate production (in surface sediments) and consumption (in deep sediments). O_2 , NO_3^- , dissolved Fe^{2+} profiles are re-plotted from previous Chapters.

Sulfate production

Understanding the sulfate production processes in the sediments of Lake Superior is important as these reactions provide > 50% of sulfate for sulfate reduction. Production of sulfate in surface sediments may result from two major processes: re-oxidation of dissolved sulfides (HS^- , H_2S and other polysulfide S_n^{2-} ; we use $\sum\text{H}_2\text{S}$ to represent all in later discussion), and hydrolysis of sulfate-esters during mineralization of organic matter. Re-oxidation of $\sum\text{H}_2\text{S}$ is considered to be a minor contributor to the net sulfate production in Lake Superior sediments, as maximum sulfate production occurs well within the oxic zone (e.g., ~ 2 cm at Sta. FWM and < 1 cm at Sta. IR) rather than at the redox boundaries (e.g., ~5 cm at Sta. FWM and 2 cm at Sta. IR) where $\sum\text{H}_2\text{S}$ can be rapidly oxidized. Hydrolysis of sulfate-esters, therefore, must be the main process that produces sulfate in Lake Superior. This is in contrast to a previous suggestion in eutrophic systems where this source was thought to contribute <10% of sulfate for reduction, whereas re-oxidation of reduced sulfur dominated (King and Klug 1980, 1982; Marnette et al. 1992). The stoichiometric ratio of carbon mineralized to sulfate produced (for hydrolysis of sulfate-esters) is poorly understood. The results suggest an average $R^*_{\text{SO}_4^2\text{-prod.}}: R^*_\text{C}$ ratio of ~ 0.006 (average $R^*_\text{C}: R^*_{\text{SO}_4^2\text{-prod.}}$ of ~ 167; Table. 4.1). This ratio is greater than but broadly consistent with the S: Organic C ratio of ~ 0.004 that was previously estimated in the surface sediments of Lake Superior (Nriagu 1984).

Sulfate reduction

Net sulfate reduction accounts for 0.3 – 3% of organic carbon mineralization in Lake Superior sediments. This contribution is an order of magnitude smaller than from

denitrification (1 -31%; Table 2.4, Chapter 2) and similar to that from iron reduction (1%; Table. 3.2, Chapter 3). The net sulfate reduction rates in the sediments from low-sedimentation offshore sites are low ($0.0069\text{-}0.023\text{ mmol m}^{-2}\text{ d}^{-1}$; average $0.012\text{ mmol m}^{-2}\text{ d}^{-1}$), whereas sulfate reduction rates at high-sedimentation nearshore sites are higher (average $0.085\text{ mmol m}^{-2}\text{ d}^{-1}$). As in the offshore areas the sulfate for sulfate reduction is sourced within the sediment rather than supplied from the water column, the sulfate reduction rates there are not expected to be limited by sulfate concentrations in the overlying water. Instead, they are likely regulated by the supply of organic matter (organic S sedimentation). This idea is supported by a comparison between the sediment sulfate reduction rates in freshwater lakes (where sulfate concentrations are 5 to 500 μM) and in marine environments (28 mM) (Fig. 4.5): despite the difference in sulfate concentrations, the rates of sulfate reduction in oligotrophic lakes are similar to those in marine sediments of similar sedimentation rates (Canfield 1989). The sediment sulfate reduction in oligotrophic freshwater systems is thus controlled by the sedimentation flux (organic S sedimentation) and should be less sensitive to sulfate concentrations in the overlying waters.

In addition to the dependence on organic matter sedimentation through the supply of organic sulfur, the rates of sulfate reduction are affected by the organic matter sedimentation through the supply of organic carbon. As sulfate reduction occurs below the zones of oxic respiration and denitrification, the rates of sulfate reduction depend on the depths of oxygen and nitrate penetrations. These penetration depths regulate the amount and reactivity of organic carbon that reaches the sulfate reduction zone, and for deeply oxygenated sediments depend on the supply of organic carbon nonlinearly. Figure

4.6 shows the negative correlation between the OPD and/or NPD and the net sulfate reduction rates in Lake Superior. Similarly to the correlation described in Chapter 2 between denitrification and sediment oxygen penetration (Fig. 2.8), a similar relationship may exist in other systems characterized by low organic carbon sedimentation, such as in the deep oceans.

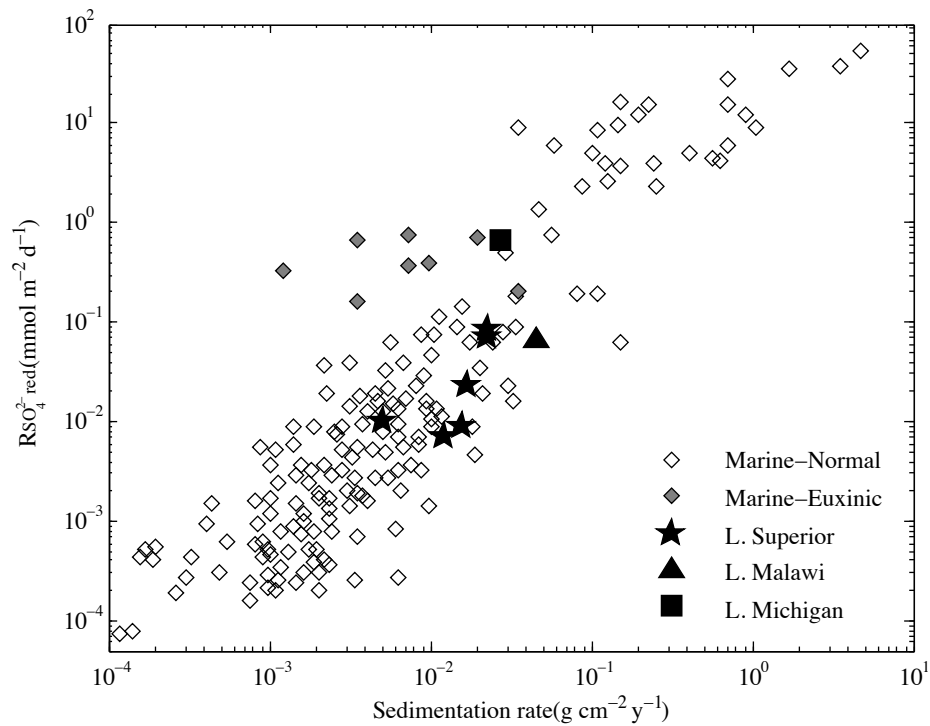


Figure 4. 5 Sediment sulfate reduction rates vs. sedimentation rates. The data are from Lake Superior (this study), Lake Malawi (Chapter 5), Lake Michigan (Thomsen et al. 2004), and marine sediments (Canfield 1989).

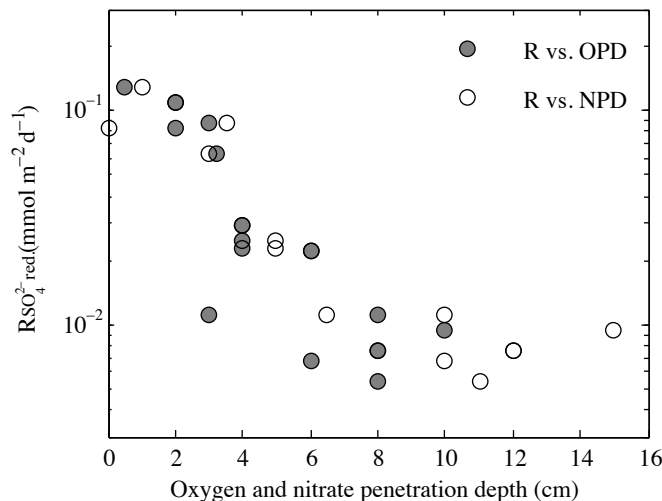


Figure 4. 6 The rates of sediment sulfate reduction vs. oxygen and nitrate penetration (See previous Chapters for OPD and NPD).

Lake Superior sediments as sinks for sulfur

Sediments in Lake Superior serve as net sinks for sulfur from the system, with the long-term burial of non-reactive sulfur compounds (reduced S in iron-sulfide minerals and C-bound organic sulfur) at the rate of $0.012 \text{ mmol m}^{-2} \text{ d}^{-1}$ offshore and $0.085 \text{ mmol m}^{-2} \text{ d}^{-1}$ nearshore. This possibly underestimates the burial rates as some refractory organic sulfur compounds deposited into the sediment may also be buried. The effluxes of sulfate from the offshore sediments (average $\sim 0.020 \text{ mmol m}^{-2} \text{ d}^{-1}$) suggest a sulfate recycling efficiency of $< 43\%$ (Table 4.1). The high concentrations of dissolved Fe^{2+} in the deep sediments (Fig. 4.4 A and more profiles in Chapter 3) and the sediment pH of $\sim 7-8$ (see data in Appendix) suggest that the concentrations of dissolved $\Sigma\text{H}_2\text{S}$ should be low, as ferrous iron strongly reacts with dissolved sulfides to precipitate iron sulfides (Morse et al. 1987). Deep oxygen penetrations imply negligible fluxes of dissolved sulfide across

the SWI. The concentrations of H₂S were not directly measured as of writing of this Thesis.

The proposed insensitivity of sulfate reduction to sulfate concentrations in carbon-poor sediments suggests that in such sediments the sediment storage of sulfur may not be an appropriate proxy for understanding the historical changes in the water column sulfate concentrations. The organic matter supply (both organic carbon and organic sulfur) is instead a more important control on the sediment sulfate reduction and storage rates. The increases in sulfate concentration in the water of Lake Superior over the 20th century should not have significantly increased the sediment sulfate reduction rates, at least offshore. To the contrary, the concomitant increase in nitrate concentrations (see Chapter 2), by potentially increasing the depth of nitrate penetration, may have led to a decrease in the rates of sulfate reduction (Fig. 4.6).

Extrapolating these findings to carbon-poor low-sulfate environments of the past, such as in the Precambrian Ocean (Gaines et al. 2012), regeneration of sediment organic sulfur into the sulfate pool may have contributed significantly to the support of sulfate reduction in addition to sulfate supplied from the water column. Using the ³²S/³⁴S isotope fractionation between the water column sulfate and sedimentary pyrites in these conditions may be inaccurate as a paleoreconstruction tool, as additional fractionation processes may be involved. Sulfur isotope fractionation associated with assimilatory sulfate reduction in the water column (sulfate uptake and incorporation into organic matter) is small ($\sim\Delta^{34}\text{S}$ sulfate-sulfite of 0.9 to 2.8‰), but may be significant considering the small fractionation detected in ancient pyrites resulted from low rates of sulfate

reduction (e.g, < 10‰ in Archean pyrites; Habicht et al. 2002). The isotopic fractionation during the hydrolysis of sulfate-esters is not known.

CONCLUSIONS

- The sulfur cycle in Lake Superior sediments is characterized by strong spatial heterogeneity. In offshore low-sedimentation areas, sulfate flux is directed out from the sediments into the water column ($0.020 \text{ mmol m}^{-2} \text{ d}^{-1}$), whereas in some nearshore high-sedimentation areas, sulfate fluxes are into the sediments ($0.063 \text{ mmol m}^{-2} \text{ d}^{-1}$).
- Sulfate is produced within the sediments, most likely by regeneration of organic sulfur (hydrolysis of sulfate-esters). In Lake Superior, this process contributes up to > 50% of sulfate that supports sulfate reduction (100% in the offshore low-sedimentation areas and 50% in the nearshore high-sedimentation areas). This strongly contrasts previous suggestions made for eutrophic systems that this source of sulfate plays only a minor role. The sulfate production rate of $\sim 0.05 \text{ mmol m}^{-2} \text{ d}^{-1}$ suggests a $R^*_{\text{SO}_4^{2-}\text{prod.}} : R^*_C$ ratio (i.e. the S:C release during organic matter mineralization) of ~ 0.006 .
- Sulfate reduction in Lake Superior sediments (average $0.012 \text{ mmol m}^{-2} \text{ d}^{-1}$ offshore and $0.085 \text{ mmol m}^{-2} \text{ d}^{-1}$ nearshore) accounts for > 0.3-3% of carbon mineralization. The rates of sulfate reduction in oligotrophic lake sediments (e.g., Lake Superior) are similar to those in marine sediments of similar sedimentation rates, despite the low sulfate concentrations in freshwater. Sulfate reduction in these low-sedimentation

low-carbon systems is controlled mainly by the supply of organic matter (through the sedimentation of both organic S and organic C) and the penetration depths of oxygen and nitrate. The sulfate reduction rates are not expected to be sensitive to the concentrations of sulfate in the overlying waters.

- Sediment sulfur storage may not be an appropriate proxy for tracing the changes of sulfate concentrations in oligotrophic systems.

Chapter 5 Sediment carbon and nutrient cycling in tropical meromictic Lake Malawi

Most of the results in this Chapter have been compiled into a paper, to be submitted to Limnology and Oceanography with authors listed below:

¹Jiying Li, ¹Erik T. Brown, ²Sean A. Crowe, and ^{1,3}Sergei Katsev

¹ Large Lakes Observatory, University of Minnesota Duluth

² Departments of Microbiology and Immunology and Earth, Ocean, and Atmospheric Sciences, University of British Columbia

³ Department of Physics, University of Minnesota Duluth

SUMMARY

To characterize the water column and sediment geochemistry and constrain carbon and nutrient budgets in the East African Lake Malawi, we measured geochemical distributions in the water column and sediments at 4 locations (in 100 to 650 m depth). The results reveal that in deep anoxic sediments of the lake organic carbon is buried with high efficiency (44%), though the area-specific rates of carbon mineralization ($4.6 \text{ mmol m}^{-2} \text{ d}^{-1}$) are similar to those in temperate large lakes and marine sediments in similar water depths. Ammonium effluxes from the sediments ($0.44 \text{ mmol m}^{-2} \text{ d}^{-1}$) supply 17- 21% of all nitrogen entering the water column. Sediment denitrification (average $0.035 \text{ mmol m}^{-2} \text{ d}^{-1}$) and burial of organic nitrogen ($0.27 \text{ mmol m}^{-2} \text{ d}^{-1}$) remove >16% of the total nitrogen input into Lake Malawi. The recycling efficiency of phosphorus in the sediments is high (64%). Sediment SRP effluxes ($0.037 \text{ mmol m}^{-2} \text{ d}^{-1}$) are comparable to the external P inputs into the lake estimated in 1990s, which are likely exceeded by the present-day external loads. This high phosphorus recycling efficiency suggests that sediments are only weak sinks for water column phosphorus, which leads to higher sensitivity of the water column P levels to external phosphorus inputs.

INTRODUCTION

The East African Lake Malawi is the fifth largest lake in the world by volume, the second deepest (maximum depth >700 m) in Africa, and an important source of fish protein for local populations (Bootsma and Hecky 2003). Like other East African Great Lakes, Lake Malawi is under considerable stress from both anthropogenic changes in their watersheds and climate warming (Bootsma and Hecky 2003; Hecky et al. 2003; Otu et al. 2011). Intensification of agriculture has led to increased erosion and nutrient inputs: since the 1940s, the lake has been experiencing increases in sedimentation, concentrations of total sedimentary phosphorus, and abundances of eutrophic diatom taxa in the Southern basin (Hecky et al. 1999; Otu et al. 2011). Historic water temperature data reveals that the deep waters have warmed by ~ 0.7 °C between 1940s and early 2000s (Vollmer et al. 2005).

Lake-wide budgets of nitrogen, phosphorus and silica were last estimated in the mid-1990s (Bootsma and Hecky 1999). Since then increases in population and agricultural activity have led to further losses of forest cover, altered river discharges, and significantly increased nutrient loadings (Hecky et al. 2003). In addition, sediment contributions to the carbon and nutrient cycles in the lake have not been quantified, and both carbon and nutrient lake-wide budgets remain uncertain. As shown in previous chapters, sediment processes can be a significant component of carbon and nutrient cycling. Understanding this contribution is crucial for understanding not only the geochemical cycling in the lake but also the sensitivity of the ecosystem to external stress (e.g. increasing nutrient inputs). The goal of this chapter is to fill this gap.

In addition to understanding the sediments' contribution to carbon and nutrient cycles in Lake Malawi, investigating the sediments in this large meromictic lake provides an opportunity to study geochemical controls of these processes in hypoxic/anoxic conditions. Lake Malawi's water column is permanently stratified by temperature and weak salinity gradients (Halfman 1993). As a result, oxygen concentrations decrease below a diffuse thermocline at ~100 m, and waters below 200 m are permanently anoxic (Halfman 1993). The bottom waters in the shallower (<200 m) southern region of the lake are hypoxic (<20% O₂ saturation). Results from previous chapters (chapters 1 and 2) showed that sediment carbon and nitrogen cycles in well-oxygenated large temperate freshwater lakes follow relationships similar to those in marine systems. Whereas tropical large lakes with anoxic water columns may be hypothesized to be analogous to tropical anoxic marine basins, no quantitative comparisons have yet been made. This chapter will use the study in Lake Malawi to make cross-system comparisons that may lead to a better understanding of the fundamentals of carbon mineralization and nutrient cycling.

This chapter reports on the results from three cruises conducted on Lake Malawi in 2011, 2012 and 2014. In addition to recording changes in lake temperature and chemical distributions in the water column, sediment organic matter mineralization and nutrient cycling were characterized at 4 locations across the lake, in water depths from 100 to 650 m. Efficiency of carbon preservation was analyzed in these warm anoxic sediments, compare the results to those in marine and cold freshwater sediments, and quantify sediment contributions to the C, N and P cycles and the lake-wide C and nutrient geochemical budgets.

METHODS

Sampling and analyses

Sediment and water samples were taken on two cruises aboard *R/V Ndunduma* in 2011 and 2014 (Fig. 5.1; Table 5.1). Water column temperature and dissolved oxygen distributions were measured using a Sea&Sun 90M Conductivity-Temperature-Depth (CTD) probe with Oxyguard dissolved oxygen sensor. Water samples taken using Niskin bottles were drawn into a syringe directly from the bottle spigot and filtered through WHATMAN 0.2 μm PP w/GMF filters before being preserved according to the type of analysis. Sediment cores of 94-mm inner diameter with undisturbed sediment-water interfaces were recovered using an Ocean Instruments multi-corer. The cores were immediately sealed from the atmosphere and porewaters were extracted using Rhizon porous polymer micro samplers (0.1 μm membrane pore size) (Dickens et al. 2007) through ports drilled in core tube sidewalls, at intervals varying from 0.5 cm at the sediment surface to 5 cm below 20 cm. The ports were sealed with silicone to prevent contamination with air. Samples for nitrate, ammonium and sulfate analyses were frozen at -18°C until measurements. Samples for dissolved Fe(II), Mn(II) and SRP analyses were acidified with hydrochloric acid (1% of 6N HCl) immediately after collection and stored at 4°C . Samples for dissolved inorganic carbon (DIC) were poisoned with HgCl_2 and stored at 4°C in septum-cap vials filled with no headspace. Separate intact sediment cores were split, photographed and analyzed for gamma-density (bulk density) on a Geotek multisensory core logger at the LacCore facility of the University of Minnesota, and scanned for major elements at 200 μm spatial resolution using an ITRAX X-ray fluorescence (XRF) scanning sediment analyzer at the Large Lakes Observatory,

University of Minnesota Duluth. Separate sediment cores were sectioned onboard and frozen at -18 °C for further analyses.

Sediment sections from stations CD, S2 and ND were measured for organic carbon content (by carbon coulometry; Kistner 2013). Sediment sections from stations CD and S2 were analyzed for ^{210}Pb activity and dry bulk density (dry mass per volume of wet sediment) at the University of Manitoba for the calculation of sediment accumulation rates ($\text{g cm}^{-2} \text{yr}^{-1}$) using a constant rate of supply (CRS) model (Appleby and Oldfield 1978). Burial velocities U (cm yr^{-1}) were calculated from the obtained age- vs.-depth relationships as a function of depth x as $U = dx/dt$. Dating of the ND core was performed by varve counting and tying to the existing chronology at that site. Porosity of sediments at sites S2 and CD was calculated from dry bulk density ($\text{g dry sediment per cm}^3$ wet sediment) as $\varphi = 1 - \rho_{\text{dry bulk}}/\rho_{\text{dry sed.}}$, assuming a 2.65 g cm^{-3} density of dry sediments ($\rho_{\text{dry sed.}}$; Burdige 2006). Porosity of sediments at site SM and ND were calculated as $\varphi = (\rho_{\text{dry sed.}} - \rho_{\text{bulk sed.}}) / (\rho_{\text{dry sed.}} - \rho_w)$, where ($\rho_{\text{dry sed.}}$ is the density of dry sediments (2.65 g cm^{-3}), ρ_w is the density of water (1.00 g cm^{-3}) and $\rho_{\text{bulk sed.}}$ is the density of the bulk sediments (wet sediments) measured.

Dissolved oxygen distributions in sediment porewater at Station SM were measured using a Unisense (Clark-type) microelectrode (Revsbech 1989) calibrated at O_2 saturation in lake water at in situ temperature ($\sim 22^\circ\text{C}$) and at zero oxygen level in a buffered sodium ascorbate solution. Profiling was performed onboard in subsampled cores shortly after their recovery. Dissolved nitrate and sulfate concentrations in collected samples were determined by ion chromatography (DIONEX ICS 1100). Soluble reactive phosphorus (SRP) was measured by the Molybdenum Blue Method on a Lachat Quickchem 8000 flow injection auto-analyzer (Grasshoff 1999). Ammonium and DIC concentrations were determined by

flow injection (Hall and Aller 1992) using a Lazar COND-158BL-XS micro flow-through conductivity measurement system. Dissolved Fe(II) concentrations were measured spectrophotometrically (on a GENESYS™ 6 spectrophotometer) as a Fe-Ferrozine complex detected at 562 nm wavelength (Viollier et al. 2000); dissolved Mn concentrations were obtained by atomic absorption spectroscopy (AAS).

Table 5. 1 Sampling dates and locations

Date	Station	Depth (m)	Latitude (S)	Longitude (E)
Jan 2011	SM.1	182	13° 30.997'	34° 46.219'
Jan 2014	SM.2	180	13° 28.424'	34° 43.937'
Jan 2012	S2.1	110	13° 45.718'	34° 39.546'
Jan 2014	S2.2	104	13° 50.230'	34° 52.373'
Jan 2012	CD.1	650	11° 18.607'	34° 21.875'
Jan 2014	CD.2	650	11° 05.846'	34° 20.108'
Jan 2012	ND.1	358	10° 01.070'	34° 11.480'
Jan 2014	ND.2	358	10° 24.945'	34° 20.333'

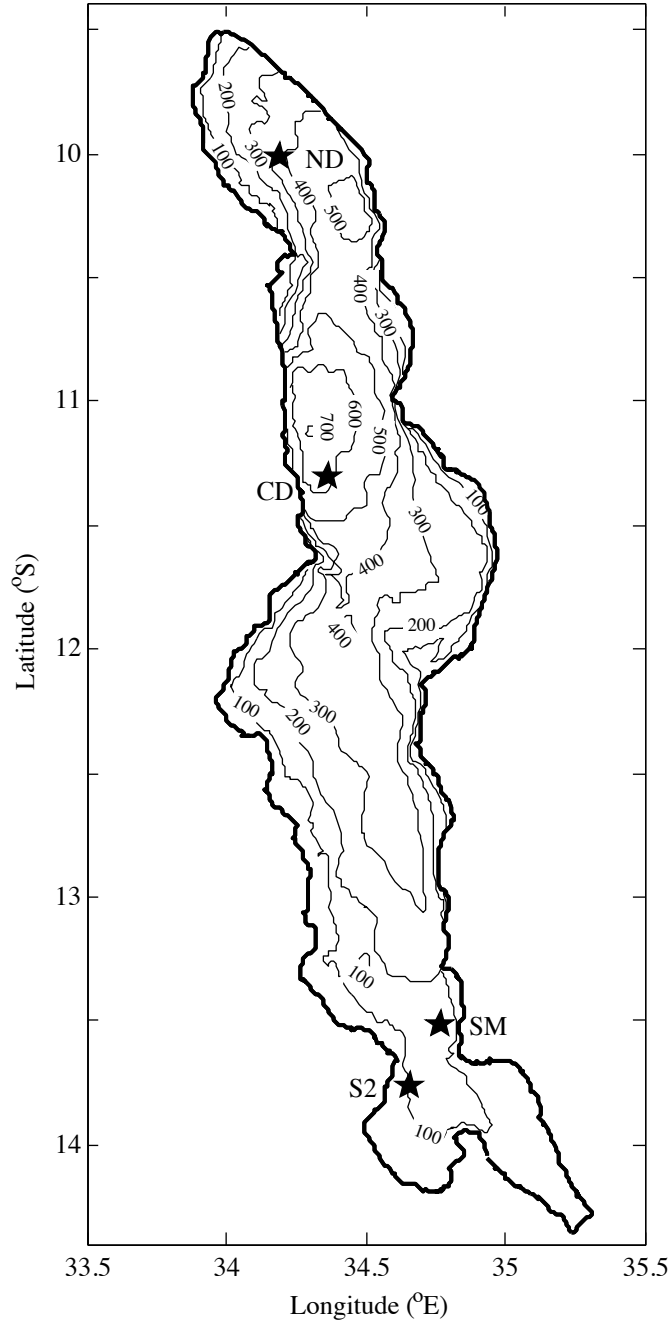


Figure 5. 1 Sampling locations in Lake Malawi.

Calculation of fluxes

Molecular diffusion fluxes (F_i) of nitrate, ammonium, sulfate, SRP, DIC and dissolved Fe^{2+} were calculated using Fick's law of diffusion:

$$F_i = -\varphi D_s \frac{dC_i}{dx} \quad (5.1)$$

where x is the depth below the sediment-water interface, C_i is the solute concentration (mmol per porewater volume), φ is porosity, and $D_s = D_i/(1 - \ln\varphi^2)$, is the diffusion coefficient corrected for sediment tortuosity (Boudreau 1997) from the infinite (free solution) molecular diffusion coefficient D_i at in-situ temperature 23°C. In determining the fluxes of DIC (mostly CO_2 and HCO_3^-) and SRP (mostly HPO_4^{2-} and H_2PO_4^-), the diffusion coefficients for the two possible ionic species were averaged with uncertainty presented and the calculated fluxes are presented with uncertainties that including possible variations in composition ratios. The values of D_i and D_s used for different species are given in Table 5.2. Porosity (φ) values at the SWI were used (*see Results for porosity*); at the ND station where porosity was not measured, an average φ of 0.92 was used, with range of uncertainties included in the calculation of diffusion coefficients. The concentration gradients (dC_i/dx) at the SWI were calculated using the porewater concentrations in the surface 1-2 cm, by linear fitting. Values are not used for profiles with concentration gradients that were poorly resolved (e.g., DIC concentration gradient at S2). The total fluxes of these substances at the sediment water interface are assumed to be close to diffusive fluxes, as bioturbation and bioirrigation in these anoxic/hypoxic sediments are inhibited (Pilskaln and Johnson 1991).

RESULTS

Stratification and oxygen distributions

Temperature profiles in the water column (Fig. 5.2A) at all stations indicate stable stratification. Temperature decreases from > 28 °C at the surface to ~ 23 °C in bottom waters, with the steepest gradient found between 50 and 100 m depth. The temperature in the deep waters (> 300 m) is currently higher than at any time since at least the 1940s (Fig. 5.2). The warming rate over the past decade is consistent with the trend in Lake Malawi over the preceding decades (Fig. 5.2B).

Dissolved oxygen levels were close to saturation in surface waters and decreased with depth, reaching zero at around 200 m (Fig. 5.2A). At stations SM and S1 in the Southern basin (182 m at SM and 110 m at S2), bottom waters were characterized by $\sim 20\%$ and 30% oxygen saturation at time of sampling, respectively. Oxygen in the sediments at these stations was depleted within 0.5 mm of the sediment-water interface (SWI). Oxygen fluxes into the sediments, as determined from microelectrode profiles near the SWI, were small: $0.24\text{-}0.52$ mmol m⁻² d⁻¹, averaging 0.39 mmol m⁻² d⁻¹ (Table 2). Sediments in the deeper Central and Northern basins (650m at CD and 358 m at ND) were anoxic.

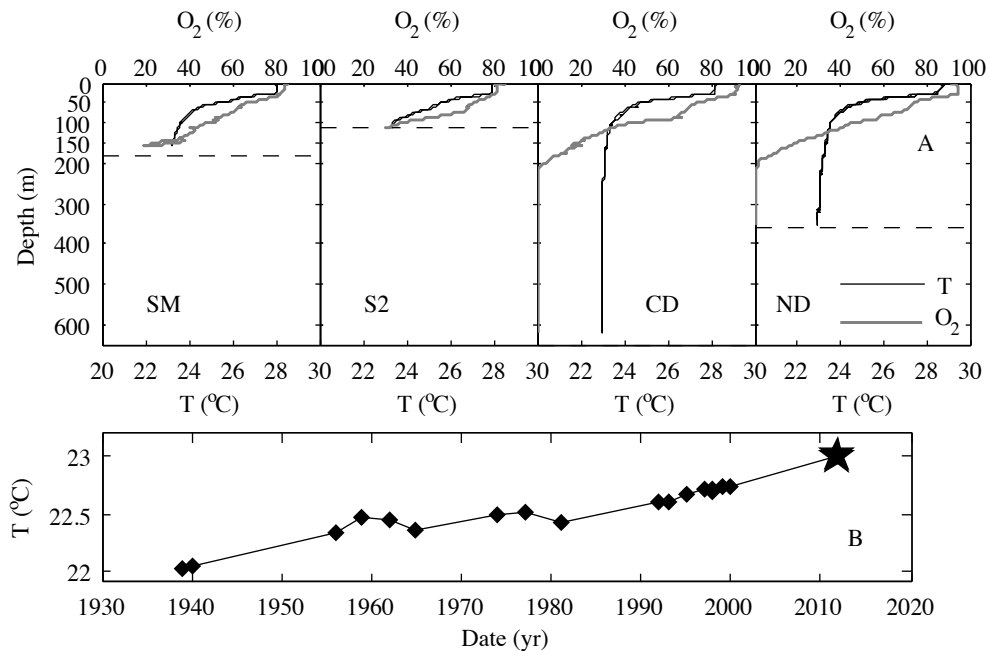


Figure 5.2 A) Vertical distributions of temperature and dissolved oxygen in the water column of Lake Malawi. B) Deep water (> 300 m) temperature in Lake Malawi. Horizontal dashed lines indicate lake bottom. Data prior to 2000 are from Vollmer et al. (2005).

Sediment properties

Sediments exhibited strong variability in their visual appearances and vertical zonation. Sediments from the Central and Northern sites (CD and ND) show alternating dark-and-light laminations, with thicknesses of 0.5 – 1.5 mm per dark-light couplet (Fig. 5.3). At station CD, distinct non-laminated layers were observed at depth intervals 8-14 cm and below 20 cm (Fig. 5.3). Sediments from shallower stations (S2 and SM) were not laminated (Fig. 5.3). Scanning XRF profiles (Fig. 5.3) reveal prominent multiple Fe and Mn enrichments located at several depth intervals in the sediments at Sta. S2 and CD,

Sediment at Sta. ND (taken close to the site of the International Drilling Program) showed no such metal-rich layers.

Sediment accumulation rates ($\text{g cm}^{-2} \text{yr}^{-1}$) and burial efficiencies (cm yr^{-1}) determined from ^{210}Pb analyses at Sta. S2 and CD are shown in Fig. 5.4. The light-dark laminations observed in sediments at Sta. CD and ND (Fig. 5.4) are annual varves that result from seasonal sedimentation patterns (Pilska and Johnson 1991) and thus can be used for sedimentation dating: light layers rich in diatoms are deposited during the high-productivity windy dry season (May to September), whereas dark sediments rich in minerals and terrigenous material are deposited during the rainy season (November to March) when riverine sediment transport is greater. The valve-counting dates and calculated sediment burial velocities (cm yr^{-1}) are shown in Fig. 5.4. The site in the south basin (Sta. S2) exhibits higher sedimentation rate and burial velocity than the sites in the central and northern basins (Sta. CD and ND). The organic carbon contents of the sediments are shown in Fig. 5.5, with values generally decreasing down core but varying non-monotonically. The density and porosity of the sediments are shown in Fig. 5.6.

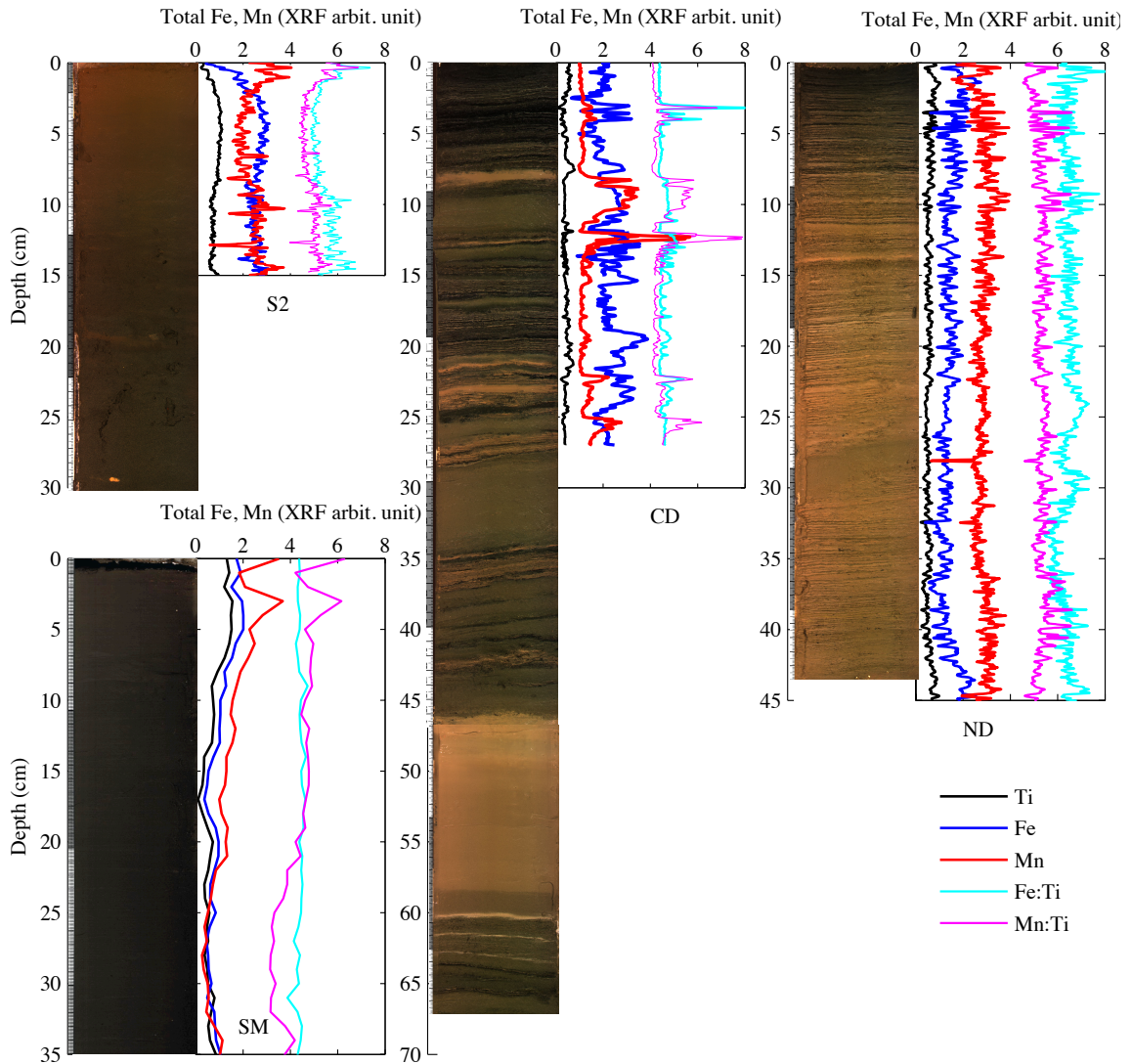


Figure 5.3 Optical images and x-ray fluorescence scanning of total iron, manganese and titanium in Lake Malawi sediment cores.

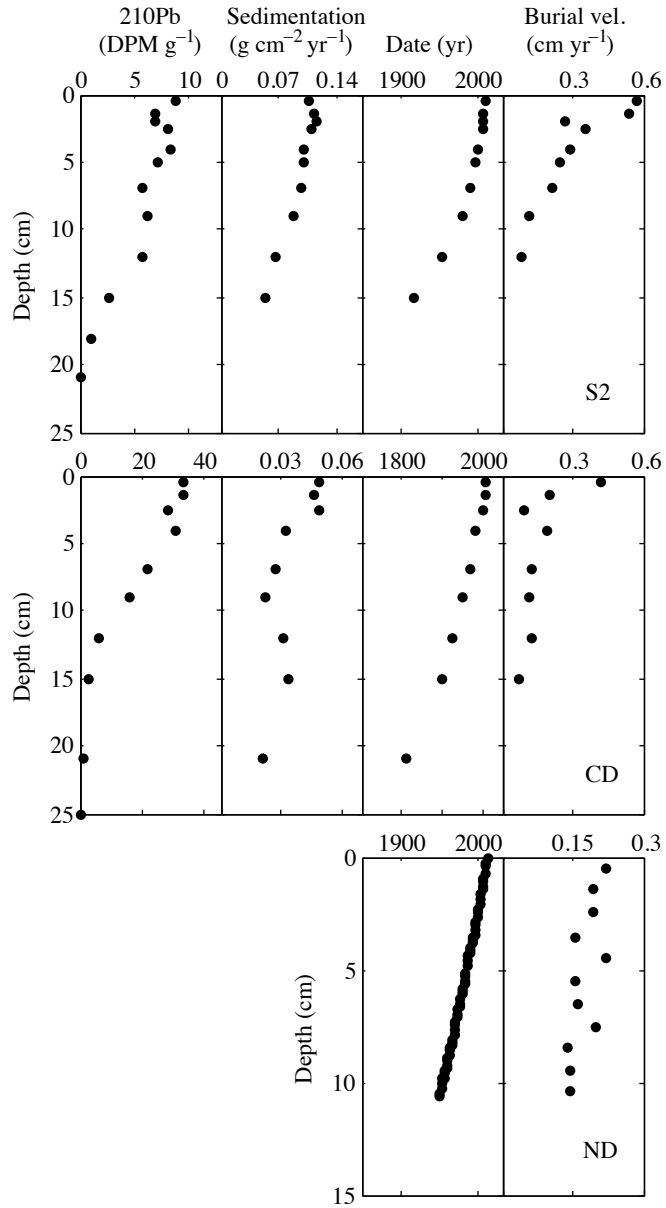


Figure 5. 4 Unsupported ^{210}Pb activity, sediment accumulation rates, sediment ages, and burial velocities.

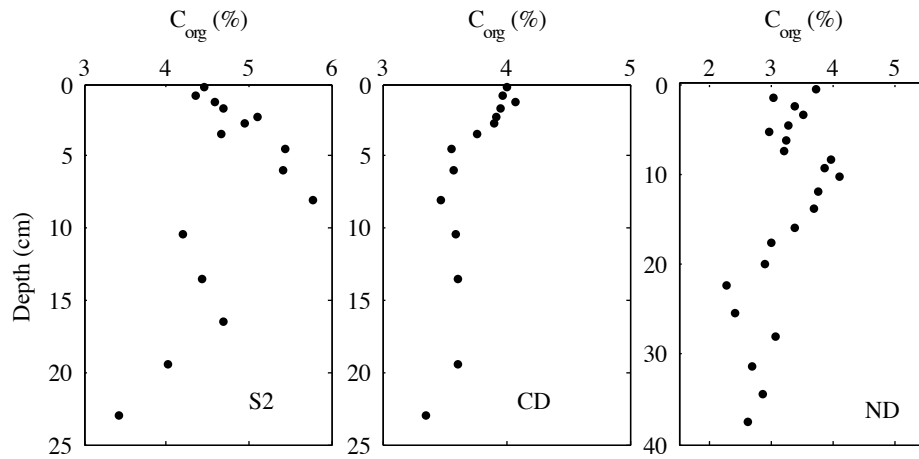


Figure 5.5 Organic carbon content in Lake Malawi sediments

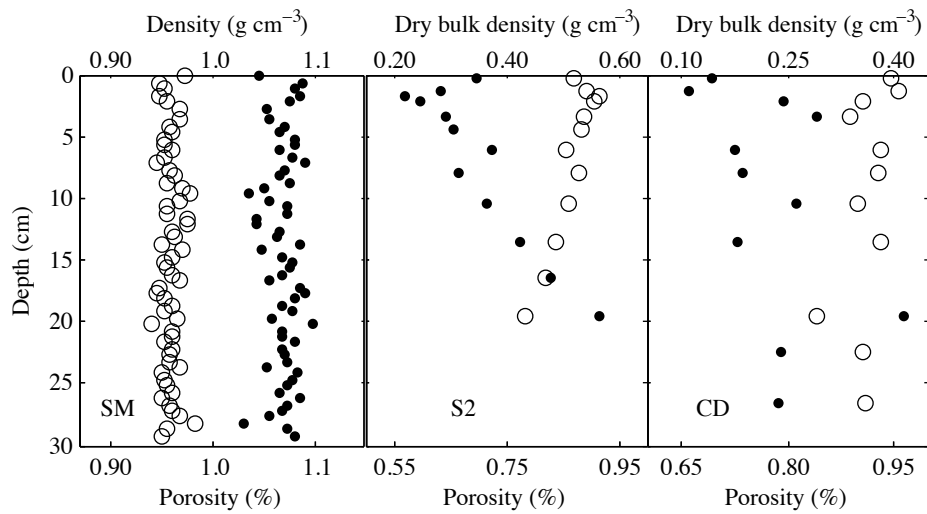


Figure 5.6 Porosity and density (dry bulk density ($\rho_{\text{dry bulk}}$; g dry sediment per cm^3 wet sediment) or bulk density ($\rho_{\text{bulk sed.}}$; g wet sediment per cm^3 wet sediment) in Lake Malawi sediments

Dissolved inorganic carbon in water and sediments

Dissolved inorganic carbon (DIC) increased with depth (from ~ 2 mmol L⁻¹ in the surface water to 2.5 mmol L⁻¹ in deep waters, and ~ 5 mmol L⁻¹ in the deep sediments; Fig. 5.7), consistent with organic carbon mineralization that produces DIC. Diffusive fluxes of DIC across the SWI, which approximate the depth-integrated rates of carbon degradation in sediments, are shown in Table 5.3.

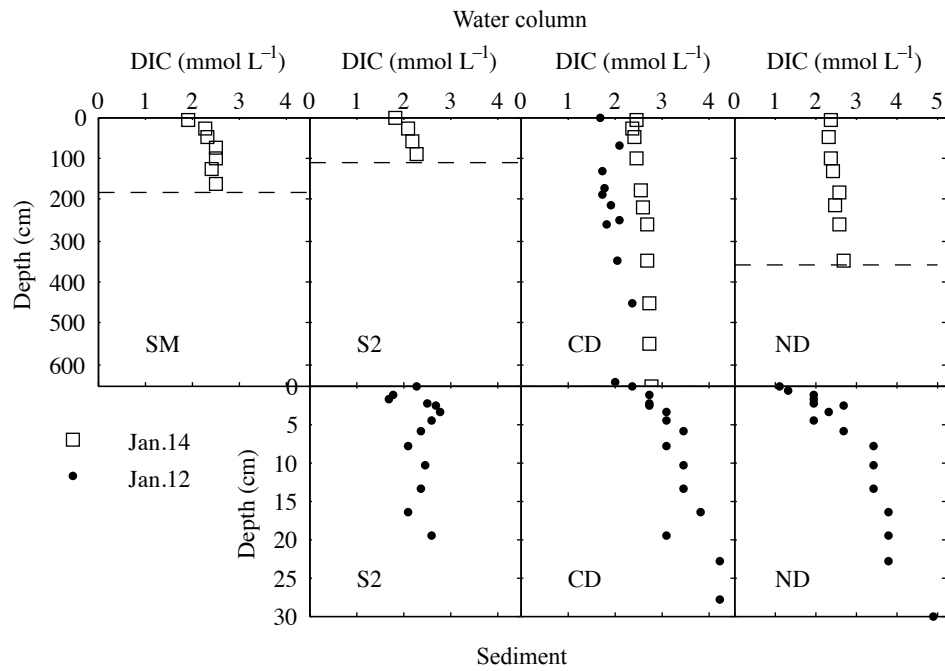


Figure 5. 7 Dissolved inorganic carbon (DIC) concentrations in water column and sediment porewaters. Dashed lines indicate sediment-water interface.

Table 5. 2 Porosity, infinite dilution molecular diffusion coefficients (D_i) and the tortuosity-corrected diffusion coefficients D_s .

		O ₂	NH ₄ ⁺	NO ₃ ⁻	HCO ₃ ⁻	CO ₃ ²⁻	DIC	SO ₄ ²⁻	H ₂ PO ₄ ⁻	HPO ₃ ²⁻	SRP	
Station	Porosity at SWI	716	599	581	359	281		322	289	231		D_i (cm ² yr ⁻¹)
SM	0.95	649	543	527	326	255	290±35	292	262	209	236±26	
S2	0.87	560	469	454	281	220	250±31	252	226	181	203±23	D_s (cm ² yr ⁻¹)
CD	0.95	649	543	527	326	255	290±35	292	262	209	236±26	
ND	0.92	614	513	498	308	241	274±33	276	248	198	223±25	

Table 5. 3 Fluxes of O₂, NH₄⁺, DIC, NO₃⁻, SO₄²⁻ and SRP at the sediment-water interface (mmol m⁻² d⁻¹). Negative values indicate flux from sediment into the water column.

Stations	F _{O₂}	F _{DIC}	F _{NH₄⁺}	F _{NO₃⁻}	F _{SO₄²⁻}	F _{SRP}
SM			-0.63 ±0.08	0.043	0.042 ±0.011	-0.056 ±0.006
S2	0.33± 0.04		-0.15 ±0.01	0.026 ±0.004	0.022 ±0.013	-0.026 ±0.012
CD	0	-5.4 ±3.0	0.56 ±0.07	- 0.009 ±0.004		-0.029 ±0.003
ND	0	-4.2 ±1.2	-0.40 ±0.21	- 0.15		-0.037 ±0.025
Average		-4.8 ±1.6	-0.44 ±0.12			-0.037 ±0.014

Ammonium concentrations in water and sediments

Ammonium (NH_4^+) concentrations in oxygenated epilimnetic waters were low at all stations (typically $< 1 \mu\text{mol L}^{-1}$ with a few exceptions that may be due to contaminations during sampling; Fig. 5.8). The concentrations increased into the anoxic waters below 200 m (20-25 and 10-16 $\mu\text{mol L}^{-1}$ respectively in the bottom waters at Sta. CD and ND). In sediments, ammonium concentrations increased markedly below the SWI at all locations (Fig. 5.8), consistent with organic carbon mineralization that releases NH_4^+ . Ammonium diffusive fluxes from sediments into the water column are shown in Table 5.3 (0.15 - 0.63 $\text{mmol m}^{-2} \text{d}^{-1}$, average 0.44 $\text{mmol m}^{-2} \text{d}^{-1}$). Fluxes of DIC (average 4.8 $\text{mmol m}^{-2} \text{d}^{-1}$) were about an order of magnitude higher, consistent with the $\sim 10\text{C} : 1\text{N}$ ratio in Lake Malawi sediments (Pilskaln 2004; Hecky et al. 1999; Otu et al. 2011).

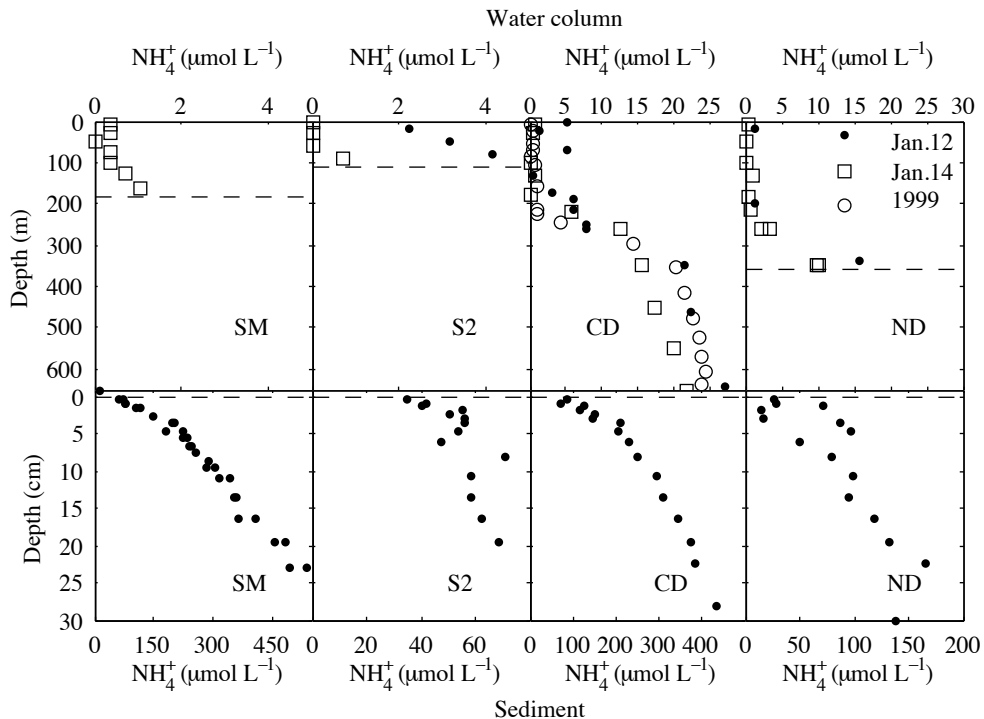


Figure 5. 8 Ammonium concentrations in water column and sediments. Dashed lines indicate sediment-water interface. Historical data are from Bootsma and Hecky 1999.

Nitrate concentrations in water and sediments

Nitrate concentrations in the water column near the lake surface were low ($< 4 \mu\text{mol L}^{-1}$) but increased with depth (Fig. 5.9), indicating remineralization of organic material and oxidation of the released ammonium to nitrate. The nitrate levels peaked at around 150 m and decreased below, until complete nitrate depletion at around the oxycline (Fig. 5.9), indicating denitrification and/or anammox. In sediment at Sta. SM, porewater nitrate was depleted immediately below the SWI. At S2, nitrate concentrations in the surface sediment were also low ($\sim 4 \mu\text{mol L}^{-1}$) but exhibited a peak at ~ 8 cm, below which NO_3^- decreased to $< 2 \mu\text{mol L}^{-1}$ in the deep sediment. At CD, nitrate concentrations at the SWI were low, consistent with the absence of nitrate in the bottom water, but peaked at 2 cm depth, below which the levels decreased (Fig. 5.9). Nitrate reappeared at one depth interval in the deeper sediment, exhibiting a peak at around 10 cm. At the northern anoxic site, ND, porewater nitrate also exhibited a sub-surface peak, reaching $13 \mu\text{mol L}^{-1}$ within the upper 1 cm and decreasing to near depletion below 5 cm. Molecular diffusion fluxes of nitrate across the sediment-water interface estimated from concentration gradients are listed in Table 5.3. At stations SM and S1 where oxygen and nitrate were both present in the bottom water, nitrate fluxes were directed into the sediments, at the average rate of $0.035 \text{ mmol m}^{-2} \text{ d}^{-1}$. At anoxic deep stations CD and ND, nitrate fluxed out of the sediments.

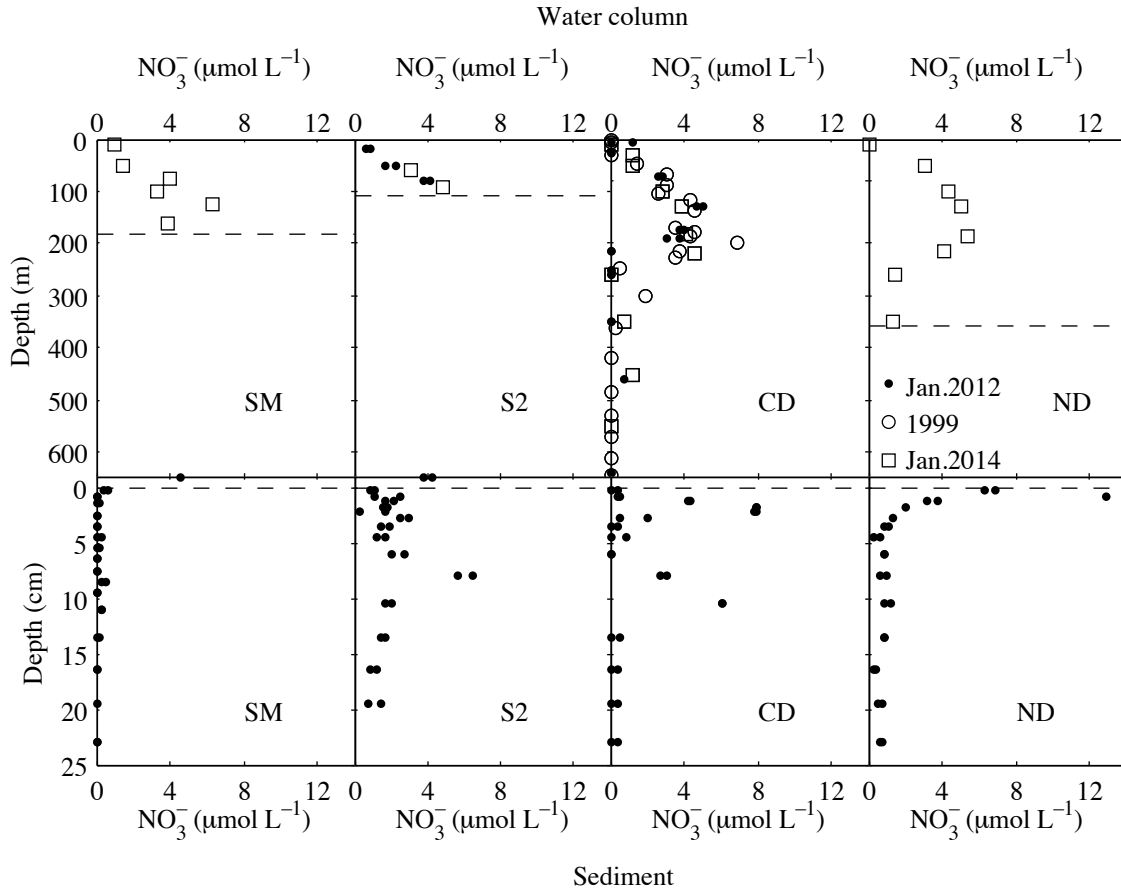


Figure 5. 9 Nitrate concentrations in water column and sediments. Historical data are from Bootsma and Hecky 1999. Dashed lines indicate sediment-water interface.

Sulfate concentrations in water column and sediments

Sulfate concentrations ranged 15-17 $\mu\text{mol L}^{-1}$ in the oxygenated surface waters and decreased with depth into the anoxic waters (Fig. 5.10) to $\sim 2\text{-}5 \mu\text{mol L}^{-1}$. Sulfate levels in sediment porewaters generally decreased with depth below the SWI (Fig. 5.10). Sulfate profiles exhibited peaks at depths that matched the depths of the nitrate peaks (Fig. 5.10). The flux of sulfate at SM was $0.056 \text{ mmol m}^{-2} \text{ d}^{-1}$ and at S2 it was $0.026 \text{ mmol m}^{-2} \text{ d}^{-1}$ into the sediment. At the deep anoxic stations CD and ND, the sediments appeared to be weak sources of sulfate to the overlying waters (Fig. 5.10; Table 5.3).

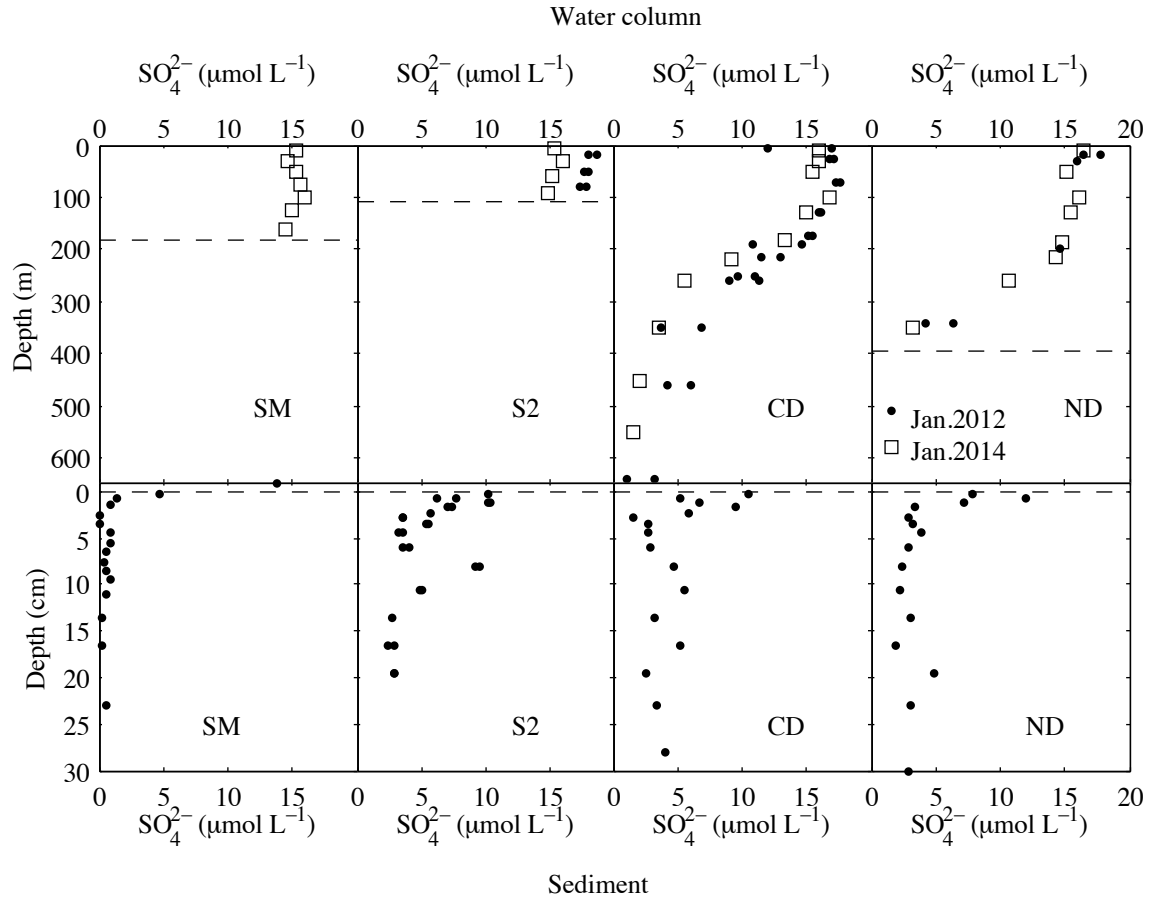


Figure 5. 10 Sulfate concentrations in water column and sediments. Dashed lines indicate sediment-water interface.

Dissolved manganese, iron, and phosphorus

Dissolved Mn was low ($< 5 \mu\text{mol L}^{-1}$) in the water column (as measured at Sta. ND and CD; also measured to be ~ 3.6 in the deep waters (500 m) of the central basin, and $\sim 1.8 \mu\text{mol L}^{-1}$ at 240 m in the shallower southern basin (253 m depth)). Mn concentrations increased with depth in the sediments (to $> 50 \mu\text{mol L}^{-1}$ at SM and CD, and $> 8 \mu\text{mol L}^{-1}$ at ND; Fig. 5.12). The distribution of porewater Mn(II) at Sta. ND exhibited a peak at around 4 cm depth. Dissolved iron (Fe^{2+}) was not detectable (< 2

$\mu\text{mol L}^{-1}$) in the water column (as measured by ferrozine method at Sta. S1, CD and ND). It was also absent in sediment porewaters at Sta. S2. At stations SM, CD and ND, porewater Fe^{2+} concentrations increased markedly ($> 50 \mu\text{mol L}^{-1}$; Fig. 5.12) into the sediments, suggesting Fe reduction. Total phosphorus (TP) and soluble reactive phosphorus (SRP) concentrations in the oxygenated epilimnetic waters were low at all stations (typically $< 2 \mu\text{mol L}^{-1}$; Fig. 5.11). The concentrations increased into the anoxic waters below 200 m ($4\text{-}5 \mu\text{mol L}^{-1}$ in the bottom waters at Sta. CD and ND). The concentrations of TP and SRP are similar at all sites, and the TP levels at Sta. CD (Figs. 5.11) are similar to those reported by Bootsma and Hecky (1999). However the SRP concentrations reported by Bootsma and Hecky were significant smaller. SRP concentrations in sediments generally increased with depth, indicating release of inorganic phosphorus during organic matter mineralization and potentially from Fe oxides (Fig. 5.12), but exhibited peaks near the sediment-water interface (< 2 cm) and troughs between 2 and 5 cm at all locations (Fig. 5.12). At Sta. SM, the SRP concentrations decreased from the sub-interface peak into the deep sediment, leveling off at $\sim 30 \mu\text{mol L}^{-1}$ below 10 cm (Fig. 5.12). Phosphorus fluxes from sediments into the water column averaged $0.037 \pm 0.014 \text{ mmol m}^{-2} \text{ d}^{-1}$ (Table 5.3).

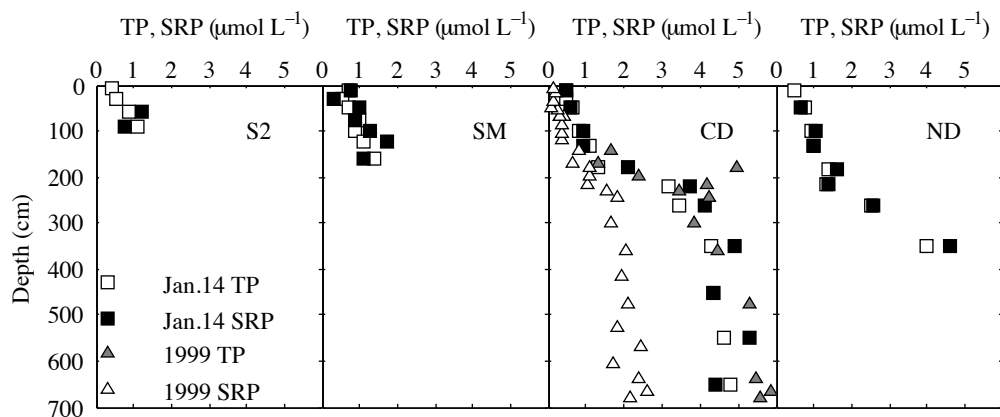


Figure 5.11 Vertical distribution of phosphorus in the water column of Lake Malawi. Historical data are from Boostma and Hecky 1999.

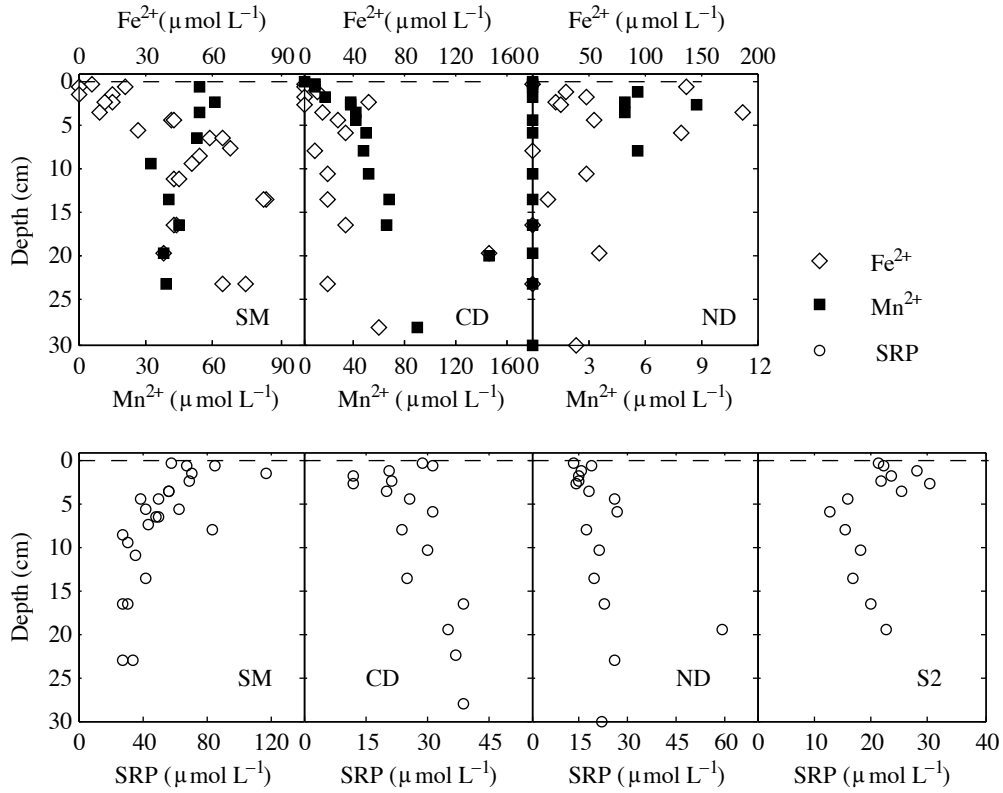


Figure 5.12 Dissolved iron (II) and soluble reactive phosphorus (SRP) concentrations in sediments. Dashed lines indicate sediment-water interface.

DISCUSSION

Geographic variability and non-steady state sedimentation

The large size and geographic variability of Lake Malawi is reflected in the differences in sediments properties among the different parts of the lake. The annual light-dark laminations observed in sediments at Sta. CD and ND are common in Lake Malawi deep sediments, as anoxic conditions inhibit biological mixing and foster preservation of undisturbed depositional structures (Anderson and Dean 1988). Non-laminated massive-clay sediments (Stas. S2, SM; Fig. 5.3) are typically found in the South, in shallower areas underlying oxygenated bottom waters (Pilskaln and Johnson 1991). The non-laminated layers within permanently anoxic sediments (e.g. at Sta. CD) likely reflect non-steady state sedimentation, such as deposition of turbidites. High-resolution seismic profiles indicated sediment flow channels even offshore in water depths of several hundred meters (Johnson and Davis 1989). It has been suggested previously that non-laminated layers could also result from localized episodic water column mixing events and sediment aeration that promotes bioturbation (Pilskaln and Johnson 1991), as well as causes precipitation of Fe and Mn oxyhydroxides (Brown et al. 2000). This hypothesis agrees with the presence of enrichments in Fe and Mn at the approximate depths of some non-laminated layers (e.g., ~ 10-15 cm at Sta. CD; Fig. 5.3), though cannot be confirmed at present as such enrichment could also be depositional, as these metal-enriched sediments may have come from shallower oxic locations. The northern site Sta. ND (near the site of the International Drilling Program) contains the best-preserved record of all stations, with consistent lamination and no signs of turbidites or post-depositional alteration. The distributions of porewater substances at all sites are

expected to be only insignificantly affected by non-steady state deposition, as solutes adjust on much faster time scales than solid sediment accumulation. The site in the south (Sta. S2) exhibits a relatively high sedimentation rate and has experienced a faster increase in sedimentation (from 0.04 to 0.11 g cm⁻² yr⁻¹ during the last century) than the sites in the central and northern parts of the lake (Sta. CD and ND). Similar increase in the sedimentation rate has been reported at other locations in the Southern basin (Otu et al. 2011), which was suggested to reflect an increasing anthropogenic eutrophication and shoreline erosion (Otu et al. 2011). Our results suggest that this increase in sedimentation rates has occurred also in the central basin (Fig. 5.4).

Carbon mineralization and preservation

The obtained fluxes of porewater NH₄⁺ (Table 5.3) allow estimating the rates of sediment carbon mineralization (Table 5.4), as organic carbon mineralization is accompanied by the production of ammonium from organic nitrogen. The typical stoichiometry of sediment organic matter in Lake Malawi is ~9-11C:1N (Pilskaln 2004; Hecky et al. 1999; Otu et al. 2011). The consumption of ammonium by nitrification is estimated at < 0.03 mmol m⁻² d⁻¹, based on the oxygen consumption of 0.33 mmol m⁻² d⁻¹ (Table 5.3). Thus, even in the presence of oxygen (Sta. S1 and SM), the ammonium consumption within the sediment is an order of magnitude slower than ammonium production (0.44 mmol m⁻² d⁻¹; Table 5.3) and can be neglected. The potential anaerobic oxidation of ammonium to nitrate (see discussion below) can be taken into account by correcting the calculated ammonium fluxes for the nitrate effluxes at the SWI (Table 5.3; included in uncertainty). The ammonium fluxes in Table 5.3 thus suggest that the total rates of carbon mineralization in Lake Malawi sediments are between 1.5 and 6.5 mmol

$\text{m}^{-2} \text{d}^{-1}$ (average $4.6 \text{ mmol m}^{-2} \text{d}^{-1}$; Table 5.4). This matches the DIC effluxes (Table 5.3). These carbon mineralization rates in Lake Malawi are similar to those in marine sediments and sediments in temperate large lakes (Lakes Superior, Michigan and Baikal) in similar water depths (Fig. 5.13).

Table 5. 4 Rates of organic carbon mineralization ($R^*_{\text{C total}}$), organic carbon burial ($F_{\text{C burial}}$; percentages indicate burial efficiency), total organic carbon flux ($F_{\text{C total}}$), denitrification ($\text{mmol m}^{-2} \text{d}^{-1}$; estimated similarly to those described in Chapter 2 (see Eq. 2.9)), and sulfate reduction ($\text{mmol m}^{-2} \text{d}^{-1}$; estimated from the sulfate in-fluxes at the SWI).

Stations	$R^*_{\text{C total}}$	$F_{\text{C burial}}$	$F_{\text{C total}}$	Denitrification		SO_4^{2-} reduction	
				$R^*_{\text{denitr.}}$	$R^*_{\text{denitr.}} : R^*_{\text{C total}}$	$R^*_{\text{sulf.}}$	$R^*_{\text{sulf.}} : R^*_{\text{total}}$
SM	6.3 ± 0.8			0.043	0.9%	0.042	1.3%
S2	1.5 ± 0.1	3.6 (71%)	5.1	0.026	2.2%	0.022	2.9%
CD	5.6 ± 0.8	2.0 (26%)	7.6				
ND	4.8 ± 2.9	2.5 (34%)	7.3				
Average	4.6 ± 2.1	2.7 (44%)	6.7				

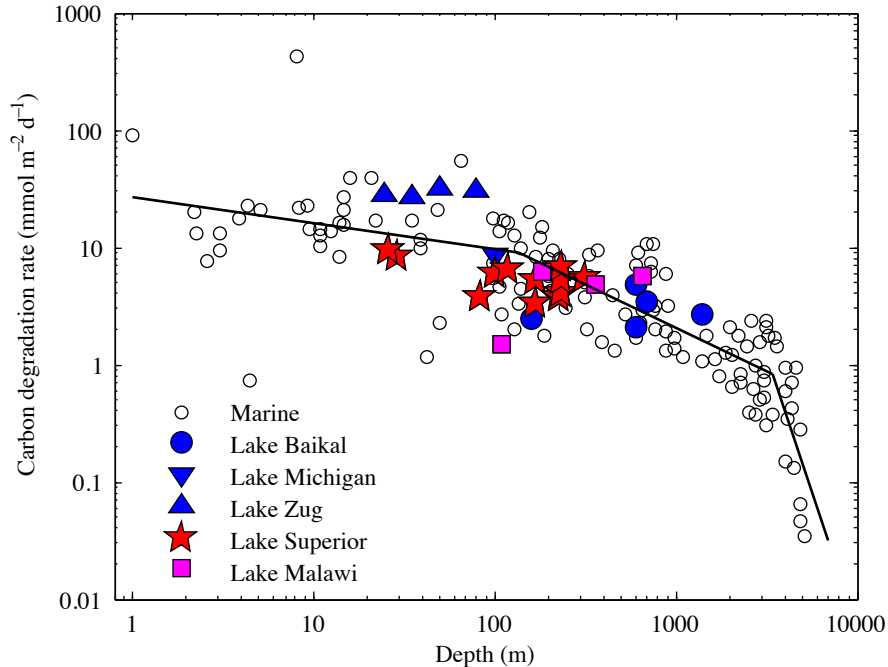


Figure 5.13 Integrated rates of organic carbon degradation as a function of water depth. Data are from Lake Malawi (this study), Lake Superior (*see* previous Chapters; estimated from oxygen uptake rates), Lake Baikal (Martin et al. 1998; Müller et al. 2005; Maerki et al. 2006), Lake Michigan (Thomsen et al. 2004), Lake Zug (Maerki et al. 2009), and marine sediments (Burdige 2007).

Exposure to oxygen has been shown to strongly affect the organic matter preservation in sediments (Burdige 2007; Hartnett et al. 1998): organic materials, especially those with diagenetic maturity, are degraded slower under anoxic conditions, and organic carbon burial efficiency correlates inversely with oxygen exposure time (Fig. 5.14 A), which can be estimated as the depth of oxygen penetration divided by the average sediment burial velocity. In this regard, the anoxic sediments of Lake Malawi conform to the relationships identified in both freshwater and marine systems (Fig. 5.14). The efficiency of organic carbon burial into the deep sediment and the C burial rates (Table 5.4) were estimated by calculating the downward carbon fluxes at the sediment-

water interface and in the deep sediment, based on the sedimentation velocities (Fig. 5.4 and Hecky et al. 1999, Otu et al. 2011) and the organic carbon contents (about 3.5% below 20 cm; Fig. 5.5). The sum of the calculated burial fluxes ($F_{C \text{ burial}}$ in Table 5.4) and the in-sediment carbon degradation rates ($R_{C \text{ total}}^*$) must equal approximately (if an approximate steady state can be assumed; the burial fluxes measured in the deep sediments may be underestimated as the sedimentation rates likely have increased.). The total organic carbon flux to the sediment was surface: $5.1 - 7.6 \text{ mmol m}^{-2} \text{ d}^{-1}$ ($F_{C \text{ total}}$ in Table 5.4). The average carbon burial efficiency (calculated by dividing the burial flux by the sedimentation flux) in Lake Malawi is 44%. This is higher than the typical values in well-oxygenated sediments and is similar to the values in marine sediments underlying waters that are low in dissolved oxygen (Fig. 5.14). It is well recognized that anoxic sediments bury more carbon than oxic sediments (Fig. 5.14; Li et al. 2012; Canfield 1994; Hartnett et al. 1998). The 44% organic carbon burial efficiency, however, appears to be lower than in marine sediments with similar sedimentation rates ($\sim 60\%$ burial efficiency; Fig. 5.14B). The difference may reflect the non-steady state deposition: As the deposition rates for both the solid sediment and organic carbon likely have increased in the past decades (Fig. 5.4; Hecky et al. 1999; Otu et al. 2011), the burial fluxes measured in the deep sediments likely underestimate the present burial rates (i.e., the difference between the carbon concentrations at the top and bottom of our sediment cores is likely greater than what would be expected without the increase in sedimentation rates). The actual organic carbon burial efficiency thus may be higher than calculated above.

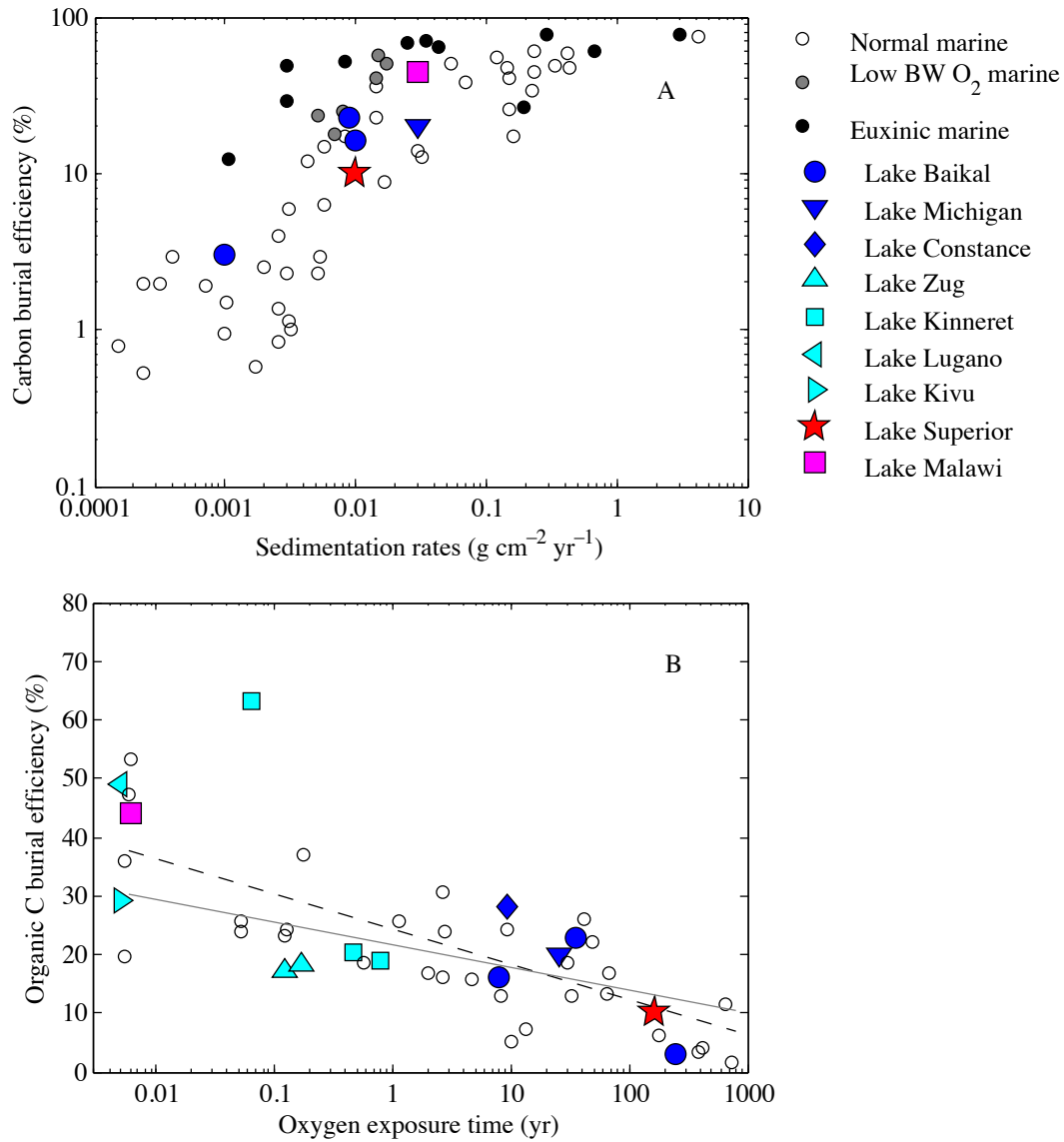


Figure 5. 14 Organic carbon burial efficiency in Lake Malawi sediments in comparison to those in marine environments and other large lakes: (A) Organic carbon burial efficiency relative to oxygen exposure time, estimated as the depth of oxygen penetration divided by the average sediment burial velocity. (B) Organic carbon burial efficiency relative to sedimentation rates. Reference: Marine (Suess 1980, Hartnett et al. 1998); Lake Lugano (Hofmann 1996); Lake Kivu and Constance (Sobek et al. 2009); Lake Kinneret (Sobek et al. 2009; Koren and Klein 2000); and reference in Fig 5.13 (*see* Fig 5.13 Caption). The dashed line and the solid line give the linear relationship for marine sediments (Hartnett et al. 1998) and autochthonous lake sediments (Sobek et al. 2009), respectively.

Nitrogen cycling

The nitrate and ammonium distributions in the water column (Figs. 5.8 and 5.9) are similar to those reported by Bootsma and Hecky (1999). Nitrate concentrations exhibit a peak at around 150 m depth as a result of the oxidation of upward-diffusing ammonium, and decrease to nearly zero below the oxycline at 200 m (Fig. 5.9). In sediments, despite the low concentrations of nitrate in the water columns overlying the deep sediments, nitrate was found in significant concentrations in the anoxic sediment porewaters at Sta. S2, CD and ND (Fig. 5.9), below the depth where the nitrate diffusing from the water column was depleted. Barring the oxidation of porewater samples, this suggests an in-sediment production of nitrate. Though unusual, similar peaks in dissolved nitrate have been observed in marine sediments where they were linked to the anaerobic oxidation of ammonium (Mortimer et al. 2004), possibly coupled to Mn reduction (Mortimer et al. 2002; Anschutz et al. 2000; Hulth et al. 1999; Luther et al. 1997). For example, porewater nitrate was found at a layer of diagenetically formed Mn oxides buried into the sediment by a catastrophic flood deposit (Deflandre et al. 2002). This process of Mn oxide-catalyzed anaerobic nitrification was also proved to occur in anoxic coastal marine sediments (intertidal salt marsh) where concentrations of ammonium and reactive manganese oxides were high (Lin and Taillefert 2014). That in our sediments the nitrate peaks are also found near the sediment layers enriched in Mn leads us to speculate that these peaks may be produced from ammonium via Mn reduction (Fig. 5.3 and 5.8).

In aquatic sediments, nitrogen supplied from the water column in the form of organic nitrogen and dissolved nitrate is removed from sediments primarily through the long-term burial of organic nitrogen and diagenetic conversion of nitrate and produced

ammonium to N_2 via denitrification and anammox (See Chapter 2). Using calculations similar to those described in Chapter 2 (see Eq. 2.9), the integrated rates of nitrate consumption in sediments (in $\text{mmol m}^{-2} \text{d}^{-1}$) can be estimated from the fluxes of nitrate. This then yields the nitrate reduction rates at stations Sta. SM and S2 that are shown in Table 5.4. Assuming that nitrate reduction is accomplished predominantly by N_2 producing processes (e.g., denitrification), it accounts for $< 10\%$ of the total sediment nitrogen removal, with the other $\sim 90\%$ of nitrogen removal occurring via the long-term burial of organic nitrogen. The role of denitrification in carbon mineralization in the deep sediments of Lake Malawi is minor: if all of the N_2 production were carried out by denitrification, it would contribute $< 3\%$ to the total sediment carbon mineralization (Table. 5.4).

Sulfur cycling

The decrease in the sulfate concentrations with depth in the anoxic water column suggests sulfate reduction (Fig. 5.10). The concentrations of sulfate in the waters overlying the sediments are low (Fig.5.10), on the order of a few μM . Sulfate persisted at residual concentrations ($\sim 2\text{-}5 \mu\text{mol L}^{-1}$) into the deep water column (Sta. CD; Fig. 5.10), as well as into the deep sediment at Sta. S2, CD and ND. Though an oxidation of sulfides to sulfate during sampling cannot be completely excluded, the low concentrations of measured hydrogen sulfide in the deep water ($< 0.8 \mu\text{mol L}^{-1}$; S. Crowe, unpubl.) suggest an incomplete sulfate reduction. Similar residual sulfate concentrations were observed in other freshwater sediments where they remained at $5\text{-} 20 \mu\text{mol L}^{-1}$ (Lovely and Klug 1983; Sinke et al. 1992; Thomsen et al. 2004; Katsev and Dittrich 2013). This behavior,

which is certainly not universal (e.g., Sta. SM in Fig. 5.10, or Crowe et al. 2008 in water column), was suggested to result from threshold concentrations for sulfate reduction (Roden and Tuttle 1993), possibly as a result of thermodynamic limitation (LaRowe and Van Cappellen 2012), or represent a physiological limit for sulfate reducers. Methanogens in sediments were suggested to outcompete sulfate reducers under some conditions, which could cause sulfate concentrations to leveled off at $\sim 20 \mu\text{mol L}^{-1}$ (Kuivila et al. 1989). Incomplete reduction of sulfate was also reported in culture incubations of *Desulfobacter postgatei* (Ingvorsen et al. 1984), suggesting sulfate uptake by *D. postgatei* was an energy-requiring process that ceased at $< 5 - 20 \mu\text{mol L}^{-1}$.

Using the approach similar to the one for nitrate reduction above, the rates of sulfate reduction are estimated from the sulfate in-fluxes at the SWI at $0.031 \text{ mmol m}^{-2} \text{ d}^{-1}$ average (Table 5.4). Sulfate reduction at this rate accounts for only $< 3\%$ of total carbon mineralization. The peaks in dissolved sulfate in the upper cm of stations CD and ND, as well as the peak at the 8 cm depth at S2, however, suggest an intriguing production of sulfate within the sediment. High rates of sulfate reduction sustained by rapid replenishment of porewater sulfate from internal sources were reported in low-sulfate environments (Roden and Tuttle 1993). In anaerobic sediments, sulfate may come from two major pathways: mineralization of organic sulfur via sulfate ester hydrolysis (King and Klug, 1982; Roden and Tuttle 1993; and Chapter 4) and anaerobic oxidation of hydrogen sulfide. The latter pathway has been observed in both freshwater and marine systems (Holmer and Storkholm 2001; King and Klug 1982). The absence of Fe^{2+} in the deep sediments at S2 and near the sediment surface at CD and ND (Fig. 5.12) allows for the possibility of H_2S presence there. To produce sulfate, the anaerobic oxidation of

sulfide may be coupled, for example, to the reduction of manganese oxides (Burdige and Nealson 1986; Aller and Rude 1988; Elsgaard and Jørgensen 1992). In a recently proposed “cryptic sulfur cycle” (Canfield et al. 2010), the oxidation of sulfide by nitrate was also suggested to be an important and previously overlooked source of sulfate in anoxic marine sediment; the resultant sulfate reduction contributed 33% to the total carbon mineralization (Canfield et al. 2010). Although a similar coupling of sulfur, nitrogen and manganese cycles in Lake Malawi sediments would only be speculative, the consistent overlapping of peaks in dissolved SO_4^{2-} , nitrate, and solid-phase Mn, as well as Mn^{2+} accumulation (Figs. 5.3, 5.9, 5.10, and 5.12) is very intriguing and worth pointing out. Regeneration of organic sulfur may also contribute to these sulfate peaks (*see* Chapter 4 for discussion of sulfate peaks in Lake Superior sediments and references therein). This cannot, however, explain the sulfate peak below the surface sediment at Sta. S2 (at ~ 8- 10 cm), where the rate of organic matter remineralization should not have exceeded that in the surface sediments.

Sediment contributions to carbon and nutrient budgets in Lake Malawi

Organic carbon sedimentation in Lake Malawi was estimated in the 1990s in sediment traps deployed at 100 m depth. It was estimated in the South basin at ~4.0 $\text{mmol m}^{-2} \text{d}^{-1}$ (Bootsma and Hecky 1999) and in the Central and Northern basins at <2.0 $\text{mmol m}^{-2} \text{d}^{-1}$ (Pilskaln 2004). Our present estimates, based on the calculated rates of carbon degradation and burial, are higher: 5.1–7.6 $\text{mmol m}^{-2} \text{d}^{-1}$, average 6.7 $\text{mmol m}^{-2} \text{d}^{-1}$. The sediment traps are known to underestimate fluxes of settling particles relative to sediment cores (Ramlal et al. 2003), and settling organic material may undergo substantial

degradation while in sediment traps (Gardner 2000). There is also significant evidence that both sedimentation fluxes and nutrient inputs into Lake Malawi have increased substantially over the past 10 years, as intensified agriculture and fertilizer use led to greater soil erosion and nutrient runoff from the catchment (Brown and Katsev 2012). The average organic carbon sedimentation flux of $6.7 \text{ mmol m}^{-2} \text{ d}^{-1}$, if applicable to the entire lake, corresponds to about 7% of previously estimated primary production ($94 \text{ mmol m}^{-2} \text{ d}^{-1}$; Ramlal et al. 2003). This fraction is similar to marine sediments in similar water depths ($\sim 300 \text{ m}$; Fig. 5.15) and lower than in shallower large temperate lakes: 20% in Lake Superior (200 m; Li et al. 2012) and 27% in Lake Michigan (100 m; Thomsen et al. 2004). The trend is consistent with the relationship found in marine sediments: C export efficiency from the water column decreases with increasing water depths (Fig. 5.15; Suess 1980). As about 56% of the deposited carbon is mineralized in the sediment (average burial efficiency of 44%), only about 3% of the organic carbon produced in the lake becomes buried into the deep sediment, with the rest being recycled, primarily to CO_2 , in the water column and upper sediment.

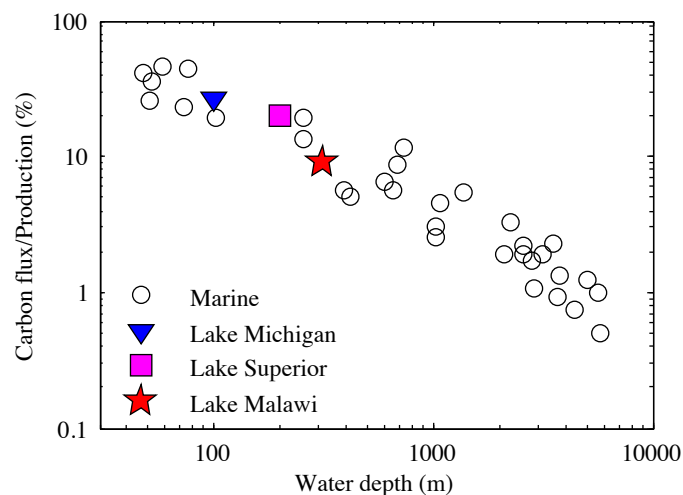


Figure 5. 15 Carbon export efficiency as a function of water depth. Marine data are from Hartnett et al. 1998.

The nitrogen budget in Lake Malawi has been partially quantified by Bootsma and Hecky (1999), including nitrogen inputs with atmospheric deposition ($0.41 \text{ mmol m}^{-2} \text{ d}^{-1}$), watershed inflow ($0.39 - 0.90 \text{ mmol m}^{-2} \text{ d}^{-1}$), and outputs with the riverine outflow ($0.01 \text{ mmol m}^{-2} \text{ d}^{-1}$) and organic nitrogen sedimentation ($0.35 - 0.65 \text{ mmol m}^{-2} \text{ d}^{-1}$). The latter was estimated from sediment traps. Gondwe et al. (2008) have quantified biological fixation ($0.036 \text{ mmol m}^{-2} \text{ d}^{-1}$). Denitrification in the water column was not quantified but suggested to be significant (Bootsma and Hecky 1999). Sediment-water exchanges of nitrate and ammonium, as well as long-term burial of organic nitrogen, were not quantified. Table 5.5 summarizes our updated nitrogen budget with contributions from sediments. Our estimate of organic nitrogen sedimentation ($6.7/10=0.67 \text{ mmol m}^{-2} \text{ d}^{-1}$) is again higher but broadly consistent with the earlier estimates from sediment traps ($0.35 - 0.65 \text{ mmol m}^{-2} \text{ d}^{-1}$). The fluxes of inorganic nitrogen from deep (anoxic) sediments into the water column are $0.44 \text{ mmol m}^{-2} \text{ d}^{-1}$ (mostly as ammonium). This corresponds to 24-34% of all inputs of nitrogen into the water column ($1.3-1.8 \text{ mmol m}^{-2} \text{ d}^{-1}$; Table 5.5), suggesting a significant contribution of sediments to nutrient recycling. Thus, about $0.67/1.1=61\%$ of all N entering Lake Malawi reaches the sediment, of which $\sim 66\%$ is returned into the water column as ammonium, and the rest is buried into the deep sediment or removed as N_2 . These numbers may be somewhat different for the coastal parts of the lake underlying shallower and oxic waters.

Table 5. 5 Total nitrogen budget for the Lake Malawi water column. Contributions from this work are in italic. All others are from Bootsma and Hecky (1999) and Gondwe et al. (2008). All rates are reported on an area-specific basis ($\text{mmol m}^{-2} \text{d}^{-1}$). Results from this work are based on data from hypoxic and anoxic sediments. Surface area of Lake Malawi is 29,600 km^2 .

Source or sink	Contribution to N budget		
	Water column	Sediment	Entire Lake
Atmospheric deposition	0.41		0.41
Watershed input	0.39- 0.90		0.39- 0.90
N fixation	0.036		0.036
Water column denitrification	Unknown		Unknown
Outflow	-0.01		-0.01
Organic N sedimentation	<i>-0.67</i>	<i>0.67</i>	
Effluxes at SWI (NH_4^+ and NO_3^-)	<i>0.44</i>	<i>-0.44</i>	
Sediment denitrification		<i>-0.035</i>	<i>-0.035</i>
Long term burial		<i>-0.27</i>	<i>-0.27</i>
Total input	<i>1.3- 1.8</i>	<i>0.67</i>	<i>0.84- 1.3</i>
Total output	<i>-0.68</i>	<i>-0.75</i>	<i>-0.32</i>

The total phosphorus budget in Lake Malawi was previously considered as being close to balance (Bootsma and Hecky (1999); Table 5.6). The total inputs from atmosphere and watershed were estimated at $0.045 - 0.058 \text{ mmol m}^{-2} \text{d}^{-1}$, and outputs with sedimentation flux ($0.027 - 0.052 \text{ mmol m}^{-2} \text{d}^{-1}$) and river outflow ($0.0004 \text{ mmol m}^{-2} \text{d}^{-1}$) (Table 5.6). Our estimate for phosphorus sedimentation, $0.046 - 0.069 \text{ mmol m}^{-2} \text{d}^{-1}$ (average $0.58 \text{ mmol m}^{-2} \text{d}^{-1}$, based on average 110 C:1P stoichiometry, Mohd-Rozhan Zakaria, unpublished data), is again higher but broadly consistent with previous estimates. However, our estimate for the SRP efflux from sediments (average $0.037 \text{ mmol m}^{-2} \text{d}^{-1}$, accounting $\sim 42\%$ of the total input into water column; Table 5.3) suggests a significant and previously unquantified important contribution. The updated phosphorus

budget suggests a significant imbalance for both the water column and the entire lake, with total inputs exceeding outputs (Table 5.6).

The significant internal source of phosphorus from sediments (42% of the total P input into water column) suggests that sediment dynamics may have important effects on the ecosystem's functioning. The water column exchange time between the hypolimnion (>220 m) and metalimnion (105 to 220 m) is ~19- 22 years and 5 -7 years between metalimnion and epilimnion (< 220 m) (Vollmer et al. 1999). This suggests that, while the lakes primary productivity (mostly occurring in the well mixed epilimnion (< 105 m)) may respond faster to external input of P, dynamics in sediment phosphorus cycling may affect the ecosystem in longer (decadal) time scale. The comparable magnitude of phosphate efflux to the phosphorus sedimentation flux suggests a high recycling efficiency (~ 64%), which is typical in anoxic sediments as phosphorus retention there is low with the low availability and long-term preservation of iron oxyhydroxides (e.g., Katsev and Dittrich 2013). The weaker phosphorus retention in Lake Malawi than in well-oxygenated oligotrophic lakes (Caraco et al. 1990; Heinen and McManus 2004; Katsev et al. 2006) suggests that phosphorus dynamics in the water column of Lake Malawi may be more sensitive to the external inputs of phosphorus, as sediment burial removes a relatively small fraction of phosphorus from circulation. Phosphorus inputs from watershed into Lake Malawi likely have drastically increased in the last two decades, as sales of phosphorus fertilizers increased many-fold (Brown and Katsev 2012). These conditions may lead to the accumulation of total phosphorus in the lake and in the long-term increases in primary productivity.

Table 5. 6 Total phosphorus budget for Lake Malawi. Contributions from this work are in italic. All others are from Bootsma and Hecky (1999). All rates are reported on an area-specific basis ($\text{mmol m}^{-2} \text{d}^{-1}$). Results from this work are based on data from hypoxic and anoxic sediments. Surface area of Lake Malawi is 29,600 km^2 .

Source or sink	Contribution to P budget		
	Water column	Sediment	Entire Lake
Atmospheric deposition	0.022		0.022
Watershed input	0.023- 0.036		0.023- 0.036
Outflow	-0.0005		-0.005
Organic P sedimentation	<i>-0.058</i>	<i>0.058</i>	
Effluxes at SWI (SRP)	<i>0.037</i>	<i>-0.037</i>	
Long term burial		<i>-0.025</i>	<i>-0.025</i>
Total input	<i>0.082-0.095</i>	<i>0.058</i>	<i>0.045- 0.058</i>
Total output	<i>-0.059</i>	<i>-0.062</i>	<i>-0.026</i>

CONCLUSIONS

- Lake Malawi has been experiencing increasing sedimentation rates over the last century, especially in the south basin.
- The temperature in the deep waters (> 300 m) is currently higher than at any time since at least the 1940s. The warming rate over the past decade is consistent with the trend in Lake Malawi over the preceding decades.
- In the deep anoxic sediments of Lake Malawi, organic carbon is buried with high efficiency (44%), consistent with trends found in marine sediments that carbon remineralization efficiency is controlled by the duration of organic carbon exposure to oxygen. Carbon export efficiency (sedimentation per primary productivity) and sediment remineralization rates in Lake Malawi are similar to those of marine

environments under similar water depth. Our compilation of data from other freshwater large lakes (including temperate and tropical, oligotrophic and eutrophic, well-oxygenated and meromictic lakes) suggests that carbon mineralization in sediments in freshwater large lakes in general follows the relationship that was established in marine systems (*see* also Chapter 1 for more trends and data).

- Sediments contribute significantly to the carbon, nitrogen and phosphorus cycles in Lake Malawi and cannot be neglected in geochemical budget estimates. Sediment effluxes contribute ~ 20% of nitrogen, and ~ 42% of phosphorus entering the water column. Whereas the internal loading of P to the water column is significant (but smaller than the combined loading from watershed and atmosphere), the high efficiency of P regeneration in the sediments suggests that sediments are weak sinks of total phosphorus. The lake should be more sensitive to external P inputs compared to temperate lakes where sediment P regeneration efficiencies are low (sediments are strong P sinks). The lake may be more vulnerable to increases in external P inputs as its productivity may be affected by increases in P loading from agricultural lands.

CONCLUSIONS

In this Thesis diagenetic cycles and sediment-water exchanges were characterized in two large freshwater lakes: temperate Lake Superior and tropical Lake Malawi. Geochemical rates and fluxes were investigated for the cycles of organic carbon, oxygen, nitrogen, phosphorus, iron, and sulfur. Sediment processes were compared for different diagenetic regimes, as well as between temperate and tropical lakes and between freshwater sediments and marine coastal and abyssal sediments. The obtained results allow us to draw the following main conclusions.

The sediments in Lake Superior exhibit strong spatial heterogeneity. Striking variations were observed for the oxygen penetration depth (OPD) in Lake Superior: sediments in low-sedimentation areas (typically offshore) are characterized by deep OPDs (4 to > 12 cm), whereas sediments in high-sedimentation nearshore areas are typically characterized by shallow OPDs (< 4 cm). In agreement with ideas previously postulated for the deep Arctic ocean, the OPDs in Lake Superior were found to vary temporally by as much as 2 cm, in response to seasonal variations in organic carbon sedimentation and oxygen levels in the bottom waters. The depth of oxygen penetration (OPD) was found to strongly affect the dynamics of carbon and nutrients. The low-sedimentation, deeply oxygenated sediments are typically characterized by low rates of oxygen uptake ($5.8 \pm 1.2 \text{ mmol m}^{-2} \text{ d}^{-1}$), low denitrification rates ($0.10 \text{ mmol m}^{-2} \text{ d}^{-1}$), and low sulfate reduction rates ($0.012 \text{ mmol m}^{-2} \text{ d}^{-1}$). These sediments typically serve as sources of both nitrate and sulfate to the overlying water column (nitrate and sulfate

average effluxes of, respectively, 0.26 and 0.020 mmol m⁻² d⁻¹). Both nitrate and sulfate in these sediments are produced within the sediment (by, respectively, nitrification and organic-sulfur regeneration), sustaining the corresponding reduction processes. The sediments in high-sedimentation areas with shallow OPDs, in contrast, are typically characterized by high rates of oxygen uptake (8.7 ± 2.1 mmol m⁻² d⁻¹), and high rates of denitrification (0.76 mmol m⁻² d⁻¹) and sulfate reduction (0.085 mmol m⁻² d⁻¹). There, nitrate and sulfate flux into the sediment from the water column, and sediment denitrification and sulfate reduction (fluxes in 0.16 and 0.063 mmol m⁻² d⁻¹, respectively) serve as sinks for the corresponding water column substances. The depth of oxygen penetration also affects the recycling efficiency of phosphorus: in deeply oxygenated sediments the flux of P is controlled by the balance between organic P regeneration and its adsorption in the oxic surface sediments. It is only weakly affected by iron reduction, which leads to a low P recycling efficiency (13%). In contrast, the anoxic sediments of Lake Malawi exhibit a high P recycling efficiency (~ 64%).

Sediments contribute significantly to the geochemical budgets in both lakes. These contributions are documented in our revised budgets for the lakes and hold clues to changes observed in their water columns. In Lake Superior, organic carbon sedimentation corresponds to 20% of primary production. Sediments serve as important nitrogen sinks for the entire lake via nitrogen removal to N₂ and long-term burial of non-reactive N, which together account for 73% of the total nitrogen removal in the lake. Sediment nitrification, which leads to the net efflux of nitrate into the water column (estimated 0.27 mmol m⁻² d⁻¹), is a major source of nitrate to the system, contributing 84% of nitrate inputs. This suggests that changes in the rates of N sediment processes can strongly

influence the nitrate concentrations in Lake Superior. Our updated budget for TN and nitrate in Lake Superior is closer to balance than previous budgets. Having low phosphorus recycling efficiency ($\sim 13\%$), sediments in Lake Superior serve as a major phosphorus sink (burial flux of $43 \mu\text{mol m}^{-2} \text{d}^{-1}$). The flux of dissolved phosphorus across the SWI accounts for approximately 13% of total P inputs into the water column. In Lake Malawi, sediment effluxes contribute $\sim 20\%$ of nitrogen, and $\sim 42\%$ of phosphorus entering the water column. The high efficiency of P regeneration in the sediments there suggests that over decadal time scales the water column P content and the lake's productivity are controlled by the external P inputs. The lake is therefore more sensitive to the increased P loadings than temperate well-oxygenated lakes as any new inputs are likely to remain active in the lake for longer (i.e., there is a less efficient removal mechanism).

Carbon and nitrogen cycling in large freshwater systems conforms to many of the same trends as in marine systems. Organic carbon mineralization rates (average $5.7 \text{ mmol m}^{-2} \text{d}^{-1}$ in Lake Superior and $4.6 \text{ mmol m}^{-2} \text{d}^{-1}$ in Lake Malawi), organic carbon export efficiencies (20% in Lake Superior and 7% in Lake Malawi), and carbon burial efficiencies (12% in Lake Superior and 44% in Lake Malawi) are similar to those in marine counterparts for comparable sedimentation rates, water depths, and redox conditions. Reactivity of organic carbon was found to decrease with carbon age similarly to the power law documented in marine environments. Comparisons between cold Lake Superior and warm Lake Malawi suggests that carbon mineralization and preservation rates are within their typical ranges for the respective sedimentation rates, with temperature effect not explicitly discernable. The carbon mineralization efficiency is

controlled primarily by oxygen exposure. Quantitative relationships established in freshwater sediments can be used to draw inferences for the carbon and nutrient cycles in marine sediments. For example, correlations between the freshwater sediment denitrification rates and OPD can likely be extrapolated to estimate denitrification rates in deep Ocean sediments. The rates of denitrification in deeply oxygenated sediments cannot be described by the same relationship with total oxygen uptake as in shallow oxygenated sediments, suggesting that these sediments should be treated differently in global models. The unusual sulfur cycle driven by the oxidation of organic sulfur to sulfate, as revealed in the organic-poor deeply-oxygenated sediments of Lake Superior, suggests alternative controls on sediment sulfate reduction, such as the supply of organic carbon and the depth of oxygen penetration. This has implications for interpreting sediment sulfur storage as records for sulfate levels in the water column.

REFERENCES

- Aller, R. C., V. Madrid, A. Chistoserdov, J. Y. Aller, and C. Heilbrun. 2010. Unsteady diagenetic processes and sulfur biogeochemistry in tropical deltaic muds: Implications for oceanic isotopic cycles and the sedimentary record. *Geochimica et Cosmochimica Acta* **74**: 4671-4692.
- Alin, S., and T. C. Johnson. 2007. Carbon cycling in large lakes of the world: A synthesis of production, burial, and lake-atmosphere exchange estimates. *Glob. Biogeochem. Cycles* **21**: GB3002, doi: 10.1029/2006GB002881
- Anderson, R. Y., and W. E. Dean. 1988. Lacustrine varve formation through time. *Paleogeogr. Paleoclimatol. Paleoecol.* **62**: 215- 235
- Anschutz, P., B. Sundby, L. Lefrancois, G. W. Luther, A. Mucci. 2000. Interaction between metal oxides and species of nitrogen and iodine in bioturbated marine sediments. *Geochim Cosmochim Acta* **64**: 2751- 2762
- van Alstine, J. D. 2006. A high resolution study of the spatial and temporal variability of natural and anthropogenic compounds in offshore Lake Superior sediments. M.Sc. thesis. University of Minnesota.
- Appleby, P. G., and F. Oldfield. 1978. The calculation of lead-210 dates assuming a constant rate of supply of unsupported ^{210}Pb to the sediment. *Catena* **5**: 1-8.
- Austin, J., and S. Colman. 2008. A century of temperature variability in Lake Superior. *Limnol. Oceanogr.* **53**: 2724-2730.
- Baehr, M. M., and J. McManus. 2003. The measurement of phosphorus and its spatial and temporal variability in the western arm of Lake Superior. *J. Great. Lakes Res.* **29**: 479- 487

- Baker, J. E., S. J. Eisenreich, and B. J. Eadie. 1991. Sediment trap fluxes and benthic recycling of organic carbon, polycyclic aromatic hydrocarbons, and polychlorobiphenyl congeners in Lake Superior. *Environ. Sci. Technol.* **25**: 500-509.
- Bennington, V., G. A. McKinley, N. Kimura, and C. H. Wu. 2010. General circulation of Lake Superior: Mean, variability, and trends from 1979 to 2006. *Journal of Geophysical Research* **115**: C12015, doi:10.1029/2010JC006261
- Berner, R. A. 1980. *Early diagenesis: A theoretical approach*. Princeton University Press.
- Benz, M., A. Brune, and B. Schink. 1998. Anaerobic and aerobic oxidation of ferrous iron at neutral pH by chemoheterotrophic nitrate-reducing bacteria. *Archives of Microbiology* **169**: 159- 165
- Boehrer, B., and M. Schultze. 2008. Stratification of lakes. *Rev. Geophys.* **46** RG2005, doi:10.1029/2006RG000210.
- Bootsma, H. A., R. E. Hecky, and E. G. Ave. 2003. A Comparative Introduction to the Biology and Limnology of the African Great Lakes. **29**: 3–18.
- Bootsma, H., and R. Hecky. 1999. Nutrient cycling in Lake Malawi/Nyasa. In *Water Quality Report*, eds. H. A. Boostsma and R. E. Hecky, Lake Malawi/Nyasa Biodiversity Conservation Project.
- Boström, K. 1970. Origin of manganese-rich layers in Arctic sediments. *AAPG Bull.* 2471-2472.
- Boudreau, B. P. 1997. *Diagenetic models and their implementation: Modeling transport and reactions in aquatic sediments*. Springer.

- Boudreau, B. P. 1998. Mean mixed depth of sediments: The wherefore and the why. *Limnol. Oceanogr.* **43**: 524-526.
- Brown, E. T., L. L. Callonnet, and C. R. Cerman. 2000. Geochemical cycling of redox-sensitive metals in sediments from Lake Malawi: A diagnostic paleotracer for episodic changes in mixing depth. *Geochimica et Cosmochimica Acta.* **64**: 3515-3523
- Brown, E.T., Johnson, T.C., Scholz, C.A., Cohen, A.S. and King, J., 2007, Abrupt Change in Tropical African Climate Linked to the Bipolar Seesaw Over the Past 55,000 Years, *Geophys. Res. Lett.*, 34, doi:10.1029/2007GL031240.
- Brown E.T. and Katsev S. 2012, Southern East African climate recorded in laminated sediments of Lake Malawi, Abstract PP33A-2113, AGU 2012 Fall Meeting, San Francisco, Calif., 3-7 Dec.
- Burdige, D. J. and K. H. Nealson.1986. Chemical and microbiological studies of sulfide-mediated manganese reduction. *Geomicrobiology Journal* **4**: 36- 387.
- Burdige, D. J. 1993. The biogeochemistry of manganese and iron reduction in marine sediments. *Earth-Science Reviews* **35**: 249-284.
- Burdige, D. J., and S. Zheng. 1998. The biogeochemical cycling of dissolved organic nitrogen in estuarine sediments. *Limnol. Oceanogr.* **43**: 1796-1813.
- Burdige, D. J. 2006. *Geochemistry of marine sediments*. Princeton Univ. Press.
- Burdige, D. J. 2007. Preservation of organic matter in marine sediments: controls, mechanisms, and an imbalance in sediment organic carbon budgets? *Chem. Rev.* **107**: 467-485.

- Canfield, D. E. 1989. Sulfate reduction and oxic respiration in marine sediments: implications for organic carbon preservation in euxinic environments. *Deep-Sea Res.* **36**: 121-138.
- Canfield, D. E. 1989. Reactive iron in marine sediments. *Geochimica et Cosmochimica Acta* **53**: 619- 632
- Canfield, D. E., B. B. Jørgensen, H. Fossing, R. Glud, J. Gundersen, N. B. Ramsing, B. Thamdrup, J. W. Hansen, L. P. Nielsen, and P. O. J. Hall. 1993. Pathways of organic carbon oxidation in three continental margin sediments. *Marine Geology.* **113**: 27- 40.
- Canfield, D. E. 1994. Factors influencing organic carbon preservation in marine sediments. *Chemical Geology* **114**: 315-329
- Canfield, D. E. 2001. Biogeochemistry of sulfur isotopes. *Reviews in Mineralogy and Geochemistry* 43: 607– 636.
- Canfield, D. E., F. J. Stewart, B. Thamdrup, L. D. Brabandere, T. Dalsgaard, E. F. Delong, N. P. Revsbech, and O. Ulloa. 2010. A cryptic sulfur cycle in oxygen-minimum-zone waters off the chilean coast. *Science* **330**: 1375- 1377
- Capone, D. G. and R. P. Kiene. 1988. Comparison of microbial dynamics in marine and freshwater sediments: Contrasts in anaerobic carbon catabolism. *Limnology and Oceanography* **33**: 725- 749
- Caraco, N, J. Cole, G. E. Likens. 1990. A Comparison of Phosphorus Immobilization in Sediments of Freshwater and Coastal Marine. *Biogeochemistry* 9: 277- 290
- Caraco, N., J. Cole, G. E. Likens. 1993. Sulfate control of phosphorus availability in lakes. *Hydrobiologia* **253**: 275-280

- Carignan, R. and R. J. Flett. 1981. Postdepositional mobility of phosphorus in lake sediments. *Limnology and Oceanography* **26**: 361- 366
- Carlton, R. G., G. S. Walker, M. J. Klug, and R. G. Wetzel. 1989. Relative values of oxygen, nitrate, and sulfate to terminal microbial processes in the sediments of Lake Superior. *J. Great Lakes Res.* **15**: 133- 140.
- Chapra, S., and D. M. Dolan. 2012. Great Lakes total phosphorus revisited: 2. Mass balance modeling. *Journal of Great Lakes Research* **38**: 74- 754
- Chapra S.C. and W.C. Sonzogni. 1979. Great Lakes total phosphorus budget for the mid 1970s. *J. WPCF* 51: 2524-2532.
- Chapra, S., A. Dove, and G. J. Warren. 2012. Long-term trends of Great Lakes major ion chemistry. *Journal of Great Lakes Research* 38: 55- 560
- Christensen, J. P., and G. T. Rowe. 1984. Nitrification and oxygen consumption in northwest Atlantic deep-sea sediments. *Journal of Marine Research* **42**: 1099- 1116.
- Cole, J. J., Y. T. Prairie, N. F. Caraco, W. H. McDowell, L. J. Tranvik, R. G. Striegl, C. M. Duarte, P. Kortelainen, J. A. Downing, J. J. Middelburg, and J. Melack. 2007. Plumbing the global carbon cycle: Integrating inland waters into the terrestrial carbon budget. *Ecosystems* **10**:171–184.
- Coloway, F., and M. Bender. 1982. Diagenetic models of interstitial nitrate profiles in deep sea suboxic sediments. *Limnol. Oceanogr.* **27**: 624- 638.
- Codispoti, L. A., J. A. Brandes, J. P. Christensen, A. H. Devol, S. W. A. Naqvi, H. W. Paerl, and T. Yoshinari. 2001. The oceanic fixed nitrogen and nitrous oxide budgets: Moving targets as we enter the anthropocene? *Scientia Marina* **65**: 85-

105.

- Cotner, J. B., B. A. Biddanda, W. Makino, and E. Stets. 2004. Organic carbon biogeochemistry of Lake Superior. *Aquat. Ecosystem Health & Management* **7**: 451-464.
- Dale, A. W., S. Sommer, M. Haeckel, K. Wallmann, P. Linke, G. Wegener, O. Pfannkuche. 2010. Pathways and regulation of carbon, sulfur and energy transfer in marine sediments overlying methane gas hydrates on the Opouawe Bank (New Zealand). *Geochimica et Cosmochimica Acta* **74**: 5763-5784.
- Dalsgaard, T., B. Thamdrup, and D. Canfield. 2005. Anaerobic ammonium oxidation (anammox) in the marine environment. *Research in Microbiology* **156**: 457- 464.
- Deflandre. B., A. Mucci, J. P. Gagné, C. Guignard, and B. Sundby. 2002. Early diagenetic processes in coastal marine sediments disturbed by a catastrophic sedimentation event. *Geochimica et Cosmochimica Acta*. **66**: 2547- 2558
- Devol, A. H., and J. P. Christensen. 1993. Benthic fluxes and nitrogen cycling in sediments of the continental margin of the eastern North Pacific. *J. Mar. Res.* **51**:345-372.
- Devol, A. H., L. A. Codispoti, and J. P. Christensen. 1997. Summer and winter denitrification rates in western Arctic shelf sediments. *Continental Shelf Research* **17**: 1029–1050.
- Dickens, G. R., M. Koelling, D. C. Smith, L. Schnieders, and the IODP Expedition 302 Scientists. 2007. Rhizon sampling of pore waters on scientific drilling expeditions: An example from the IODP expedition 302, Arctic Coring

- Expedition (ACEX). Scientific Drilling 4, March, doi:10.2204/iodp.sd.4.08.2007
- Elsgaard L. and B. B. Jørgense. 1992. Anoxic transformations of radiolabeled hydrogen sulfide in marine and freshwater sediments. *Geochimica et Cosmochimica Acta*. **56**: 2425- 2435.
- Evans, J. E., T. C. Johnson, E. C. Alexander Jr., R. S. Lively, and S. J. Eisenreich. 1981. Sedimentation rates and depositional processes in Lake Superior from ^{210}Pb geochronology. *Journal of Great Lakes Research* **7**: 299-310.
- Fennel, K., D. Brady, D. DiToro., R. W. Fulweiler, W. S. Gardner, A. Giblin, M. J. McCarthy, A. Rao, S. Seitzinger, M. Thouvenot-Korppoo, and C. Tobias. 2009. Modeling denitrification in aquatic sediments. *Biogeochemistry* **93**: 159-178.
- Finlay, J. C., R. W. Sterner, and S. Kumar. 2007. Isotopic evidence for in lake production of accumulating nitrate in Lake Superior. *Ecol. Appl.* **17**: 2323-2332.
- Finlay, J. C., G. E. Small, and R. W. Sterner. 2013. Human influences on nitrogen removal in Lakes. *Science* **342**: 247.
- Gaines, R. R., E. U. Hammarlund, X. Hou, C. Qi, S. E. Gabbott, Y. Zhao, J. Peng, and D. Canfield. 2012. Mechanism for burgess shale-type preservation. *PNAS* **109**: 5180- 5184
- Gardner, W. D. 2000. Sediment Trap Sampling in Surface Waters, *The Changing Ocean Carbon Cycle: A midterm synthesis of the Joint Global Ocean Flux Study*. Cambridge University Press: 240-281
- Gehlen, M., C. Rabouille, U. Ezat, and L. D. Guidi-Guilvard. 1997. Drastic changes in deep-sea sediment porewater composition induced by episodic input of organic matter. *Limnol. Oceanogr.* **42**: 980-986.

- Glud, R. N., B. Thamdrup, H. Stahl, F. Wenzhoefer, A. Glud, H. Nomaki, K. Oguri, N. P. Revsbech, and H. Kitazato. 2009. Nitrogen cycling in a deep ocean margin sediment (Sagami Bay, Japan). *Limnol. Oceanogr.* **54**: 723-734.
- Glud, R. N. 2008. Oxygen dynamics of marine sediments, *Mar. Biol. Res.* **4**: 243–289.
- Giblin, A. E., G. E. Likens, A. White, and R. W. Howarth. 1990. Sulfur storage and alkalinity generation in New England lake sediments. *Limnol. Oceanogr.* **35**: 852-869
- Gobeil, C., B. Sundby, R. W. Macdonald, and J. N. Smith. 2001. Recent change in organic carbon flux to Arctic Ocean deep basins: Evidence from acid volatile sulfide, manganese and rhenium discord in sediments. *Geophys. Res. Lett.* **28**: 1743–1746.
- Gondwe, M. J., S. J. Guildford, and R. E. Hecky. 2008. Planktonic nitrogen fixation in Lake Malawi/Nyasa. *Hydrobiologia* **596**: 251- 267
- Gonfiantini, R., G. M. Zuppi, D. H. Eccles, and W. Ferro. 1979. Isotope investigations of Lake Malawi. In: *Isotope in Lake Studies*. International Atomic Energy Agency Panel Proceedings Series **51**:192-205.
- Gudasz, C., D. Bastviken, K. Steger, K. Premke, S. Sobek, and L. J. Tranvik. 2010. Temperature-controlled organic carbon mineralization in lake sediments. *Nature* **466**: 478–481.
- Guildford, S. J., and R. E. Hecky. 2000. Total nitrogen, total phosphorus and nutrient limitation in lakes and oceans: Is there a common relationship? *Limnol. Oceanogr.* **45**: 1213-1223.
- Grasshoff, K., K. Kremling, and M. Ehrhardt [eds.]. 1999. *Methods of sea water analysis*.

Wiley-VCH.

- Halfman, J. D. 1993. Water column characteristics from modern CTD data, Lake Malawi, Africa. *J. Great Lakes Res.* **19**: 512- 520
- Habicht, K. S., M. Gade, B. Thamdrup, P. Berg, and D. E. Canfield. 2002. Calibration of Sulfate levels in the Archean Ocean. *Science* **298**: 2372- 2374
- Hall, P. O. J., and R. C. Aller. 1992. Rapid, small-volume, flow injection analysis for total CO₂ and NH₄⁺ in marine and freshwaters. *Limnology and Oceanography.* **37**: 1113- 1119.
- Hartnett, H. E., R. G. Keil, J. I. Hedges, and A. H. Devol. 1998. Influence of oxygen exposure time on organic carbon preservation in continental margin sediments. *Nature.* **391**: 572 – 574.
- Hecky, R. E., and P. Kilham. 1988. Nutrient limitation of phytoplankton in freshwater and marine environments: A review of recent evidence on the effects of enrichment. *Limnol. Oceanogr.* **33**: 796- 822
- Hecky, R. E., H. J. Kling, T. C. Johnson, H. A. Bootsma, P. Wilkinson. 1999. Algal and sedimentary evidence for recent changes in the water quality and limnology of Lake Malawi/Nyasa. In *Water Quality Report*, eds. H. A. Bootsma and R. E. Hecky, Lake Malawi/Nyasa Biodiversity Conservation Project.
- Hecky, R. E., H. A. Bootsma, and M. L. Kingdon. 2003. Impact of land use on sediment and nutrient yields to Lake Malawi/Nyasa (Africa). *J. Great Lakes Res.* **29**: 139 -158
- Heinen E. A., and J. McManus. 2004. Carbon and nutrient cycling at the sediment-water boundary in western Lake Superior. *J. Great Lakes Res.* **30**: 113-132.

- den Heyer, C., and J. Kalff. 1998. Organic matter mineralization rates in sediments: A within- and among-lake study. *Limnol. Oceanogr.* **43**: 695–705.
- den Heyer, C. and J. Kalff. 1998. Organic matter mineralization rates in sediments: A within-and among-lake study. *Limnology and oceanography* **43**: 695–705
- Hietanen, S., and J. Kuparinen. 2008. Seasonal and short-term variation in denitrification and anammox at a coastal station on the Gulf of Finland, Baltic Sea. *Hydrobiologia* **596**: 67- 77.
- Hoehler, T. M., M. J. Alperin, D. B. Albert, and C. S. Martens. 1994. Field and laboratory studies of methane oxidation in an anoxic marine sediment: Evidence for a methanogen-sulfate reducer consortium. *Global Biogeochem. Cycles* **8**: 451–463
- Holmer, M, and P. Storkholm. 2001. Sulphate reduction and sulphur cycling in lake sediments: a review. *Freshwater Biology* **46**: 431- 451
- Holmes, R. M., A. Aminot, R. K erouel, B. A. Hooker, and B. J. Peterson. 1999. A simple and precise method for measuring ammonium in marine and freshwater ecosystems. *Can. J. Fish. Aquat. Sci.* **56**: 1801-1808.
- Hulth, S., R. C. Aller, D. E. Canfield, T. Dalsgaard, P. Engstrom, F. Gillbert, K. Sundback, and B. Thamdrup. 2005. Nitrogen removal in marine environments: Recent findings and future research challenges. *Marine Chemistry* **94**: 125-145.
- Hupfer, M., and J. Lewandowski. 2008. Oxygen controls the phosphorus release from lake sediments- a long-lasting paradigm in limnology. *Internat. Rev. Hydrobiol.* **93**: 415- 432

- Ingvorsen, K., A. J. B. Zehnder, and B. B. Jørgensen. 1984. Kinetics of sulfate and acetate uptake by *Desulforbacter postgatei*. *Applied Environmental Microbiology* **47**: 403- 408
- Johnson, T. C., and T. W. Davis. 1989. High resolution seismic profiles from Lake Malawi, east Africa. *African Earth Sci.* **8**: 383- 392
- Johnson, T. C., Brown, E. T., McManus, J., Barry, S., Barker, P., & Gasse, F. 2002. A high-resolution paleoclimate record spanning the past 25,000 years in southern East Africa. *Science*, 296(5565), 113-132.
- Johnson, T. C., J. E. Evans, and S. J. Eisenreich. 1982. Total organic carbon in Lake Superior sediments: Comparisons with hemipelagic and pelagic marine environments. *Limnol. Oceanogr.* **27**: 481-491.
- Jorgensen, B. B. 1982. Mineralization of organic matter in the sea bed – the role of sulphate reduction. *Nature* **296**: 643-645.
- Katsev, S., I. Tsandev, I. L'Heureux, D. G. Rancourt. 2006. Factors controlling long-term phosphorus efflux from Lake sediments: Exploratory reactive-transport modeling. *Chemical Geology* **24**: 127- 147
- Katsev, S., B. Sundby, A. Mucci. 2006. Modeling vertical excursions of the redox boundary in sediments: Application to deep basins of the Arctic Ocean. *Limnol. Oceanogr.* **51**: 1581- 1593
- Katsev, S., G. Chaillou, and B. Sundby. 2007. Effects of progressive oxygen depletion on sediment diagenesis and fluxes: A model for the lower St. Lawrence River Estuary. *Limnol. Oceanogr.* **52**: 2555- 2568.
- Katsev, S., S. A. Crowe, A. Mucci, B. Sundby, S. Nomosatryo, G. D. Haffner, and D. A.

- Fowle. 2010. Mixing and its effects on biogeochemistry in persistently stratified, deep, tropical Lake Matano, Indonesia. *Limnol. Oceanogr.* **55**: 763-776
- Katsev, S. and M. Dittrich. 2013. Modeling of decadal scale phosphorus retention in lake sediment under varying redox conditions. *Ecological Modelling* **251**: 246- 259
- Kemp A. L. W., C. I. Dell, and N. S. Harper. 1978. Sedimentation rates and a sediment budget for Lake Superior. *J. Great Lakes Res.* **4**: 276-287.
- Klump, J.V., R. Paddock, C. C. Remsen, S. Fitzgerald, M. Boraas, and P. Anderson. 1989. Variation in accumulation rates and the flux of labile organic matter in eastern Lake Superior basins. *J. Great Lakes Res.* **15**: 104–122.
- King, G. M., and M. J. Klug. 1980. Sulfhydrolase activity in sediments of Wintergreen Lake, Kalamazoo County, Michigan. *Appl. Environ. Microbiol.* **39**:950-956.
- King, G. M and M. J. Klug. 1982. Comparative aspects of sulfur mineralization in sediments of a eutrophic lake. *Appl. Environ. Microbiol.* **43**: 1406-1412
- Kistner, M. M., 2013. Organic carbon reactivity in Lake Superior. M.Sc. thesis. University of Minnesota.
- Kuivila, K. M., J. W. Murray, and A. H. Devol 1989. Methane production, sulfate reduction and competition for substrates in the sediments of Lake Washington. *Geochimica et Cosmochimica Acta* **53**: 409- 416
- LaRowe, D. E., A. W. Dale, J. P. Amend, and P. van Cappellen. 2012. Thermodynamic limitations on microbially catalyzed reaction rates. *Geochimica et Cosmochimica Acta* **90**: 96- 109
- Laursen, A. E., and S. P. Seitzinger. 2002. The role of denitrification in nitrogen removal

- and carbon mineralization in Mid-Atlantic Bight sediments. *Continental Shelf Research* **22**: 1397-1416.
- Lesht, B. M., T. D. Fontaine III, and D. M. Dolan. 1991. Great Lakes total phosphorus model: post audit and regionalized sensitivity analysis. *J. Great Lakes Res.* **17**: 3-17.
- Li, J. 2011. Diagenesis and sediment-water exchanges in organic-poor sediments of Lake Superior. M.Sc. thesis, University of Minnesota.
- Li, H., E. C. Minor, and P. K. Zigah. 2013. Diagenetic changes in Lake Superior sediments as seen from FTIR and 2D correlation spectroscopy. *Organic Geochemistry* **58**: 125- 136
- Lorke, A., B. Muller, M. Maerki, and A. Wüest. 2003. Breathing sediments: The control of diffusive transport across the sediment-water interface by periodic boundary-layer turbulence. *Limno. Oceanogr.* **48**: 2077-2085
- Lovley, D. R. and M. J. Klug. 1983. Sulfate reducers can outcompete methanogens at freshwater sulfate concentrations. *Applied Environmental Microbiology* **45**: 187-192
- Luther, G. W. III, B. Sundby, B. L. Lewis, P. J. Brendel, and N. Silverberg. 1997. Interactions of manganese dioxide by nitrite: an anaerobic nitrification reaction. *Aquat. Geochem.* **8**: 15- 36
- MacIntyre, S. (2013). Climatic variability, mixing dynamics, and ecological consequences in the African Great Lakes. *Climatic Change and Global Warming of Inland Waters: Impacts and Mitigation for Ecosystems and Societies*, 311-336.
- Maerki, M., B. Müller, and B. Wehrli. 2006. Microscale mineralization pathways in

- surface sediments: A chemical sensor study in Lake Baikal. *Limnol. Oceanogr.* **51**: 1342- 1354.
- Maerki, M., B. Müller, C. Dinkel, and B. Wehrli. 2009. Mineralization pathways in lake sediments with different oxygen and organic carbon supply. *Limnol. Oceanogr.* **54**: 428–438.
- März, C., A. Stratmann, J. Matthießen, A. K. Meinhardt, S. Eckert, B. Schnetger, C. Vogt, R. Stein, and H. J. Brumsack. 2011. Manganese-rich brown layers in Arctic Ocean sediments: composition, formation mechanisms, and diagenetic overprint. *Geochimica et Cosmochimica Acta* **75**: 7668-7687
- Martin, P., L. Granina, K. Martens, and B. Goddeeris. 1998. Oxygen concentration profiles in sediments of two ancient lakes: Lake Baikal (Siberia, Russia) and Lake Malawi (East Africa). *Hydrobiologia* **367**: 163- 174
- Matisoff, G., and X. Wang. 1998. Solute transport in sediments by freshwater infaunal bioirrigators. *Limnol. Oceanogr.* **43**: 1487- 1499
- McDonald, C. P., N. R. Urban, and C. M. Casey. 2010. Modeling historical trends in Lake Superior total nitrogen concentrations. *Journal of Great Lakes Research* **36**: 715- 721
- McManus, J., W. M. Berelson, K. H. Coale, K. S. Johnson, and T. E. Kilgore. 1997. Phosphorus regeneration in continental margin sediment. *Geochimica et Cosmochimica Acta.* **61**: 2891- 2907
- McManus, J., E. A. Heinen, and M. M. Baehr. 2003. Hypolimnetic oxidation rates in Lake Superior: Role of dissolved organic material on the lake's carbon budget. *Limnol. Oceanogr.* **48**:1624-1632.

- Meile, C., and P. Van Cappellen. 2003. Global estimates of enhanced solute transport in marine sediments. *Limnol. Oceanogr.* **48**: 777-786
- Meile, C., P. Berg, P. Van Cappellen, and K. Tuncay. 2005. Solute-specific pore water irrigation: Implications for chemical cycling in early diagenesis. *Journal of Marine Research* **63**: 601- 621
- Meysman, F. J. R., B. P. Boudreau, and J. J. Middelburg. 2005. Modeling reactive transport in sediments subject to bioturbation and compaction. *Geochim. Cosmochim. Acta.* **69**: 3601-3617.
- Middelburg, J. J. 1989. A simple rate model for organic matter decomposition in marine sediments. *Geochimica et Cosmochimica Acta.* **53**:1577-1581.
- Middelburg, J. J., T. Vlug, F. Jaco, and W. A. van der Nat. 1993. Organic matter mineralization in marine systems. *Global Planet. Change* **8**: 47-58.
- Middelburg, J., K. Soetaert, P. M. J. Herman, and C. H. R. Heip. 1996. Denitrification in marine sediments: A model study. *Global Biogeochemical Cycles* **4**: 661-673.
- Middelburg, J. J., K. Soetaert, and P. M. J. Herman. 1997. Empirical relationships for use in global diagenetic models. *Deep-Sea Research I* **44**: 327-344
- Morse, J. W., F. J. Millero, J. C. Cornwell, and D. Rickard. 1987. The chemistry of the hydrogen sulfide and iron sulfide systems in natural waters. *Earth-Science Reviews* **24**: 1-42
- Mortimer, C. H. 1942. The exchange of dissolved substances between mud and water in lakes. *J. Ecology* **30**: 147- 201

- Mortimer, R. J. G., M. D. Krom, S. J. Harris, P. J. Hayes, I. M. Davies, W. Davison, H. Zhang. 2002. Evidence for suboxic nitrification in recent marine sediments. *Mar. Ecol. Prog. Ser.* **236**: 31- 35
- Mortimer, R. J. G., S. J. Harris, M. D. Krom, T. E. Freitag, J. I. Prosser, J. Barnes, P. Anschutz, P. J. Hayes, I. M. Davies. 2004. Anoxic nitrification in marine sediments. *Mar. Ecol. Prog. Ser.* **276**: 37- 51
- Mouret, A., P. Anschutz, B. Deflandre, G. Chaillou, C. Hyacinthe, J. Deborde, H. Etcheber, J.-M. Jouanneau, A. Grémare, and P. Lacroart. 2010. Oxygen and organic carbon fluxes in sediments of the Bay of Biscay. *Deep-Sea Res. I* **57**: 528-540.
- Müller, B., M. Maerki, M. Schmid, E. G. Vologina, B. Wehrli, A. Wüest, and M. Sturm. 2005. Internal carbon and nutrient cycling in Lake Baikal: sedimentation, upwelling, and early diagenesis. *Global and Planet. Change* **46**: 101-124.
- Munawar, M., and I. F. Munawar. 1978. Phytoplankton of Lake Superior 1973. *J. Great Lakes Res., Internat. Assoc. Great Lakes Res.* **4**: 415-442.
- Nalewajko, C., K. Lee, and H. Shear. 1981. Phosphorus kinetics in Lake Superior: light intensity and phosphate uptake in algae. *Can. J. Fish. Aquat. Sci.* **38**: 224-232.
- Nriagu, J. O. 1984. Role of inland water sediments as sinks for anthropogenic sulfur. *The Science of the Total Environment* **38**: 7- 13
- Ostrom, N. E., D. T. Long, E. M. Bell, and T. Beals. 1998. The origin and cycling of particulate and sedimentary organic matter and nitrate in Lake Superior. *Chemical Geology* **152**: 13-28

- Otu, M. K., P. Ramlal, P. Wilkinson, R. I. Hall, R. E. Hecky. 2011. Paleolimnological evidence of the effects of recent cultural eutrophication during the last 200 years in Lake Malawi, East Africa. *J. Great Lakes. Res.* **37**: 61- 74
- Pallud, C., C. Meile, A. M. Laverman, J. Abell, P. Van Cappellen. 2007. The use of flow-through sediment reactors in biogeochemical kinetics: Methodology and examples of applications. *Marine Chemistry* **106**: 256- 271
- Pilskaln, C. H. and T. C. Johnson. 1991. Seasonal signal in Lake Malawi sediments. *Limnol. Oceanogr.* **36**: 544- 557
- Pilskaln, C. H. 2004. Seasonal and interannual particle export in an African rift valley lake: A 5-yr record from Lake Malawi, southern East Africa. *Limnol. Oceanogr.* **49**: 964- 977
- Poulton S.W. and D.E. Canfield. 2005. Development of a sequential extraction procedure for iron: implications for iron partitioning in continentally derived particulates. *Chem. Geol.* **214**: 209-221.
- Ramlal, P. S., R. E. Hecky, H. A. Bootsma, S. L. Schiff, and M. J. Kingdon. 2003. Sources and Fluxes of organic carbon in Lake Malawi/Nyasa. *J. Great Lakes Res.* **29**: 107- 120
- Reimers, C. E., and E. Suess. 1983. The partitioning of organic carbon fluxes and sedimentary organic matter decomposition rates in the ocean. *Marine Chemistry* **13**: 141-168
- Revsbech, N. P. 1989. An oxygen microelectrode with a guard cathode. *Limnology and Oceanography* **34**: 472-476
- Roden, E. E. and J. H. Tuttle. 1993. Inorganic sulfur turnover in oligohaline estuarine

- sediments. *Biogeochemistry* **22**: 81- 105
- Roden, E. E., and J. W. Edmonds. 1997. Phosphate mobilization in iron-rich anaerobic sediments: Microbial Fe(III) oxide reduction versus iron-sulfide formation. *Arch. Hydrobiol.* **139**: 347- 378
- Roden, E.E. and R.G. Wetzel. 2002. Kinetics of microbial Fe(III) oxide reduction in freshwater wetland sediments. *Limnol. Oceanogr.* **47**: 198-211
- Rudd J.W.M., Kelly C.A. & Furutani A. 1986. The role of sulfate reduction in long term accumulation of organic and inorganic sulfur in lake sediments. *Limnology and Oceanography* **31**: 1281-1291.
- Ruttenberg K.C. 1992. Development of a sequential extraction method for different forms of phosphorus in marine sediments. *Limnol. Oceanogr.* **37**: 1460-1482.
- Rysgaard, S., N. Risgaard-Petersen, N. P. Sloth, K. Jensen, and L. P. Nielsen. 1994. Oxygen regulation of nitrification and denitrification in sediments. *Limnol. Oceanogr.* **39**: 1643-1652.
- Sauter, E. J., M. Schluter, and E. Suess. 2001. Organic carbon flux and remineralization in surface sediments from the northern North Atlantic derived from pore-water oxygen microprofiles. *Deep-Sea Research I* **48**: 529-553.
- Sayles, F. L., W. R. Martin, and W. G. Deuser. 1994. Response of benthic oxygen-demand to particulate organic-carbon supply in the deep-sea near Bermuda. *Nature* **371**: 686–689.
- Schubert, C. J., E. Durisch-Kaiser, B. Wehrli, B. Thamdrup, P. Lam, and M. M. M. Kuypers. 2006. Anaerobic ammonium oxidation in a tropical freshwater system (Lake Tanganyika). *Environmental Microbiology* **8**: 1857- 1863,

doi:10.1111/j.1462-2920.2006.001074.x

- Seitzinger, S. P., S. W. Nixon, and M. E. Q. Pilson. 1984. Denitrification and nitrous oxide production in a coastal marine ecosystem. *Limnol. Oceanogr.* **29**: 73-83.
- Seitzinger, S. P. 1988. Denitrification in freshwater and coastal marine ecosystems: Ecological and geochemical significance. *Limnol. Oceanogr.* **33**: 702-724.
- Seitzinger, S. P., and A. E. Giblin. 1996. Estimating denitrification in North Atlantic continental shelf sediments. *Biogeochemistry* **35**: 235-260.
- Seitzinger, S. P., J. A. Harrison, J. K. Böhlke, A. F. Bouwman, R. Lowrance, B. Peterson, C. Tobias, and G. Van Drecht. 2006. Denitrification across landscapes and waterscapes: A synthesis. *Ecological Applications*. **16**: 2064- 2090.
- Sinke, A. J. C, A. A. Cornelese, T. E. Cappenberg, and A. J. B. Zehnder. 1992. Seasonal variation in sulfate reduction and methanogenesis in peaty sediments of eutrophic Lake Loosdrecht, The Netherlands. *Biogeochemistry* **16**: 43- 61
- Small, G. E., G. S. Bullerjahn, R. W. Sterner, B. F. N. Beall, S. Brovold, J. C. Finlay, R. M. L. McKay, and M. Mukherjee. 2013. Rates and controls of nitrification in a large oligotrophic lake. *Limnol. Oceanogr.* **58**: 276–286.
- Sobek, S., E. Durisch-Kaiser, R. Zurbrügg, N. Wongfun, M. Wessels, N. Pasche, and B. Wehrli. 2009. Organic carbon burial efficiency in lake sediments controlled by oxygen exposure time and sediment source. *Limnol Oceanogr.* **54**: 2243–2254.
- Solan, M., and L. G. Herringshaw. 2008. Bioturbation in aquatic environments: linking past and present. *Aquatic Biology* **2**: 201-205
- Stark, R. A. 2009. Nitrate production and nitrogen and carbon cycling in Lake Superior Sediments. M.Sc. thesis. University of Minnesota.

- Sterner, R.W., T. M. Smutka, R. M. L. McKay, X. Qin, E. T. Brown, and R. M. Sherrell. 2004. Phosphorus and trace metal limitation of algae and bacteria in Lake Superior. *Limnol. Oceanogr.* **49**:495-507
- Sterner R. W., E. Anagnostou, S. Brovold, G. S. Bullerjahn, J. C. Finlay, S. Kumar, R. M. McKay, and R. M. Sherrell. 2007. Increasing stoichiometric imbalance in North America's largest lake: Nitrification in Lake Superior. *Geophys. Res. Lett.* **34**: L10406, doi:10.1029/2006GL028861
- Sterner, R. W., T. Andersen, J. J. Elser, D. O. Hessen, J. M. Hood, E. McCauley and J. Urabe. 2008. Scale-dependent carbon : nitrogen : phosphorus seston stoichiometry in marine and freshwaters. *Limnol. Oceanogr.* **53**: 1169- 1180.
- Sterner, R. W. 2010. In situ-measured primary production in Lake Superior. *Journal of Great Lakes Research* **36**: 139-149.
- Straub, K. L., and B. E. E. Buchholz-Cleven. 1996. Enumeration and detection of anaerobic ferrous iron-oxidizing, nitrate-reducing bacteria from diverse European sediments. *Applied and Environmental Microbiology* **64**: 4846-4856.
- Suess, E. 1980. Particulate organic carbon flux in the oceans: Surface productivity and oxygen utilization. *Nature* **288**: 260- 263
- Sundby, B., C. Gobeil, N. Silverberg, and A. Mucci. 1992. The phosphorus cycle in coastal marine sediments. *Limnology and Oceanography* **37**: 1129- 1145
- Sweerts, J.-P. R.A., C. A. Kelly, J. W. M. Rudd, R. Hesslein, and T. E. Capenberg. 1991. Similarity of whole-sediment molecular diffusion coefficients in freshwater sediments of low and high porosity. *Limnol. Oceanogr.* **36**: 335-342.
- Thomsen, U., B. Thamdrup, D. A. Stahl, and D. E. Canfield. 2004. Pathways of organic

- oxidation in deep lacustrine sediment, Lake Michigan. *Limnol. Oceanogr.* **46**: 2046-2057.
- Tranvik, L. J., J. A. Downing, J. B. Cotner, S. A. Loiselle, R. G. Striegl, T. J. Ballatore, P. Dillon, K. Finlay, K. Fortino, L. B. Knoll, P. L. Kortelainen, T. Kutser, S. Larsen, I. Laurion, D. M. Leech, Y. Prairie, W. H. Renwick, F. Roland, B. S. Sherman, D. W. Schindler, S. Sobek, A. Tremblay, M. J. Vanni, A. M. Verschoor, E. von Wachenfeldt, and G. A. Weyhenmeyer. 2009. Lakes and impoundments as regulators of carbon cycling and climate. *Limnol. Oceanogr.* **54**:2298–2314.
- Viollier, E., P. W. Inglett, K. Hunter, A. N. Roychoudhury, and P. Van Cappellen. 2000. The ferrozine method revisited: Fe(II)/Fe(III) determination in natural waters. *Applied Geochemistry* **15**: 785-790.
- Vollmer, M. K., H. A. Bootsma, R. E. Hecky, G. Patterson, J. D. Halfman, J. M. Edmond, D. H. Eccles, and R. F. Weiss. 2005. Deep-water warming trend in Lake Malawi, East Africa. *Limnol. Oceanogr.* **50**: 727- 732.
- Vollmer, M. K., R. F. Weiss, and H. A. Bootsma. 2002. Ventilation of Lake Malawi/Nyasa. *The East African Great Lakes: Limnology, Palaeolimnology and Biodiversity. Advances in Global Change Resercah* **12**: 209- 233
- Weiler, R.R. 1978. Chemistry of Lake Superior. *J. Great Lakes Res.* 4:370–385.
- Wüest, A., G. Piepke, and J. D. Halfman. 1996. Combined effects of dissolved solids and temperature on the density stratification of Lake Malawi, in Johnson, T.C. and E.O. Odada (eds.), *The limnology, climatology and paleoclimatology of the East African lakes.* Gordon and Breach, Toronto:183- 202
- Zhu, Guibing, S. Wang, W. Wang, Y. Wang, L. Zhou, B. Jiang, H. J. M. Op den Camp,

- N. Risgaard-Petersen, L. Schwark, Y. Peng, M. M. Hefting, M. S. M. Jetten, and C. Yin. 2013. Hotspots of anaerobic ammonium oxidation at land-freshwater interfaces. *Nature Geoscience* **6**: 103-107.
- Zigah, P. K., E. C. Minor, J. P. Werne, and L. McCallister. 2011. Radiocarbon and stable carbon isotope insights into provenance and cycling of carbon in Lake Superior. *Limnol. Oceanogr.* **56**: 867-886.
- Zigah, P. K., E. C. Minor, and J. P. Werne. 2012. Radiocarbon and stable-isotope geochemistry of organic and inorganic carbon in Lake Superior. *Global Biogeochemical Cycles* **26**: GB1023

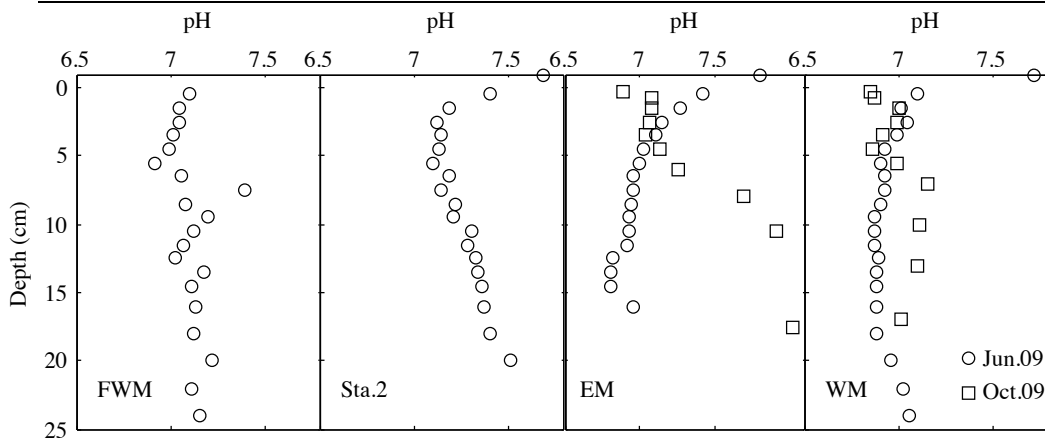
APPENDICES

Appendix 1. Parameters used in calculations.

	Parameter	Unit
φ	Porosity	
θ	Tortuosity: $\theta^2 = 1 - \ln(\varphi^2)$	
M_w	Weight of interstitial water	g
M_d	Weight of dry sediment	g
ρ	Density of dry sediment	g cm^{-3}
$\rho_{\text{bulk sed.}}$	Density of the bulk sediments (wet sediments)	g cm^{-3}
$\rho_{\text{dry bulk}}$	Dry bulk density (g dry sediment per volume wet sediment)	g cm^{-3}
U	Burial velocity	cm yr^{-1}
x	Depth below SWI	cm
t	Time or age	yr
C_i	Concentration of a chemical species i	mol g^{-1} (solid); mol L^{-1} (porewater)
C_i^0	Concentration of species i at SWI	mol L^{-1}
C_i^{burr}	Concentration of species i in bioirrigated burrows	mol L^{-1}
D_i	Diffusion coefficient of species i	$\text{cm}^2 \text{yr}^{-1}$
D_s	$D_s = D/\theta^2$	$\text{cm}^2 \text{yr}^{-1}$
D_b	Bioturbation coefficient	$\text{cm}^2 \text{yr}^{-1}$
ξ	$(1-\varphi)\rho$	g cm^{-3}
α_{irr}	Bioirrigation coefficient	s^{-1}
R_i	Reaction rate of species or reaction i	$\text{mol cm}^{-3} \text{yr}^{-1}$
R_i^*	Integrated rate of reaction of species or reaction i	$\text{mol m}^{-2} \text{d}^{-1}$
F_i	Diffusive flux of species i	$\text{mol m}^{-2} \text{d}^{-1}$
$F_{i \text{ bur}}$	Burial flux of species i	$\text{mol m}^{-2} \text{d}^{-1}$
k	First order rate parameter (reactivity)	yr^{-1}
τ	Half-life of reaction $\tau = \ln(2) / k$	yr

Appendix 2. Lake Superior sediment pH values

Depth (cm)	FWM.1	Sta.2	EM.1	WM.1	EM.2		WM. 2	
	pH				Depth (cm)	pH	Depth (cm)	pH
-1	7.82	7.68	7.8	7.72	0.25	6.88	0.25	6.84
0.5	7.1	7.4	7.41	7.1	0.75	7.08	0.75	6.87
1.5	7.04	7.18	7.26	7.01	1.5	7.07	1.5	7.00
2.5	7.04	7.12	7.15	7.04	2.5	7.06	2.5	6.99
3.5	7.01	7.14	7.1	6.99	3.5	7.03	3.5	6.91
4.5	6.99	7.13	7.02	6.92	4.5	7.13	4.5	6.86
5.5	6.91	7.09	7.00	6.9	6	7.25	5.5	6.99
6.5	7.05	7.18	6.95	6.92	8	7.68	7	7.15
7.5	7.39	7.14	6.96	6.92	10.5	7.90	10	7.11
8.5	7.07	7.22	6.94	6.9	13.5	8.16	13	7.10
9.5	7.19	7.21	6.93	6.87	17.5	8.01	17	7.01
10.5	7.12	7.3	6.93	6.87				
11.5	7.06	7.28	6.91	6.87				
12.5	7.02	7.33	6.82	6.89				
13.5	7.17	7.34	6.81	6.88				
14.5	7.11	7.36	6.8	6.88				
16	7.13	7.37	6.95	6.88				
18	7.12	7.4		6.88				
20	7.22	7.51		6.95				
22	7.11			7.02				
24	7.15			7.05				
27.5				6.92				



Appendix 3. Lake Superior sediment water content (WC) values

FWM.1		FWM.2		FWM.3		FWM.4		FWM.5		FWM.6		FWM.7	
Depth (cm)	WC												
0.5	0.85	0.5	0.89	0.25	0.87	0.25	0.87	0.25	0.87	0.05	0.95	0.25	0.88
1.5	0.77	1.5	0.76	0.75	0.83	0.75	0.84	0.75	0.84	0.25	0.86	0.75	0.83
2.5	0.71	2.5	0.68	1.5	0.76	1.5	0.80	1.5	0.79	0.75	0.81	1.5	0.75
3.5	0.67	3.5	0.72	2.5	0.70	2.5	0.75	2.5	0.73	1.5	0.77	2.5	0.70
4.5	0.69	4.5	0.74	3.5	0.69	3.5	0.74	3.5	0.74	2.5	0.73	3.5	0.71
5.5	0.72	5.5	0.74	4.5	0.71	4.5	0.74	4.5	0.75	3.5	0.74	4.5	0.72
6.5	0.73	6.5	0.74	6	0.74	5.5	0.75	5.5	0.75	4.5	0.75	5.5	0.73
7.5	0.76	7.5	0.73	8	0.70	6.5	0.74	6.5	0.75	5.5	0.75	6.5	0.75
8.5	0.74	8.5	0.72	10.5	0.69	8	0.73	7.5	0.74	6.5	0.76	7.5	0.75
9.5	0.75	9.5	0.72	13.5	0.69	10.5	0.75	9	0.70	7.5	0.75	8.5	0.75
10.5	0.72	11	0.74	16.5	0.72	13.5	0.75	11	0.71	9.5	0.75	9.5	0.75
11.5	0.71	13.5	0.74	19.5	0.73	16.5	0.72	13.5	0.71	10.5	0.74	11	0.74
12.5	0.71	17.5	0.73	23	0.72	19.5	0.71	16.5	0.71	11.5	0.72	13.5	0.74
13.5	0.68									13	0.73	16.5	0.73
14.5	0.70									15.5	0.74	19.5	0.72
16	0.70									18.5	0.73		
18	0.70									22.5	0.73		
20	0.72												
22	0.71												
24	0.71												

Appendix 3, continued

IR.1		IR.2		IR.3		IR.4		IR.5		IR.6		KW.1	
Depth (cm)	WC												
0.25	0.91	0.25	0.89	0.25	0.90	0.25	0.91	0.25	0.89	0.25	0.9	0.25	0.88
0.75	0.87	0.75	0.85	0.75	0.87	0.75	0.84	0.75	0.84	0.75	0.87	0.75	0.86
1.5	0.84	1.5	0.84	1.5	0.83	1.5	0.77	1.5	0.83	1.25	0.85	1.5	0.84
2.5	0.81	2.5	0.81	2.5	0.81	2.5	0.79	2.5	0.79	1.75	0.75	2.5	0.81
3.5	0.78	3.5	0.79	3.5	0.78	3.5	0.79	3.5	0.79	2.25	0.82	3.5	0.79
4.5	0.75	4.5	0.77	4.5	0.76	4.5	0.77	4.5	0.76	2.75	0.82	4.5	0.77
6	0.76	6	0.76	6	0.76	5.5	0.77	5.5	0.76	3.5	0.8	6	0.72
8	0.76	8	0.76	8	0.76	6.5	0.77	6.5	0.76	4.5	0.82	8	0.72
10.5	0.76	10.5	0.76	10.5	0.76	8	0.77	8	0.76	5.5	0.8	10.5	0.76
13.5	0.76	13.5	0.76	13.5	0.75	10.5	0.76	10.5	0.77	6.5	0.77	13.5	0.75
16.5	0.76	17.5	0.75	17.5	0.75	13.5	0.76	13.5	0.76	7.5	0.78	16.5	0.69
19.5	0.75	22.5	0.75	22.5	0.75	16.5	0.77	16.5	0.76	8.5	0.77	19.5	0.73
23	0.71					19.5	0.76	19.5	0.76	10.5	0.77	23	0.72
										13.5	0.77		
										16.5	0.77		
										19.5	0.76		
										22.5	0.76		

Appendix 3, continued

EM.1		EM.2		EM.3		EM.4		EM.5		EM.6		Sta. 2	
Depth (cm)	WC												
0.5	0.88	0.25	0.90	0.25	0.89	0.25	0.91	0.25	0.90	0.25	0.84	0.5	0.73
1.5	0.86	0.75	0.88	0.75	0.88	0.75	0.90	0.75	0.86	1.25	0.82	1.5	0.62
2.5	0.83	1.5	0.91	1.5	0.86	1.5	0.87	1.5	0.84	1.75	0.8	2.5	0.51
3.5	0.80	2.5	0.83	2.5	0.82	2.5	0.82	2.5	0.81	2.25	0.81	3.5	0.45
4.5	0.77	3.5	0.79	3.5	0.79	3.5	0.80	3.5	0.79	2.75	0.76	4.5	0.44
5.5	0.74	4.5	0.78	4.5	0.78	4.5	0.77	4.5	0.77	3.5	0.79	5.5	0.42
6.5	0.71	6	0.70	6	0.75	5.5	0.76	5.5	0.75	4.5	0.77	6.5	0.41
7.5	0.69	8	0.65	8	0.73	6.5	0.75	6.5	0.74	5.5	0.56	7.5	0.40
8.5	0.68	10.5	0.63	10.5	0.70	7.5	0.73	7.5	0.73	6.5	0.74	8.5	0.40
9.5	0.68	13.5	0.61	13.5	0.68	8.5	0.72	9	0.72	7.5	0.73	9.5	0.39
10.5	0.65	17.5	0.61	16.5	0.68	9.5	0.68	11	0.69	8.5	0.7	10.5	0.39
11.5	0.65			19.5	0.69	11	0.71	13.5	0.70	10.5	0.61	11.5	0.34
12.5	0.65			23	0.68	13.5	0.71	16.5	0.69	13.5	0.68	12.5	0.35
13.5	0.64					16.5	0.71	19.5	0.69	16.5	0.68	13.5	0.34
14.5	0.64					19.5	0.71	23	0.70	19.5	0.58	14.5	0.34
16	0.63					23	0.71			22.5	0.64	16	0.42
												18	0.43
												20	0.40

Appendix 3, continued

WM.1		WM.2		WM.3		WM.4		WM.5		WM.6		NIP.1	
Depth (cm)	WC												
0.5	0.87	0.25	0.89	0.25	0.89	0.25	0.89	0.25	0.90	0.25	0.87	0.25	0.85
1.5	0.84	0.75	0.87	0.75	0.87	0.75	0.87	0.75	0.86	0.75	0.86	0.75	0.79
2.5	0.81	1.5	0.84	1.5	0.84	1.5	0.84	1.5	0.82	1.5	0.83	1.25	0.72
3.5	0.76	2.5	0.69	2.5	0.80	2.5	0.80	2.5	0.77	2.5	0.81	1.75	0.68
4.5	0.75	3.5	0.66	3.5	0.77	3.5	0.77	3.5	0.75	3.5	0.77	2.25	0.6
5.5	0.74	4.5	0.63	4.5	0.75	4.5	0.76	4.5	0.74	4.5	0.67	2.75	0.53
6.5	0.73	6	0.60	6	0.68	5.5	0.75	5.5	0.71	5.5	0.66	3.5	0.55
7.5	0.72	8	0.60	8	0.65	6.5	0.73	6.5	0.66	6.5	0.65	4.5	0.56
8.5	0.70	10.5	0.59	10.5	0.64	8	0.70	7.5	0.65	7.5	0.64	5.5	0.54
9.5	0.70	13.5	0.57	13.5	0.63	10.5	0.73	8.5	0.64	8.5	0.63	6.5	0.55
10.5	0.69	17.5	0.54	16.5	0.62	13.5	0.72	10.5	0.63	9.5	0.62	7.5	0.55
11.5	0.68			19.5	0.62	17.5	0.70	13.5	0.65	11	0.61	8.5	0.49
12.5	0.67			23	0.60	22.5	0.70	16.5	0.61	13.5	0.60	10.5	0.49
13.5	0.67							19.5	0.61	16.5	0.59	13.5	0.52
14.5	0.66							22.5	0.58			16.5	0.49
16	0.67											19.5	0.53
18	0.65											22.5	0.52
20	0.65												
22	0.64												
24	0.62												
27.5	0.61												

Appendix 3, continued

CM.1		CM.2		CM.3		CM.4		ED.2		ED.3	
Depth (cm)	WC										
0.25	0.91	0.25	0.89	0.25	0.90	0.25	0.97	0.25	0.92	0.25	0.93
0.75	0.88	0.75	0.87	0.75	0.87	0.75	0.84	0.75	0.90	0.75	0.87
1.5	0.85	1.5	0.84	1.5	0.82	1.5	0.81	1.5	0.88	1.5	0.85
2.5	0.82	2.5	0.82	2.5	0.79	2.5	0.78	2.5	0.82	2.5	0.82
3.5	0.79	3.5	0.78	3.5	0.77	3.5	0.77	3.5	0.81	3.5	0.81
4.5	0.78	4.5	0.77	4.5	0.75	4.5	0.76	4.5	0.79	4.5	0.78
6	0.75	5.5	0.75	5.5	0.73	5.5	0.73	5.5	0.76	5.5	0.77
8	0.68	6.5	0.74	6.5	0.73	6.5	0.73	6.5	0.75	6.5	0.76
10.5	0.72	7.5	0.73	7.5	0.72	7.5	0.72	7.5	0.74	7.5	0.75
13.5	0.72	8.5	0.72	8.5	0.71	8.5	0.71	8.5	0.70	8.5	0.73
16.5	0.71	9.5	0.70	9.5	0.70	9.5	0.71	9.5	0.74	9.5	0.71
19.5	0.70	11	0.68	11	0.69	10.5	0.70	11	0.71	10.5	0.73
23	0.71	13.5	0.70	13.5	0.65	11.5	0.70	13.5	0.68	11.5	0.75
		17.5	0.69	16.5	0.63	13	0.69	16.5	0.69	13	0.73
		22.5	0.68	19.5	0.61	15	0.67	19.5	0.71	15	0.72
				23	0.60	17.5	0.67	23	0.74	17.5	0.72
						20.5	0.68				

Appendix 3, continued

SW.1		SW.2		BB.1		NB.1		TB.1	
Depth (cm)	WC								
0.25	0.92	0.25	0.94	0.25	0.66	0.25	0.68	0.25	0.89
0.75	0.85	0.75	0.88	0.75	0.69	0.75	0.68	0.75	0.81
1.5	0.81	1.25	0.86	1.25	0.67	1.25	0.42	1.25	0.78
2.5	0.77	1.75	0.84	1.75	0.61	1.75	0.56	1.75	0.8
3.5	0.75	2.25	0.81	2.25	0.65	2.25	0.54	2.25	0.78
4.5	0.73	2.75	0.77	2.75	0.62	2.75	0.53	2.75	0.78
5.5	0.74	3.5	0.75	3.5	0.43	3.5	0.52	3.5	0.77
6.5	0.74	4.5	0.71	4.5	0.58	4.5	0.45	4.5	0.77
8	0.71	5.5	0.68	5.5	0.58	5.5	0.54	5.5	0.77
10.5	0.73	6.5	0.7	6.5	0.56	6.5	0.53	6.5	0.75
13.5	0.70	7.5	0.7	7.5	0.56	7.5	0.54	7.5	0.74
16.5	0.70	8.5	0.61	8.5	0.56	8.5	0.55	8.5	0.75
19.5	0.73	10.5	0.66	10.5	0.57	10.5	0.54	10.5	0.75
		13.5	0.6	13.5	0.57	13.5	0.53	13.5	0.71
		16.5	0.6	16.5	0.57	16.5	0.51	16.5	0.76
		19.5	0.6	19.5	0.49	19.5	0.48	19.5	0.74
		22.5	0.57	22.5	0.57	22.5	0.47	22.5	0.75

Appendix 4. Calculated porosity (φ) values for Lake Superior sediments

FWM.1		FWM.2		FWM.3		FWM.4		FWM.5		FWM.6		FWM.7	
Depth (cm)	φ												
0.5	0.94	0.5	0.96	0.25	0.95	0.25	0.94	0.25	0.95	0.05	0.98	0.25	0.95
1.5	0.90	1.5	0.89	0.75	0.93	0.75	0.93	0.75	0.93	0.25	0.94	0.75	0.93
2.5	0.86	2.5	0.85	1.5	0.90	1.5	0.91	1.5	0.91	0.75	0.92	1.5	0.89
3.5	0.84	3.5	0.87	2.5	0.86	2.5	0.89	2.5	0.88	1.5	0.90	2.5	0.86
4.5	0.85	4.5	0.88	3.5	0.85	3.5	0.88	3.5	0.88	2.5	0.88	3.5	0.87
5.5	0.87	5.5	0.88	4.5	0.87	4.5	0.89	4.5	0.89	3.5	0.88	4.5	0.87
6.5	0.88	6.5	0.88	6	0.88	5.5	0.89	5.5	0.89	4.5	0.89	5.5	0.88
7.5	0.89	7.5	0.88	8	0.86	6.5	0.88	6.5	0.89	5.5	0.89	6.5	0.89
8.5	0.88	8.5	0.87	10.5	0.85	8	0.88	7.5	0.88	6.5	0.89	7.5	0.89
9.5	0.89	9.5	0.87	13.5	0.86	10.5	0.89	9	0.86	7.5	0.89	8.5	0.89
10.5	0.87	11	0.88	16.5	0.87	13.5	0.89	11	0.87	9.5	0.89	9.5	0.89
11.5	0.87	13.5	0.88	19.5	0.88	16.5	0.87	13.5	0.87	10.5	0.89	11	0.88
12.5	0.86	17.5	0.88	23	0.87	19.5	0.87	16.5	0.87	11.5	0.87	13.5	0.88
13.5	0.85									13	0.88	16.5	0.88
14.5	0.86									15.5	0.88	19.5	0.87
16	0.86									18.5	0.88		
18	0.86									22.5	0.88		
20	0.87												
22	0.87												
24	0.87												

Appendix 4, continued

IR.1		IR.2		IR.3		IR.4		IR.5		IR.6		KW.1	
Depth (cm)	φ												
0.25	0.96	0.25	0.95	0.25	0.96	0.05	0.98	0.25	0.95	0.25	0.96	0.25	0.95
0.75	0.95	0.75	0.94	0.75	0.95	0.25	0.94	0.75	0.93	0.75	0.95	0.75	0.94
1.5	0.93	1.5	0.93	1.5	0.93	0.75	0.92	1.5	0.93	1.25	0.94	1.5	0.93
2.5	0.92	2.5	0.92	2.5	0.92	1.5	0.90	2.5	0.91	1.75	0.89	2.5	0.92
3.5	0.91	3.5	0.91	3.5	0.90	2.5	0.88	3.5	0.91	2.25	0.92	3.5	0.91
4.5	0.89	4.5	0.90	4.5	0.90	3.5	0.88	4.5	0.89	2.75	0.92	4.5	0.90
6	0.89	6	0.89	6	0.89	4.5	0.89	5.5	0.89	3.50	0.91	6	0.87
8	0.89	8	0.89	8	0.89	5.5	0.89	6.5	0.89	4.50	0.92	8	0.87
10.5	0.90	10.5	0.89	10.5	0.89	6.5	0.89	8	0.90	5.50	0.91	10.5	0.89
13.5	0.89	13.5	0.89	13.5	0.89	7.5	0.89	10.5	0.90	6.50	0.90	13.5	0.89
16.5	0.89	17.5	0.89	17.5	0.89	9.5	0.89	13.5	0.89	7.50	0.90	16.5	0.86
19.5	0.89	22.5	0.89	22.5	0.89	10.5	0.89	16.5	0.89	8.50	0.90	19.5	0.88
23	0.87					11.5	0.87	19.5	0.89	10.50	0.90	23	0.87
										13.50	0.90		
										16.50	0.90		
										19.50	0.89		
										22.50	0.89		

Appendix 4, continued

EM.1		EM.2		EM.3		EM.4		EM.5		EM.6		Sta. 2	
Depth (cm)	φ												
0.5	0.95	0.25	0.96	0.25	0.96	0.25	0.96	0.25	0.96	0.25	0.93	0.5	0.88
1.5	0.94	0.75	0.95	0.75	0.95	0.75	0.96	0.75	0.94	1.25	0.92	1.5	0.81
2.5	0.93	1.5	0.97	1.5	0.94	1.5	0.95	1.5	0.93	1.75	0.91	2.5	0.74
3.5	0.91	2.5	0.93	2.5	0.92	2.5	0.92	2.5	0.92	2.25	0.92	3.5	0.69
4.5	0.90	3.5	0.91	3.5	0.91	3.5	0.91	3.5	0.91	2.75	0.89	4.5	0.67
5.5	0.88	4.5	0.90	4.5	0.90	4.5	0.90	4.5	0.90	3.5	0.91	5.5	0.66
6.5	0.87	6	0.86	6	0.89	5.5	0.89	5.5	0.89	4.5	0.90	6.5	0.65
7.5	0.85	8	0.83	8	0.88	6.5	0.89	6.5	0.88	5.5	0.77	7.5	0.64
8.5	0.85	10.5	0.82	10.5	0.86	7.5	0.88	7.5	0.88	6.5	0.88	8.5	0.64
9.5	0.85	13.5	0.81	13.5	0.85	8.5	0.87	9	0.87	7.5	0.88	9.5	0.63
10.5	0.83	17.5	0.81	16.5	0.85	9.5	0.85	11	0.86	8.5	0.86	10.5	0.63
11.5	0.83			19.5	0.85	11	0.87	13.5	0.86	10.5	0.81	11.5	0.58
12.5	0.83			23	0.85	13.5	0.87	16.5	0.85	13.5	0.85	12.5	0.59
13.5	0.82					16.5	0.86	19.5	0.85	16.5	0.85	13.5	0.58
14.5	0.82					19.5	0.87	23	0.86	19.5	0.79	14.5	0.58
16	0.82					23	0.87			22.5	0.82	16	0.65
												18	0.67
												20	0.63

Appendix 4, continued

WM.1		WM.2		WM.3		WM.4		WM.5		WM.6		NIP.1	
Depth (cm)	φ												
0.5	0.95	0.25	0.96	0.25	0.96	0.25	0.95	0.25	0.96	0.25	0.94	0.25	0.94
1.5	0.93	0.75	0.95	0.75	0.95	0.75	0.95	0.75	0.94	0.75	0.94	0.75	0.91
2.5	0.92	1.5	0.93	1.5	0.93	1.5	0.93	1.5	0.92	1.5	0.93	1.25	0.87
3.5	0.89	2.5	0.86	2.5	0.92	2.5	0.91	2.5	0.90	2.5	0.92	1.75	0.85
4.5	0.89	3.5	0.84	3.5	0.90	3.5	0.90	3.5	0.89	3.5	0.90	2.25	0.80
5.5	0.88	4.5	0.82	4.5	0.89	4.5	0.89	4.5	0.88	4.5	0.84	2.75	0.75
6.5	0.88	6	0.80	6	0.85	5.5	0.89	5.5	0.87	5.5	0.84	3.5	0.76
7.5	0.87	8	0.80	8	0.83	6.5	0.88	6.5	0.84	6.5	0.83	4.5	0.77
8.5	0.86	10.5	0.79	10.5	0.82	8	0.86	7.5	0.83	7.5	0.83	5.5	0.76
9.5	0.86	13.5	0.78	13.5	0.82	10.5	0.88	8.5	0.82	8.5	0.82	6.5	0.76
10.5	0.85	17.5	0.76	16.5	0.81	13.5	0.87	10.5	0.82	9.5	0.81	7.5	0.76
11.5	0.85			19.5	0.81	17.5	0.86	13.5	0.83	11	0.81	8.5	0.72
12.5	0.84			23	0.80	22.5	0.86	16.5	0.81	13.5	0.80	10.5	0.72
13.5	0.85							19.5	0.81	16.5	0.79	13.5	0.74
14.5	0.84							22.5	0.79			16.5	0.72
16	0.84											19.5	0.75
18	0.83											22.5	0.74
20	0.83												
22	0.83												
24	0.81												
27.5	0.81												

Appendix 4, continued

CM.1		CM.2		CM.3		CM.4		ED.2		ED.3	
Depth (cm)	φ										
0.25	0.96	0.25	0.96	0.25	0.96	0.25	0.99	0.25	0.97	0.25	0.97
0.75	0.95	0.75	0.95	0.75	0.94	0.75	0.93	0.75	0.96	0.75	0.95
1.5	0.94	1.5	0.93	1.5	0.93	1.5	0.92	1.5	0.95	1.5	0.94
2.5	0.93	2.5	0.92	2.5	0.91	2.5	0.90	2.5	0.92	2.5	0.93
3.5	0.91	3.5	0.90	3.5	0.90	3.5	0.90	3.5	0.92	3.5	0.92
4.5	0.90	4.5	0.90	4.5	0.89	4.5	0.89	4.5	0.91	4.5	0.91
6	0.89	5.5	0.89	5.5	0.88	5.5	0.88	5.5	0.89	5.5	0.90
8	0.85	6.5	0.88	6.5	0.87	6.5	0.87	6.5	0.89	6.5	0.89
10.5	0.87	7.5	0.88	7.5	0.87	7.5	0.87	7.5	0.89	7.5	0.89
13.5	0.87	8.5	0.87	8.5	0.87	8.5	0.87	8.5	0.86	8.5	0.88
16.5	0.87	9.5	0.86	9.5	0.86	9.5	0.87	9.5	0.88	9.5	0.86
19.5	0.86	11	0.85	11	0.85	10.5	0.86	11	0.87	10.5	0.88
23	0.86	13.5	0.86	13.5	0.83	11.5	0.86	13.5	0.85	11.5	0.89
		17.5	0.85	16.5	0.82	13	0.86	16.5	0.86	13	0.88
		22.5	0.85	19.5	0.81	15	0.84	19.5	0.87	15	0.87
				23	0.80	17.5	0.84	23	0.88	17.5	0.87
						20.5	0.85				

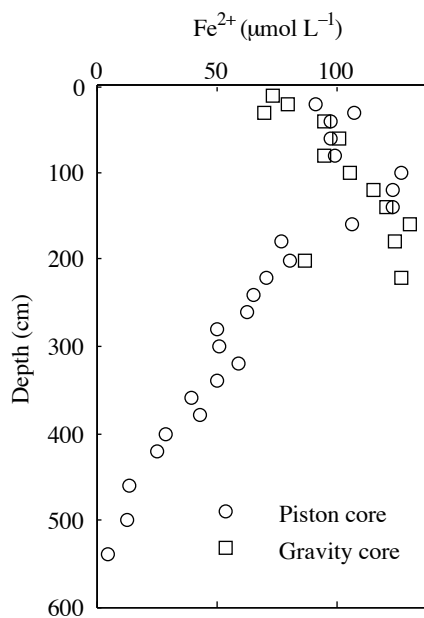
Appendix 4, continued

SW.1		SW.2		BB.1		NB.1		TB.1	
Depth (cm)	φ								
0.25	0.97	0.25	0.98	0.25	0.84	0.25	0.85	0.25	0.96
0.75	0.94	0.75	0.95	0.75	0.86	0.75	0.85	0.75	0.92
1.5	0.92	1.25	0.94	1.25	0.84	1.25	0.66	1.25	0.90
2.5	0.90	1.75	0.93	1.75	0.81	1.75	0.77	1.75	0.91
3.5	0.89	2.25	0.92	2.25	0.83	2.25	0.76	2.25	0.90
4.5	0.88	2.75	0.90	2.75	0.81	2.75	0.75	2.75	0.90
5.5	0.89	3.5	0.89	3.5	0.67	3.5	0.74	3.5	0.90
6.5	0.88	4.5	0.87	4.5	0.79	4.5	0.68	4.5	0.90
8	0.87	5.5	0.85	5.5	0.79	5.5	0.76	5.5	0.90
10.5	0.88	6.5	0.86	6.5	0.77	6.5	0.75	6.5	0.89
13.5	0.86	7.5	0.86	7.5	0.77	7.5	0.76	7.5	0.88
16.5	0.86	8.5	0.81	8.5	0.77	8.5	0.76	8.5	0.89
19.5	0.88	10.5	0.84	10.5	0.78	10.5	0.76	10.5	0.89
		13.5	0.80	13.5	0.78	13.5	0.75	13.5	0.87
		16.5	0.80	16.5	0.78	16.5	0.73	16.5	0.89
		19.5	0.80	19.5	0.72	19.5	0.71	19.5	0.88
		22.5	0.78	22.5	0.78	22.5	0.70	22.5	0.89

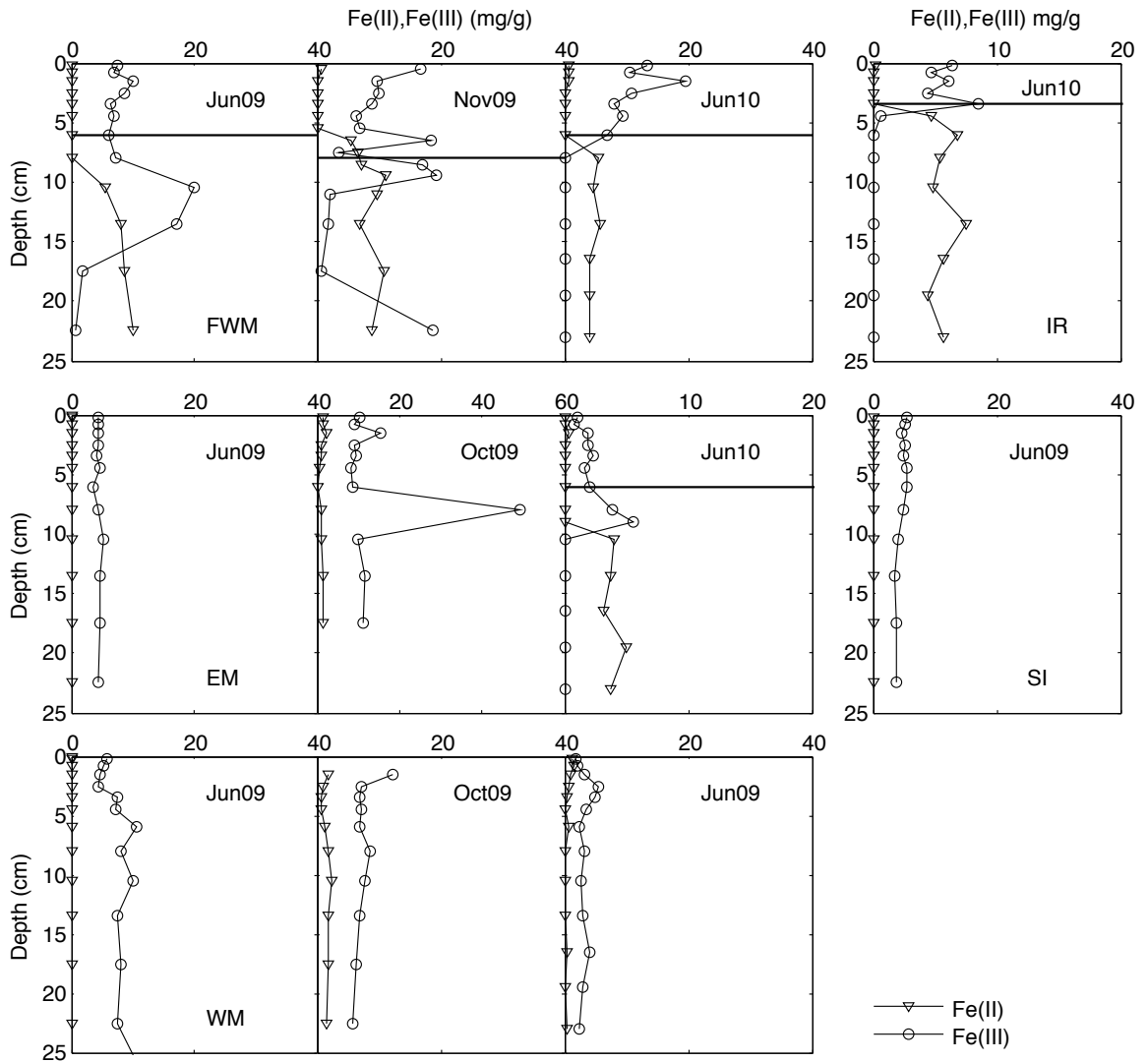
Appendix 5. Dissolved Fe(II) in piston and gravity cores at Sta. IR. 6, Lake Superior

Depths indicate the distance to the top of the cores.

Piston core		Gravity core	
Depth (cm)	Fe ²⁺ (μmol L ⁻¹)	Depth (cm)	Fe ²⁺ (μmol L ⁻¹)
20	91.1	10	73.4
30	107.1	20	80.2
40	97.5	30	70.1
60	97.4	40	94.6
80	99.7	60	101.1
100	127.1	80	94.7
120	123.7	100	105.9
140	123.2	120	115.4
160	106.8	140	121.1
180	77.5	160	131.0
200	80.5	180	124.8
220	70.9	200	86.6
240	65.2	220	127.2
260	63.3		
280	50.5		
300	51.4		
320	59.3		
340	50.7		
360	40.0		
380	42.9		
400	29.1		
420	25.1		
460	13.4		
500	12.5		
540	4.8		
Deep	96.4		



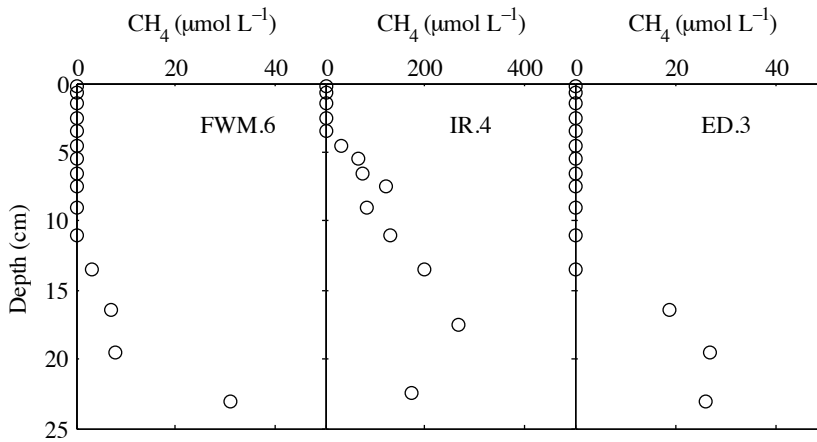
Appendix 6. Distributions of HCl (0.5 N)- extractable iron, Lake Superior sediments



Appendix 7. Distributions of methane in Lake Superior sediments

(measurements provided by S.A. Crowe)

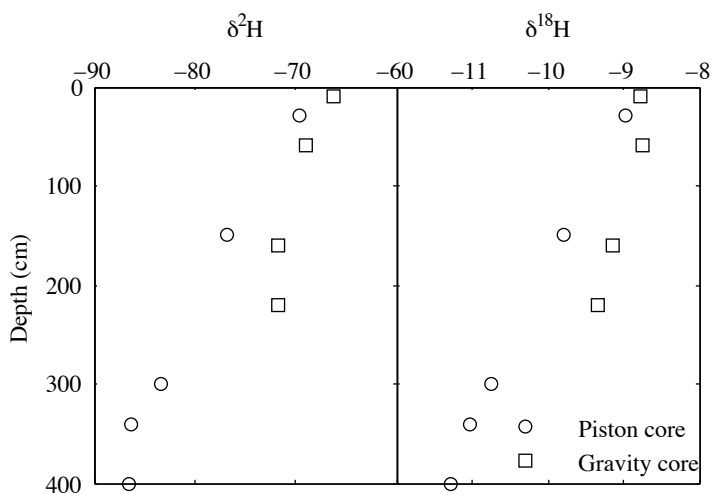
IR.4		ED.3		FWM.6	
Depth (cm)	CH ₄ ($\mu\text{mol L}^{-1}$)	Depth (cm)	CH ₄ ($\mu\text{mol L}^{-1}$)	Depth (cm)	CH ₄ ($\mu\text{mol L}^{-1}$)
0.25	1	0.25	0	0.25	0
0.75	1	0.75	0	0.75	0
1.5	1	1.5	0	1.5	0
2.5	0	2.5	0	2.5	0
3.5	2	3.5	0	3.5	0
4.5	33	4.5	0	4.5	0
5.5	67	5.5	0	5.5	0
6.5	73	6.5	0	6.5	0
7.5	122	7.5	0	7.5	0
9	83	9	0	9	0
11	131	11	0	11	0
13.5	197	13.5	0	13.5	3
17.5	265	16.5	19	16.5	7
22.5	174	19.5	27	19.5	8
		23	26	23	31



**Appendix 8. Distributions of $\delta^2\text{H}$ and $\delta^{18}\text{O}$ in piston and gravity cores at Sta. IR.
6, Lake Superior**

Samples were analyzed at the GEOTOP-UQAM geochemical laboratories with the help of Dr. Alfonso Mucci. Depths indicate the distance from the top of the cores.

Piston core			Gravity core		
Depth (cm)	$\delta^2\text{H}$ (‰)	$\delta^{18}\text{O}$ (‰)	Depth (cm)	$\delta^2\text{H}$ (‰)	$\delta^{18}\text{O}$ (‰)
30	-69.7	-8.98	10	-66.3	-8.77
150	-76.7	-9.78	60	-69.0	-8.74
300	-83.3	-10.75	160	-71.8	-9.15
340	-86.3	-11.03	220	-71.8	-9.34
400	-86.5	-11.27			



Appendix 9. Results from sediment flow-through reactor experiments, Sta. ED, Lake Superior.

These experiments were conducted using sediment flow-through reactors (designed in Pallud et al. 2007), which consist of sediment slices 0.9 cm thick and 4 cm in diameter (sediment volume $V=11 \text{ cm}^3$). The input concentrations of nitrate and chloride (C_0) were 25 – 32 and 10 – 12 $\mu\text{mol L}^{-1}$ respectively (*see* measured values in table below). The imposed flow rate (Q) was $\sim 1.7 \text{ mL h}^{-1}$ (measured values are in the Table). The outflows were analyzed for concentrations (C_{out}) of nitrate, nitrite and soluble reactive phosphate (SRP). The experiments were conducted at room temperature ($\sim 20^\circ\text{C}$). The consumption/production rates of nitrate, nitrite and SRP (R ; negative values indicate consumption) were calculated as $R = \frac{(C_0 - C_{\text{out}})Q}{V}$.

Reactor 3-4 cm

Time (h)	Flow rate (mL h^{-1})	Input ($\mu\text{mol L}^{-1}$)		Outflow ($\mu\text{mol L}^{-1}$)				Rate ($\mu\text{mol cm}^{-3} \text{ d}^{-1}$)		
		Cl^-	NO_3^-	Cl^-	NO_3^-	NO_2^-	SRP	NO_3^-	NO_2^-	SRP
0	1.68	11.4	26.9	123.1	0	0	0	-0.099	0	0
8.9	1.68	11.4	26.9	16.9	40.9	4.8	1.5	0.051	0.018	0.0054
24.1	1.68	11.4	26.9	10.0	49.7	0	3.7	0.083	0	0.014
35.5	1.73	11.3	26.9	10.1	38.1	0	2.9	0.042	0	0.012
48.8	1.73	11.3	31.6	8.5	35.3	0	3.3	0.014	0	0.013
77.1	1.73	11.3	31.6	8.4	19.5	0	1.7	-0.046	0	0.0065
97.1	1.56	11.3	31.6	8.3	6.7	0.9	2.6	-0.085	0.003	0.0087
108.4	1.56	11.3	31.6	11.5	10.0	0	1.5	-0.073	0	0.0050
156.5	1.56	10.7	28.3	11.6	15.0	0	1.5	-0.045	0	0.0050

Appendix 9, continued

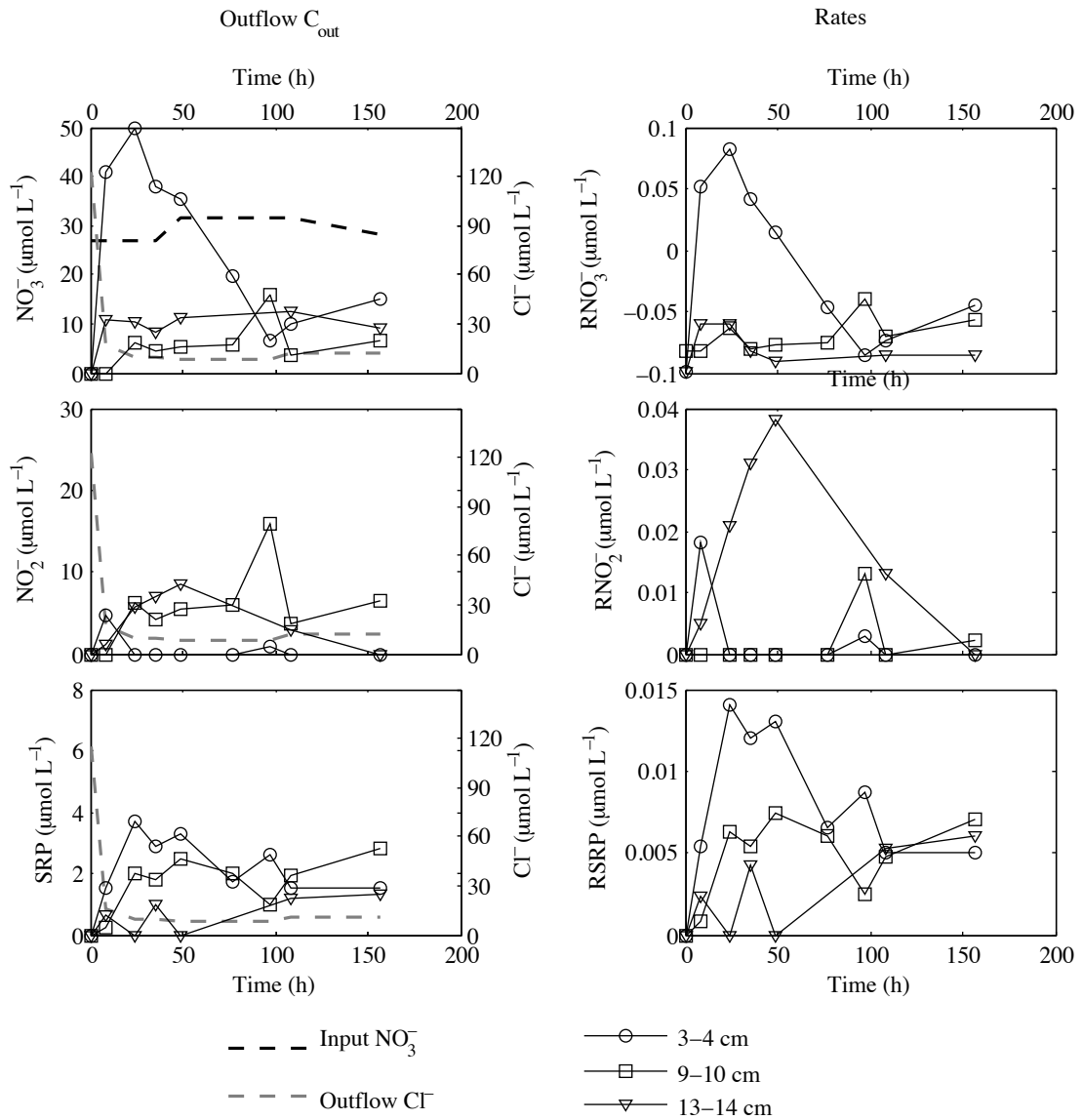
Reactor 9-10 cm

Time (h)	Flow rate (mL h ⁻¹)	Input ($\mu\text{mol L}^{-1}$)		Outflow ($\mu\text{mol L}^{-1}$)				Rate ($\mu\text{mol cm}^{-3} \text{d}^{-1}$)		
		Cl ⁻	NO ₃ ⁻	Cl ⁻	NO ₃ ⁻	NO ₂ ⁻	SRP	NO ₃ ⁻	NO ₂ ⁻	SRP
0	1.41	11.4	26.9	132.5	0	0	0	-0.083	0	0
8.9	1.41	11.4	26.9	17.4	0	0	0.27	-0.083	0	0.0008
24.1	1.41	11.4	26.9	15.1	6.2	6.2	2.0	-0.064	0	0.0063
35.5	1.35	11.3	26.9	10.5	4.3	4.3	1.8	-0.080	0	0.0054
48.8	1.35	11.3	31.6	9.4	5.5	5.5	2.5	-0.077	0	0.0075
77.1	1.35	11.3	31.6	14.3	5.9	5.9	2.0	-0.076	0	0.0060
97.1	1.17	11.3	31.6	7.8	15.8	15.8	0.99	-0.040	0.013	0.0025
108.4	1.56	11.3	31.6	9.4	3.8	3.8	1.9	-0.071		0.0048
156.5	1.56	10.7	28.3	10.2	6.4	6.4	2.8	-0.056	0.0023	0.0071

Reactor 13-14 cm

Time (h)	Flow rate (mL h ⁻¹)	Input ($\mu\text{mol L}^{-1}$)		Outflow ($\mu\text{mol L}^{-1}$)				Rate ($\mu\text{mol cm}^{-3} \text{d}^{-1}$)		
		Cl ⁻	NO ₃ ⁻	Cl ⁻	NO ₃ ⁻	NO ₂ ⁻	SRP	NO ₃ ⁻	NO ₂ ⁻	SRP
0	1.68	11.4	26.9	97.86	0	0	0	-0.099	0	0
8.9	1.68	11.4	26.9	27.13	10.62	1.245	0.6535	-0.060	0.005	0.0024
24.1	1.68	11.4	26.9	12.24	10.21	5.635	0	-0.061	0.021	0
35.5	2.03	11.3	26.9	12.395	8.11	6.92	0.952	-0.083	0.031	0.0042
48.8	2.03	11.3	31.6	8.94	11.265	8.565	0	-0.090	0.038	0
108.4	2.03	11.3	31.6	12.915	12.31	2.865	1.19	-0.085	0.013	0.0053
156.5	2.03	10.7	28.3	7.325	9.18	0	1.355	-0.085	0	0.0060

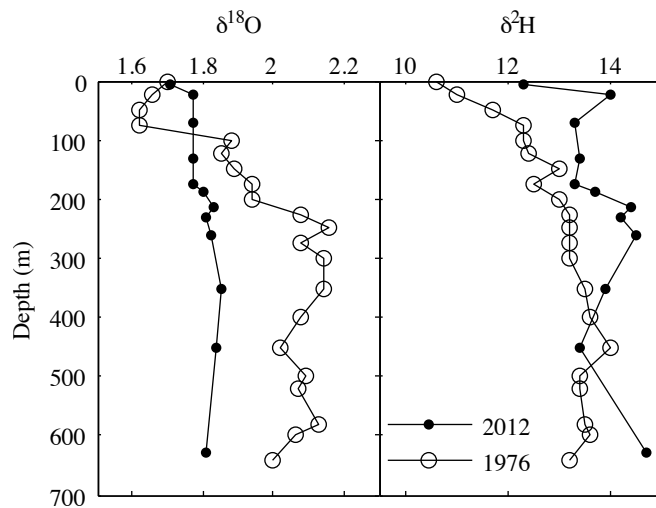
Appendix 9, continued



Appendix 10. Distributions of $\delta^2\text{H}$ and $\delta^{18}\text{O}$ in Lake Malawi water column at Sta. CD.

Historical data for comparison are taken from Gonfiantini et al. 1979. Samples were analyzed at the GEOTOP-UQAM geochemical laboratories with the help of Dr. Alfonso Mucci.

Depth (m)	$\delta^2\text{H}$ (‰)	$\delta^{18}\text{O}$ (‰)
5	12.3	1.71
25	14	1.77
70	13.3	1.77
130	13.4	1.77
175	13.3	1.77
190	13.7	1.8
215	14.4	1.83
230	14.2	1.81
260	14.5	1.82
350	13.9	1.85
450	13.4	1.84
630	14.7	1.81



Appendix 11. Data for other freshwater large lakes.

The Data are from Lake Baikal (Maerki et al. 2006), Lake Michigan (Thomsen et al. 2004), and Lake Zug (Maerki et al. 2009).

1. Rates of carbon mineralization ($\text{mmol m}^{-2} \text{d}^{-1}$) vs. water depth (Fig. 5.13)

Lake Baikal		Lake Michigan		Lake Zug	
Depth (m)	R_c	Depth (m)	R_c	Depth (m)	R_c
600	4.9	100	8.6	25	27.9
700	3.4			35	26.9
160	2.5			50	31.2
600	2.1			80	30.1
1400	2.7			120	26.9
				160	33.3
				180	34.9

2. Rates of total oxygen uptake (TOU; $\text{mmol m}^{-2} \text{d}^{-1}$) vs. water depth (Fig. 1.14 A)

Lake Baikal		Lake Michigan		Lake Zug	
Depth (m)	TOU	Depth (m)	TOU	Depth (m)	TOU
600	5.1	100	5.7	25	26.2
700	3.6			35	25.4
160	2.6			50	29.7
600	2.2			80	28.4
1400	2.8			120	1.90

3. Oxygen penetration as functions of water depth (Fig. 1.14 B)

Lake Baikal		Lake Michigan	
Depth (m)	OPD (cm)	Depth (m)	OPD (cm)
600	2.5	100	2.1
700	2		
160	2		
600	2.5		
1400	2.5		

4. Rate of sediment denitrification ($\text{mmol m}^{-2} \text{d}^{-1}$) vs. water depth (Fig. 2.7 C, Fig. 2.8 A)

Lake Baikal		Lake Michigan		Lake Zug	
Depth (m)	$R_{\text{denitr.}}$	Depth (m)	$R_{\text{denitr.}}$	Depth (m)	$R_{\text{denitr.}}$
600	0.51	100	0.19	25	0.70
700	0.35			35	0.67
160	0.26			50	0.57
600	0.22			80	0.65
1400	0.28			120	0.63
				160	0.38